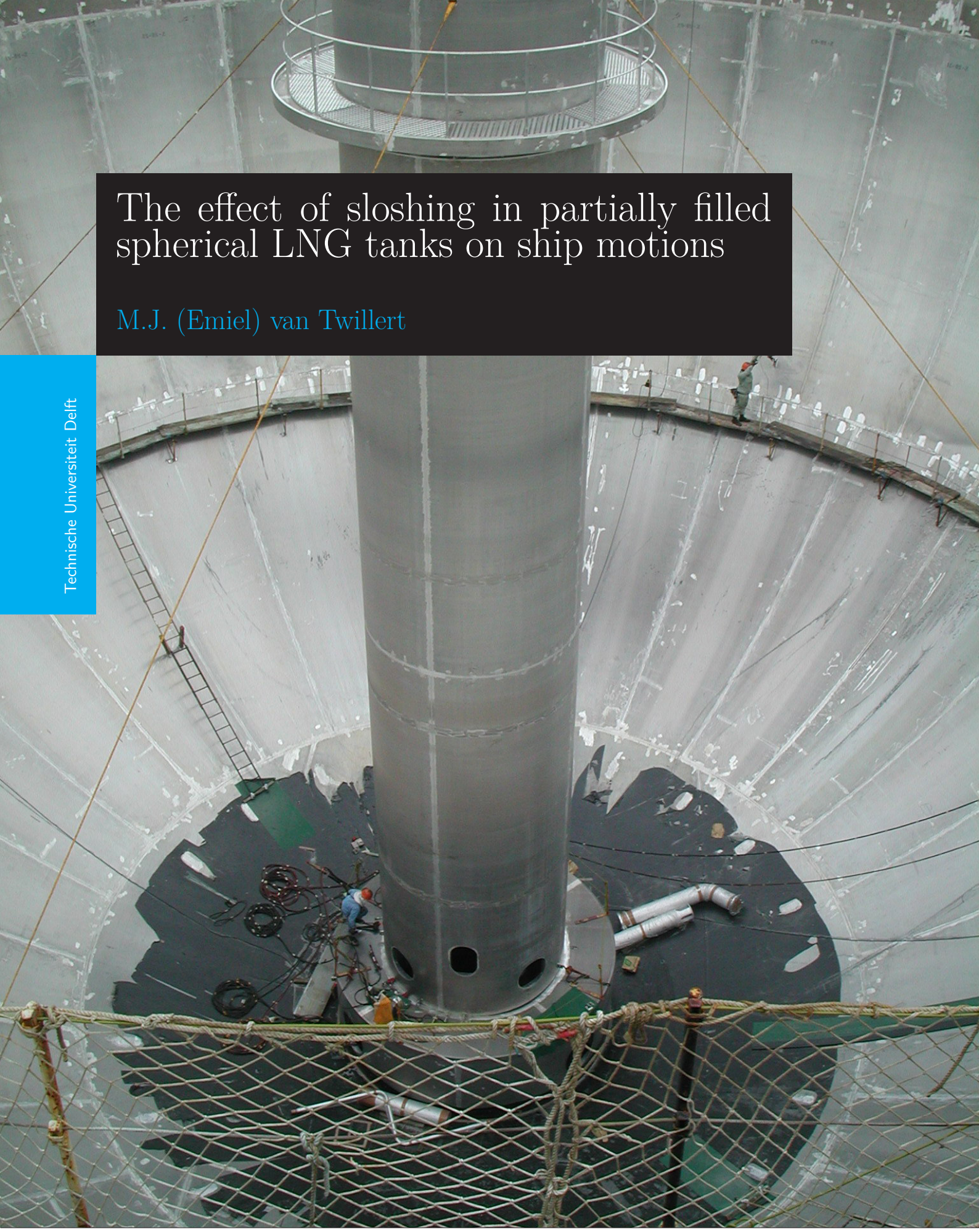

The effect of sloshing in partially filled spherical LNG tanks on ship motions

M.J. (Emiel) van Twillert

Technische Universiteit Delft

TU Delft Delft University of Technology

Challenge the future

The effect of sloshing in partially filled spherical LNG tanks on ship motions

by

M.J. (Emiel) van Twillert

in partial fulfillment of the requirements for the degree of

Master of Science

in Offshore Engineering

at the Delft University of Technology,

to be defended on Tuesday March 17, 2015 at 13:30 PM.

Chairman:	Prof. dr. ir. R.H.M. Huijsmans	TU Delft
Thesis committee:	Dr. ir. I. Akkerman	TU Delft
	Dr. ir. G.H. Keetels	TU Delft
	Ir. F. Lange	Shell
	Dr. O.E. Sequeiros	Shell
	F. McPhail MEng ACGI	Shell

This thesis is confidential and cannot be made public.

TU Delft

Abstract

Ships with partially filled spherical cargo tanks may experience sloshing of the cargo in the internal tanks when exposed to waves. Besides impact forces on the tank wall, sloshing may also have an effect on the ship motions. No previous research on the effect of sloshing in partially filled spherical tanks on ship motions was identified. Therefore Shell has decided to perform scale model tests in which the behaviour of a barge with two spherical tanks was investigated for different loading and environmental conditions. The focus of these tests was on the roll motions of the barge as this degree of freedom is expected to be influenced most by sloshing in the internal tanks. The scale model test results clearly showed two peaks in the roll RAO response. The first peak is around the natural frequency of the barge, while the second and smaller peak is around the first mode natural sloshing frequency. Significant roll responses of the barge due to higher free surface modes were not identified in the tests. It was however identified that the first mode natural sloshing frequency is in the area of wind wave frequencies, which might be encountered during an offloading operation. It was furthermore identified that the first roll RAO peak decreases in height and frequency for increasing loading condition. The sloshing induced roll RAO peak also decreases in height, but showed an increasing frequency for increasing loading condition. Non-linear sloshing was observed in the tanks when the barge was excited by waves around the first mode natural sloshing frequency.

This report describes two methods to analyse the effect of sloshing on ship motions. The first method applies linear potential theory on both the barge and the internal tanks. For the barge the radiation, diffraction and incoming wave potentials are solved. For the internal tanks only the radiation potential is calculated, as there are obviously no incoming or diffracted waves in the tanks. The potentials are then used to solve the added mass, damping and wave forces for the coupled barge-tank system in the frequency domain. By comparing the frequency domain results with the scale model tests results a good agreement was identified for all loading conditions. On top of this the frequency domain approach is very fast and relatively easy to set up. However, linearity is assumed while in the scale model test non-linear sloshing was observed. It is expected that non-linearity will damp out the roll motion of the vessel and it is therefore expected that for increasing wave height the frequency domain solution will overestimate the response. It was also found that both roll RAO peaks are very sensitive to the wave direction. By comparing the roll RAO's for liquid and frozen cargo in the tanks it was found that sloshing significantly decreases the height of the main roll RAO peak and also creates a lower barge natural frequency.

The second method is a more complex time domain model that is based on a coupling between Volume of Fluid solver ComFLOW and ship motions solver aNySIM. In the coupled model the motions of the barge due to waves, without internal tanks, are obtained by using linear potential flow and are calculated in aNySIM. The ship motions calculated in aNySIM are used as input in ComFLOW that calculates the more complex and potentially non-linear motions of the liquid in the spherical cargo tanks. The resulting sloshing loads are again used as input in aNySIM, creating a two-way coupling between the dynamics of the ship and cargo tanks. The time domain results showed a reasonably good agreement with the scale model tests. However, the second, sloshing induced, roll RAO peak is underestimated in the coupled model. This might be due to the type of waves used in the test, uncertainty in the RAO's and due to the properties of the coupling between ComFLOW and aNySIM. The time domain method is time consuming and complex to set up, but offers more insight in what is really happening. It was shown that non-linear motions of the barge occur due to sloshing in the tanks. It was also found that with partially filled tanks the response of the barge is irregular when exposed regular waves. The influence of the pump tower was also investigated, which showed that due to the damping created by the pump tower the overall roll response is lower and the barge natural frequencies moves to a lower frequency.

Preface and Acknowledgments

This report describes the research conducted as part of my thesis to obtain the Master of Science degree in Offshore Engineering. Although I obtained a BSc degree in Civil Engineering I have always been interested in the sea and its extremes. This is one of the reasons for me to pursue a degree in Offshore Engineering, which is largely focused on challenging the extreme sea environments all around the world. During my studies I enjoyed the classes about hydromechanics and decided to graduate by specialising in floating structures. The professor for this specialisation is René Huijsmans, which I would like to thank for being the chairman of my graduation committee and for providing me with valuable feedback throughout my MSc project. But I would also like to thank René for his confidence in me and for connecting me with André van der Stap, Team Lead of the Offshore Structures department of Shell. I would like to thank André and Shell for offering me the opportunity to work on a very up-to-date and interesting topic that finally resulted in the report presented to you.

During the duration of the project I have been supported by many people. At Shell I would like to thank my daily supervisors; Frank Lange, Octavio Sequeiros and Finlay McPhail for their support, time and for sharing their valuable insights with me. I would also like to thank Jason McConochie and Emilio Caputano for sharing their experiences with me and for looking critically at my work. At the TU Delft I would also like to thank Ido Akkerman for explaining me the basics of numerical schemes, for looking at my results critically and for providing me with valuable feedback after reading my report. Geert Keetels joined the graduation committee in the final weeks of the project and I would like to thank him for his contribution to this project.

A special thank you is reserved for my family and friends that always supported me during my journey from a MAVO diploma, via the army, to obtaining a masters degree from Delft University of Technology.

I wish you an interesting read.

Delft, March 2015

Emiel

Summary

This is a summary of the MSc project in which the effect of sloshing in partially filled spherical tanks on ship motions is investigated. First the problem will be described, followed by a literature review and the goal of the project. Then both models that are used for this project are discussed and the results are compared with scale model test results. Finally the conclusions and recommendations are presented.

Introduction and problem description

With floating liquefied natural gas (FLNG) the natural gas is transported from the offshore wellhead to the FLNG facility where it is purified and liquefied. After liquefaction the Liquefied Natural Gas is stored in the storage tanks of the FLNG until an LNG carrier (LNGC) arrives. The LNG carrier will berth itself alongside the FLNG, in which the distance between the LNGC and FLNG is approximately 4 meters, the size of the fenders used to separate both vessels. After the LNG carrier is brought into position the LNG is transported from the FLNG to the LNG carrier via mechanical loading arms. During the offloading operations the tanks of the LNG carrier are gradually filled from empty to full. During this process the free surface area of the LNG in the tanks changes depending on the filling level and the type of tank used. Due to the free surface of the cargo and the waves exciting the LNG carrier, the cargo may slosh inside the cargo tanks possibly inducing additional vessel motions. As the FLNG and LNG carrier are positioned so close to each other it is very important to understand the motions of the LNG carrier with partially filled tanks, which is the main focus of this project.

LNG carriers are mainly built with two types of containment system; membrane and Moss type tanks. Membrane type tanks are mostly prismatic tanks that are not self supporting. Sloshing has always been considered a major challenge with membrane tanks because of the vertical walls. These are vulnerable to wave slamming forces that may damage the tanks and/or create additional vessel motions. Because of this a lot of research has been performed on the effect of sloshing in prismatic tanks on ship motions, which is currently considered relatively well understood. Moss type tanks are spherical self-supporting tanks that are structurally stronger than prismatic tanks. Due to the spherical shape slamming forces are not expected to occur. Damage to the tanks due to sloshing has therefore never been considered a major issue. It was however also assumed that for ship motions the ballasted loading condition (empty tanks) would be the critical condition and that for increasing loading condition the ship motions would decrease. However, there is no evidence identified in the public domain to support these assumptions. Therefore one of the main goals of this project is to develop a model that can be used to gain more insight in the effect of sloshing on ship motions.

Literature review

During the literature review the effects of sloshing on ship motions is investigated for both prismatic- and spherical cargo tanks.

Spherical tanks

For sloshing in spherical tanks the only research identified was focused on obtaining the natural sloshing frequency, that is of interest because violent sloshing motions are expected around that frequency. Budiansky (1958) performed numerical work to determine the natural frequencies of an almost full, half-full and near empty spherical tank. McCarty and Stephens (1960) performed experimental research to obtain the first 4 natural sloshing frequencies of spherical tanks. Mikishev and Dorozhkin

(1981) performed experimental research to develop an empirical equation to calculate the first mode natural sloshing frequency for an arbitrary filling depth and tank radius. Rattayya (1965) also developed an empirical equation for the first mode natural sloshing frequency, but used a numerical approach. Additionally, Andrew and Alfred (1962) showed by experiments that the natural sloshing frequencies do not seem to be strongly dependent on the fluid properties such as density and viscosity. From this part of the literature study it is learnt that the first mode natural sloshing frequency is in the area of wind wave frequencies, which are likely to be encountered during a side-by-side operation.

This research gave insight for which frequencies the most extreme sloshing may be expected, but it did not give any insight in the effect of sloshing in spherical tanks on ship motions. Therefore Shell decided to initiate a joint experiment research program together with The Centre for Offshore Foundation (COFS) at The University of Western Australia (UWA) and the State Key Laboratory of Ocean Engineering (SKLOE) at Shanghai Jiao Tong University (SJTU). The main goal of the scale model test campaign was to gain an understanding of the motions of a vessel with partially filled spherical tanks in waves. The barge used in the scale model test had a full scale length of 200 meter, breadth of 46 meter and depth of 25 meter. A scaling ratio of 1:60 was used. During the test the 0, 25, 50, 75 and 100 percent loading conditions were considered. The results obtained during these scale model tests are used to validate the frequency and time domain models.

Prismatic tanks

Molin et al. (2010), Zhao et al. (2014), Gaillarde et al. (2003) and Claus et al. (2010) all published scale model test results and found that in case of sloshing there are two peaks in the response, just as is found for spherical tanks. However, the sloshing induced roll Response Amplitude Operator (RAO) peak for prismatic tanks is found to be generally larger than what is found for spherical tanks. Molin et al. (2010) also showed that non-linear sloshing may occur for certain sea states. Bunnik and Veldman (2010), Claus et al. (2010), Lee (2008) and Gaillarde et al. (2003) all developed frequency domain models to simulate the effect of sloshing in membrane type tanks on ship motions. These models are based on linear potential theory for both the response of the ship to waves and the sloshing inside the cargo tanks. The linear assumptions are expected to be valid for the ship motions, as offloading conditions are considered, that generally result in small ship motions. However, for the sloshing in the tank the linear assumption may not be valid. The results of the frequency domain models did not show a good agreement with scale model tests. Bunnik and Veldman (2010) developed, next to a frequency domain model, also a time domain model to simulate the effect of sloshing in membrane type tanks on ship motions. The model consisted of a coupling between ship motion solver aNySIM and Volume of Fluid CFD solver ComFLOW. A very good agreement is found between model tests and time domain results, even for a relatively coarse grid in ComFLOW.

Research goal

The effect of sloshing in partially filled spherical tanks on ship motions is identified as a gap. The research goal of this thesis is formulated as follows: “To develop a coupled sloshing-ship motion model that is validated with scale model tests, to be used to simulate, and to gain a better understanding of, the effect of sloshing in partially filled spherical tanks on ship motions under operational conditions.” To reach this goal, the knowledge obtained during the literature review is used as a basis for further research. As a result of comparing different solution strategies a time domain model consisting of a coupling between ComFLOW and aNySIM has been identified as most promising. This is expected to be mainly because of ComFLOWs ability to simulate non-linear sloshing. However, sloshing is expected to be less violent in spherical tanks than in prismatic tanks. Therefore the frequency domain approach may also show good results for spherical tanks. It would be very interesting to provide a final comparison between the roll RAOs obtained from the scale model test, linear frequency domain approach and non-linear time domain approach. Therefore it was decided to create both a frequency- and time domain model, to validate both models with the scale model tests and to use the models to gain additional insight in the effects of sloshing on ship motions.

Frequency domain approach

WAMIT is used to model both the barge and tank in the frequency domain. The main assumption in the frequency domain approach is linearity. This means that the ship motions are supposed to be small. According to Denis (1974) small vessel motions give heave amplitudes smaller than $1/5^{th}$ of the draft, roll amplitudes smaller than 15 degrees and pitch amplitudes smaller than 5 degrees. This assumption is generally believed to be valid for ships without a large free surface in operational conditions. However, the linear assumptions may not be valid for the sloshing in the tanks; during the scale model tests non-linear sloshing was observed. Other assumptions made include that the fluid is considered frictionless, homogeneous, incompressible, free of surface tension and irrotational. Because of this viscous effects are not taken into account, which are especially important for the roll motion of a ship. Therefore additional linear roll damping was added to the equation of motion to mimic the effects of non-linear viscous damping. This was done by matching the height of the local maxima around the natural frequency of the barge to the model test results. The equation of motion solved by WAMIT in the frequency domain is:

$$\left[-\omega^2 \left(\boldsymbol{M}_b + \boldsymbol{A}_b(\omega) - \boldsymbol{A}_t(\omega)\right) + i\omega(\boldsymbol{B}_b(\omega) + \boldsymbol{B}_{ext}) + (\boldsymbol{C}_b - \boldsymbol{C}_t + \boldsymbol{C}_{ext})\right] \hat{\boldsymbol{\zeta}} = \hat{\boldsymbol{F}}(\omega) \tag{1}$$

Here the subscripts b and t are used to identify the barge and tank respectively. The subscript ext is used to refer to the external damping or restoring coefficient matrix, which can also be used to add additional damping to the system. In Equation 1 ω is the wave frequency, $\boldsymbol{M}$ is the mass matrix, $\boldsymbol{A}$ the added mass matrix, $\boldsymbol{B}$ is the damping matrix, $\boldsymbol{C}$ is the restoring coefficients matrix, $\hat{\boldsymbol{\zeta}}$ is the complex motion amplitude vector and $\hat{\boldsymbol{F}}$ is the complex wave force amplitude vector. In the frequency domain approach the panel models of the barge and tank are used to obtain the potentials when the barge is is excited by waves. The sensitivity of the results to the mesh size of both panel models is checked. By taking into account the convergence of the results and the calculation times a final mesh size was chosen for both the barge and tank separately. For the barge the radiation, diffraction and incoming wave potentials were solved. For the tanks only the radiation potential is solved to calculate the added mass of the cargo. In WAMIT the mass of the cargo is included in the frequency dependent added mass of the cargo. Once the added mass, damping, restoring coefficients and wave forces in Equation 1 are known the RAOs can be obtained by taking the modulus of the complex motion amplitudes:

$$RAO_j = |\hat{\zeta}_j| \tag{2}$$

Where j=1,2,..6 and identifies the degrees of freedom of the barge.

Time domain approach

In a time domain approach non-linear effects can be taken into account. However, modelling the non-linear response of the barge to waves is still considered too time consuming. Additionally, the linear assumptions for a barge in waves (without large free surface) is expected to be valid under operational conditions. Therefore it is decided to take non-linear sloshing into account and to model the barge without cargo tanks with linear potential theory. The challenge in this approach is to develop a coupling that can create an (almost) real time coupling between the sloshing in the tanks and the motions of the barge.

For this project a coupling between ComFLOW (Volume of Fluid solver) and aNySIM (ship motion solver) is developed. The principle of the coupling is shown in Figure 1. In aNySIM the motions, velocities and accelerations of the barge are calculated at the present time level. ComFLOW uses the motions calculated in aNySIM to place the tank in a new position and to progress in time until it has passed the current aNySIM time. During its march in time the motions, velocities and accelerations calculated by aNySIM are linearly interpolated. When ComFLOW has passed the current aNySIM time the most recent sloshing loads are sent to aNySIM. aNySIM then includes the sloshing loads in the equation of motion to progress to the next time level.

ComFLOW uses the Navier-Stokes equations to solve fluid flows. However, as very high Reynolds numbers were observed in both model- and full scale, viscous effects have been neglected. Therefore the Navier-Stokes equations solved by ComFLOW reduce to the Euler equations:

$$\frac{\partial \boldsymbol{u}}{\partial t} + \boldsymbol{u} \cdot \nabla \boldsymbol{u} = -\frac{1}{\rho} \nabla p + \boldsymbol{F}_{ext} \tag{3}$$

With $\boldsymbol{u} = (u, v, w)$ the velocity vector, ∇ the divergence, ρ the density of the cargo, p the pressure and $\boldsymbol{F}_{ext}$ is the external force vector, by which, for example, gravity is taken into account. Ship motion solver aNySIM requires the frequency dependent added mass, damping and wave forces as input to solve the linearised response of the barge to waves. However, due to non-linear sloshing in the cargo tanks the response of the barge is also expected to be non-linear.

Results and validation

This section will discuss the results and validation of both the frequency and time domain model. Validation of the numerical models will be done against the scale model test results. Sloshing in the internal tanks has shown to have the largest impact on the roll motion. Furthermore, roll is considered a critical degree of freedom during an offloading operation. Therefore the focus of the results will be on the roll motion of the barge.

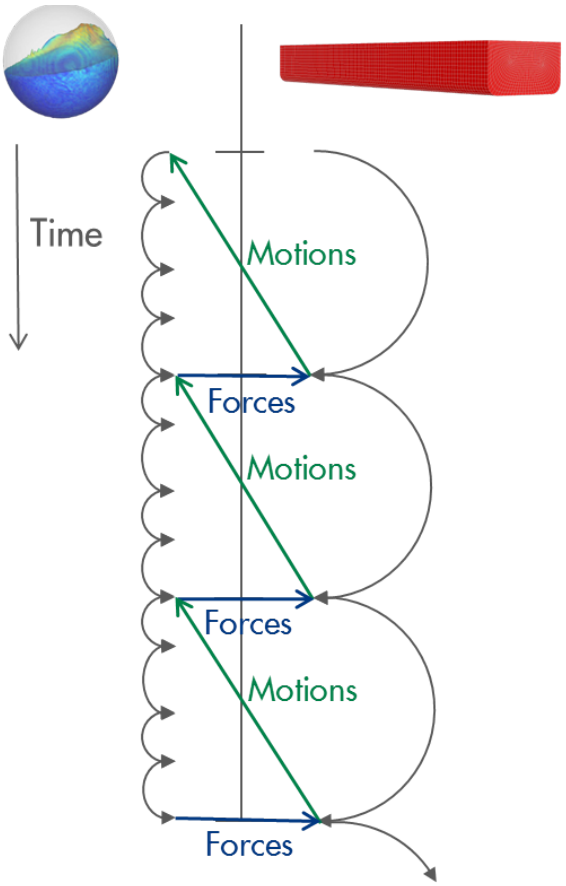

Figure 1: Principe of the coupling

It is expected that the roll radius of gyration may not have been measured correctly during the scale model tests. Therefore the roll radius of gyration is corrected so that the barge natural frequency found in the frequency domain approach matches the barge natural frequency found during the scale model tests. Correcting the roll radius of gyration created a difference of about one to five percent in the barge natural frequency. The uncertainty that comes from the unknown roll radius of gyration should be considered when reading the results. Correcting the roll radius of gyration does not have a significant effect on the width of the response curve around the barge natural frequency and also does not have a significant influence on the location and height of the sloshing induced roll RAO peak.

Frequency domain results

The main results that are obtained in the frequency domain are shown in Figure 2 for 45 and 90 degree incoming waves and for the 25, 50 and 75 percent loading conditions. The left peak in the roll RAO response is around the barge natural frequency. The right and smaller peak is induced by the sloshing and is around the first free surface mode natural frequency. It can also be observed that for quartering waves the sloshing induced roll RAO peak has almost disappeared.

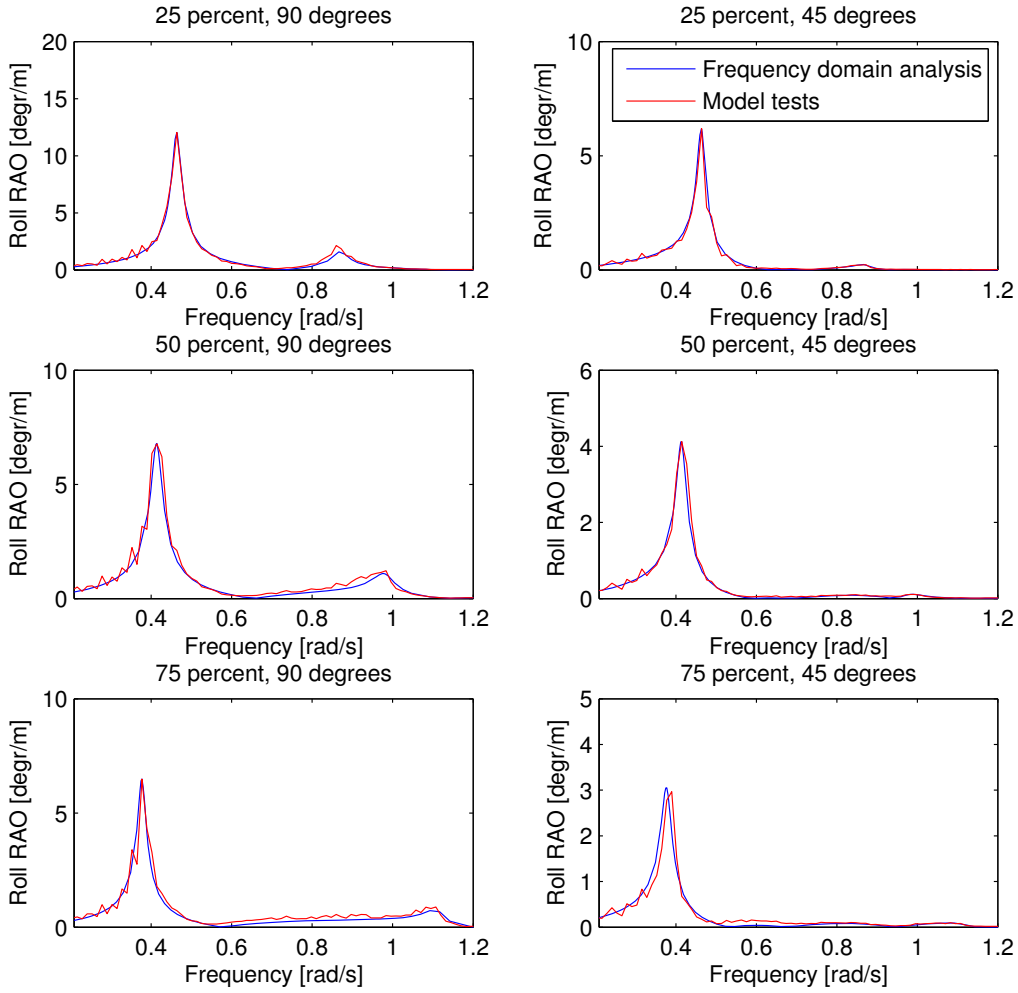

Figure 2: Model tests- and frequency domain analysis results for liquid cargo.

Figure 2 shows that the results obtained from the scale model tests and frequency domain approach match well. The location of the left peak is matched by correcting the roll radius of gyration. But also the width of the left peak and the overall response around the sloshing induced roll RAO peak matches very well and is not significantly influenced by the roll radius of gyration. Additionally, the pitch and heave RAOs obtained during the scale model tests were modelled accurately in the frequency domain without any correction.

Figure 3 shows the differences in roll response for the 50 percent loading condition when liquid or frozen cargo is considered. The results clearly show that frozen cargo results in a higher roll RAO peak around the barge natural frequency, and that this peaks occurs at a higher frequency. The shift in frequency was expected by the literature study performed, and was for example shown by Molin (2008) for membrane type tanks. Now it also shown that this occurs for spherical tanks. The results shows that sloshing of the cargo actually damps the roll motions of the barge around the barge natural frequency, rather than increasing it. The results also show that sloshing creates a lower barge natural frequency due to a loss of hydrostatic stability. This is beneficial as it brings the natural frequency further away from commonly experienced sea states. Obviously there is no sloshing induced roll RAO peak for the frozen cargo, as is the case with liquid cargo.

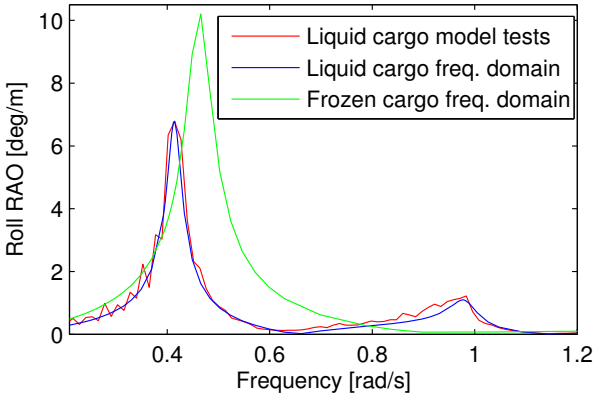

Figure 3: Frozen vs liquid cargo (50% loaded)

Figure 4 below shows how the roll RAOs are depending on the wave direction.

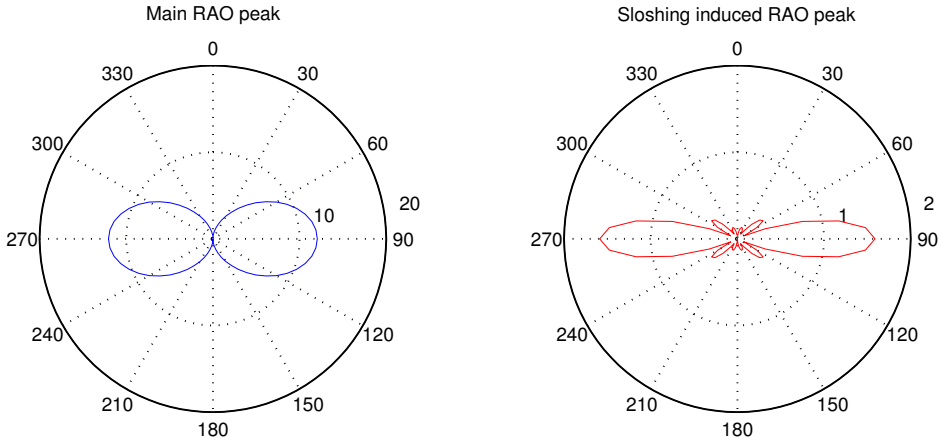

Figure 4: Influence of wave direction on the roll RAO peaks for the 25% loading condition.

It is known that the roll motion of a barge is very sensitive to the wave direction. But it was unknown how the sloshing induced roll RAO peak is influenced by the wave direction. The results indicate that the height of the sloshing induced roll RAO peak is even more influenced by the wave direction than the height of the main roll RAO peak. There are three main explanations for this. The first one is that for for 45 degree waves the barge may start to yaw. Because of yaw sloshing in one tank goes out of phase with the other tank, decreasing the sloshing induced roll. The second explanation is that for 45 degree incoming waves the roll and sway of the barge are smaller, and smaller sloshing loads are therefore expected. The third and final explanation is that for 45 degree waves the sloshing does not occur from starboard to port side, but also at an angle of 45 degrees creating a smaller moment around the x-axis.

Time domain results

Response Ampltitude Operators

In Figure 5 the results of the time domain approach are shown, including scale model test results. During the model tests the RAOs are determined by white noise tests. Because of computational time considerations the RAOs from the coupled model are mainly determined with regular waves.

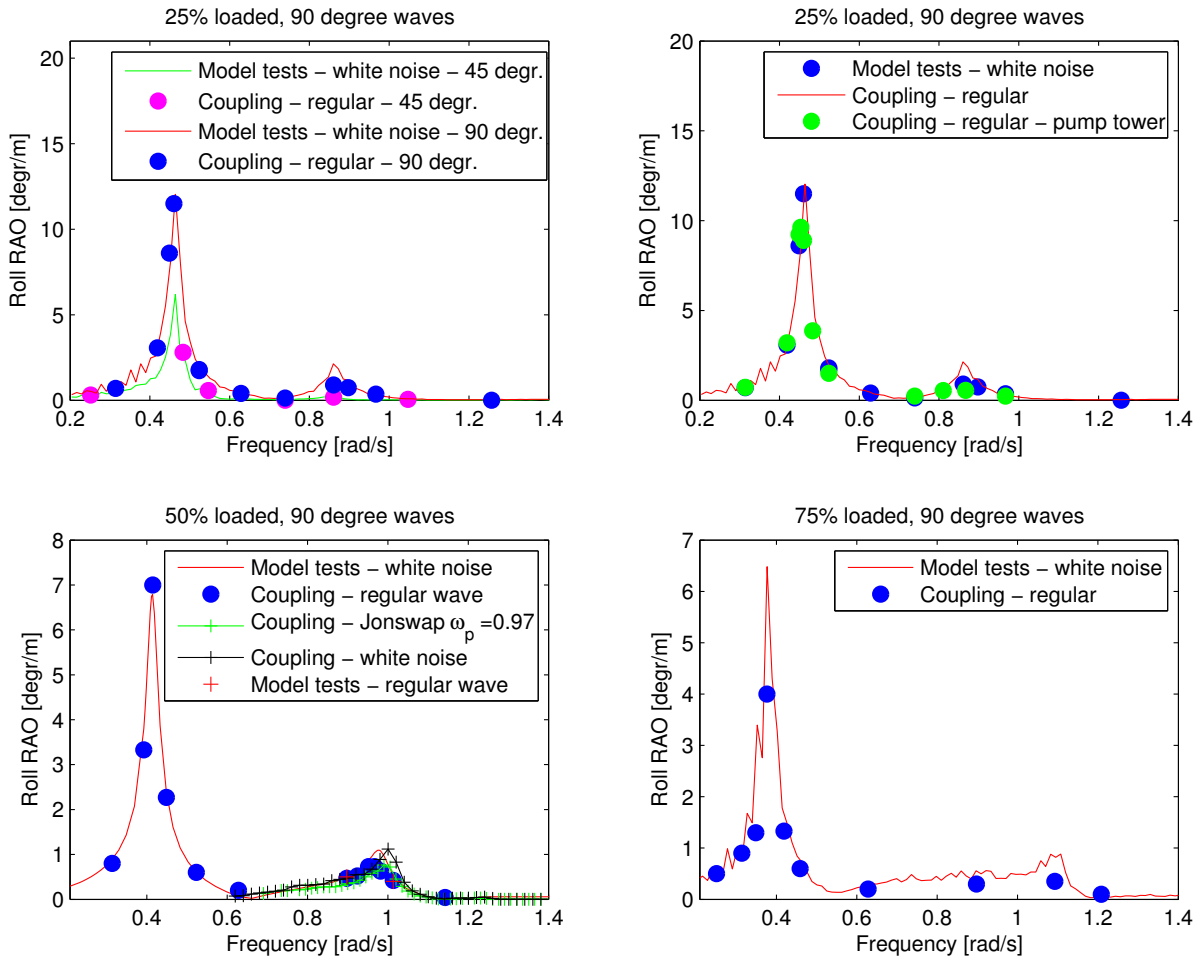

Figure 5: Results for a 3 meter (significant) wave height.

In general the results match well with the model test results. The response around the barge natural frequency is predicted correctly for the 25 and 50 percent loading condition. For the 75% loading condition the response is significantly underestimated. This may be partly because of the damping chosen based on the roll decay tests. The sloshing induced roll RAO peak is underestimated for all loading conditions. Two main explanations for this are identified. The first explanation is that there is too much damping created by the coupling between aNySIM and ComFLOW. This will be explained in more detail on page xv. The second explanation is that the response to a regular wave is different then what may be expected based on RAOs determined during a white noise test. This may be because during a white noise test different wave frequencies are transported into the tank. The RAOs however are determined from a cross spectral analysis between time, the motions of the barge and the waves. The motions of the barge however are influenced by the sloshing in the tank, in which frequencies from the past may still be present and are not taken into account in the cross spectral analysis. Therefore frequencies other than the frequencies on the x-axis may be present in the response. The RAOs from a

white noise test determined with the time domain model are also shown for the 50% loading condition and show a better match than the regular waves.

The results for the 25% loading condition are shown for 45 and 90 degree waves. It can be seen that the overall response for both wave directions is modelled correctly. For 45 degree incoming waves the peak around the barge natural frequency is smaller and the sloshing induced roll RAO peak has almost disappeared in both results. For the 25% loading condition also the effect of the pump tower is investigated. The results show that with a pump tower in the middle the barge natural frequency moves to a lower frequency and that in general the response is smaller. This makes sense as the pump tower adds damping to the system, creating a smaller response and lower natural frequency.

It is expected that there is some uncertainty in both the scale model test- and time domain results. The uncertainty from the scale model tests is introduced by the cross spectral analysis to obtain the RAOs. The RAOs determined from the time domain model contain uncertainties as the response of the barge was often irregular when exposed to regular waves. This is because the partially filled tanks introduce other frequencies into the response. It was found that for a regular wave three frequencies are present in the barge roll response: the wave frequency, barge natural frequency and first free surface mode natural frequency. Higher free surface modes should be present in the response, but their contribution is expected to be so low that it cannot be detected because of the noise in the data. The fact that multiple frequencies are present in the response is a clear indication of non-linearity. This is further investigated by looking into the RAOs for different wave heights.

For the 50% loading condition the non-linearity of the response is investigated. The barge is exposed to a regular wave with frequency $\omega = 097$ rad/s (close to the first mode natural frequency). This test was repeated for different wave heights. If the response would be linear then the obtained RAOs would be the same independent of the wave height. However, the RAOs decreases for an increase in wave height, see figure 6. This clearly shows how non-linear the response is due to the sloshing in the tanks.

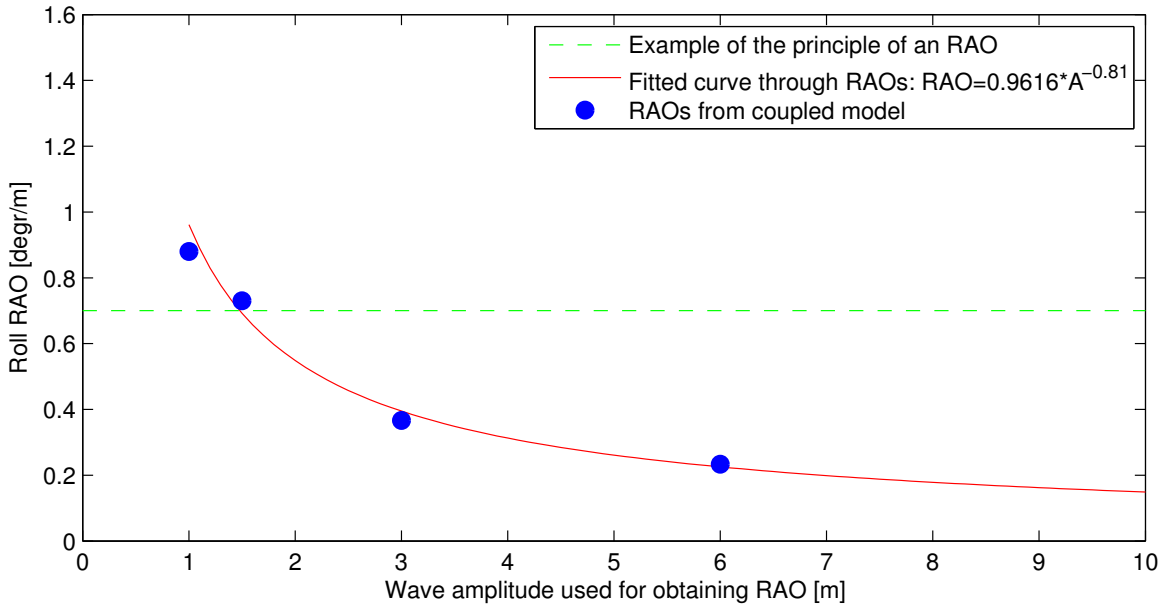

Figure 6: Roll RAOs obtained for 50% loading condition from different wave amplitudes.

Influence of the communication time step

In the coupled simulation aNySIM and ComFLOW communicate in intervals equal to the aNySIM time step. This was originally chosen to be 0.1 seconds which resulted in a stable simulation. In this section it is investigated in more detail how the communication time step influences the results. This was done by performing a roll decay test for the 50% loading condition. This was chosen because a roll decay test gives a lot of information about the damping and the natural frequency of the system, but also because the response is not chaotic and therefore results can be easily compared. The main results are shown in Figure 7. It was found that there were significant differences for communication steps of 0.1, 0.175 and 0.25 seconds. Two main explanations for this have been identified. The motions in between the aNySIM time steps, that are necessary for ComFLOW that uses smaller time steps than aNySIM, are linearly interpolated. This may increase some inaccuracies in the model as the motions do not show a linear time trace, but more a sine shape response. The second explanation may be related to the assumption that ComFLOW has a much smaller time step than aNySIM. This is however not always the case. When the ComFLOW time steps becomes almost as large as the aNySIM time step the difference between the aNySIM- and ComFLOW current time may become large when the sloshing loads are exchanged. The result of this is that aNySIM uses sloshing loads that may be smaller or larger than expected at the current aNySIM time.

To propose solutions for the observations three strategies have been investigated in more detail. The first one is third order interpolation of the motions. The second strategy is linear interpolation of the forces. The third and final strategy is a fixed and exactly the same time step for both ComFLOW and aNySIM. The last strategy ensures that both ComFLOW and aNySIM reach exactly the same time levels and interpolation is therefore not necessary. The results are shown in Figure 7 on the next page.

The results show that the simulation with a communication interval of 0.25 seconds and linear interpolation of the motions is not stable, which is clearly visible after 80 seconds. The results with linear interpolation, and a communication interval of 0.175 shows a stable response (in the time considered). For all other results presented in this summary a communication interval of 0.1 seconds has been considered. A communication interval of 0.1 seconds shows larger amplitudes than the results obtained with communication intervals of 0.175 and 0.25 seconds. This makes sense as with linear interpolation the estimated motions are underestimated for a sine shaped response. When the interval between known points increases the motions are expected to be estimated less accurately and more significantly underestimated.

The dark blue curve shows the results when third order cubic spline interpolation of the motions is used, still no interpolation of the forces, and a communication interval of 0.1 seconds (just as for the green line). The absolute amplitudes are larger compared to the results obtained with linear interpolation of the motions. This was expected as with linear interpolation the results are underestimated. With third order interpolation the estimated motions are expected to be larger and more accurate for a sine shaped response. When linear interpolation of the forces is also taken into account (red line) the results show a smaller amplitude than without linear interpolation of the forces.

The dotted black- and cyan coloured line represent results obtained with a simulation in which ComFLOW and aNySIM both use the same time step and exchange information at the same time levels. This strategy has been tested for a time step of 0.025 and 0.06 seconds. A time step of 0.06 seconds is often used by ComFLOW. However, depending on the flow velocities ComFLOW normally changes the time step based on the CFL condition. The implications of using a fixed time step is that ComFLOW cannot decrease the time step anymore to create a more stable simulation in case of high fluid velocities or increase the time step to decrease the calculation time. The results obtained with a synced simulation show a small phase difference of about 0.33% and a significantly larger absolute amplitude compared to the results found with a communication interval of 0.1 seconds. The differences between the amplitude found in the two synced simulations is expected to be partly caused by the smaller time step that is also used in ComFLOW. In case of a smaller ComFLOW time step the peaks in the sloshing loads may be better captured and could produce a larger response.

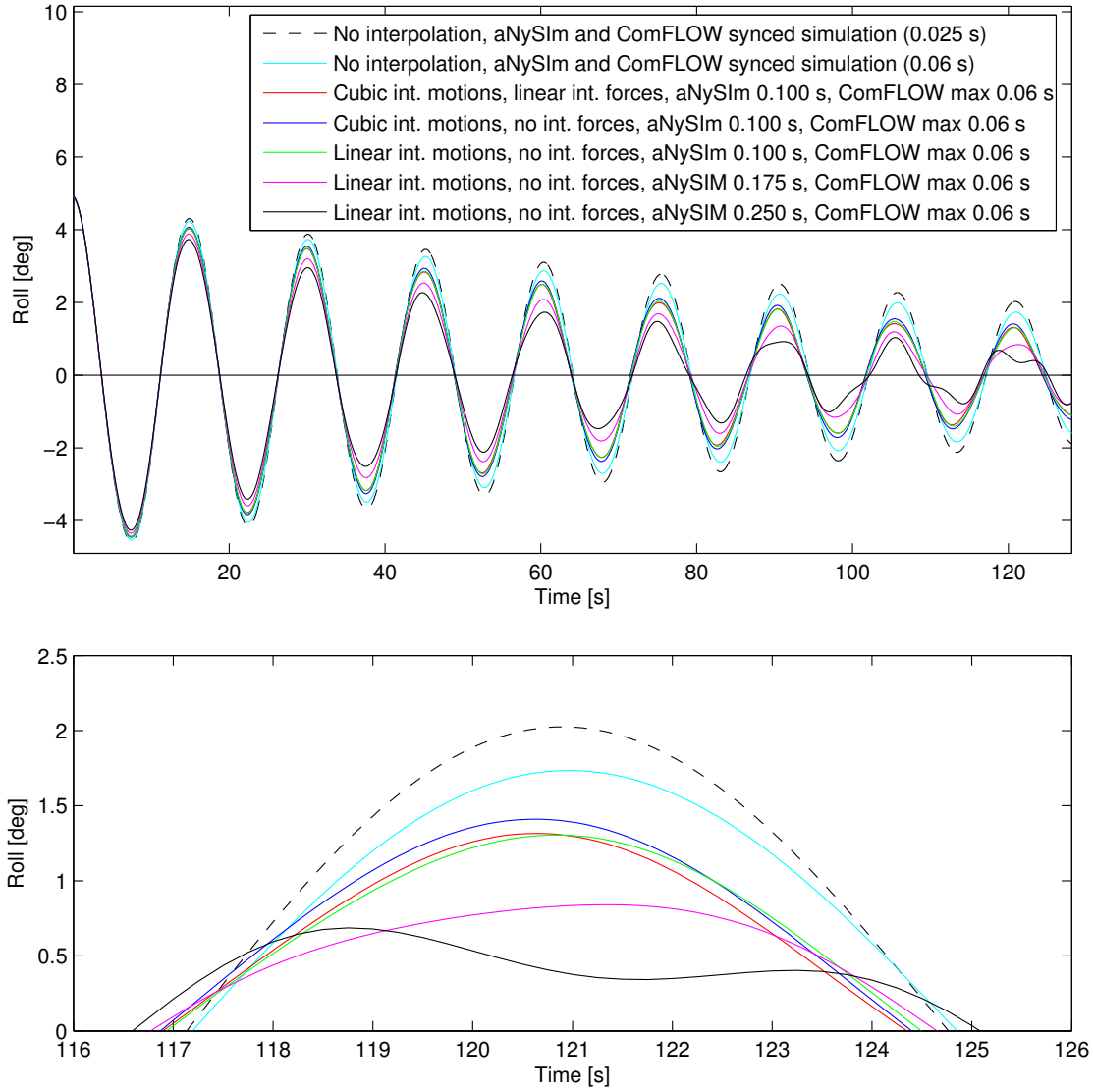

Figure 7: Roll decay test with different communication strategies for 50% loaded tanks

Conclusion

Experimental results obtained by Shell were used to validate both the frequency- and time domain model. In the frequency domain model both the response of the barge to waves and the sloshing in the tanks is modelled under linear assumptions. In the time domain model linear assumptions have been made for the response of the barge to waves, but the sloshing in the tank is modelled by the non-linear Euler equations.

The frequency domain model provides accurate results compared to the scale model tests (45 and 90 degree incoming waves) and is very fast; running the model only takes about one hour and is relatively easy to set up. However, linearity of the solution is assumed, while it was found that the response (especially around the natural sloshing frequency) is non-linear. This means that the agreement between the roll RAOs obtained from the frequency domain approach and the scale model tests strongly depend on the wave height used during the scale model tests. The effect of the tank size was investigated and it was shown that the effects due to sloshing (lower barge natural frequency, smaller roll RAO peak around the barge natural frequency and a larger sloshing induced roll RAO peak) becomes larger for

an increase in tank size. This is believed to be caused by an increase of the sloshing moments for a larger tank. The influence of sloshing was also investigated by comparing the vessel response for frozen and liquid cargo. It was shown that sloshing decreases the height of the main roll RAO peak and creates a lower barge natural frequency. Obviously no sloshing induced roll RAO peak was present in the response with frozen cargo. Variation of the wave direction signified the dependence of the sloshing induced roll RAO peaks on the wave direction.

The time domain model showed reasonable results compared to the roll RAOs obtained from the scale model tests. An overall trend in the results is that the sloshing induced roll RAO peak was underestimated in the time domain model. This could be due to uncertainties in the RAOs determined from the scale model test, but also due to uncertainties following from the modelling approach (for example type of wave tests used and the chosen grid). A white noise test was also performed in the time domain model and the resulting RAOs showed a better match compared to the scale model tests than the RAOs obtained from regular waves. It was also found that the pump tower adds damping to the system, decreasing the barge natural frequency and the overall roll response. The effect of the communication time step was also investigated. Additional strategies were developed to increase the effectiveness of the coupling, for example third order interpolation of the motions, first order interpolation of the forces and a simulation in which ComFLOW and aNySIM use exactly the same time step and therefore do not require any interpolation. The results were significantly different for the different communication time steps and interpolation schemes.

To conclude, both the frequency domain and time domain approach showed promising results and can both be used to investigate the effect of sloshing on ship motions. Both approaches have their advantages and disadvantages. The frequency domain approach is very accurate for the sea states considered in the model tests, fast, robust and easy to set up. But due to the linear assumptions the frequency domain approach should be used with caution outside the sea states that it is validated for. On the other hand, the time domain approach is very time consuming and more complex to set up, but also shows good results. More importantly, the time domain approach can be used to investigate the non-linear response of the vessel in more complex sea states and gives more insight into what is actually happening.

Recommendations

The main recommendations have been separated into two groups. The first group focuses on increasing the knowledge of the effects of sloshing in spherical tanks on ship motions and the different approaches to model this. The second group is more focused on other areas that the developed coupling between ComFLOW and aNySIM could also be used for.

It is recommended to gain more insight in the influence of the wave height and the type of wave spectrum on the response. To decrease the roll motions of the tank the use of baffles or anti roll tanks can be investigated. This could also be done by using the coupling. It is also recommended to investigate in more detail the numerical schemes used in the coupling, which is shown to have a significant influence on the results. An operability study, by considering an offloading scenario including fenders and mooring lines, is recommended to investigate the effect of sloshing on the uptime of an offloading operation. This would ideally be done by considering a more realistically shaped LNG carrier with 4 or 5 tanks on board. For this project mainly water was used as cargo, it would be of interest what the effect of LNG sloshing on the response is. The LNG is transported under pressure, which could be simulated by a two-phase simulation in ComFLOW and by using the coupling with aNySIM. The effect of sloshing on a sailing vessel could also be investigated. The coupling developed for this project could also be used to simulate green water effects and the interaction between flow in a riser and ship motions.

Contents

List of Figures

List of Tables

1

Introduction

1.1. Background information

Currently natural gas is transported by pipeline from the (offshore) wellhead to a (nearby) facility for treatment during which impurities in the natural gas may be removed. In case of a nearby market, the natural gas can then be transported by pipeline from the facility to its destination. In case of a market further away, transportation via pipeline is too expensive and the gas is liquefied for transportation by ship or truck. However, in case of an offshore reservoir the liquefaction facility might be located far away at an onshore location. This significantly increases the costs for transportation via pipeline, making the project economically less attractive. This problem is solved by Shell with a Floating Liquefied Natural Gas (FLNG) facility, located above or near the offshore field, see Figure 1.1 below.

Figure 1.1: Artist impression of FLNG in a side by side offloading situation (Shell, 2014)

With FLNG the natural gas is transported from the wellhead to the FLNG facility where it is purified and liquefied. After liquefaction the Liquefied Natural Gas is stored in the storage tanks of the FLNG until an LNG carrier (LNGC) arrives. The LNG carrier will berth alongside the FLNG, in which the

distance between the LNGC and FLNG is approximately 4 meters, the size of the fenders used to separate both vessel. After the LNG carrier is brought into position the LNG is transported from the FLNG to the LNG carrier via mechanical loading arms. During the offloading operations the tanks of the LNG carrier are gradually filled from empty to full. During this process the free surface area of the LNG in the tanks changes depending on the filling level and the type of tank used. Due to the free surface of the cargo and the waves exciting the LNG carrier, the cargo may slosh inside the cargo tanks possibly inducing additional vessel motions. Because the FLNG and LNG carrier are positioned so close to each other it is very important to understand the motions of the LNG carrier with partially filled tanks, which is the main focus of this project.

1.2. Problem definition

Before the concept of FLNG was introduced LNG was only produced in onshore facilities and preferably transported to the LNG carrier in areas where the LNG carrier is protected from waves and swell. In this situation sloshing in the internal tanks is not expected to be an issue, as sloshing of the cargo is initially induced by vessel motions created by waves and swell. This means that currently LNG carriers are only exposed to swell and waves in (near) ballasted or (almost) fully loaded conditions, when the LNG carrier is in transit. Both these conditions are not expected to create a significant effect of sloshing on ship motions. However, with FLNG the LNG carrier with partially filled tanks is relatively unprotected from the offshore environment and sloshing is likely to occur and therefore may have a significant effect on the ship motions.

LNG carriers are mainly built with two types of containment system; membrane and Moss type tanks. Membrane type tanks are mostly prismatic tanks that are not self supporting. Sloshing has always been considered a major challenge with membrane tanks because of its vertical walls that are vulnerable to wave slamming forces that may damage the tanks and/or create additional vessel motions. Because of this a lot of research has been performed on the effect of sloshing in prismatic tanks on ship motions, which is currently considered well understood. Moss type tanks are spherical self-supporting tanks that are structurally stronger than prismatic tanks. Due to the spherical shape slamming forces are not expected to occur. Damage to the tanks due to sloshing has therefore never been considered a major issue. It was however also assumed that sloshing in the partially filled spherical tanks would not have a significant impact on ship motions. Based on this was assumed that the ballasted loading condition would be the critical condition and that for increasing loading condition the ship motions would decrease. However, there was no evidence in the public domain to support this assumptions. Therefore one of the main goals of this project is to develop a model that can be used to gain more insight in the effect of sloshing on ship motions.

1.3. Literature review

This section is divided in two; the first part will discuss the literature identified for sloshing in spherical tanks while the second part is dedicated to sloshing in prismatic tanks.

1.3.1. Spherical tanks

There was no literature identified that focused on the effect of sloshing in spherical tanks on ship motions. Because there was no literature available Shell decided to initiate a joint experiment research program together with The Centre for Offshore Foundation (COFS) at The University of Western Australia (UWA) and the State Key Laboratory of Ocean Engineering (SKLOE) at Shanghai Jiao Tong University (SJTU). There was however literature available that investigates the natural sloshing frequencies of the liquid in partially filled spherical tanks. Both the literature review for obtaining the natural sloshing frequency, and the scale model test campaign will be discussed in the two next sections.

Natutal sloshing frequency of liquid in spherical tanks

The natural sloshing frequency of the liquid in the spherical tanks is of interest because violent sloshing motions are expected around that frequency. Budiansky (1958) performed numerical work to determine the natural frequencies of an almost full, half-full and near empty spherical tank. This research showed that the natural sloshing frequency is mainly dependent on the tank radius and a dimensionless parameter that was identified in the project. By using the dimensionless parameter Budiansky created a formula that could be used to estimate the first three natural sloshing frequencies for the considered filling condition and an arbitrary tank radius. McCarty and Stephens (1960) performed experimental research to obtain the first 4 natural sloshing frequencies of spherical tanks with diameters of 0.16, 0.33 and 0.67 meter. McCarty and Stephens (1960) used a similar relationship between the natural sloshing frequency and a dimensionless frequency parameter as Budiansky (1958). However, McCarty and Stephens (1960) investigated a wider range of filling conditions and showed that the first mode natural frequency increases monotonically with increasing filling level, while the higher modes show a minimum natural frequency around the 50% filling condition. Budiansky (1958) and McCarty and Stephens (1960) both showed that the natural sloshing frequency increases for higher free surface modes and decreases for a larger tank radius. Later performed research focused on sloshing in spherical tanks showed very similar results. For example, Mikishev and Dorozhkin (1981) performed experimental research to develop an empirical equation to calculate the first mode natural sloshing frequency for an arbitrary filling depth and tank radius. Rattayya (1965) also developed an empirical equation for the first mode natural sloshing frequency, but used a numerical approach. Additionally, Andrew and Alfred (1962) showed by experiments that the natural sloshing frequencies do not seem to be significantly depending on the fluid properties such as density and viscosity.

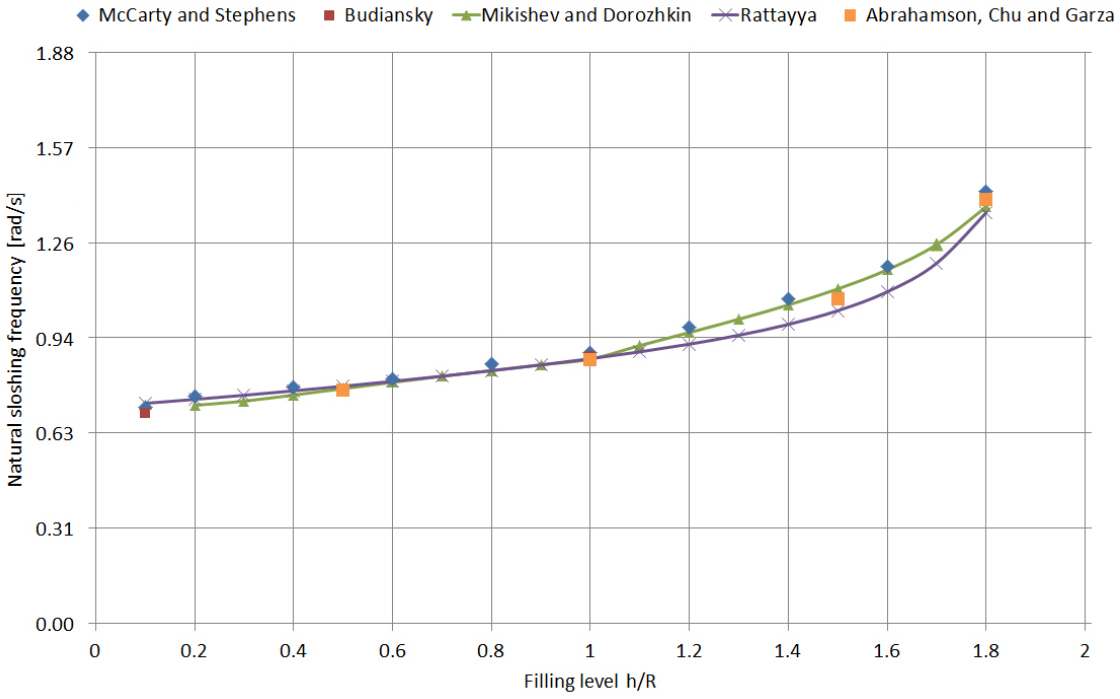

Figure 1.2: First mode natural sloshing frequencies for a spherical tank with $R = 19.25$ m

In Figure 1.2 an overview is given of the main findings of the literature review focused on the natural sloshing frequencies of partially filled spherical tanks. The comparison is made for a spherical tank with a radius of 19.25 meter, the same radius as used in the scale model tests performed by Shell. From the comparison can be clearly seen that the different sources show very similar results. Furthermore, an important conclusion from this part of the literature study is that the first mode natural sloshing frequency for a spherical tank with a realistic radius for LNG carriers is in the range of wind wave frequencies, which are likely to be encountered during an offloading operation.

Effect of sloshing in spherical tanks on ship motions

During the model test campaign that Shell initiated the motions of a scale model of a barge with two spherical tanks on board was investigated for different loading- and environmental conditions. The main goals of these scale model tests were to:

- Obtain key knowledge on the general motions of vessels with partially filled spherical tanks and to identify the governing loading condition, if there is only a single governing loading condition.
- Gain insight in what type of sloshing occurs in the spherical tanks for different loading conditions
- Obtain detailed information on quantities that are hard to predict without scale model tests, such as the viscous roll damping of the barge for the different loading conditions
- Obtain reliable model test results that can be used to validate the numerical models that are developed in this MSc- and possibly future project.

Barge particulars

The properties of the barge that was used in these scale model tests will also be used during the MSc project. Additionally, the results of the developed models will be validated by using the results of this model test campaign. Therefore the scale model test campaign and the main results found will be discussed in this section. The model tests have been performed on a 1:60 scale and a photograph of the barge during the scale model tests is given in Figure 1.3 below:

Figure 1.3: Picture of the barge during the model tests.

The full scale particulars of the barge are given in Table 1.1 below. The barge is equipped with bilge keels, one on each side. The bilge keel is designed to create hydrodynamic resistance so that the barge has a lower tendency to roll. It has a length and width of 15 and 0.8 meter respectively. The bilge itself has a radius of 5.5 meter. Two spherical tanks with a radius of 19.25 meter are placed on board and can be partially filled with fresh water. The size of the two spherical tanks is chosen so that the mass of the cargo in it is approximately equal to the mass transported by realistic Moss type LNG carriers. Moss carriers transport approximately 135.000 cubic meters of gas, of which the mass is approximately $W = V \cdot \rho = 135.000 * 435 = 58.73 \cdot 10^3$ tonne. The tank radius chosen for the model tests is 19.25 meters, which results in a mass of the fresh water cargo of $\frac{4}{3} \cdot \pi \cdot R^3 \cdot 2 \cdot 1000 = 59.76 \cdot 10^3$ tonne.

Designation	Unit	0%	25%	50%	75%	100%
After cargo loading						
Length betw. perpend.	m	200	200	200	200	200
Breadth	m	46	46	46	46	46
Depth	m	25.5	25.5	25.5	25.5	25.5
Draft	m	9.12	10.24	11.12	11.22	11.24
Displacement	m^3	81482.83	90859.18	99297.9	100235.53	100235.53
LCG from a.p.	m	100.0	100.0	100.0	100.0	100.0
VCG excl. free surface	m	12.71	15.50	14.00	15.90	20.00
Prior to cargo loading (for modelling barge without tanks)						
Roll radius of gyration	m	19.82	19.56	19.14	19.08	22.80
Pitch radius of gyration	m	69.28	69.76	68.80	68.80	68.44
Yaw radius of gyration	m	69.28	69.76	68.80	68.80	68.44
VCG excl. cargo	m	12.71	13.02	13.86	14.25	17.10
∇	m^3	81475.2	75816.0	69444.0	55728.0	40500.0

Table 1.1: Full scale barge particulars before and after cargo loading

Test conditions
During the model tests the following loading conditions were considered: 0%, 25% liquid cargo, 50% liquid cargo, 50% frozen cargo during which the natural frequency of the total system was matched by adding weights, 75% liquid cargo and 100% liquid cargo. The motions of the barge will be investigated for these loading by considering regular, white noise and decay tests. The goals for the different tests were to:

- Obtain the natural frequencies of the system and damping coefficients during decay tests for roll, heave and pitch
- Obtain the RAOs by exposing the barge to a white noise wave spectrum
- Validate the RAO's found from the white noise tests with regular wave test cases

For the white noise- and regular wave test cases bow (0°), bow-quartering (45°) and beam (90°) waves were considered. The barge is double symmetrically designed, so the results obtained for the first quadrant incoming wave direction can be extrapolated to the remaining three quadrants.

- Bow waves, 0°
- Bow quartering waves, 45°
- Beam waves, 90°

Results obtained during the tests

Next the main results found during the model tests campaign will be summarised. These results are focused on the roll motion of the barge during beam and bow quartering seas. For other degrees of freedom- and incoming wave directions the effect of sloshing is believed to be of less impact on the motions of the barge. Generally the roll motion is the largest for beam waves, also without sloshing involved. It was however uncertain how sloshing would influence the roll motion. The roll RAO's for beam waves are shown in figure 1.4 below.

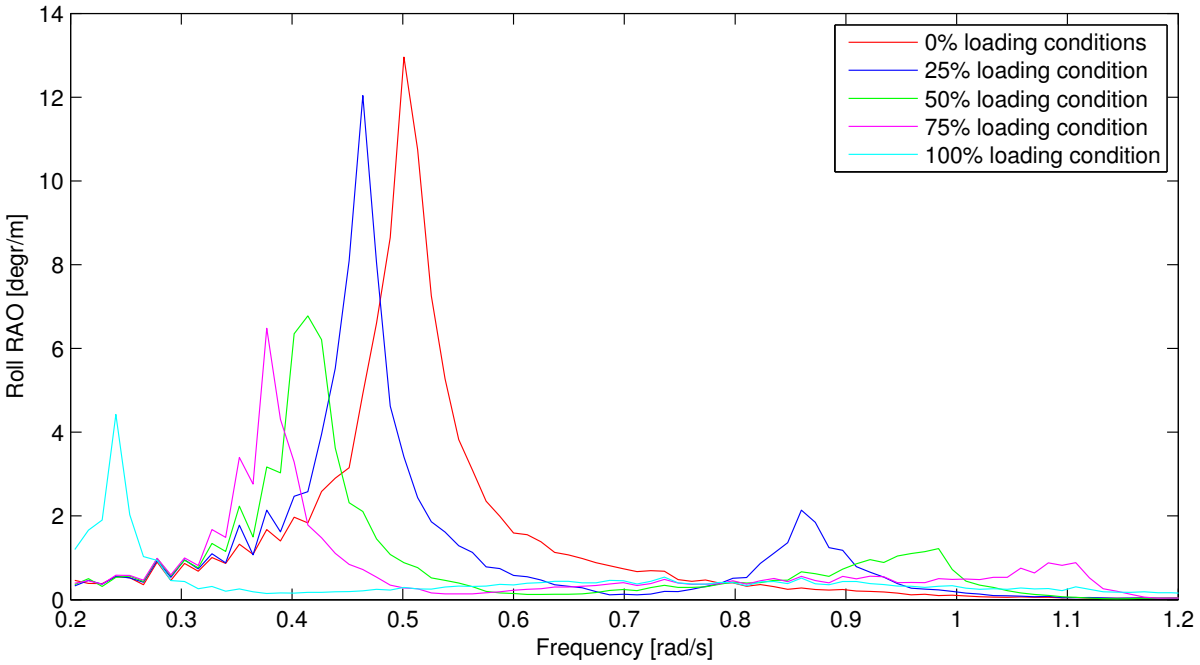

Figure 1.4: Model test results for the roll motions in beam waves

The presented results clearly indicate there is a significant effect of sloshing on ship motions. The following three main trends have been identified based on the results:

- Two local maxima in the roll response are observed for every partially loaded conditions. The left maxima is the natural frequency of the barge and tank system together. The right maxima is the sloshing induced peak, that does not exist for empty- or completely filled loading conditions.
- The left- and right local maxima both decrease with increasing filling condition. This indicates sloshing damps out the roll motion of the barge and that the ballasted loading condition results in the largest roll response.
- The frequency of the left local maxima moves to the left- and the frequency of the right local maxima moves to the right for increasing loading condition. The left local maxima moves to the left because for an increase in loading condition the total mass of the system increases, the centre of gravity of the cargo becomes higher and due to sloshing in the tanks (shown by Molin et al. (2010) for prismatic tanks). That the right local maxima moves to the right for increasing filling condition is because the natural sloshing frequency becomes larger for increasing filling ratios of the tank (McCarty and Stephens, 1960).

The bow-quartering wave cases showed one very clear trend; the sloshing induced roll RAO peak almost completely disappeared compared to the beam wave roll response. See Figure 1.5 for more details. This is believed to be caused by the sloshing motions in the two tanks that are now moving in anti-phase with each other, rather than in phase for the beam waves. Furthermore, as expected also the main peak has decreased for bow quartering waves.

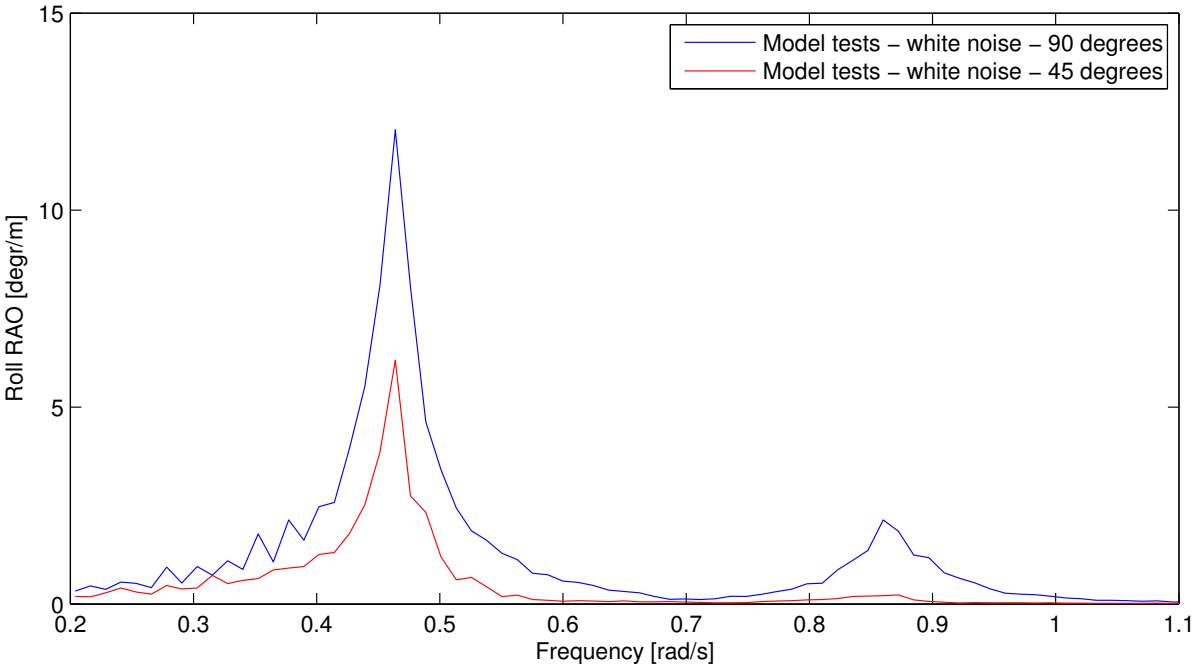

Figure 1.5: Roll motions in beam- and bow quartering waves for the 25% loading condition.

Conclusion
From the model tests key knowledge has been obtained on the influence of sloshing in partially filled spherical tanks on ship motions. Examples of this are the general motions (RAO's) of a barge with partially filled spherical tanks in waves, information on the damping from the roll decay tests and validation material for to-be-developed numerical models. The obvious next step is to develop the models and to compare them with the results obtained in the scale model tests.

Future work
From the obtained results can be concluded that sloshing in partially filled spherical tanks does have a significant influence on ship motions, especially roll. Now that the effect of the sloshing in the spherical tanks is better understood, the knowledge can be applied to more realistic vessel shapes with 4 or 5 spherical tanks on board or a wider range of environmental conditions. To start a scale model test campaign for every change in environmental conditions, hull shape or tank properties is very expensive. Therefore the most important step for future work at this moment is believed to be the development of a numerical model that can accurately describe the effect of sloshing in the spherical tanks on ship motions. With the to-be-developed numerical model it is the goal that a wide range of environmental- and loading conditions, but also a more complex offloading scenario can be simulated without having to perform additional model tests.

1.3.2. Prismatic tanks

The focus of the next paragraphs will be the effect of sloshing in prismatic tanks on ship motions. First a number of scale model tests will be discussed, followed by frequency- and time domain models that were used to simulate the effect of sloshing in partially filled prismatic tanks on ship motions. Bunnik and Huijsmans (2007) performed large scale (1:10) model tests on a section of a prismatic tank to obtain validation material for a 2-phase Volume of Fluid method (Wemmenhove et al., 2005). It was shown that due to the inertia of the cargo there was a large spreading in the peak pressure on the walls, while the tank was moved with a periodic motion. Also, mixing of air and water was shown for high- and low filling ratios. Molin et al. (2010) performed scale model tests to investigate the coupling between sloshing in a rectangular tank and ship motions. Tests were done with (1) a ceiling placed on top of the free surface to prevent sloshing and (2) with an open free surface so that sloshing could occur. The focus of the tests was on the roll motion of the ship, that is considered to be the degree of freedom that is most significantly influenced by sloshing. Molin et al. (2010) identified that there was only one roll RAO peak without free surface and two roll RAO peaks when sloshing in the tank could occur. The first RAO peak is at the natural frequency of the barge including tanks and the second RAO peak (not visible when the ceiling is on the free surface) is around the natural sloshing frequency of the cargo in the tanks. In case of sloshing the first peak is smaller than for without sloshing, this indicates that sloshing damps the motions of the vessel around the first roll RAO peak. Furthermore, due to a loss of hydrostatic stability the first roll RAO peak moves to a lower frequency when sloshing occurs. Molin et al. (2010) also identified that for an increasing wave height, mainly the second, but also the first roll RAO peak becomes smaller. This indicates that the sloshing inside the tank is non-linear which also creates non-linear ship motions. This is an important observation as linearity and non-linearity are important consideration in choosing a modelling approach.

In contradiction to Molin et al. (2010), Zhao et al. (2014) found during model tests that the roll RAO's in case of sloshing were larger than with a frozen cargo. Zhao et al. (2014) also found that even though higher free surface modes are excited, they do not necessarily have an effect on the ship motions. This may be because the higher sloshing modes do not contain enough energy to significantly influence the vessel motions. Claus et al. (2010) found, by performing scale model tests, that around the first RAO peak, where large roll amplitudes are observed, the ship is rotating around the cargo and that the free surface of the cargo stays relatively horizontal. Around the sloshing natural frequency, smaller roll motions are observed, but the liquid inside the tank sloshes violently. It was also found that sloshing had a significant influence on the pitch motions as well, but in this case a longitudinal tank was used, which is not representative for spherical tanks on board LNG carriers. Gaillarde et al. (2003) published the results of the SALT JIP in which the roll RAO's were investigated for different loading- and environmental conditions. Results showed that in some cases the roll RAO's are larger for partially filled tanks than for the ballasted condition, which is an interesting observation as was one of the assumptions for spherical tanks was that the ballasted condition is the most critical condition. It is expected that the first mode natural sloshing frequency is close to the natural frequency of the barge and tank together. However, no information on the natural sloshing frequencies of the cargo in the tanks were available.

Bunnik and Veldman (2010), Claus et al. (2010), Lee (2008) and Gaillarde et al. (2003) all developed frequency domain models to simulate the effect of sloshing in prismatic tanks on ship motions. These models are based on linear potential theory for both the ship motions and the sloshing inside the cargo tanks. The linear assumptions are expected to be valid for the ship motions, as offloading conditions are considered, that generally result in small ship motions. However, for the sloshing in the tank the linear assumption may not be valid. Molin et al. (2010) clearly showed that the sloshing in the tank may be non-linear, and that non-linear sloshing damps the response around the natural sloshing frequency. Therefore it is expected that the roll RAO is overestimated in the frequency domain approach compared to model tests, this however also depends on the wave height considered in the model tests. Bunnik and Veldman (2010) created a coupled ship-tank model in DIFFRAC, developed by MARIN, and used the model tests from Molin et al. (2010) to validate the model. It was found that the height and frequency of the first roll RAO peak were predicted correctly. The height and frequency of the second, sloshing induced, second roll RAO peak however, were not modelled correctly. The peak was overestimated, as expected, by about 20% and the frequency was underestimated by 5%. Lee (2008) presented a coupled

ship-tank model in WAMIT and compared this with the results found in the SALT JIP (2004). The results in the frequency domain did not show a good agreement with the model tests for different filling conditions. Gaillarde et al. (2003) compared a Diodore model with the SALT JIP results and found good results around the natural frequency of the ship-tank model, but the frequency and height of the sloshing induced roll RAO peak were not modelled correctly. Based on previously done research it is concluded that the frequency domain approach does not accurately describes the effect of sloshing in prismatic tanks on ship motions.

A completely different approach of solving the effect of sloshing in internal tanks on ship motions includes the use of mechanical analogies in the time domain. The principle behind it is that every free surface mode can be represented by an equivalent pendulum or mass-spring-damper system. Depending on the approach chosen, every free surface mode is represented by a certain frozen mass, moving mass, pendulum arm, spring stiffness and damping. Under linear assumptions these parameters have been identified in Ibrahim (2005) for rectangular and cylindrical tanks, and in Sumner (1965) for spherical tanks. However, for spherical tanks the focus was only on frequencies much lower than the natural frequencies of the different modes. A non-linear approach was developed by Bauer (1966e) for cylindrical tanks and by Miles (1984c) for spherical tanks. However, mechanical analogy models have not been validated for the effect of sloshing on ship motions. Bunnik and Veldman (2010) developed, next to a frequency domain model, also a time domain model to simulate the effect of sloshing in membrane type tanks on ship motions. The model consisted of a coupling between ship motion solver aNySIM and Volume of Fluid CFD solved ComFLOW. A very good agreement was found between model tests (Molin et al., 2010) and the results of the time domain, even for a relatively coarse grid in ComFLOW. Both roll RAO peaks were modelled with a high accuracy in terms of the frequency and height of the peaks. Bunnik and Veldman (2010) also showed that, because of the non-linear sloshing that can be simulated with ComFLOW, the sloshing induced roll RAO peak became smaller in amplitude with increasing wave height. However, because a CFD solver is part of the model, computation times are significant and depend very much on the grid used.

1.4. Research goal

Based on the literature review a fundamental understanding of the effect of sloshing in partially filled spherical tanks on ship motions has been identified as a gap. No information at all was identified that describes the above mentioned effect. The research goal of this thesis is therefore formulated as:

> To develop a coupled sloshing-ship motion model that is validated with scale model tests, to be used to simulate, and to gain a better understanding of, the effect of sloshing in partially filled spherical tanks on ship motions under operational conditions.

1.5. Solution strategy evaluation

During the literature review several solution strategies have been identified and evaluated. However, because no previous research was identified on the effect of sloshing in spherical tanks on ship motions, the focus of the literature study review has been on sloshing in membrane type tanks. Based on this four solution strategies were identified, with decreasing confidence in an accurate solution: model tests, time domain coupling between a ship motions solver and a CFD solver, a frequency domain approach and mechanical analogies. All these potential solution strategies are discussed in this section.

Model tests are believed to be the most accurate and reliable solution strategy available. However, model tests data for a ship with partially filled spherical tanks are not available. Therefore Shell has decided to perform scale model tests in the summer of 2014. These model tests consisted of a barge with two spherical tanks on board that were filled with fresh water. A range of loading- and environmental conditions were considered in the model tests to obtain the behavior of the barge with partially filled spherical tanks in waves. These tests were also used to obtain critical information (for example roll damping of the barge) that is not straight forward to calculate, but also to obtain validation material for any to-be-developed numerical models. The information obtained in these model tests can be used in this MSc project and therefore additional model tests are not required.

A coupling between a ship motion- and CFD solver has shown to be an accurate tool to simulate the effects of non-linear sloshing in membrane tanks on ship motions. As it is expected that sloshing in spherical tanks will be less violent than in membrane tanks, it is believed that the ship motion- and CFD solver coupled model will also provide accurate results for spherical tanks. As there are no known models that can simulate the effect of sloshing in partially filled spherical tanks on ship motions and this is believed to be the most accurate solution strategy, this method is chosen as main strategy in this MSc project. Additionally, the model tests performed by Shell can be used to validate the numerical model. After validation the model can be used to gain insight in situations (different environment, hull, tank or fluid properties) that have not been covered during the model tests.

During the literature review the frequency domain approach has not shown very accurate results for membrane type tanks. Although sloshing is expected to be less violent in spherical tanks than in membrane type tanks, and therefore produce more accurate results in the frequency domain, it was initially decided not to develop a frequency domain model during this project. However, WAMIT was used to obtain the frequency dependent input for the time domain model of the barge without tanks. During the development of the frequency dependent input it was found that it would be less complicated to include the internal tanks in the frequency domain analysis. Therefore, as an addition, the frequency domain approach was also included in this project.

The mechanical analogies for simulating sloshing have not been thoroughly tested for the effect of sloshing on ship motions. Furthermore, many assumptions are made that decrease the confidence in this approach. Therefore the use of mechanical analogies has not been identified as a valuable solution strategy in this stage of the project with so many unknowns about the actual bahaviour of a ship in waves with partially filled spherical tanks.

To conclude the solution strategy evaluation; during this project a frequency- and time domain model will be developed. For the frequency domain model WAMIT is used and for the time domain model a coupling between aNySIM and ComFLOW will be developed. Results from both the frequency- and time domain model can be validated with the model tests performed by Shell in August 2014. This strategy will finally yield a very complete comparison between model test-, time domain- and frequency domain results. It is expected that from this clear conclusions and recommendations can be drawn, and that significant academic steps have been taken in the field of sloshing in spherical tanks and its influence on ship motions. Furthermore, it will enable Shell to make an educated decision on which modelling approach to take for different purposes, for example statistics or the analysis of complex offloading scenarios in which non-linear sloshing, fender behaviour and mooring lines are included.

1.6. Objectives

As discussed in Section 1.4 the goal for this MSc project is to develop a coupled sloshing- ship motion model that is validated with scale model tests and can be used to simulate, and to gain a better understanding of, the effect of non-linear sloshing in partially filled spherical tanks on ship motions under operational conditions. To reach this goal a number of objectives are defined.

For setting up the frequency domain model the following objectives were set:

- Create panel model of the spherical tanks
- Set up coupled frequency domain model for hull and internal tanks

The objectives for development and validation of the coupled aNySIM - ComFLOW model are:

- Create a panel model of the barge
- Create a WAMIT model without internal tanks and obtain hydrodynamic database
- Set up and validate model of the barge including mooring system in aNySIM
- Set up and validate a model of two spherical tanks in ComFLOW to simulate sloshing
- Develop a coupling between aNySIM and ComFLOW

After the above objectives are completed, the following final objectives can be met:

- Validate coupled frequency domain model with scale model test results
- Validate coupled aNySIM - ComFLOW time domain model with the scale model test results
- Analysis and interpretation of data
- Depending on the time left after meeting all the objectives above, new situations may be investigated. For example, LNG as cargo rather than water, new environmental conditions or a different number of spherical tanks on board
- Brainstorming about- and writing of conclusions and recommendations
- Delivering a final report and summary to the graduation committee

1.7. Coordinate systems

The main coordinate system used in this report is the body fixed reference frame. It has its origin in the centre of gravity of the vessel, the positive x-axis is in the direction of the bow, the positive y-axis is in the direction of port side and the positive z-axis is upward. This is visualised in Figure 1.6 below.

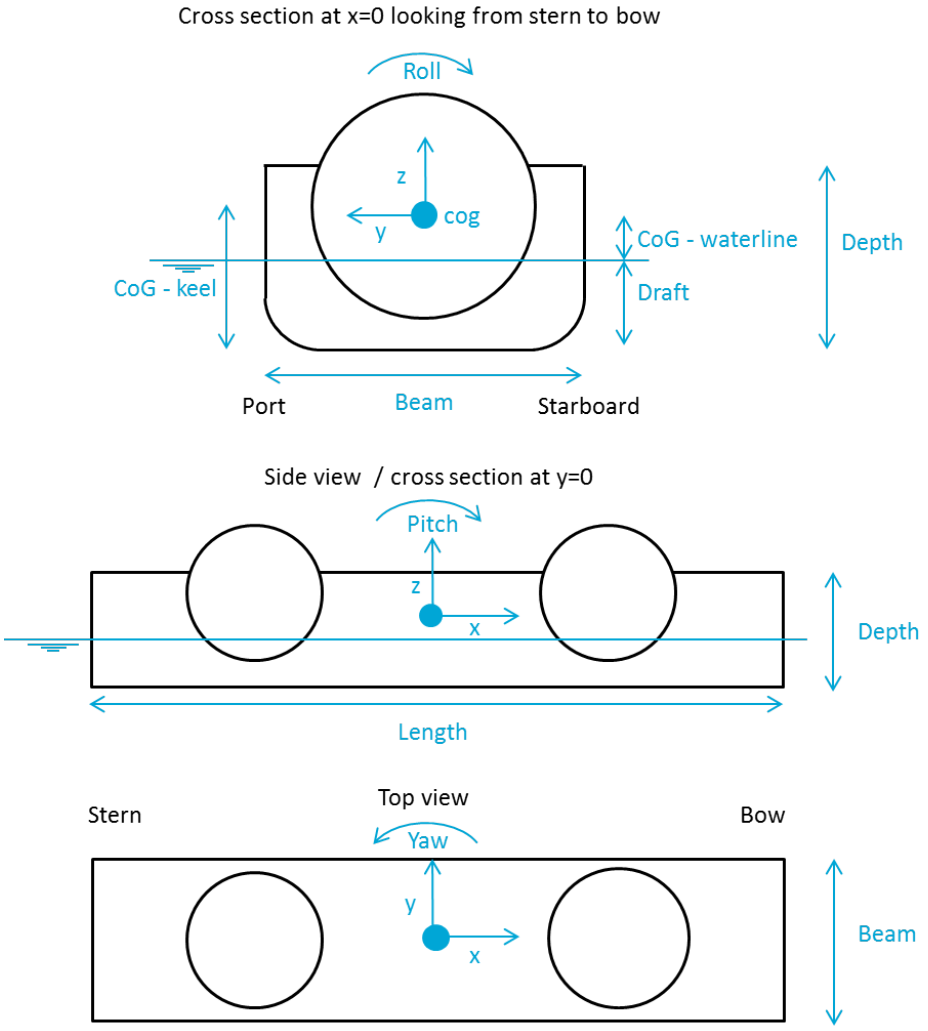

Figure 1.6: Body fixed coordinate system and barge particulars

Only the fixed ends of the mooring lines are defined in the earth fixed coordinate system. The earth fixed coordinate system has its origin in the waterline and below the centre of gravity (at t=0). The earth fixed coordinate frame follows the same conventions as the body fixed reference frame. The angle of wave direction is taken to be zero at the stern and follows the same positive direction as yaw. Additionally, the wave frequency is given in rad/s.

The six degrees of freedom of the barge and their most relevant notations are given in Table 1.2.

DoF	Description	Positions	Velocities	Forces and moments
1	motion in x-direction (surge)	x [m]	u [m s^{-1}]	F_x [kN]
2	motion in y-direction (sway)	y [m]	v [m s^{-1}]	F_y [kN]
3	motion in z-direction (heave)	z [m]	w [m s^{-1}]	F_z [kN]
4	rotation around x-axis (roll)	ϕ [rad]	p [rad s^{-1}]	M_x [kN m]
5	rotation around y-axis (pitch)	θ [rad]	q [rad s^{-1}]	M_y [kN m]
6	rotation around z-axis (yaw)	ψ [rad]	r [rad s^{-1}]	M_z [kN m]

Table 1.2: Degrees of freedom and notations used

1.8. Thesis outline

This thesis report is organised as follows. Chapter 1 is an introduction to the project in which the context, goals and objectives are discussed.

Chapter 2 contains a description of the frequency domain model in which sloshing in the internal tanks is included. In Chapter 3 the ComFLOW model of the spherical tanks is described. Chapter 4 contains the description of the aNySIM ship motions model. Chapter 5 describes the coupling between aNySIM and ComFLOW. In chapter 6 the results obtained with both the frequency- and time domain model are discussed and validated with the scale model test results.

Finally, in chapter 7 conclusions following from this project are discussed and recommendations for future research are presented.

2

Coupling in the frequency domain

2.1. Introduction

In this section the development of the frequency domain model is discussed for the ballasted- and partially loaded tanks. For this the software package WAMIT is used. The main assumption in this approach is linearity (see Section B), while it is already known from model tests that the sloshing in the spherical tanks may become non-linear for some loading- and environmental conditions. However, it is expected that non-linear sloshing in the tank will decrease the motions of the vessel. As of such the frequency domain model may overestimate the vessel motions for increasing wave heights.

First the equation of motion are discussed in Section 2.2, followed by the approach for the ballasted loading condition in Section 2.3, the approach for the partially loading conditions with liquid cargo in Section 2.4 and with frozen cargo in Section 2.5. In Section 6.1 the results of all developed frequency domain models are discussed and compared with the scale model test results.

2.2. Equation of motion

This section discusses the equation of motion for both the barge alone, and for the coupled barge-tank model. Furthermore, it is described how the forces and RAOs of the coupled model are obtained in the frequency domain approach.

2.2.1. Barge only

Without internal tanks the equation of motion solved in WAMIT for the barge only is given by:

$$\boldsymbol{M}_b \ddot{\boldsymbol{x}}_b(t) = \sum \boldsymbol{F}_b(t) \tag{2.1}$$

Where the subscript b is used to identify the barge. Furthermore, $\boldsymbol{M}$ is the 6×6 mass matrix, $\ddot{\boldsymbol{x}}(t)$ is the 6×1 acceleration matrix and $\boldsymbol{F}_t(t)$ is the 6×1 matrix of forces acting on the barge. In more detail these are given by:

$$\boldsymbol{F}_b(t) = \begin{bmatrix} F_1(t) \\ F_2(t) \\ F_3(t) \\ F_4(t) \\ F_5(t) \\ F_6(t) \end{bmatrix} \qquad \ddot{\boldsymbol{x}}_b(t) = \begin{bmatrix} \ddot{x}_1(t) \\ \ddot{x}_2(t) \\ \ddot{x}_3(t) \\ \ddot{x}_4(t) \\ \ddot{x}_5(t) \\ \ddot{x}_6(t) \end{bmatrix} \tag{2.2}$$

And the mass matrix is given by (Fossen, 1994):

$$\boldsymbol{M}_b = \begin{bmatrix} m & 0 & 0 & 0 & m \cdot z_g & -m \cdot y_g \\ 0 & m & 0 & -m \cdot z_g & 0 & m \cdot x_g \\ 0 & 0 & m & 0 & -m \cdot x_g & 0 \\ 0 & -m \cdot z_{cm} & m \cdot y_g & I_{44} & -I_{45} & -I_{46} \\ m \cdot z_g & 0 & -m \cdot x_g & -I_{54} & I_{55} & -I_{56} \\ -m \cdot y_g & m \cdot x_g & 0 & -I_{64} & -I_{65} & I_{66} \end{bmatrix} \tag{2.3}$$

Where x_g, y_g and z_g are the coordinates of the centre of gravity with respect to the origin of the body fixed reference frame. However, for this project a double symmetrical barge (symmetrical around $x = 0$ and $y = 0$ with the origin in the centre of gravity of the barge) is considered. Because of this $x_g = y_g = z_g = 0$ and all cross inertia terms are also zero, reducing the mass matrix for the barge without internal tanks to:

$$\boldsymbol{M_b} = \begin{bmatrix} m_{11} & 0 & 0 & 0 & 0 & 0 \\ 0 & m_{22} & 0 & 0 & 0 & 0 \\ 0 & 0 & m_{33} & 0 & 0 & 0 \\ 0 & 0 & 0 & I_{44} & 0 & 0 \\ 0 & 0 & 0 & 0 & I_{55} & 0 \\ 0 & 0 & 0 & 0 & 0 & I_{66} \end{bmatrix} \tag{2.4}$$

The total forces from Equation 2.2 can be written as:

$$\boldsymbol{F}_b(t) = \boldsymbol{F}_w(t) + \boldsymbol{F}_h(t) \tag{2.5}$$

Where $\boldsymbol{F}_w(t)$ is wave force on the barge (see Equation B.98). $\boldsymbol{F}_h(t)$ is the hydromechanic reaction load from the oscillating barge in still water which consists of a static and dynamic term:

$$\boldsymbol{F}_b(t) = \boldsymbol{F}_w(t) + \boldsymbol{F}_{h,stat}(t) + \boldsymbol{F}_{h,dyn}(t) \tag{2.6}$$

The static term $\boldsymbol{F}_{h,stat}(t)$ is equal to the 6×6 restoring coefficient matrix $\boldsymbol{C}_b$ that is in phase with the displacement of the barge and caused by a change in buoyancy. The dynamic term consists of two parts:

1. The 6×6 added mass matrix $\boldsymbol{A}_b$, that is in phase with the acceleration
2. The 6×6 potential damping matrix $\boldsymbol{B}_b$ that is in phase with the velocity

So that the total force on the barge can be written as:

$$\begin{aligned} \boldsymbol{F}(t) &= \boldsymbol{F}_w(t) + \boldsymbol{F}_h(t) && (2.7) \\ &= \boldsymbol{F}_w(t) + \boldsymbol{F}_{h,stat}(t) + \boldsymbol{F}_{h,dyn}(t) && (2.8) \\ &= \boldsymbol{F}_w(t) - \boldsymbol{C}_b\boldsymbol{x}(t) - \boldsymbol{A}_b\ddot{\boldsymbol{x}}(t) - \boldsymbol{B}_b\dot{\boldsymbol{x}}(t) && (2.9) \end{aligned}$$

By substitution of Equation 2.9 in Equation 2.1 the equation of motion can be written in a new form:

$$[\boldsymbol{M}_b + \boldsymbol{A}_b]]\,\ddot{\boldsymbol{x}}(t) + \boldsymbol{B}_b\dot{\boldsymbol{x}}(t) + \boldsymbol{C}_b\boldsymbol{x}(t) = \boldsymbol{F}_w(t) \tag{2.10}$$

2.2.2. Forces excited by the internal tanks

The equation of motion for the internal tanks is derived in the same manner as was done for only the barge in Section 2.2.1. However, for the internal tanks there are no exciting wave forces. There is also no potential damping as there is no diffraction of waves away from the internal tanks. In other words, when the tank is moved, waves are generated, but they stay inside the tank and do not go to the outside

of the tank. This means all the energy is contained in the tanks (as viscous damping is not considered with potential flow). The equation of motion for the tank (subscript t) is therefore given by:

$$\boldsymbol{F}_t(t) = \boldsymbol{A}_t\ddot{\boldsymbol{x}}(t) + \boldsymbol{C}_t\boldsymbol{x}(t) \tag{2.11}$$

Here the mass of the liquid in the internal tanks is included in the added mass of the cargo $\boldsymbol{A}_t$, which is calculated from the pressures on the wall of the internal tank.

2.2.3. Coupled equation of motion

The equation of motion of the coupled barge - tank model is derived by adding the forces due to sloshing in the tanks (Equation 2.11) to the equation of motion of the barge (Equation 2.10):

$$(\boldsymbol{M}_b + \boldsymbol{A}_b)\cdot\ddot{\boldsymbol{x}}(t) + \boldsymbol{B}_b\cdot\dot{\boldsymbol{x}}(t) + \boldsymbol{C}_b\cdot\boldsymbol{x}(t) = \boldsymbol{F}_w(t) + \boldsymbol{F}_t(t) \tag{2.12}$$

$$(\boldsymbol{M}_b + \boldsymbol{A}_b - \boldsymbol{A}_t)\cdot\ddot{\boldsymbol{x}}(t) + \boldsymbol{B}_b\cdot\dot{\boldsymbol{x}}(t) + (\boldsymbol{C}_b - \boldsymbol{C}_t)\cdot\boldsymbol{x}(t) = \boldsymbol{F}_w(t) \tag{2.13}$$

Now the equation of motion in the time domain is found. The time domain solution is converted to the frequency domain solution by considering:

$$\boldsymbol{x}(t) = \Re\left[\hat{\boldsymbol{\zeta}}\cdot e^{i\omega t}\right] \tag{2.14}$$

$$\boldsymbol{F}_w(t) = \Re\left[\hat{\boldsymbol{F}}\cdot e^{i\omega t}\right] \tag{2.15}$$

Where $\hat{\boldsymbol{\zeta}}$ and $\hat{\boldsymbol{F}}$ are the complex motion- and force amplitudes respectively. The coupled equation of motion in the frequency domain is obtained by first taking the necessary derivatives of Equation 2.14 and 2.15, and substituting those in Equation 2.13. The next step is to collect all real parts for both sides of the equation. By using $\Re[a] = \Re[b]$ and dividing the results by $e^{i\omega t}$ the coupled equation of motion in the frequency domain is found:

$$\left[-\omega^2(\boldsymbol{M}_b + \boldsymbol{A}_b - \boldsymbol{A}_t) + i\omega\boldsymbol{B}_b + (\boldsymbol{C}_b - \boldsymbol{C}_t)\right]\hat{\boldsymbol{\zeta}} = \hat{\boldsymbol{F}}(\omega) \tag{2.16}$$

WAMIT also offers the possibility to include an external damping ($\boldsymbol{B}_{ext}$)- or restoring coefficient ($\boldsymbol{C}_{ext}$) matrix. This can be used to add additional damping and/or springs forces to the equation of motion:

$$\left[-\omega^2(\boldsymbol{M}_b + \boldsymbol{A}_b - \boldsymbol{A}_t) + i\omega(\boldsymbol{B}_b + \boldsymbol{B}_{ext}) + (\boldsymbol{C}_b - \boldsymbol{C}_t + \boldsymbol{C}_{ext})\right]\hat{\boldsymbol{\zeta}} = \hat{\boldsymbol{F}}(\omega) \tag{2.17}$$

Finally, by taking into consideration that $\boldsymbol{A}_b$ and $\boldsymbol{A}_t$ are frequency dependent, the final equation of motion in the frequency domain that is used WAMIT is obtained:

$$\left[-\omega^2\left(\boldsymbol{M}_b + \boldsymbol{A}_b(\omega) - \boldsymbol{A}_t(\omega)\right) + i\omega(\boldsymbol{B}_b(\omega) + \boldsymbol{B}_{ext}) + (\boldsymbol{C}_b - \boldsymbol{C}_t + \boldsymbol{C}_{ext})\right]\hat{\boldsymbol{\zeta}} = \hat{\boldsymbol{F}}(\omega) \tag{2.18}$$

2.2.4. Exciting forces

The complex wave force amptitudes $\hat{\boldsymbol{F}}$ in the WAMIT analysis are calculated by direct integration of the hydrodynamic pressures. See Section B.2.4 for more details- and the derivation of the equations below.

$$\hat{\boldsymbol{F}} = -\iint_S (p\cdot\boldsymbol{n})\cdot dS \tag{2.19}$$

Where the pressures p are obtained from the linearised Bernoulli equation:

$$p = p_s + p_d = -\rho g z - \rho\frac{\partial\Phi}{\partial t} = -\rho g z - \rho\left(\frac{\partial\Phi_w}{\partial t} + \frac{\partial\Phi_d}{\partial t} + \frac{\partial\Phi_r}{\partial t}\right) \tag{2.20}$$

$$= -\rho g z + i\rho\omega e^{-i\omega t}\left(\phi_w + \phi_d + \sum_{j=1}^{6}\phi_j\right) \tag{2.21}$$

In which ρ is the density, z the water depth, ϕ_w the incoming wave potential, ϕ_d the diffraction potential and ϕ_r the radiation potentials. Because of linearity the radiation potentials can be included separately for all 6 degrees of freedom. See Section B.2 for more details.

2.2.5. Added mass and damping coefficients

The frequency dependent (coupled) added mass- and damping coefficients are related to the radiation potential. In case there are no waves, and therefore no incoming wave- or diffraction potentials, the vessel still creates waves that are removing energy from the system (potential damping) and it experiences an inertial force (added mass). In the frequency domain approach viscous damping is not taking into account. However, additional linear damping can be added to the system to account for the non-linear roll damping as much as possible, see Equation 2.18 for more details. The frequency dependent added mass and damping in WAMIT are ultimately solved by:

$$A_{ij} = -\Re\left[\rho \iint_S n_i \phi_j \, dS\right] \tag{2.22}$$

$$B_{ij} = -\Im\left[\rho\omega \iint_S n_i \phi_j \, dS\right] \tag{2.23}$$

Where S is the wetted surface of the barge, n_i is the normal vector and ϕ_j is the radiation potential caused by a motion in the j-th degree of freedom.

2.2.6. Restoring coefficients

The restoring coefficients are calculated by considering the displaced seawater due to a motion of the vessel in a certain degree of freedom. For example, the restoring force in heave due to a heave motions is calculated by multiplying the density and gravity with the z-component of the displaced volume:

$$C(3,3) = \rho g \iint_S n_3 \, dS \tag{2.24}$$

The equations to determine all restoring forces are given in Section B.2.5.

2.2.7. Response Amplitude Operators

The RAOs are obtained by taking the modulus of the complex motion $\hat{\zeta}_j$:

$$RAO_j = |\hat{\zeta}_j| \tag{2.25}$$

The modulus of an imaginary number z=$a + bi$ is given by:

$$|z| = \sqrt{a^2 + b^2} \tag{2.26}$$

2.3. Ballasted condition

This section describes the frequency domain approach for the ballasted condition (no cargo in the tanks). Therefore the internal tanks are not taken into account. This will be the base case which, if validated successfully, can be extended to include internal tanks. The motions of the barge for the ballasted condition are analysed in the frequency domain by considering the steps shown in Figure 2.1 below.

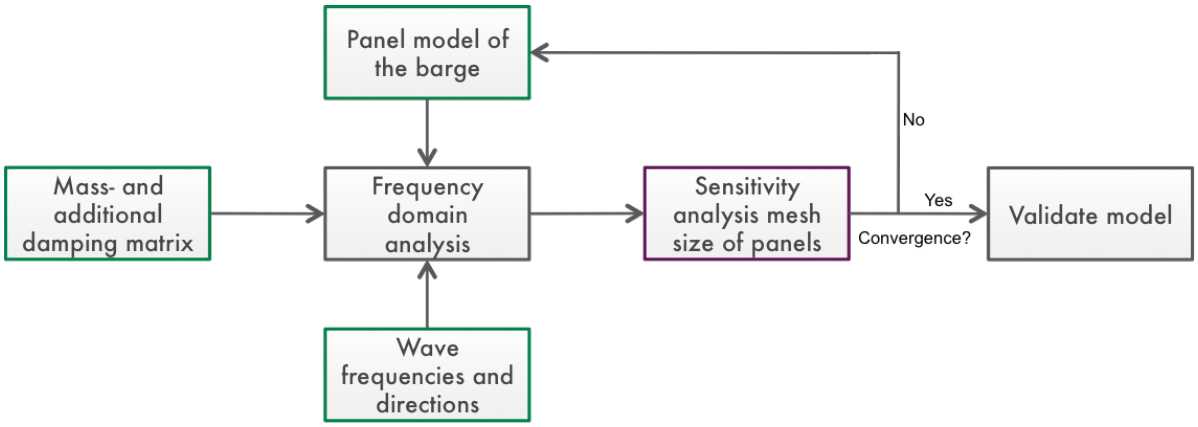

Figure 2.1: Steps for the ballasted case.

The green blocks are input for the frequency domain analysis, that is done in WAMIT. After running the simulation a sensitivity analysis (purple block) of the panel model mesh size is performed. Both the input and sensitivity analysis are described in the sections below. The validation of the model is given separately in Section 6.1.1.

2.3.1. Mass, damping and environment

The mass matrix used is based on the mass matrix defined in Section 2.2.1. For the ballasted condition the components of the mass matrix are calculated by considering a mass m=81472.2 tonnes, roll radius of gyration k_{xx}=19.92 meter and pitch- and yaw radii of gyration $k_{yy} = k_{zz} = 69.28$ meter. More details on the particulars of the barge can be found in Table 2.1. The roll, pitch and yaw inertia can now be calculated by multiplying the mass of the barge with its respective roll radius of gyration squared. This gives the following mass matrix in tonnes for the mass and tonnes$\cdot m^2$ for the inertia:

$$\boldsymbol{M_{ballasted}} = \begin{bmatrix} 8.15\text{E}4 & 0 & 0 & 0 & 0 & 0 \\ 0 & 8.15\text{E}4 & 0 & 0 & 0 & 0 \\ 0 & 0 & 8.15\text{E}4 & 0 & 0 & 0 \\ 0 & 0 & 0 & 3.23\text{E}10 & 0 & 0 \\ 0 & 0 & 0 & 0 & 3.91\text{E}11 & 0 \\ 0 & 0 & 0 & 0 & 0 & 3.91\text{E}11 \end{bmatrix} \tag{2.27}$$

The additional damping matrix is only considered for additional linear roll damping to compensate for any viscous effects (non-linear) that cannot be determined in the frequency domain approach.

The main parameters used to model the environment are wave frequency, water density and water depth. The water density is 1000 kg/m3. The water depth is important to take into account the influence of the sea floor on the waves. The influence of the sea floor can be ignored for deep water, for which the water depth is larger than half the maximum wave length considered. The wave length λ is calculated

with:

$$\lambda = \frac{g}{2 \cdot \pi} \cdot T^2 \tag{2.28}$$

$$\approx 1.56 \cdot T^2 \tag{2.29}$$

Where T is the wave period. The largest wave period considered is 25 seconds, therefore the maximum wave length is:

$$\lambda_{max} \approx 1.56 \cdot T^2 \tag{2.30}$$

$$\approx 1.56 \cdot 25^2 = 975 \text{ m} \tag{2.31}$$

The water depth is 600 meter, and as $600 > 1/2\ \lambda_{max}$ deep water can be considered.

2.3.2. Panel model barge

In the frequency domain analysis only the geometry of the barge below the mean free water line is taken into account, so only part of the geometry of the body has to be modelled. Furthermore, the origin of the coordinate frame is taken to be equal to the centre of gravity of the vessel. The particulars for the barge are given in Section 1.3, but the main particulars for the ballasted condition relevant to the panel model are also given in Table 2.1.

Length	200	[m]
Breadth	46	[m]
Depth	25.5	[m]
Mean draft	9.195	[m]
Displacement	81475.2	[m^3]
roll radius of gyration	19.92	[m]
Keel to centre of gravity	12.7	[m]

Table 2.1: Main barge particulars of the full scale barge for the ballasted condition

The panel model is generated by dividing the exterior of the wetted surface of the barge in a number of panels. The size of these panels is determined by choosing a mesh size. The mesh size should be small enough so that the pressures due to an incoming wave do not change significantly over a panel. Therefore the initial mesh size is determined from the shortest wave that is considered, as in this case the pressure differences over a panel is the largest.

According to Faltinsen (1993) a safe initial mesh size is smaller than $1/8\ \lambda$. The shortest wave considered is 3 seconds, therefore the initial panel size is estimated to be:

$$\lambda_{max} \approx \frac{1}{8} \cdot 1.56 \cdot 3^2 = 1.8 \text{ m} \tag{2.32}$$

To be on the safe side an initial mesh size of 1.5 meter is chosen. Subsequently other mesh sizes were chosen to investigate convergence of the solution and to find the mesh size that gives the best combination of calculation time and accuracy (see Section 2.3.3.

As the barge is double symmetric, meaning it is symmetrical around $x = 0$ and $y = 0$ only a quarter of the barge has to be modelled, after which WAMIT will make use of the symmetry boundary condition (see equations B.72 to B.74) to solve the potentials. A visualisation of the panel model for the barge only, including reference frame, is shown in Figure 2.2 below. For a mesh size of 1.5 meter 2741 panels were used to model a quarter of the barge, so without symmetry 10,964 panels are used for the complete barge.

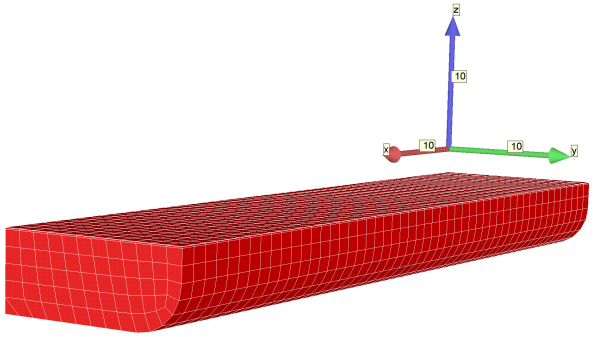

Figure 2.2: Visualisation of the mesh for the double symmetric barge (2741 panels).

2.3.3. Sensitivity of results to mesh size

To investigate the effect of the mesh size on the ship motions the RAOs, added mass- and damping are compared for different mesh sizes. The two plots at the top in Figure 2.3 show the roll RAO for different mesh sizes. At the bottom left the results are given for the heave RAO and the bottom right describes the roll added mass. All results are given for beam waves.

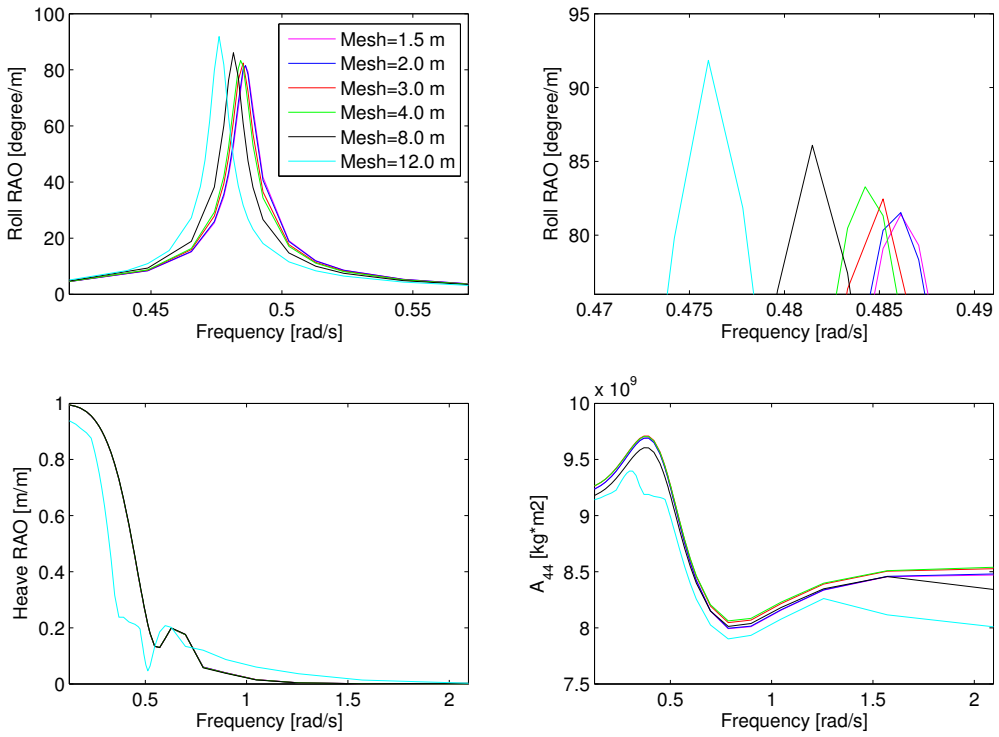

Figure 2.3: Sensitivty of the results to the mesh size for beam waves

The results clearly indicate that a mesh size of 12.0 meters gives very different results than was found for the other mesh sizes. For the roll RAOs the natural frequency and the height of the corresponding peak are significantly different from those obtained with smaller mesh sizes. Also the heave RAO and roll added mass indicate that a mesh size of 12.0 meter is not sufficient. For the other mesh sizes the solution converges for decreasing mesh size and the results obtained from a 2.0 meter mesh size are very similar to the results found with a 1.5 meter mesh. Based on the sensitivity analysis it is assumed that

the solution has converged sufficiently to choose a final mesh size by taking into account the calculation times. In Table 2.2 the calculation times are shown. This is shown by considering the time necessary to calculate the response of the barge to one wave frequency.

Mesh size [m]	**Number of panels [-]**	**Time per freq.[s]**
1.5	10,964	215.79
2.0	6,584	52.83
3.0	2,880	5.70
4.0	1,720	1.56
8.0	728	0.26
12.0	360	0.04

Table 2.2: Mesh size vs calculation time per wave frequency

From Table 2.2 above can be directly concluded that the calculation times increases significantly with decreasing mesh size. Not a constant order could be identified with which the calculation times increase for a change in mesh size. The different mesh sizes can now be compared in terms of accuracy of the results and calculation time:

- Accuracy of the results
  From Figure 2.3 it follows that the solution has converged significantly for the 1.5 meter mesh size. However, the differences between the 1.5- and 2.0 meter mesh are relatively small
- Calculation times
  The calculation times increase for decreasing mesh size. Especially the differences between the 1.5- and 2.0 meter mesh are significant.

Because the small difference in results for the 1.5- and 2.0 meter mesh, and the significant increase in calculation time for the 1.5 meter mesh with respect to the 2.0 meter mesh, the final mesh is chosen to be 2.0 meter. With a mesh size of 2.0 meter a high accuracy is achieved within a reasonable time. With this the maximum mesh size proposed by Faltinsen (1993) is exceeded. This may be because this limit is also applicable to more complex shaped vessel, while the barge has a relative simple geometry for which a larger mesh size may be sufficient.

The results obtained from the frequency domain model are given in Section 6.1.1.

2.4. Liquid cargo

In this section the approach to model the effect of sloshing in the two spherical tanks on the ship motions is discussed. Three loading conditions are considered: 25, 50 and 75 percent filled tanks. As cargo in the tanks fresh water is used, same as in the scale model tests. The main steps in the approach are:

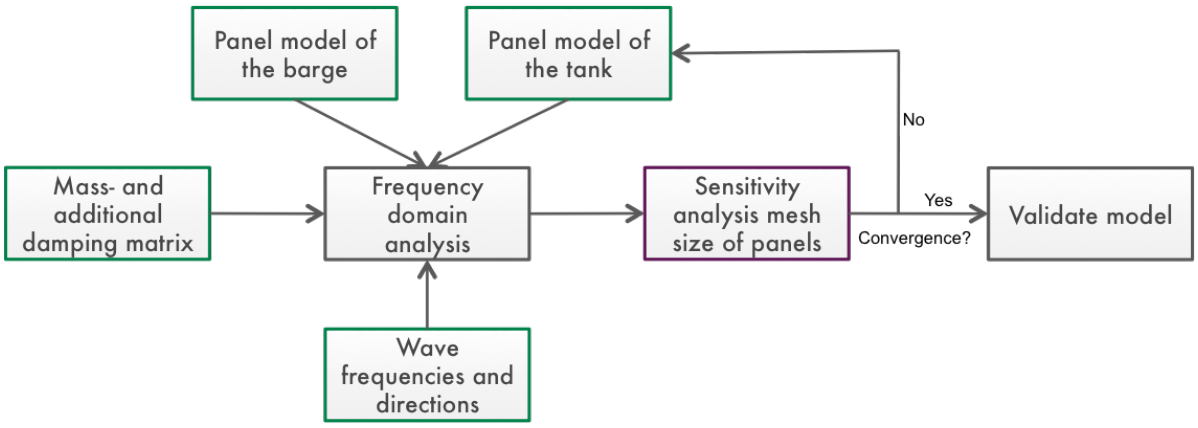

Figure 2.4: Steps in the frequency domain calculation that includes the cargo tanks.

The different steps described above are discussed in the next sections. The barge particulars used to model the effect of sloshing on the ship motions are given in Table 2.3 below.

	Unit	**25%**	**50%**	**75%**
Length ship	[m]	200	200	200
Breadth ship	[m]	46	46	46
Depth	[m]	25.5	25.56	25.5
Mean Draft (incl. cargo)	[m]	10.24	11.12	11.22
Displacement (excl. cargo)	[m^3]	75816.0	69444.0	55728.0
Roll radius (excl. cargo)	[m]	19.56	19.14	19.08

Table 2.3: Main barge particulars of the full scale barge for the 25, 50 and 75% loading condition.

To model the barge, without influence of the tanks, the displacement and roll radius of gyration are used as if no cargo is present. To analyse the effect of internal tanks on vessel motions the potentials are solved for both the hull and internal tanks separately. For the barge this includes the radiation, diffraction and incoming wave potentials. For the tanks this only includes radiation of waves on the tank wall, as there is no incoming wave potential (and therefore obviously also no diffraction potential). The RAOs are then obtained from the coupled equation of motion (Equation 2.18).

2.4.1. Mass, damping and environment

The mass matrix used in the coupled frequency domain approach only describes the mass and inertia of the hull as if there is no cargo present. Just as for the ballasted condition the additional damping matrix is used to add linear roll damping to compensate for the non-linear viscous damping that is very significant for a roll around the natural frequency of the barge. The mass of the cargo in the tanks is included in the frequency dependent added mass of the tanks. The input for the environment consists of the wave frequencies, water depth, exterior water density and the density of the cargo.

2.4.2. Panel model of hull and tank

For the coupled frequency domain simulation two panel models are generated, one for the hull and one for the tank:

- Panel model for the hull
  The mass, inertia , roll radius of gyration, centre of gravity are modelled as if no cargo is present.
- Panel model for the cargo tanks
  The panel model for the tank is loaded into WAMIT separately. Based on the panel model of the tank the the mass and inertia of the liquid cargo, as well as the (negative) restoring coefficients due to the liquid cargo (see Section 2.2.2) are determined.

The panel model of the barge hull was created in the same way, and with the same mesh size, as was done for the ballasted condition (Section 2.3.2). Therefore the panel model of the hull will not be discussed. The panel model for the tanks is developed in Multisurf. As the tank configuration is, just as the panel model for the hull, completely symmetric around $x = 0$ and $y = 0$, only half a tank is modelled.

Just as for the panel model of the hull, the panel model for the tanks is only created up to the mean free surface of the cargo in the tanks. To do this the height of the free surface and the horizontal location of the tank wall (for now z and x relative to the centre of the tank, see Figure 2.5) have to be identified. To find the mean free surface levels in the tank first the volume of the completely filled tank is calculated with:

$$V_{100\%} = \int_{-R}^{R} \pi \cdot \left[\sqrt{(R^2 - z^2)}\right]^2 dz \tag{2.33}$$

$$= \frac{4}{3}\pi R^3 \tag{2.34}$$

Where z is the vertical distance from the centre of the tank to the free surface of the liquid in the tank. From Equation 2.34 the volume of the partially filled tank can be calculated easily. However, an additional step is necessary to calculate the free surface height in the tank once the volume is known. When Equation 2.33 is integrated a more usable expression for the volume is found:

$$V_{n\%} = \int \pi \cdot \left[\sqrt{(R^2 - z^2)}\right]^2 dz \tag{2.35}$$

$$V_{n\%} = \pi \cdot \left(R^2 \cdot z - \frac{1}{3} \cdot z^3\right) \tag{2.36}$$

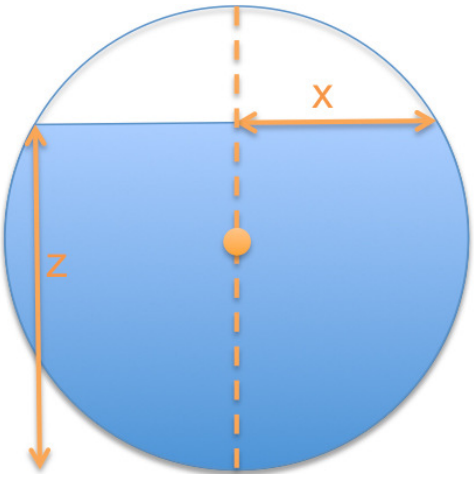

Figure 2.5: Free surface of cargo.

From this equation the vertical distance of the free surface level in the tank to the centre of the tank (x) can be solved by setting the equation equal to the volume of the partially filled tank, leaving z the only unknown. Once this is done it is easy to calculate the free surface relative to the bottom of the tank.

The horizontal location of the tank wall at the free surface level relative to the vertical line through the centre of the sphere x can be calculated with:

$$|x| = \sqrt{R^2 - (R - z)^2} \tag{2.37}$$

By using Equation 2.36 and 2.37 the results in Table 2.4 are obtained:

Loading cond. [%]	Volume [m3]	z [m]	x [m]
0	0	0.00	0.00
25	7,470	12.56	18.05
50	14,940	19.25	19.25
75	22,410	25.94	18.05
100	29,880	38.50	0.00

Table 2.4: Horizontal and vertical location of the free surface.

2.4.3. Sensitivity analysis tank mesh

In Multisurf the parameter to define the mesh is the number of panels used in the model, this in contradiction to GeniE, that was used for modelling the hull and uses the panel size as variable. Both tanks are only modelled up to the free surface of the cargo. Below in Figure 2.6 the roll RAOs are given for 4 different panel configurations around the natural sloshing frequency. As explained the maximum panel size is depending on the number of panels chosen and the height of the tank. As the height of the panel model, and therefore the panel size is at its maximum for the 75% loading condition, this loading condition is used to perform the sensitivity analysis. If the solution for a certain number of panels has converged for the 75% loading condition, it is also assumed that the solution has converged for the 25% and 50% loading condition. The considered number of panels in the sensitivity analysis are 8×8=64, 15×15=225, 30×30=900 and 45×45=2,025 panels per tank.

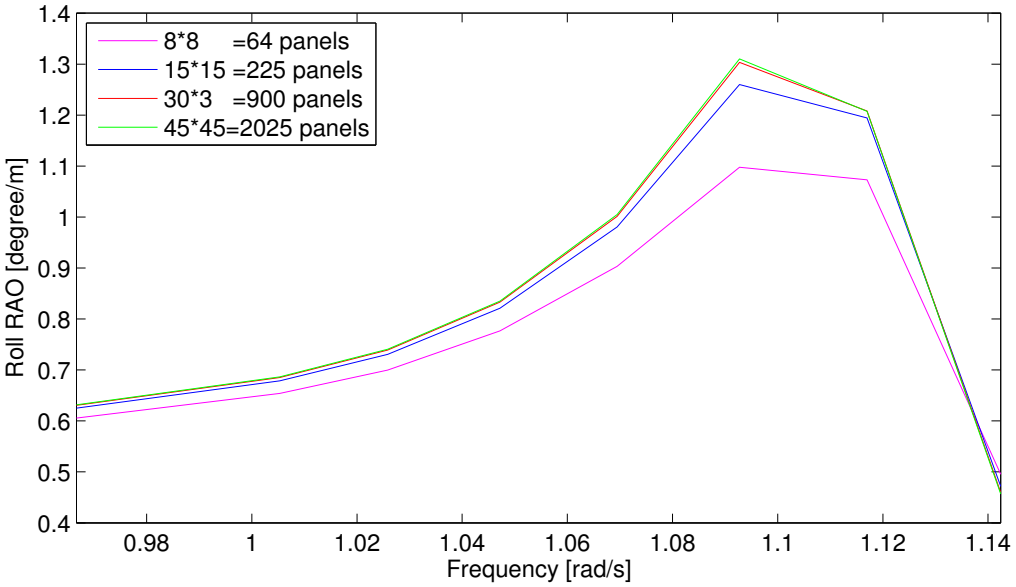

Figure 2.6: Sensitiviy analysis around the natural sloshing frequency for the 75% loading condition

From the sensitivity analysis was found that the solution when 64 panels are taken into account is significantly off. The results for the 900- and 2025 panel configuration are almost the same, and the configuration with 225 panels is only off by 3%. For a final comparison also the calculations are taken into account, see Table 2.5.

# of panels [m]	Time per frequency [min]	Time per frequency [s]
64	0.7	44
225	0.9	51
900	1.6	94
2,025	3.8	229

Table 2.5: Number of panels vs calculation time per wave frequency

Based on the results for the different panel models it is assumed that the solution has converged sufficiently for 2,025 panels. However, the computational times increase significantly with increasing number of panels. For example, the results in which 900 panels are taken into account is very close to the one with 2,025 panels. Therefore the number of panels that have to be used to obtain accurate results and good computation times for this project is determined to be 900.

In Figure 2.7 below an example of both the panel model of the hull and full tanks is shown. The results found in the coupled frequency domain analysis for the partially filled tanks are compared with the model test results in Section 6.1.2.

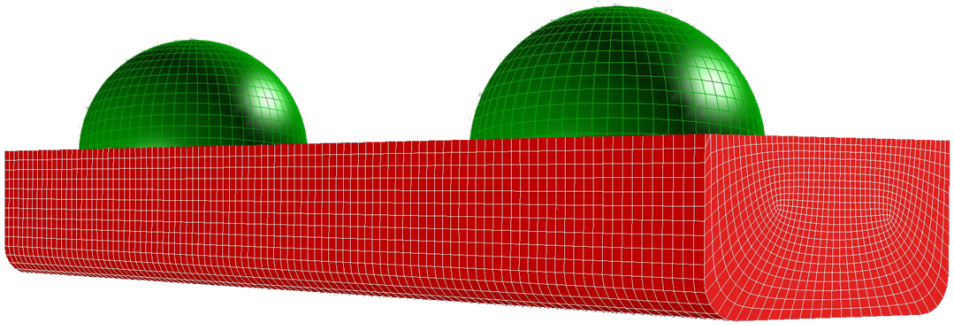

Figure 2.7: Example of panel models for both hull and tank, assumping full draft and filled tanks.

2.5. Frozen cargo

This section will describe the approach to analyse the effect of frozen cargo on the ship motions. This is of interest as in this case no sloshing occurs, and the influence of sloshing can be identified more explicitly. To analyse the roll motions of the barge with a partially filled tanks with frozen cargo the steps in Figure 2.8 are taken. First the panel model of the hull is developed, secondly the mass and moment of inertia of the cargo are calculated and added to the mass matrix of the hull. Finally the environment was modelled just as was described in Section 2.3.

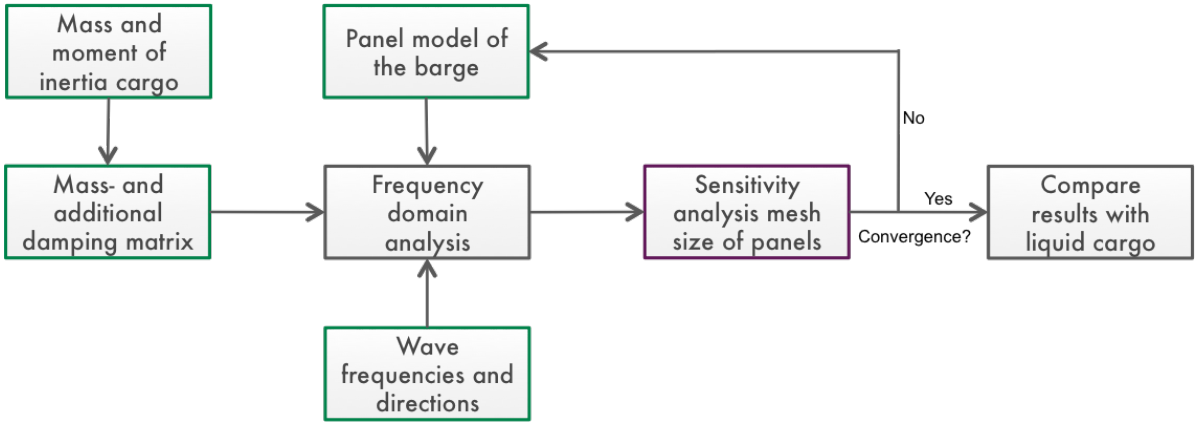

Figure 2.8: Steps for the frozen cargo conditions.

The roll motions of the barge with frozen cargo is investigated for the 50% loading conditions. The barge particulars for this can be found in Section 2.3.

2.5.1. Panel model barge and frozen cargo properties

The panel model for the barge with frozen cargo condition in the tanks is the same as for the liquid cargo condition. However, instead of using a panel model for the tanks, the mass and inertia of the frozen cargo is added to the mass matrix. The procedure for obtaining the additional mass and inertia is described in Section B.4, of which the final results for the diagonal terms are given below in table 2.6.

	Unit	**Barge**	**Tank around CoG barge**	**Total**
I_{xx}	$[kg\ m2]$	2.54E10	2.96E9	2.84E10
I_{yy}	$[kg\ m2]$	3.29E11	7.95E10	4.08E11
I_{zz}	$[kg\ m2]$	3.29E11	8.11E10	4.09E11
mass	[kg]	6.94E7	1.53E8	1.00E8

Table 2.6: Main barge particulars barge for the 50% frozen cargo condition.

By considering the results from Section B.4 the final mass matrix (kg and kgm^2) for frozen cargo is therefore given by:

$$\boldsymbol{M} = \begin{bmatrix} 1.00\text{E}8 & 0 & 0 & 0 & 2.06\text{E}7 & 0 \\ 0 & 1.00\text{E}8 & 0 & -2.06\text{E}7 & 0 & \\ 0 & 0 & 1.00\text{E}8 & 0 & 0 & 0 \\ 0 & -2.06\text{E}7 & 0 & 2.84\text{E}10 & 0 & 0 \\ 2.06\text{E}7 & 0 & 0 & 0 & 4.08\text{E}11 & 0 \\ 0 & 0 & 0 & 0 & 0 & 4.10\text{E}11 \end{bmatrix} \tag{2.38}$$

2.6. Chapter summary

This section described the approach and setup of the frequency domain model that is used to analyse the effect of sloshing on ship motions. First the main equations were described that are solved in the frequency domain model. For example the equation of motions that describe the motions of the barge including partially filled tanks. Secondly the frequency domain model for the ballasted condition was described. WAMIT, used for solving the motions of the barge in the frequency domain, was initially developed to analyse ship motions without internal tanks. It does this very accurately in situations where linear assumptions are valid, and therefore the ballasted condition can be used to investigate if the model is set up correctly. Thirdly the frequency domain model that simulates the motions of the barge with partially filled tanks is described for the 25, 50 and 75 percent loading condition. Finally a frequency domain model was discussed that is used to analyse the motions of the barge with frozen cargo in the tanks.

The results obtained with the frequency domain models for the ballasted, liquid cargo and frozen cargo conditions are compared with the scale model test results in Section 6.

3

Computational Fluid Dynamics

The setup of the CFD model that is used to simulate free surface motions, i.e. sloshing, in the partially filled spherical tanks will be described in this chapter. The CFD model is in a later state coupled to a ship motion model to investigate the effect of sloshing on ship motions. For the CFD model the Volume of Fluid solver ComFLOW is used, which can solve the Navier-Stokes equations for a viscous and incompressible fluid based on the continuity and momentum equations (see Section B.1): The continuity equation (conservation of mass) is given by:

$$\nabla \cdot \boldsymbol{u} = 0 \tag{3.1}$$

With $\boldsymbol{u} = (u, v, w)$ the velocity vector. The resulting momentum equations (Navier-Stokes equations) for incompressible flow are:

$$\frac{\partial \boldsymbol{u}}{\partial t} + \boldsymbol{u} \cdot \nabla \boldsymbol{u} = -\frac{1}{\rho}\nabla p + \frac{\mu}{\rho}\nabla \cdot \nabla \boldsymbol{u} + \boldsymbol{F}_{ext} \tag{3.2}$$

In Section 3.1 the CFD model is described more in detail and the sensitivity of the results to the grid size is investigated in Section 3.2. The CFD model itself is validated in Section 6.2. The results of the time domain coupling between ComFLOW and a ship motion solver is discussed in Section 6.4.

3.1. Description of the model

The model is created in a cartesian grid. In this section the description of the model will be discussed for geometry, grid, boundary conditions, liquid configuration, numerical schemes, forces and motions.

3.1.1. Geometry of the model

For this project spheres with a radius R=19.25 meter are used. For the flow inside a sphere the geometry in ComFLOW is set up in three steps (see Figure 3.2 for a visualisation):

1. Define the domain for the simulation
   The domain used for the ComFLOW analysis is slightly larger than the sphere
2. Create a solid block inside the complete domain
   ComFLOW requires that the complete domain is built up of cells (solid or open for flow). To meet this requirement a solid box is created that fills up the complete domain.
3. Create an empty sphere inside the block
   To create open cells in which flow is possible, a spherical shape with R=19.25 meter and -for example- origin at (x,y,z)=(0,0,0) is placed inside the solid box.

However, depending on the application of the CFD model the geometry changes. For example, in the coupled aNySIM-ComFLOW model two spheres are used that are placed at the same ship-fixed location as in the model tests. Figure 3.2 shows the geometry following from the steps above and including liquid configuration (see Section 3.1.3).

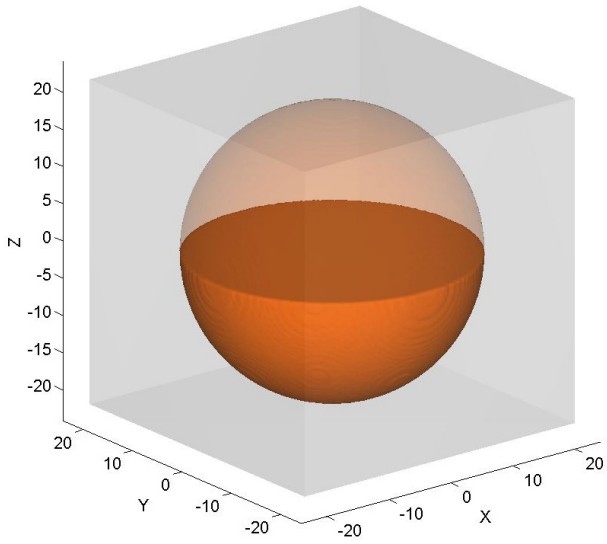

Figure 3.1: Geometry of the CFD model with a 50% filled tank.

3.1.2. Definition of the cartesian grid

The grid is set up by defining the number of grid cells that cover the box that contains the domain in the x, y, and z-direction. Based on the geometry some cells will be solid and some will be open for flow. Solid cells will not be taken into account during the simulation. See Figure 3.2 for a visualisation and Section 3.2.1 for an investigation of the effects of the grid on the results.

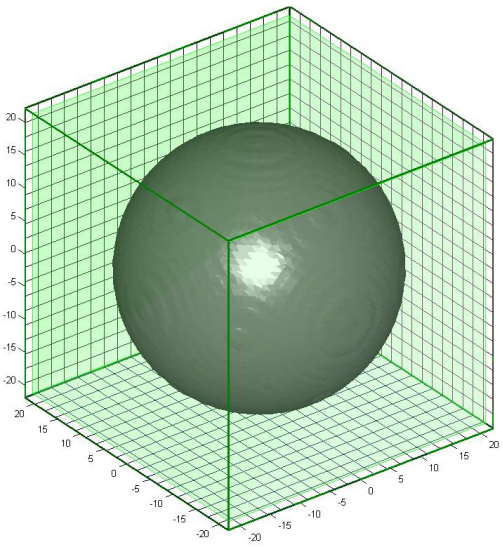

Figure 3.2: Example of a structured grid and green force box (see Section 3.1.7).

3.1.3. Initial liquid configuration

The cargo in the tanks has a density of 1000 kg/m^3. Viscous effects are neglected as the Reynolds number for both the scaled- and full scale model are far in the turbulence region. This means that the Navier-Stokes equations (Equation 3.2), reduce to the Euler equations:

$$\frac{\partial \boldsymbol{u}}{\partial t} + \boldsymbol{u} \cdot \nabla \boldsymbol{u} = -\frac{1}{\rho}\nabla p + \boldsymbol{F}_{ext} \tag{3.3}$$

The initial liquid configuration is set by defining the 3D domain in which all cells contain water at the start of the simulation. See Figure 3.2 for a visualisation of the initial liquid configuration for a 50% percent filled tank.

3.1.4. Free surface reconstruction

ComFLOW is a Volume of Fluid method. This means cells may contain no liquid at all, are completely filled with liquid or are partly filled with liquid. This gives much more freedom in defining the free surface as the free surface is not anymore depending on cell edges, but can contain any percentage of liquid. For this project this means that filling levels of 25, 50 and 75 percent can be easily reached with high accuracy. The free surface is reconstructed with the Hirt and Nichols method (geometrical reconstruction), after which the classical height-function correction is applied.

3.1.5. Time step

The time step in ComFLOW is variable during the simulation and determined by the CFL condition, which is given by:

$$CFL = \max_{i,j,k}\left(\frac{|u_{ijk}|\delta t}{h_{x,i}} + \frac{|v_{ijk}|\delta t}{h_{y,j}} + \frac{|w_{ijk}|\delta t}{h_{z,k}}\right) \tag{3.4}$$

in which u, v, w are the velocites and h_x, h_y, h_z are the mesh sizes of the cell. In case of high velocities the time step may be decreased, while for lower velocities the time step may be increased resulting in a shorter calculation time. The time step is decreased if the CFL number is greater than CFL_{max} (0.5), and doubled when the CFL number is smaller than CFL_{min} (0.2) during 10 successive time steps. CFL_{max} and CFL_{min} are chosen based on recommendations for the Euler Forward time integration method in the ComFLOW manual.

3.1.6. Numerical schemes

In ComFLOW the Navier-Stokes equations are discretised in both space and time. Both discretisation methods are discussed in this section.

Time discretisation

For the discretisation in time the (first order accurate) Forward Euler method is used:

$$y_{n+1} = y_n + h \cdot f(t_n, y_n) \tag{3.5}$$

Where $f(t_n, y_n) = y'(t)$ is the derivate of the function y at the current time step. The time discretisation could also be done with a second order accurate method, the Adams-Bashforth method. But, this would significantly increase calculation times as the recommended $CFL_{max} = 0.1$ for the Adams-Bashforth method, resulting in smaller time steps during the simulation. This is comparison to the $CFL_{max} = 0.5$ that is recommended when the Forward Euler method (see Section 3.1.5) is used.

Spatial discretisation

For spatial discretisation the second order accurate method of central-discretisation is used:

$$\Phi_e = \frac{\Phi_P + \Phi_E}{2} \tag{3.6}$$

where Φ_e is a value at point e, that is exactly in between point P and E. This method is more accurate than first-order upwind, but also less stable. Therefore a flux limiter is activated that stabilises the flow in regions where spurious oscillations might occur. When the flux limiter is used the spatial derivative is also calculated with a first-order method. In case the difference between the first- and second order method becomes too large than a spurious oscillations might occur and the first-order, but more stable, method is used. In case no spurious oscillation is expected to occur than the second-order, but less stable, method is used.

3.1.7. Forces and moments

The forces in the system are measured by means of force boxes. When a force box is defined ComFLOW calculates the net forces inside the force box, and the moments around the centre of the force box:

$$\boldsymbol{F} = \iint_S p\boldsymbol{n}\, dS \tag{3.7}$$

$$\boldsymbol{M} = \iint_S p\boldsymbol{r}\boldsymbol{n}\, dS \tag{3.8}$$

With $\boldsymbol{n}$ the outward normal vector of the surface dS and $\boldsymbol{r}$ the position vector of the surface dS relative to the centre of the force box.

3.1.8. Motions of the tank

In this project motions of the tank are prescribed by moving the complete coordinate frame. This can be done in several ways:

1. Constant- and accelerated motion (not used in this project)
2. Sinusoidal motions (used in the validation of the CFD model, see Section 6.2)
3. Time traces from text files (used in the validation of the CFD model, see Section 6.2)
4. Motions obtained from another software package (this is used in the aNySIM - ComFLOW coupled model, see Section 5)

3.2. Sensitivity of results to grid

In the sensitivity analysis it is investigated what type of grid provides accurate results within a reasonable amount of time. The sensitivity analysis is done for a spherical tank with R=19.25 that is filled for 50%. The tank is moved based on a time trace of the motions of the vessel during the scale model tests . The environment during these tests is: 90 degree waves, a 7.0 second wave period and a wave height of 1.5 meter.

During the sensitivity analysis only the fore part of the vessel (one tank) is taken into account and the point (0,0,0) in the ComFLOW coordinate frame is at the same location as the CoG (13.86 meter above the keel) of the barge with 50% filled tanks. The domain used in the ComFLOW model is therefore:

xmin	xmax	ymin	ymax	zmin	zmax
0.0	100.0	-23.0	23.0	-13.86	29.64

3.2.1. Grid sizes and calculation times

In the sensitivity analysis a range of grids, each with a different number of cells is used to compare the resulting forces and moments on the tank walls. The goal is to investigate if there is convergence of the

forces for an increasing number of cells and which grid size gives accurate results within a reasonable amount of time. The first grid is a very coarse grid with only 2,200 cells. Starting with the first grid, every next grid increased with 22 cells in x-direction, and 10 in both y- and z-direction. This is repeated up to a grid containing $154 \cdot 70 \cdot 70$ cells, which has been considered a very fine grid. Table 3.1 gives an overview of the different grids and resulting calculation times for a 400 second simulation.

Grid size	**Number of cells**	**Time**	**Realtime factor [-]**
$22 \cdot 10 \cdot 10$	2,200	5 min	1/1
$44 \cdot 20 \cdot 20$	17,600	14 min	1/2
$66 \cdot 30 \cdot 30$	59,400	1.0 hour	1/9
$88 \cdot 40 \cdot 40$	140,800	2.6 hours	1/23
$110 \cdot 50 \cdot 50$	275,000	6.7 hours	1/60
$132 \cdot 60 \cdot 60$	475,200	18.5 hours	1/167
$154 \cdot 70 \cdot 70$	754,000	47 hours	1/423

Table 3.1: Grid size and calculation times for a 400 second simulation (1 tank, 50% filled).

3.2.2. Influence of grid size on forces

This section discusses the influence of the different grid definitions on the results. For this a time series of the 6 degrees of freedom of the barge during the model tests will be used to compare the forces on the tank walls. It is expected that the weight of the liquid in the 50% filled tank is $\frac{1}{2} \cdot V_{\text{tank}} \cdot \rho \cdot g$ =146.5 MN. To be able to make a better comparison the static weight of 145.6 MN is subtracted from the actual vertical force of the liquid in the tank (Figure 3.3).

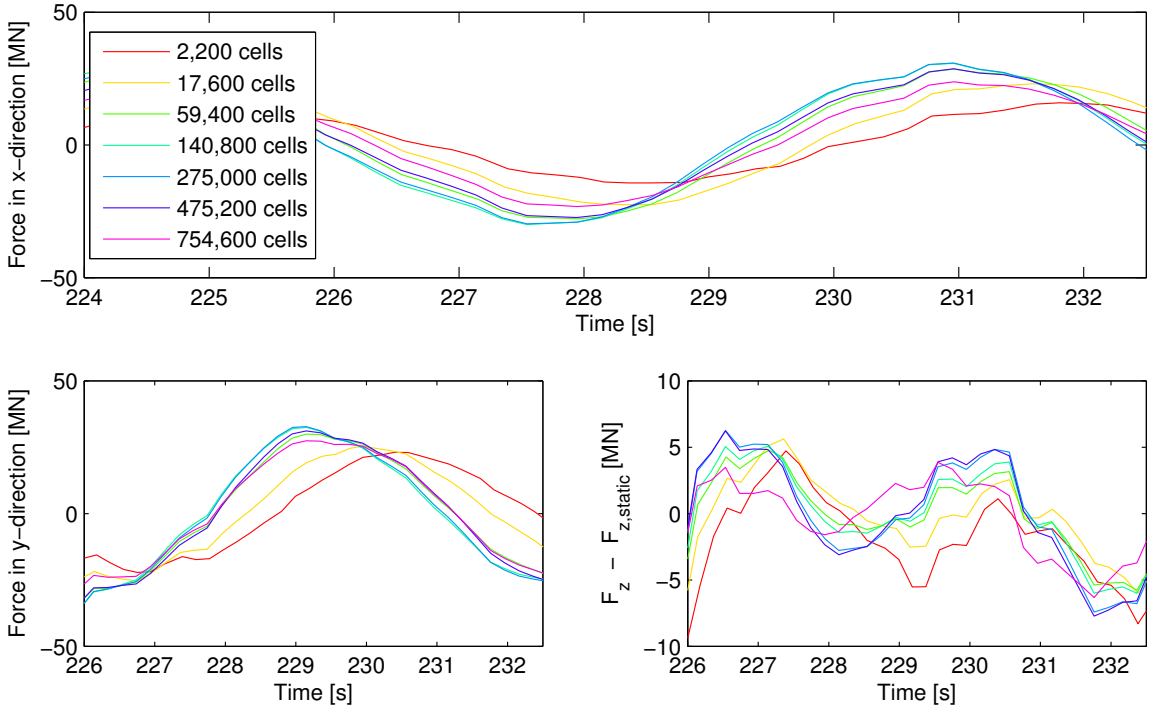

Figure 3.3: Results of sensititivy analysis for the 50% filling condition.

Figure 3.3 shows the forces in x-, y- and z-direction calculated by ComFLOW between 226 and 232.5 seconds. This interval is chosen because of the relatively large differences between the results. Approximately the same differences, or less, are found in the rest of the results. To make the results easier to interpret the static weight of the liquid in the tank is subtracted from the resulting vertical force.

From these results is clearly visible that the two smallest grids (2,200 and 17,600 cells) provide very different results than what is found for the other grid sizes. Both the size and phase are significantly off. The results for the other grid configurations are all more or less close to each other, but do not show uniform convergence. However, the results look trustworthy. To be on the safe side, and still produce trustful results in a reasonable time (the equivalent of) a grid with $88 \cdot 40 \cdot 40 = 140{,}800$ cells is used. The validation of the CFD model is described in Section 6.1.2.

3.3. Chapter summary

This chapter discussed the high level setup of the CFD model that was is to calculate the forces and moments due to the sloshing of the liquid inside the spherical tanks. The influence of the grid size on the resulting forces and moments is also investigated. This was done for one tank to minimise calculation times. The results did not show a uniform convergence for an increasing number of cells, but do seem trustworthy. Based on this a mesh size isn chosen that is believed to deliver accurate results in a reasonable time.

The ComFLOW model itself is validated in 6.2. Section 5 will discuss the coupling between ComFLOW and aNySIM. The results of the coupled aNySIM - ComFLOW simulation for the 25, 50 and 75 percent loading condition are given in Section 6.4.

4

Ship motions

This section describes the setup of the ship motion model that is used in the coupled time domain simulation. Solving the ship motions in six degrees of freedom is for this project done in aNySIM, a time-domain software package developed by MARIN. Initially the aNySIM model will be validated by using the ballasted loading condition from the scale model tests. In this case there is no liquid in the spherical tanks and thus the performance of the ship model is easily validated against model tests. The results of the validation of the ship motion model is discussed in Section 6. The coupling between aNySIM and ComFLOW is discussed in Section 5

4.1. Theory

[from aNySIM manual] In classic ship motions theory a linear mass-spring analogy is used to calculate the response of the ship to any environmental condition:

$$\sum_{j=1}^{6}(M_{kj}+a_{kj})\ddot{x}_j + b_{kj}\dot{x}_j + c_{jk}x_j = F_k \qquad \text{with k,j=1,2...6} \tag{4.1}$$

With M and a the mass and frequency dependent added mass of the vessel respectively. b represents the frequency dependent damping, c the hydrostatic restoring coefficients, F the external force and kj the different modes of the motion of the vessel. However, as aNySIM also gives the possibility to analyse non-linear effects in for example the mooring lines and fenders, the linear equation of motion (Equation 4.1) cannot be used and therefore impulse response theory is applied:

$$\sum_{j=1}^{6}(M_{kj}+m_{kj})\ddot{x}_j + \int_{-\infty}^{t} R_{kj}(t-\tau)\dot{x}(\tau)d\tau + c_{jk}x_j = F_k(t) \qquad \text{with k,j=1,2...6} \tag{4.2}$$

Where m is the frequency independent added mass and R is the retardation function (to include frequency independent damping). To solve these equations, among other things, a hydrodynamic database is required as input to aNySIM. The hydrodynamic database contains the frequency dependent added mass, damping, fist- and second order wave forces. These coefficients are calculated with linear potential theory (see Section B.2.1). The relationship between the frequency dependent added mass m, frequency independent added mass a and frequency dependent damping coefficients b is given by:

$$a_{kj} = m_{kj} - \frac{1}{\omega}\int_{0}^{\infty} R_{kj}(t)\sin(\omega t)dt \tag{4.3}$$

$$b_{kj} = \int_{0}^{\infty} R_{kj}(t)\cos(\omega t)dt \tag{4.4}$$

Where ω is the frequency of the wave and $d\omega$ is the wave frequency interval chosen in the frequency domain input. On advice of MARIN $d\omega = 0.025$ rad/s. After applying inverse Fourier transformation on Equation 4.3 and 4.4 the retardation function and frequency independent added mass can be obtained that are used in Equation 4.2:

$$R_{kj}(t) = \frac{2}{\pi} \int_0^\infty b_{kj}(\omega) \cos(\omega t)\, d\omega \tag{4.5}$$

$$m_{kj} = a_{kj}(\omega) + \frac{1}{\omega} \int_0^\infty R_{kj}(\tau) \sin(\omega t)\, d\tau \tag{4.6}$$

4.2. Overview of the model

Figure 4.1 below gives an overview of the aNySIM model setup, specifying inputs and outputs. The input for aNySIM consists of a hydrodynamic database (added mass, damping and wave forces, see Section 4.3), the vessel properties (Section 4.4), environmental conditions (Section 4.5), numerical settings (Section 4.6) and the mooring system (4.7). aNySIM processes the input and delivers the six degree of freedom motions of the vessel as output.

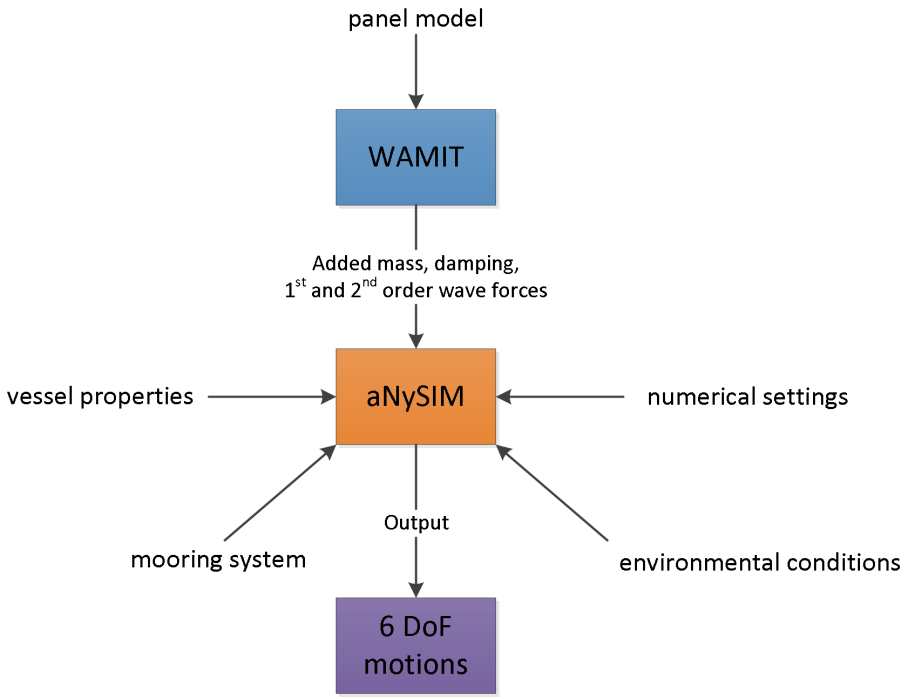

Figure 4.1: Overview of the aNySIM model including inputs and outputs

4.3. WAMIT output to hydrodynamic database

aNySIM requires a hydrodynamic database which consists of the frequency dependent added mass, damping, first order wave forces and second order wave forces. aNySIM uses this information to solve the equation of motion in the time domain. see Section 4.1 for more information on how the frequency dependent information is used in aNySIM. In this project WAMIT is used to obtain the required frequency dependent information. WAMIT requires a panel model as input and based on this calculates the potential acting on the panels, from which the required information is calculated (see Section B.2.1).

4.4. Vessel properties

aNySIM requires the vessel properties to solve the equation of motion. For the ballasted condition this mainly consists of the length, beam, draft, reference position (at the keel), centre of gravity, radii of gyration and additional roll damping. The additional roll damping is used to compensate for the viscous damping that is not considered in the frequency dependent input for aNySIM.

4.5. Environmental conditions

The environmental conditions in the aNySIM model for this project mainly consists of waves. Current and wind are not considered as these were not present in the performed model tests. In aNySIM many different types of wave conditions can be chosen, but the two main options are a wave spectrum or a regular wave. In this project mainly regular waves are used, for which aNySIM requires the wave amplitude, frequency and direction. Also the water density (1000 kg/m3) and water depth (600 meter) are included in the model. Finally a wave build up time of 75 seconds is applied to gradually expose the vessel to the waves and by this prevent a long transient response, see Figure 4.2 below.

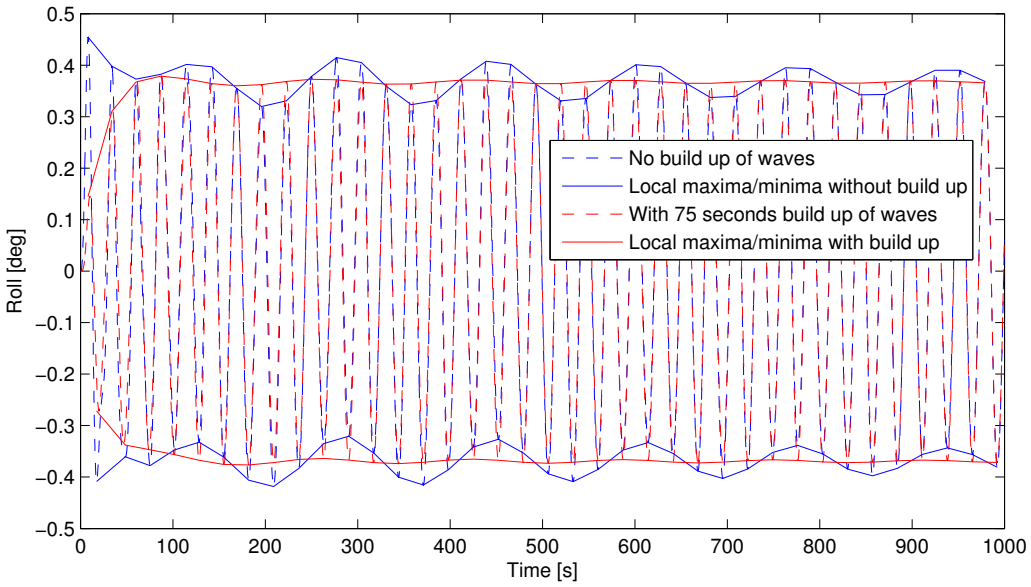

Figure 4.2: Comparison of response with- and without build up of waves

4.6. Numerical settings

The equation of motion (ordinary differential equation) is solved by using the Cash-Karp method. This method uses six function evaluation to obtain two solutions: a fourth- and a fifth order accurate solution. The difference between the two solutions is assumed to be the error of the fourth order accurate solution. To create a more stable model the time step is reduced when the difference between the two solutions becomes larger than a certain tolerance. In this project the initial time step is chosen to be 0.1 seconds and the tolerance is 0.001. Other settings are possible, for example a Runge-Kutta second order method, but Cash-Karp is expected to give the most accurate results.

4.7. Mooring system

During the model tests a soft spring mooring system was connected to the barge to prevent it from drifting off. The mooring system is also used to create a large surge and sway period so that the mooring system will not influence roll, heave and pitch motions of the barge too much. The mooring system used in the scale model tests is also used in aNySIM. The specifications of the mooring systems is given in Table 4.1 and a visualisation of the mooring system in the horizontal plane is given in Figure 4.3.

Mooring line nr	Length [m]	Stifness [kN/m]	Pre-tension [kN]
1	2065.0	93.8	2540.1
2	2065.0	93.8	2540.1
3	1912.0	93.8	2540.1
4	1912.0	93.8	2540.1

Table 4.1: Mooring system properties.

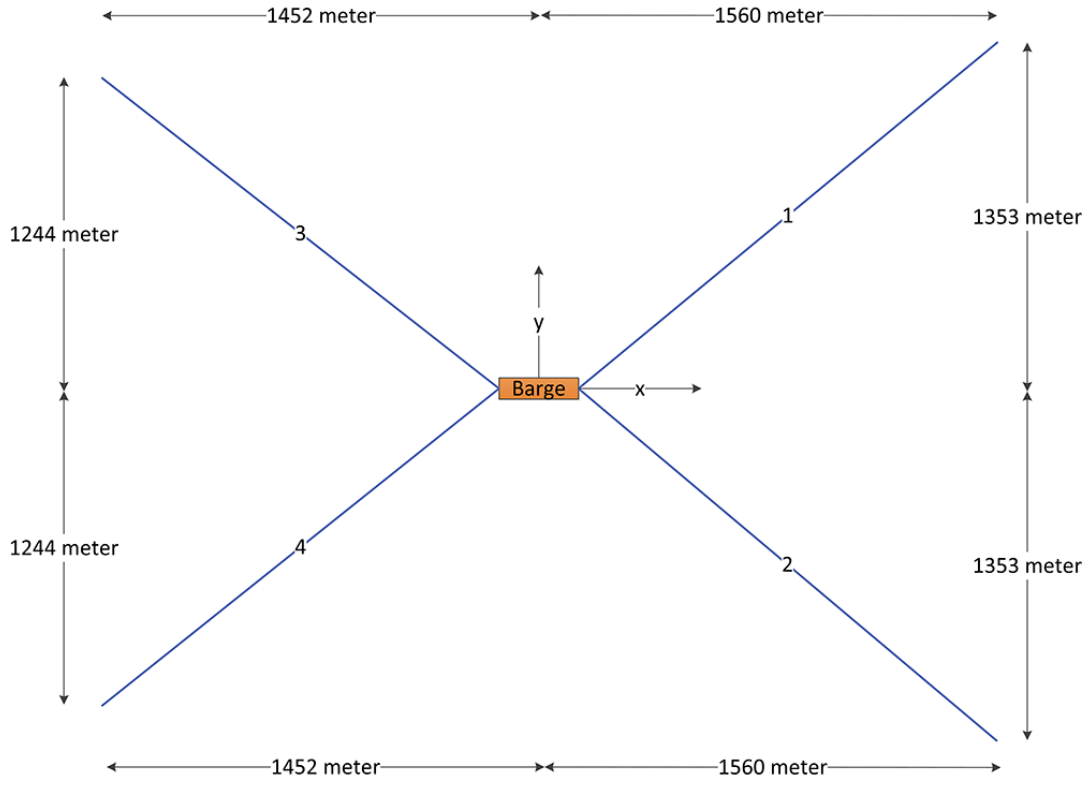

Figure 4.3: Dimensions of the soft spring mooring system in the horizontal plane.

4.8. Chapter summary

This chapter has provided a high level overview of the aNySIM model. The most important parts of the set up are the barge particulars and its location in the global- and body fixed reference frame, the mooring system and the environment. The aNySIM model will be first validated for the ballasted loading condition, without any cargo in the tanks, in Section 6.3. The next step is to develop the coupling between ComFLOW and aNySIM, this is discussed in Section 5. Finally the results from the coupled time domain model are compared with the scale model test results in Section 6.4.

5

Coupling in the time domain

The chapter will describe the development of the (64 bit) coupling between ComFLOW and aNySIM. First in Section 5.1 the general principle of the coupling is explained. Section 5.2 contains a more detailed description of the coupling, including the subroutines that are used. Finally in Section 5.3 the necessary configuration for the coupling to work is discussed for both ComFLOW and aNySIM. In Section 6 the results of the coupled time domain are discussed.

5.1. Principle of the coupling

aNySIM is developed to solve ship motions accurately and fast, but not to simulate sloshing of liquid in tanks. ComFLOW on the other hand is, among other things, developed to provide an accurate description of the flow of liquids in tanks. However, the accuracy comes with a price; it requires a lot of computational time and is therefore inefficient to be used for the simulation of a barge in waves. By using the fast and accurate code of aNySIM for solving ship motions and the capability of ComFLOW to simulate sloshing in spherical tanks, best of both worlds are combined. However, ComFLOW and aNySIM are two different software packages and a coupling has to be developed. This coupling communicates with both aNySIM and ComFLOW and makes sure both software packages have the required information at the relevant time.

The coupling is written in Fortran, and uses subroutines to communicate with both aNySIM and ComFLOW. The principle behind the coupling is that the barge, without any cargo tanks, is modelled in aNySIM. Simultaneously the tanks, without taking into account the barge, are modelled in ComFLOW. The coupling sends the motions of the barge, calculated in aNySIM, to ComFLOW that uses this information to move the reference frame in which the tanks are modelled. As a result, ComFLOW calculates the forces on the tank wall and the moments following from this. The sloshing loads are taken by the coupling and are send to aNySIM. aNySIM includes the sloshing loads in the equations of motion and calculates the motions of the barge at the next time level. The new motions are send to ComFLOW and the process repeats. See Figure 5.1 on the next page for a visualisation of the principle of the coupling.

The Fortran code consists of a number of subroutines. These subroutines are basically functions that can be called by an external programme. The Fortran code, including subroutines, is then compiled into a DLL, a Dynamic-Link Library. aNySIM uses this DLL and can call subroutine defined in the DLL. These subroutine on their turn can call ComFLOW subroutines, which have been supplied by the developers of ComFLOW in the form of a .lib (library) file; a statically linked library. This static ComFLOW library is compiled together with the developed subroutines for this project to create the DLL. In short, the developed and already available ComFLOW subroutines are both compiled into a DLL that is used by aNySIM. This means aNySIM is the leading programme in the coupled simulation.

The fact that aNySIM is the leading programme in the simulation is also shown in Figure 5.1 below. On the right hand side the activities of aNySIM are shown, on the left hand side the activities of ComFLOW are shown. First aNySIM progresses one large step in time, after which the motions are send to ComFLOW. On its turn ComFLOW will progress is time, with smaller steps, until it has reached the current aNySIM time. Then the forces on the tank wall and resulting moments are send from ComFLOW to aNySIM and the entire process repeats.

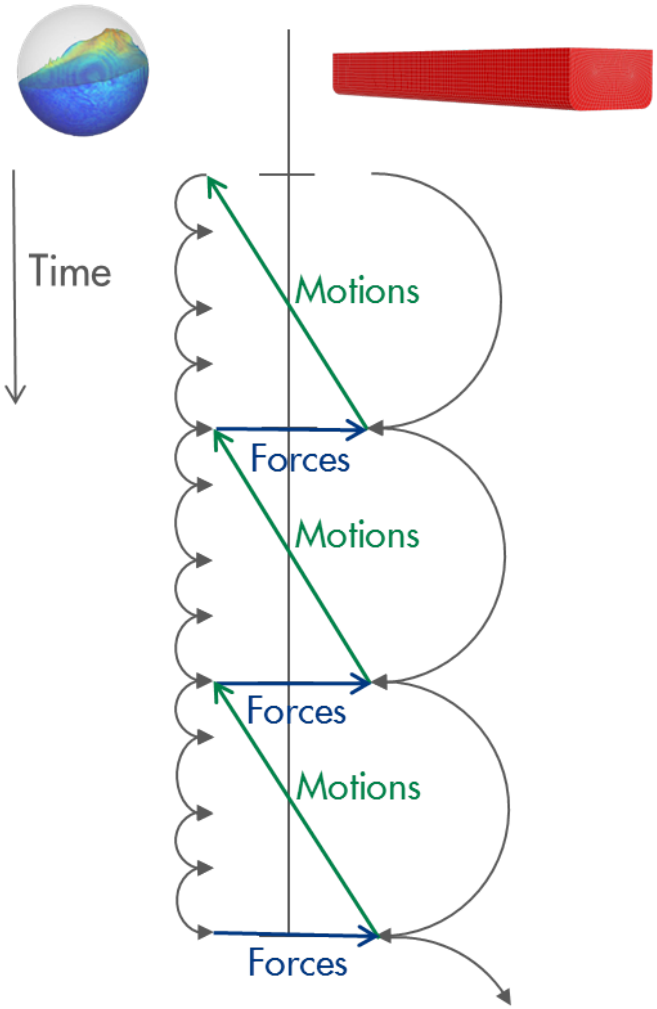

Figure 5.1: Principle of the developed Fortran coupling.

However, the visualisation above only shows the general working principle of the coupling. For example, ComFLOW requires the motions not only at the aNySIM time steps, but also in between them. Therefore interpolation methods are used to obtain the motions in between the aNySIM time steps. This and more details of the coupling are discussed within Section 5.2.

5.2. Detailed description of the coupling

The next sections will provide a more detailed description of the developed coupling. The complete code of the coupling is given in Section A.

5.2.1. Overview of the subroutines

A detailed overview of the coupling, including subroutines that can be called, is given in Figure 5.2. These subroutines; FDLL_init, FDLL_updateState, FDLL_calcForce, FDLL_getForce, FDLL_output and FDLL_close may call ComFLOW subroutines, which are also included in the DLL but are not directly called by aNySIM. From Figure 5.2 below can be clearly seen that some subroutines are called only once; in the beginning or at the end of the simulation. Other subroutines are called for every aNySIM time step. All main steps, indicated by the dark-green blocks, will be discussed in the next sections.

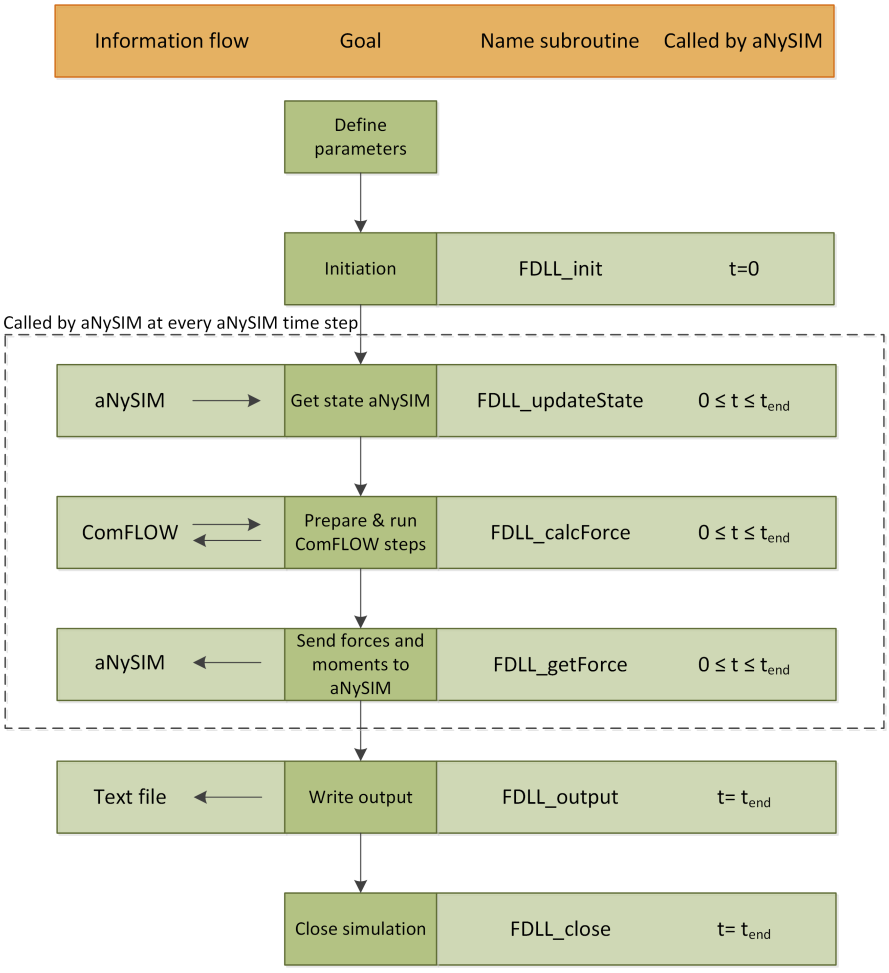

Figure 5.2: Detailed overview of the developed Fortran coupling.

5.2.2. Define parameters

In this part of the coupling the used variables are defined, for example is the variable an integer or a real value. In case of matrixes also the size is pre-determined. However, as it is possible to use multi body systems in aNySIM some variables are set to be allocatable; their size may change depending on the number of bodies. Finally, variables that are used outside of the subroutines are set to public, rather than private, so that they can be used by aNySIM and ComFLOW.

5.2.3. Initiation phase

This subroutine is called by aNySIM before the actual time domain simulation starts. The initiation phase is started when aNySIM calls the subroutine FDLL_init and specifies the number of bodies in the simulation. However not being currently used, it is possible to send an error message to aNySIM in case something goes wrong in the initiation phase. The main part of the FDLL_init subroutine is dedicated to pre-processing of ComFLOW, of which a summary is given in the code below (see Appendix A for the complete Fortran code used for the coupling).

```
subroutine FDLL_init(NBody, error)
  integer,                intent(in)  :: NBody
  integer,                intent(out) :: error

! Initisation phase of ComFLOW
call initialize(1) !<-- 1=GEODEF. Load geometry.in and create grid
call setup         !<-- process input and create liquid configuration
call closure       !<-- clean up
call initialize(0) !<-- 0=COMFLOW
! Finish initisation phase of ComFLOW
```

5.2.4. Update state of aNySIM

This subroutine will ask aNySIM for the current state (displacement, velocities and accelerations) in three reference frames for N bodies and six degrees of freedom per body:

- Earth fixed reference frame (motion, velocity and acceleration)
  The origin is located at the waterline of the model. The ship fixed reference frame is defined in the aNySIM model (XMF file) relative to the earth fixed reference frame.
- Ship fixed reference frame with the origin set at the current time (motion, velocity and acc.)
  The local reference frame is moving with the ship and is therefore always at the centre of gravity of the ship. This means position and orientation are always equal to zero.
- Ship fixed reference frame with the origin set at t_0 (motion and velocity)
  Before the simulation starts, all six degrees of freedom are set to zero in the ship fixed reference frame. After the start of the simulation the reference frame will stay at the same location and will not move with the body. This one will be used in the coupling. However, the acceleration is not known and has to be determined separately (see Section 5.2.5).

The states of the vessel that are known in the coupling are given in a bit more detail in the code below for the different reference frames: ef=earth fixed, sf=ship fixed with the reference frame set at the current time, and lif=ship fixed with reference frame set at t_0.

```
subroutine FDLL_updateState(bodyIndex, time, sfMotion, sfVeloc,
                            sfAccel, efPosition, lifMot, lifVel)
  integer,                intent(in)  ::  bodyIndex
  real,                   intent(in)  ::  time
  real,   dimension(6),   intent(in)  ::  sfMotion
  real,   dimension(6),   intent(in)  ::  sfVeloc
  real,   dimension(6),   intent(in)  ::  sfAccel
  real,   dimension(6),   intent(in)  ::  efPosition
  real,   dimension(6),   intent(in)  ::  lifMot
  real,   dimension(6),   intent(in)  ::  lifVel
```

The subroutine does not produce any output that is send to aNySIM. It only collects information that is used for changing the state of the tanks in the ComFLOW model.

5.2.5. Obtain forces

Figure 5.3 shows the subroutine in which interpolations of the motions from aNySIM takes place and in which ComFLOW is controlled. See Figure 5.2 how this fits in the total picture. All parts of the subroutine are be described separately, but for clarification all parts inside the dashed lines (loop) will be discussed in one section.

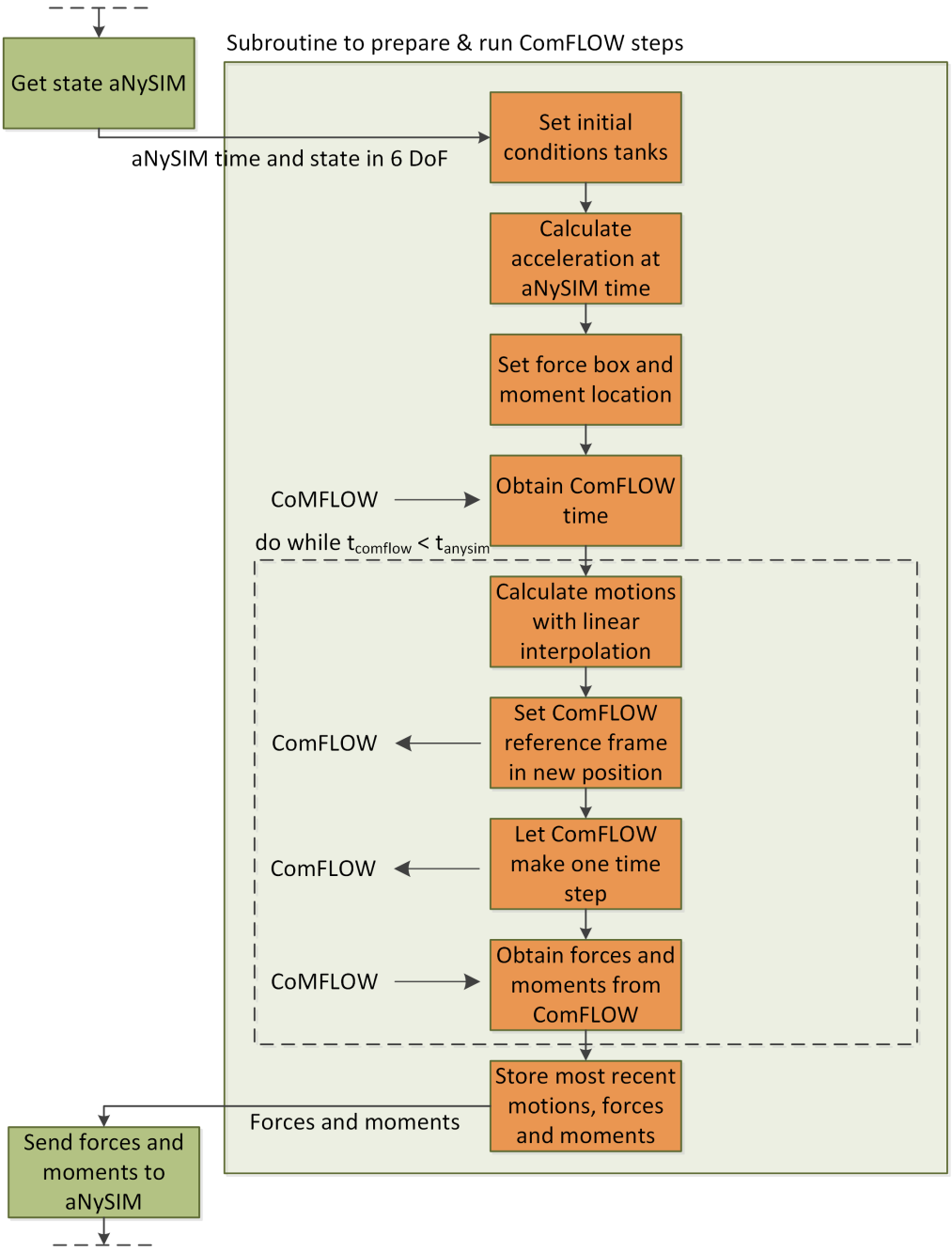

Figure 5.3: Overview of the FDLL_calcForce subroutine

Initial conditions

The initial motions of the vessel are set to zero in the aNySIM setup file. The initial positions, velocities and accelerations of the tanks in ComFLOW are set to zero in the coupling. The initial forces and moments that aNySIM takes into account are determined by ComFLOW, that makes one initial run at the beginning of the simulation. This is mainly important to determine, and take into account, the vertical force of the cargo due to gravity.

```
! Set initial positions, velocities and accelerations of ComFLOW
 pos = 0.0
 velocity = 0.0
 acceleration = 0.0
```

Pos, velocity and acceleration are (6×1) column vectors.

Calculate accelerations at aNySIM time

From aNySIM only the motions and velocities are known, as discussed in Section 5.2.4. However, ComFLOW also requires the acceleration of the tank and therefore the acceleration at the current aNySIM time has to be calculated. The accelerations are simply calculated by applying backward difference on the discrete velocities:

$$a(t_a) = \frac{v(t_a) - v(t_a - \Delta t_a)}{\Delta t_a} \tag{5.1}$$

Where the subscript "a" stands for aNySIM and the subscript "c" for ComFLOW. This means $t_a - \delta t_a$ stands for the current aNySIM time minus the aNySIM time step; so $t_a - \delta t_a$ indicates the time at the previous time level of aNySIM. In the Fortran code this is programmed in the following way:

```
! Calculate acceleration at timestep of aNySIM for body 1
if (fdll_time == 0) then
   fdll_lifAcc=0
else
   fdll_lifAcc=(fdll_lifVel(1,:)-velocity_min1)/(fdll_time-t_nmin1)
endif
```

Set force box and moment location

In ComFLOW multiple force boxes can be defined, see Section 3.1.7 for more information. In the coupling is defined which force boxes are used to determine the force and moments that are required by the coupling. Also the location around which the moments will be calculated inside this force box is defined. The location of the moments is the centre of gravity of the barge.

```
 boxnr = 1
 moment_location = 0.0
```

Obtain ComFLOW time

The coupling is developed so that first aNySIM makes one large time step, after which ComFLOW makes a number of smaller time steps as long as the ComFLOW time is smaller than the aNySIM time (before ComFLOW progresses one step in time). Now aNySIM will make one large time step, and the process repeats. Because the coupling controls when which programme is allowed to make one time step, the coupling always needs to know the latest time in both programmes. The ComFLOW time can be obtained by calling a subroutine in ComFLOW:

```
call get_time(tcycle,t,tmax,dt)
```

Calling the subroutine get_time will give as output the cycle time, current time, max time in ComFLOW and the current ComFLOW time step. In the coupling only the current time in ComFLOW is used.

Loop in which ComFLOW runs

The Fortran code that creates a loop in which ComFLOW progresses to the current aNySIM time is shown in the framed box below.

```
! Start time loop
do while (t < fdll_time)
!
if (fdll_time == 0) then
    print*, 't_n= ', fdll_time
else
    print*, 't_n-1    = ', t_nmin1
    print*, 't_n      = ', fdll_time
    print*, 't_comflow= ', t
    pos=pos_min1+(fdll_lifMot(1,:)-pos_min1)/
              (fdll_time-t_nmin1)*(t-t_nmin1)
    velocity = velocity_min1+(fdll_lifVel(1,:)-velocity_min1)/
              (fdll_time-t_nmin1)*(t-t_nmin1)
    acceleration =acceleration_min1+(fdll_lifAcc-acceleration_min1)/
              (fdll_time-t_nmin1)*(t-t_nmin1)
endif
!
! Set moving frame based on current time
call set_moving_frame(t, pos, velocity, acceleration)
! Carry out a timestep
call loop
call get_time(tcycle,t,tmax,dt)
! Obtain the forces on the tank
call get_force_frcbx(boxnr,force,moment,inertia,moment_location)
!
enddo
! End time loop
```

The first part of the code is a “do” loop. The code inside the loop is executed as long as the current ComFLOW time is smaller than the aNySIM time. The next step is to calculate the motions, velocities and accelerations of the tank at the ComFLOW times that are in between the current- and the previous aNySIM time. The is necessary because the aNySIM time step is larger than the ComFLOW time step and therefore ComFLOW also reaches time at which the motions, velocities and acceleration are not directly known. This is solved by applying linear interpolation, performed within the “if” statement, that makes sure that linear interpolation is not executed at t=0 . This is done because at t=0 no

previous motions are available and linear interpolation cannot take place. The linear interpolation used in the coupling is:

$$x(t_c) = x(t_a - \Delta t_a) + \frac{x(t_a) - x(t_a - \Delta t_a)}{\Delta t_a} \cdot (t_c - t_a + \Delta t_a) \tag{5.2}$$

$$v(t_c) = v(t_a - \Delta t_a) + \frac{v(t_a) - v(t_a - \Delta t_a)}{\Delta t_a} \cdot (t_c - t_a + \Delta t_a) \tag{5.3}$$

$$a(t_c) = a(t_a - \Delta t_a) + \frac{a(t_a) - a(t_a - \Delta t_a)}{\Delta t_a} \cdot (t_c - t_a + \Delta t_a) \tag{5.4}$$

When the motions, velocities and accelerations are known at the ComFLOW time than the subroutine set_moving_frame is called. This subroutine sets the ComFLOW reference frame in the correct position for the current time level and supplies ComFLOW with the velocities and accelerations necessary to progress one step in time. By calling the subroutine “loo” ComFLOW is told to progress one step in time, after which the new ComFLOW time is requested by the coupling and stored. Finally, the forces and moments are taken from ComFLOW by calling the subroutine get_force_frcbx and by supplying the box number and moment location to ComFLOW. Depending on the current ComFLOW time the above may be repeated or not, after which the most recent forces and moments are stored and the next subroutine, FDLL_getForce, is called by aNySIM (see Figure 5.2).

5.2.6. Send force to aNySIM

The most recent forces and moments are send to aNySIM when it calls the following subroutine:

```
subroutine FDLL_getForce(bodyIndex, force)
  integer,                intent(in)  ::  bodyIndex
  real,   dimension(6),   intent(out) ::  force
  !
  ! Body of FDLL_getForce
  force(:) = fdll_force(bodyIndex,:)
```

5.2.7. Write output

The values of all relevant variables that are used in coupled simulation are stored in a text file for every aNySIM time. For example:

- aNySIM time
- Earth fixed motions, velocities and accelerations
- Ship fixed current time motions, velocities and accelerations
- Ship fixed t_0 motions, velocities and accelerations
- Net forces on the tanks walls in x-, y and z-direction for the specified force box
- Moments around the x-, y- and z-axis for the specified force box and moment location

Next to this output is also written to the screen, but this is mostly coded in the “calc_force" subroutine. An example of the output to the screen is given in Figure 5.4 on the next page. Parts of the output were already present, but especially for (testing) the coupling additional output is written to the screen. The screenshot contains the output of three ComFLOW time steps (indicated in white) and the output of one aNySIM time step (indicated in yellow).

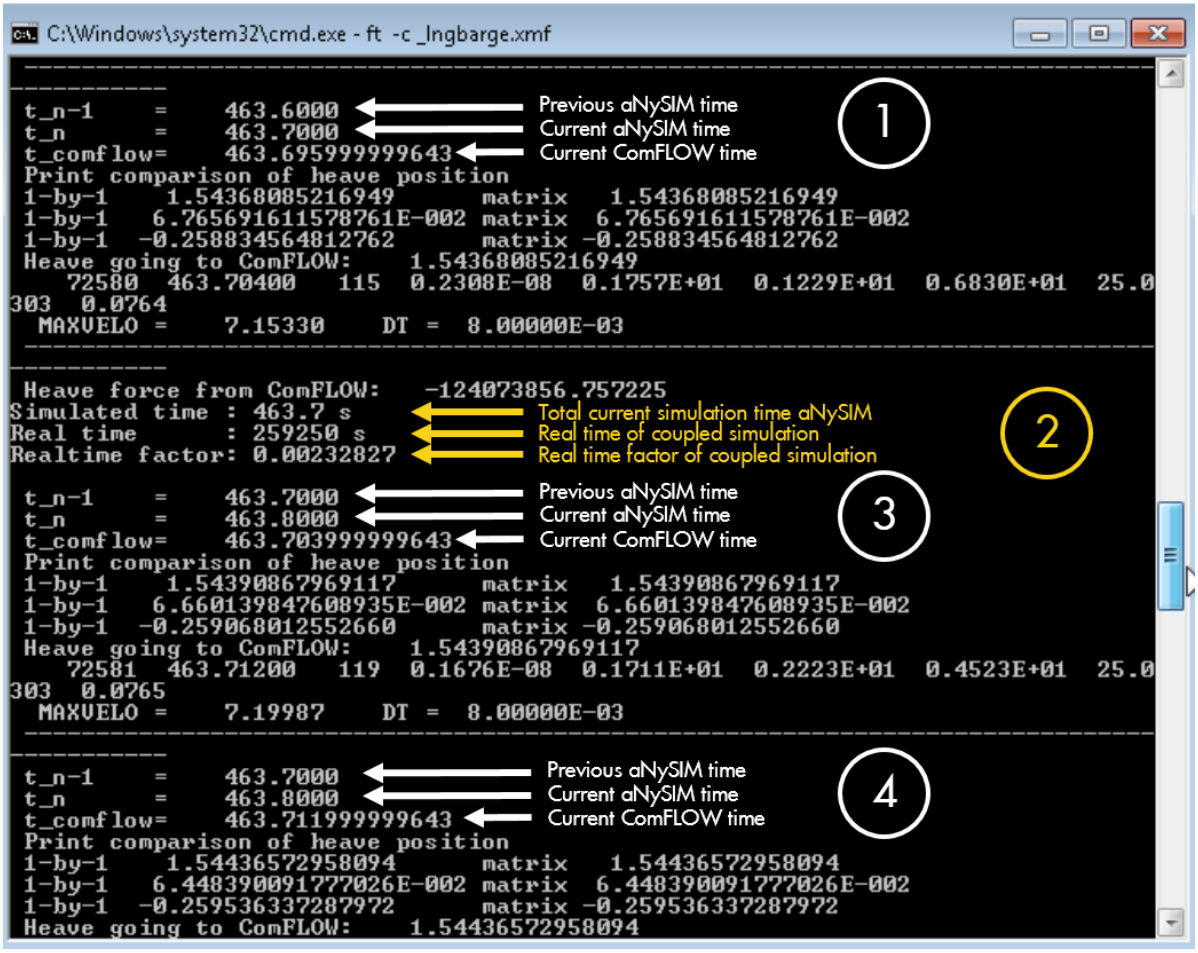

Figure 5.4: Example of output written to the screen during coupled simulation.

The four circles/times in the screenshot are described below:

1. The current aNySIM time is 463.7, the previous aNySIM time is 463.6 and the current ComFLOW time is 463.696 seconds. This indicates ComFLOW has almost reached the current aNySIM time.
2. aNySIM gives an update of the progress so far. The total simulated time is 463.7 seconds, which took 259,250 seconds to calculate. This gives a real time factor of 1/435 (multiple coupled simulations are running at the same time, which makes it very slow).
3. ComFLOW and aNySIM have progressed one step in time, the current aNySIM time is 463.8, the previous aNySIM time is 463.7 and the current ComFLOW time is 463.704 seconds.
4. CoMFLOW has progressed one step in time. The current aNySIM time is still 463.8, the current ComFLOW time is now 463.712.

This clearly shows the principle of the coupling; aNySIM leads the simulation and CoMFLOW progresses in time until it has reached the current aNySIM time.

Close simulation

The simulation is stopped and the allocated memory is made available again.

5.3. Setup of the aNySIM and ComFLOW model

Both the aNySIM and ComFLOW models have to be set up so that the influence of sloshing on ship motions is successfully modeled. A general description of the setup of the aNySIM and ComFLOW model is given in Section 4 and 3 respectively. However, in case of a coupled simulation both the ComFLOW and aNySIM model have to be set up in a specific way.

For the ComFLOW model it is very important that the origin of the reference frame is equal to the centre of gravity of the vessel model in aNySIM, and that the tanks are placed at their actual position relative to the CoG. When this is the case, the motions that are determined by aNySIM around the centre of gravity of the vessel can be directly applied on the reference frame in ComFLOW. Furthermore, to make sure that the moments determined in ComFLOW can be directly used in anySIM the moment location should be equal to the centre of gravity in ComFLOW (which should be in x,y,z=0,0,0). The force box should obviously include all tanks in the ComFLOW model.

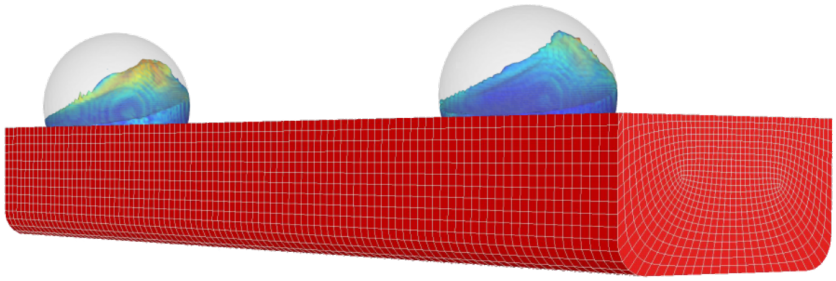

Figure 5.5: Visualisation of the coupled ComFLOW - aNySIM model.

Figure 5.5 shows the panel model of the barge and a visualisation of the tanks modelled in ComFLOW.

5.4. Chapter summary

This chapter has given a detailed overview of the developed coupling between ComFLOW and aNySIM. By using this coupling the non-linear sloshing in the tanks is modelled in ComFLOW and the ship motions are solved based on linear theory in aNySIM. For every aNySIM time step communication between ComFLOW and aNySIM takes place at which forces and motions are exchanged. Because ComFLOW can calculate non-linear flow the resulting ship motions may also become non-linear. To what expend this really occurs is investigated in Section 6.4, in which all results from the coupled simulations are discussed and compared to the scale model test results.

6

Results

In this chapter all results are discussed that are found via the frequency domain approach in section 6.1 and via the coupled time domain approach in section 6.4. Where possible the results are also validated against the scale model tests performed by Shell. The coupled time domain model consists of a coupling between aNySIM and ComFLOW. Therefore it is important to validate both ComFLOW and aNySIM separately, before they are coupled. In section 6.2 the computational fluid dynamics model in ComFLOW is discussed, followed by the validation of the aNySIM ship motions model in section 6.3. Finally the uncertainty in the results is investigated in section 6.5.

The discussion and validation of the results in the frequency domain are done for the ballasted, liquid cargo and frozen cargo condition. Additionally also the effect of wave direction and tank size are investigated in the frequency domain. The results of the time domain are presented for liquid cargo, for which the influence of wave direction, non-linear sloshing and the pump tower on the ship motions is investigated. Also the influence of the communication time step and type of interpolation used in the coupling is discussed.

Based on the results of the scale model tests and the literature study focused on prismatic tanks it has been identified that roll is most significantly influenced by sloshing in the cargo tanks. Additionally, the focus of this project is on an offloading situation (no forward speed of the vessel) in which roll is considered a critical degree of freedom that may limit the uptime of the system. Therefore this chapter will focus mainly on the roll motions of the barge.

6.1. Frequency domain model

In this section the results of the frequency domain approach are discussed and validated against the scale model tests. Section 6.1.1 will focus on the ballasted condition, followed by the liquid cargo conditions in section 6.1.2, frozen cargo in section 6.1.3. Finally the influence of wave direction and tank size are discussed in section 6.1.4 and 6.1.5 respectively.

6.1.1. Ballasted condition

The least complex loading condition is the ballasted condition, in which no cargo is present in the tanks. WAMIT is developed to analyse these types of situations, and therefore the ballasted condition is used to get an initial impression of the performance of the model. This is done by comparing results obtained in the frequency domain with the RAOs found during the scale model test campaign. These RAOs were determined by performing a cross spectrum analysis on the time series of the motions of the barge. In these tests the barge was subjected to a white noise wave spectrum.

The roll motion of the barge is subjected to a significant amount of non-linear viscous damping. The non-linear viscous damping cannot be determined in the frequency domain and is very complex to estimate without scale model tests. For this project scale model test results are available and therefore the height of the maximum response peak in the roll RAO results is matched by including additional linear damping to mimic non-linear viscous damping. The roll motions of the barge with no cargo in the tanks are given in Figure 6.1 below. Here the blue line is linked to the frequency domain results and the red line to the RAOs obtained during the scale model tests.

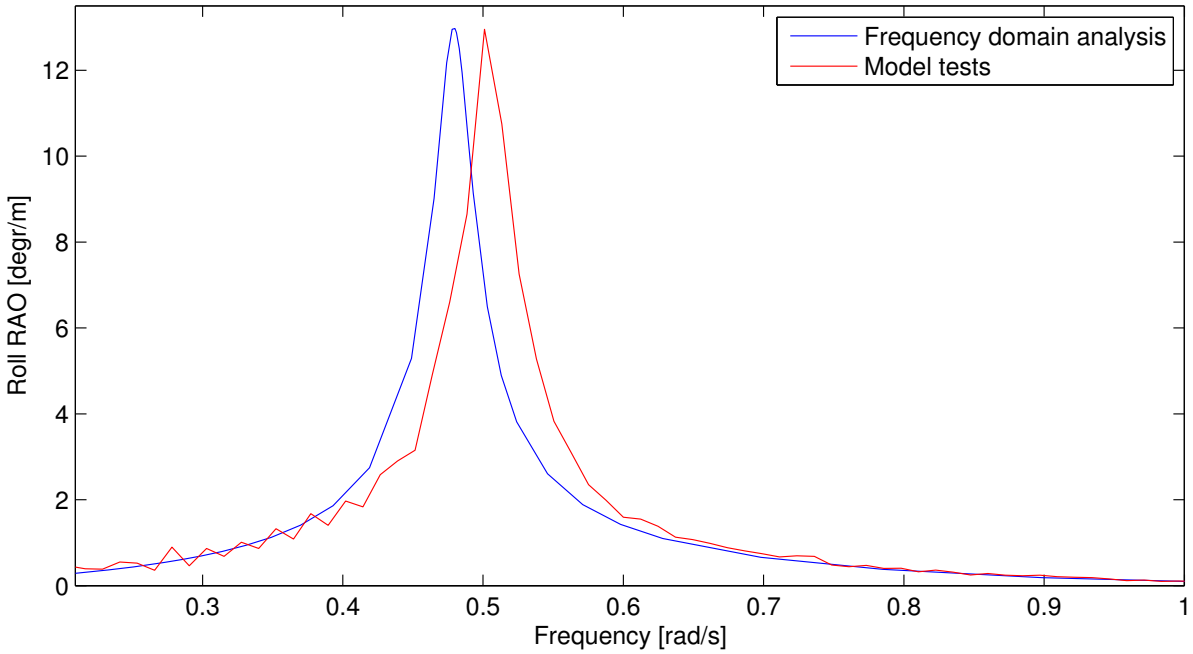

Figure 6.1: Ballasted case RAOs for beam waves.

It can be clearly seen that the natural frequency in the frequency domain model is underestimated compared to the scale model test results. However, the shape of both results are very similar and show the same trend when 0 and 1 rad/s is approached. The frequencies for which the response is maximum are given for both the model test and frequency domain results in Table 6.1 below.

Test	**Ballasted condition**
From white noise (WN) test	12.54 s / 0.501 rad/s
From frequency domain analysis	13.15 s / 0.478 rad/s
Difference	0.61 s / 0.023 rad/s

Table 6.1: Maximum response frequencies from Figure 6.1

The difference between the natural frequency found in the scale model test and frequency domain analysis is 4.86%. This is significant as it should be possible to calculate the response of a vessel with no internal tanks (or ballasted conditions as in this case) more accurately. To identify what could cause the differences the response of the barge is investigated in more detail by looking at the heave and pitch RAOs, shown in Figure 6.2 on the next page.

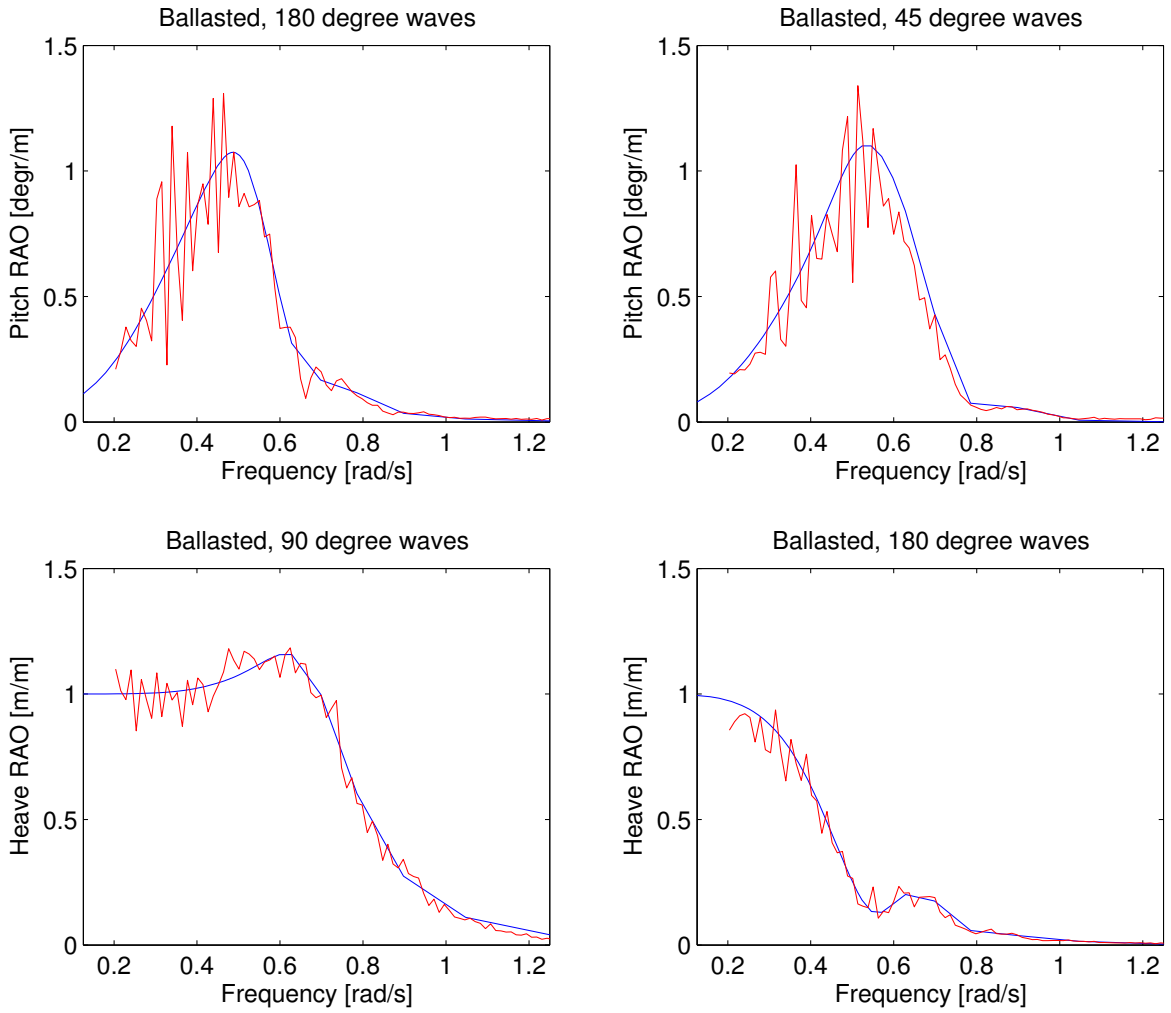

Figure 6.2: Model tests and frequency domain analysis results for pitch and heave.

Figure 6.2 shows that the results for pitch and heave match quite well for different wave directions. This is a clear indication that the panel model used in the frequency domain approach is correct, and also the hydrostatics such as the centre of gravity are modelled correctly. Furthermore, it indicates that the mass (by comparing heave results) and inertia around the y-axis (by comparing pitch results) is correct. Knowing this it can be assumed that the differences found are limited to roll. With this the source of error has not yet been identified, but it does indicate that the frequency domain model is set up correctly. Other possible sources of error are: the RAOs obtained from the scale model tests are not accurate or the vessel properties used in the frequency domain model are not correct. Both possibilities are investigated in more detail:

- The roll RAOs are not obtained correctly from the scale model tests
  It could be possible that a mistake was made in the cross spectrum analysis to determine the RAOs from the white noise tests. Also, the motions of the vessel and/or the waves could be measured incorrectly or out of phase. However, the RAOs obtained in the scale model tests have been checked with regular wave tests. The agreement found between the RAOs from the white noise- and regular wave tests is good, which indicates that the RAOs found from the white noise tests are accurate.

- One or more vessel properties are measured incorrectly during the scale model tests
  It could be possible that, for example, the roll radius of gyration is measured incorrectly during the scale model tests. This could create a shift in the response as was seen in Figure 6.1 and would not significantly change the RAOs for the other degrees of freedom. After checking this with the engineers present during the model tests it was quickly identified that there were some serious concerns about the accuracy of the measured roll radius of gyration.

By taking into account all possible reasons that could explain the differences in natural frequency it was found most probable that the roll radius of gyration was measured incorrectly during the scale model tests. This was also concluded by one of Shell's contractors, who used a different software package but also could not predict the natural frequency correctly with the measured roll radius of gyration. Therefore it has been decided to correct the roll radius of gyration so that the natural frequency matches for the frequency domain and scale model results. From this followed a roll radius of gyration of 18.90 meter (41% of the breadth), rather than the measured 19.92 meter (43% of the breadth). This is still relatively large compared to theoretical approximations. A rule of thumb that is often used states that k_{xx} can be approximated 30 to 40 percent of the breadth. Bureau Veritas proposed on the other hand ($\overline{KG}$ is the vertical distance between the keel and centre of gravity):

$$k_{xx} = 0.289 \cdot B \cdot \left(1.0 + \left(\frac{2 \cdot \overline{KG}}{B}\right)^2\right) = 0.289 \cdot 46 \cdot \left(1.0 + \left(\frac{2 \cdot 12.708}{46}\right)^2\right) = 17.35 \text{ meter} \tag{6.1}$$

This is significantly smaller than what was identified. This could be explained by a different mass distribution of the barge compared to more realistically shaped LNG carriers. By using $k_{xx} = 18.90$ meter and adding additional linear damping to account for the non-linear viscous damping the results shown in Figure 6.3 are obtained.

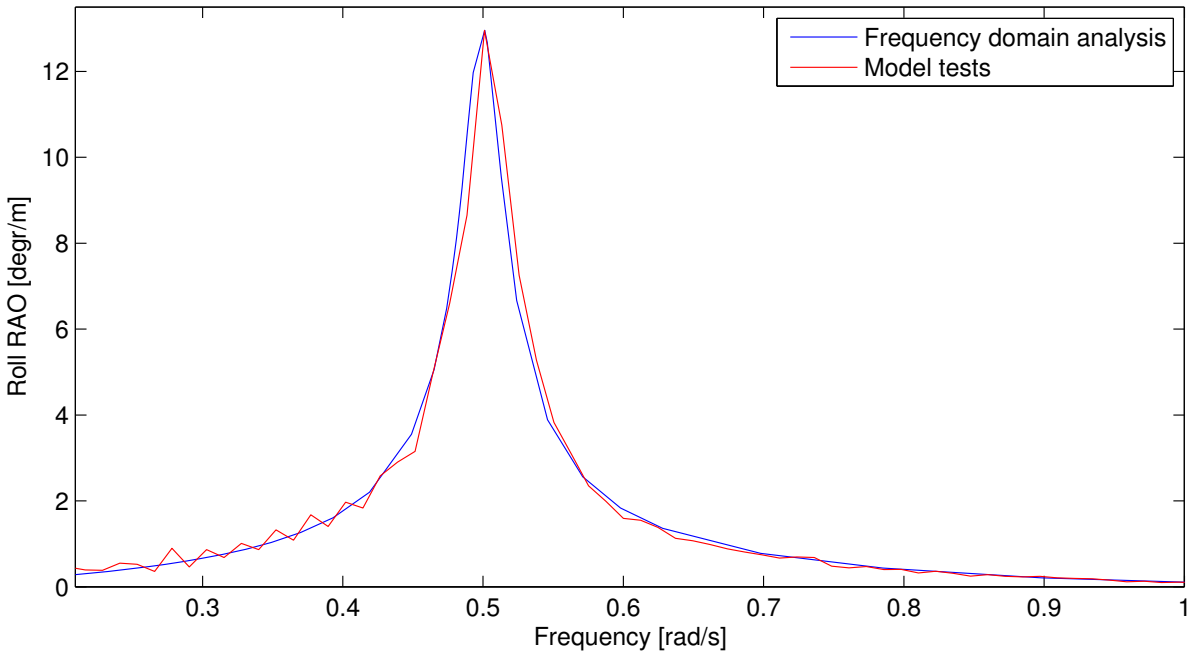

Figure 6.3: Ballasted case RAOs for beam waves with tuned roll radius of gyration.

The results clearly show great consistency between the frequency domain and scale model test results. Not only the natural frequency is predicted correctly, but also the the overall shape of the results match very well. The next step is to investigate the response of the barge with partially filled tanks.

6.1.2. Liquid cargo conditions

In this section the frequency domain results for liquid cargo are discussed and compared to the scale model test results. This is done for the 25, 50 and 75 percent loading condition. As for the ballasted condition a difference was found between the barge natural roll frequency found from the frequency domain approach and the scale model test results. Therefore the RAOs for heave and pitch are investigated and are shown in Figure 6.4 below.

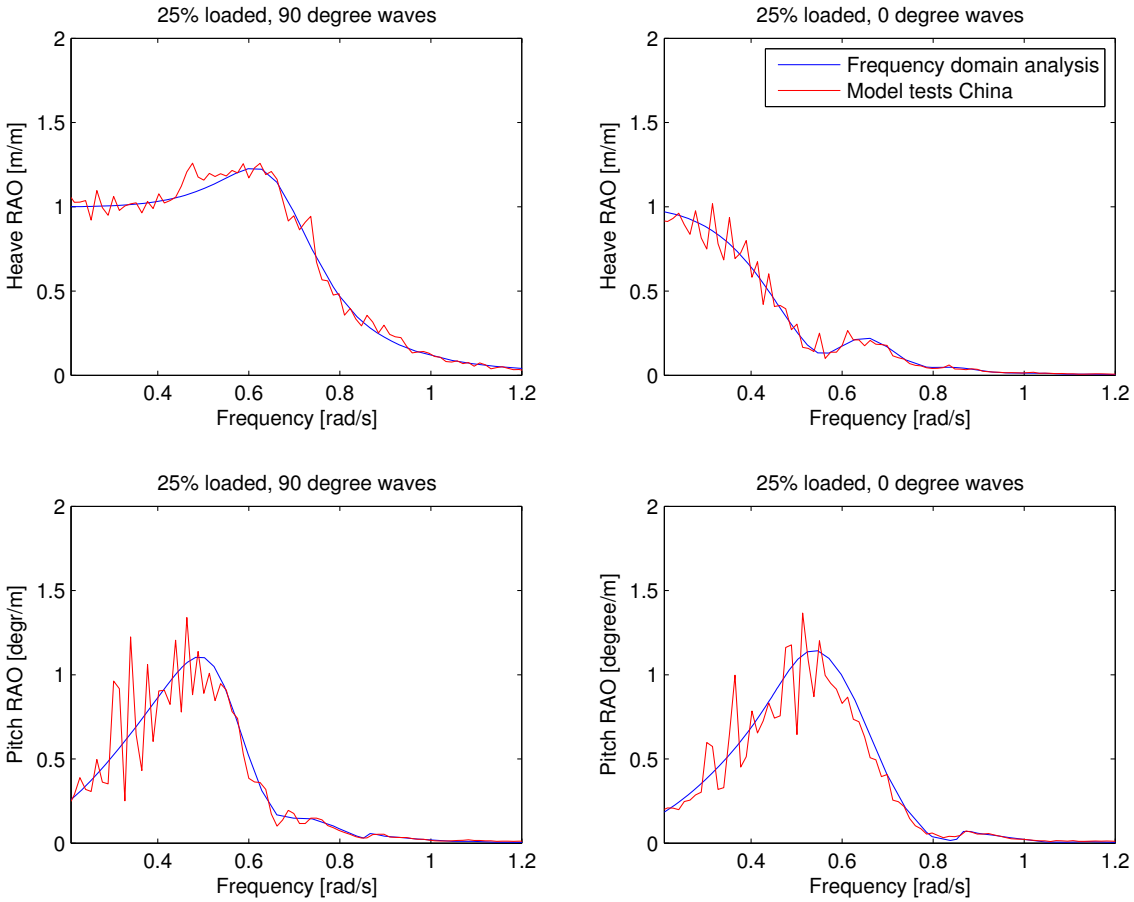

Figure 6.4: Results for heave and pitch for the 25% loading condition.

The results in Figure 6.4 clearly show that the agreement between the frequency domain and scale model test results is good for pitch and heave. This indicates that, just as for the ballasted condition, the difference in results are limited to roll. It is expected that the roll radius of gyration is not measured correctly. Therefore the roll radius of gyration has been corrected to match the natural frequency of the main roll RAO peak. The used roll radius of gyration are given in Table 6.2 below. A change in the roll radius of gyration did not have a significantly effect on the shape of the RAO curve. Also the location and height of the sloshing induced roll RAO peak is not significantly influenced by the choice of roll radius of gyration.

	Unit	**25%**	**50%**	**75%**
Measured	[m]	18.52	18.20	18.85
Corrected	[m]	19.56	19.14	19.08

Table 6.2: Measured and corrected roll radius of gyration for liquid cargo

Below in Figure 6.5 the roll RAOs are shown for the partially filled loading conditions, with corrected roll radius of gyration.

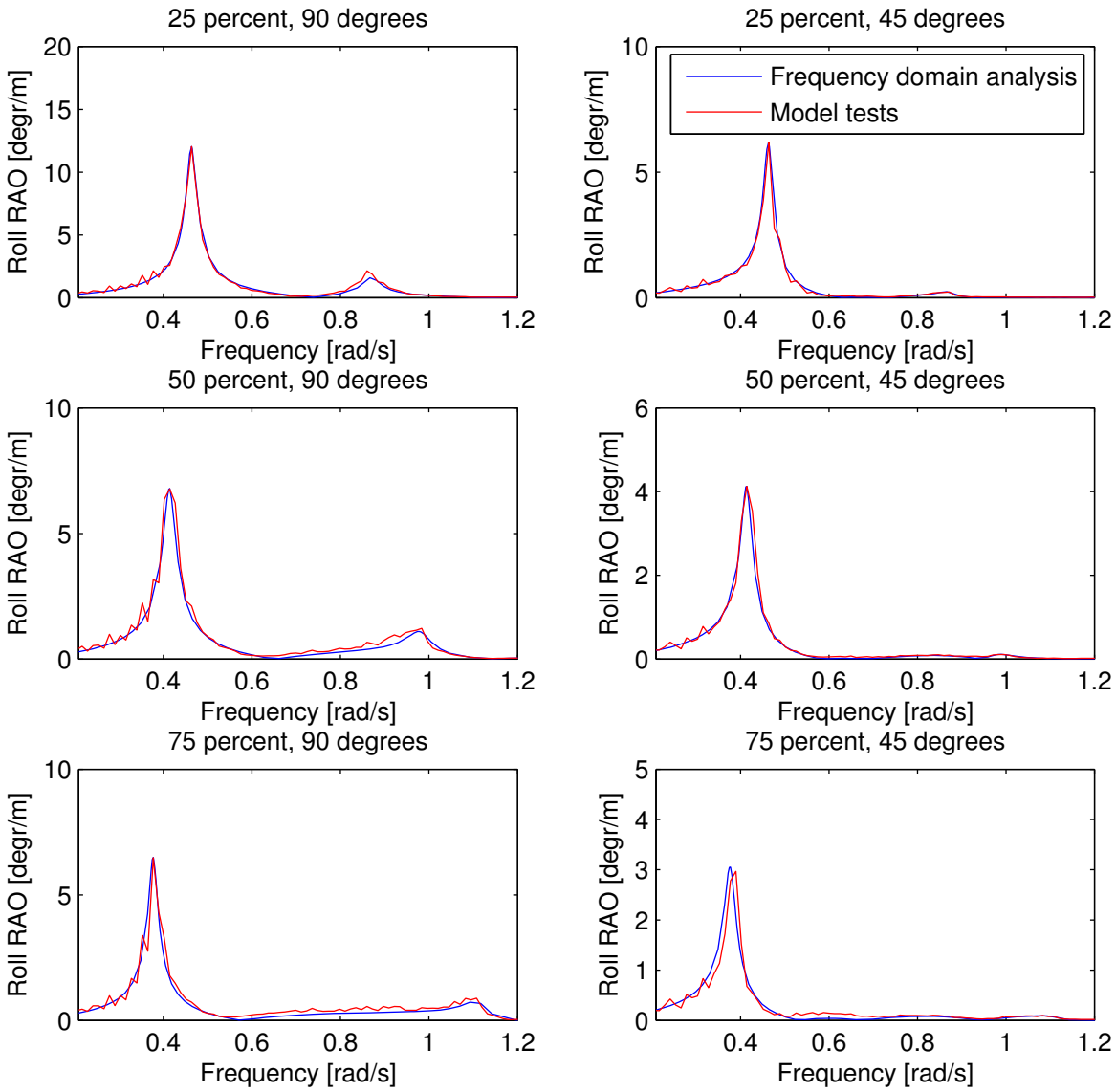

Figure 6.5: Model tests- and frequency domain analysis results for liquid cargo.

The results clearly show that the similarities between the two models are great. The location of the left peak matches very well, but this is mainly because of the corrected k_{xx}. The second peak however, is not significantly influenced by this. The overall shape of the results match very well. The second, sloshing induced roll RAO peak, is very distinctive for ship motions with partially filled cargo tanks and on first sight seems to be modelled accurately. Therefore in Figure 6.6 on the next page the results are shown with a focus on the roll RAO peak around the natural sloshing frequency. On page 58 the results are discussed in more detail.

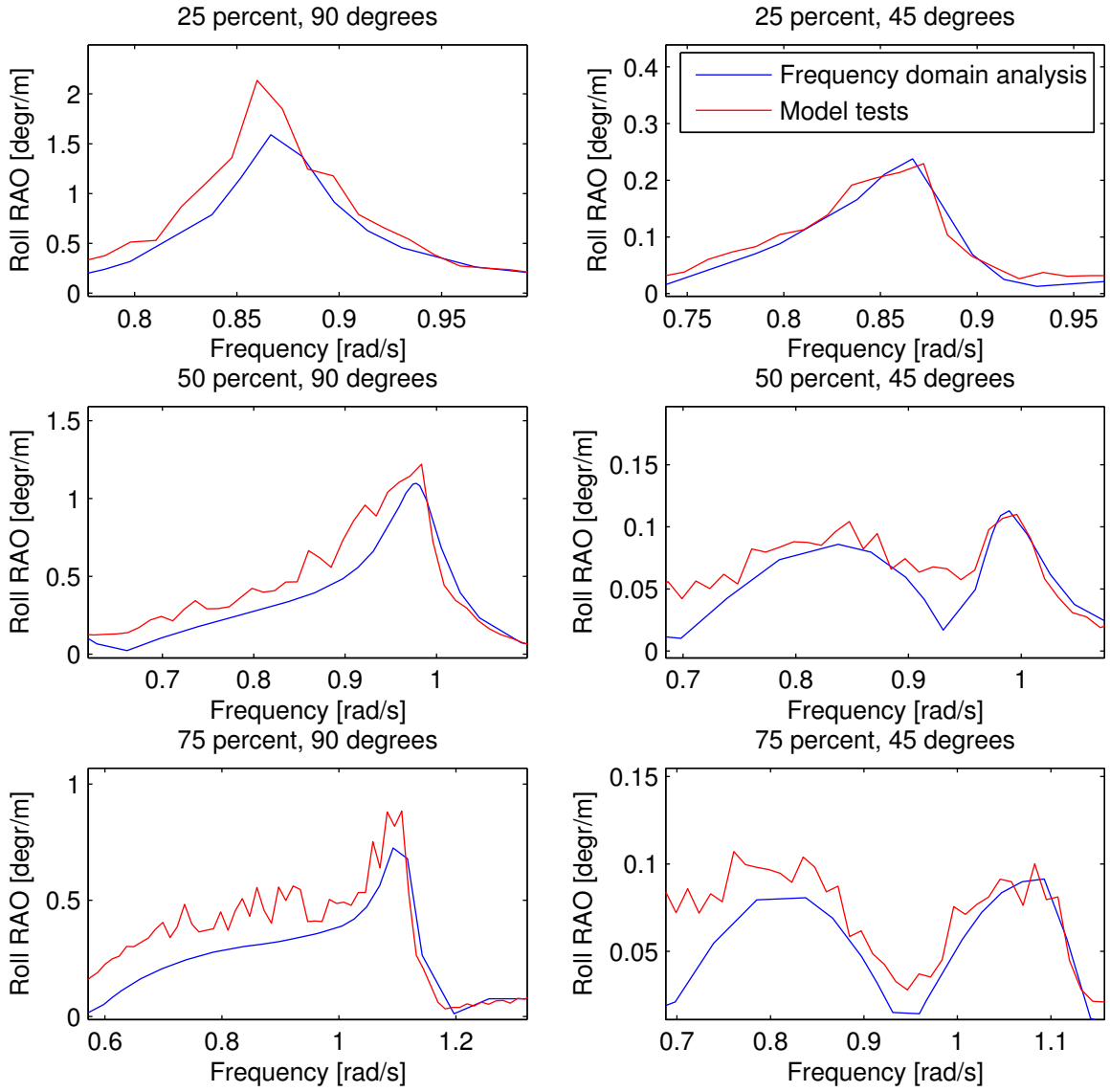

Figure 6.6: Model tests and frequency domain analysis results around natural sloshing frequency.

The results in Figure 6.6 clearly show that the height and location of the sloshing induced roll RAO peak are modelled with high accuracy for both 90 and 45 degree incoming waves. It is important to know that these results are not significantly influenced by the used roll radius of gyration of the barge.

In Figure 6.5 the roll RAOs are given for the 25, 50 and 75 percent loading condition, for 45 and 90 degree incoming waves. In Figure 6.6 the same is shown, but with a focus on the sloshing induced roll RAO peaks. A number of observations can be made from the results:

- In contrast to the results for the ballasted condition, now two roll peaks are observed for the partially filled spherical tanks;
  1. The first (left) peak occurs around the natural frequency of the barge
  2. The second (right) peak occurs around the natural sloshing frequency

  This was expected based on the results found in the literature study for rectangular tanks, for example by Molin et al. (2010). Now it is also shown that both peaks can be modelled accurately in the frequency domain.
- The roll RAO peak around the natural frequency of the barge is consistently lower for bow quartering waves compared to beam waves.
- The roll RAO peak around the natural sloshing frequency almost completely disappears for bow quartering waves compared to beam waves.
- The frequency of the second response peak, connected to the sloshing in the tank, is predicted very well. The height of this peak following from the frequency domain analysis is slightly underestimated compared to the model test results. Explanations for this could be:
  1. Uncertainty of the RAOs obtained from the model tests
     The RAOs from the model tests are obtained by performing a spectral analysis. This type of RAO analysis creates a significant uncertainty in the results. Furthermore, the equipment used in the scale model test is al subject to a certain level of uncertainty. Also the frequency domain analysis is subject to uncertainty, for example due to the mesh size chosen. This will be further discussed in section 6.5.
  2. Effects of linearisation
     The results from the frequency domain approach are all under linear assumptions. From the model tests we know that in fact sloshing is non-linear and creates non-linear ship motions. Therefore the RAOs obtained from model test are very much depending on the wave height in which they were obtained, while this is not the case for the frequency domain approach that only has one linear solution. Therefore the agreement between the scale model tests- and frequency domain results depends largely on the wave height chosen during the scale model tests. Also, due to the linearised boundary conditions in the tank only odd sloshing modes are taken into account in the frequency domain Bunnik and Veldman (2010). Although very small, this may have an influence on the roll motions of the ship.

To conclude the partially filled loading conditions with liquid cargo. Figure 6.6 showed that the frequency of the sloshing induced roll RAO peak is predicted very well by the frequency domain analysis, all frequencies found are in a 1.15% margin compared to the model tests results. The height of the roll RAO peak induced by sloshing modelled in the frequency domain underestimates the results compared to the model tests in the range of about 14- 25%. Furthermore, the overall shape of the frequency domain solutions show great similarities with the model test results. Together with the short calculation times the frequency domain proofs to be a good approach to model the effect of sloshing on ship motions.

6.1.3. Comparison frozen vs liquid cargo

In the previous section it was shown what type of roll motions can be expected when sloshing in the internal spherical cargo tanks occurs. However, this does not directly answer the question: what is the effect of sloshing on ship motions. To investigate this in more detail the liquid cargo was assumed to be frozen and therefore cannot slosh. This was modelled by calculating the inertia due to the frozen cargo and adding this to the mass matrix of the barge, see section 2.5.1 for more details. The resulting mass matrix is shown below in Equation 6.2 (in tonnes, tonnes m and tonnes m^2).

$$\boldsymbol{M} = \begin{bmatrix} 1.00\text{E}5 & 0 & 0 & 0 & 2.06\text{E}4 & 0 \\ 0 & 1.00\text{E}10^5 & 0 & -2.06\text{E}4 & 0 & 0 \\ 0 & 0 & 1.00\text{E}5 & 0 & 0 & 0 \\ 0 & -2.06\text{E}4 & 0 & 2.84\text{E}7 & 0 & 0 \\ 2.06\ \text{E}4 & 0 & 0 & 0 & 4.08\text{E}8 & 0 \\ 0 & 0 & 0 & 0 & 0 & 4.10\text{E}8 \end{bmatrix} \tag{6.2}$$

By using the mass matrix from Equation 6.2 the following frequency domain solution was found for the frozen cargo:

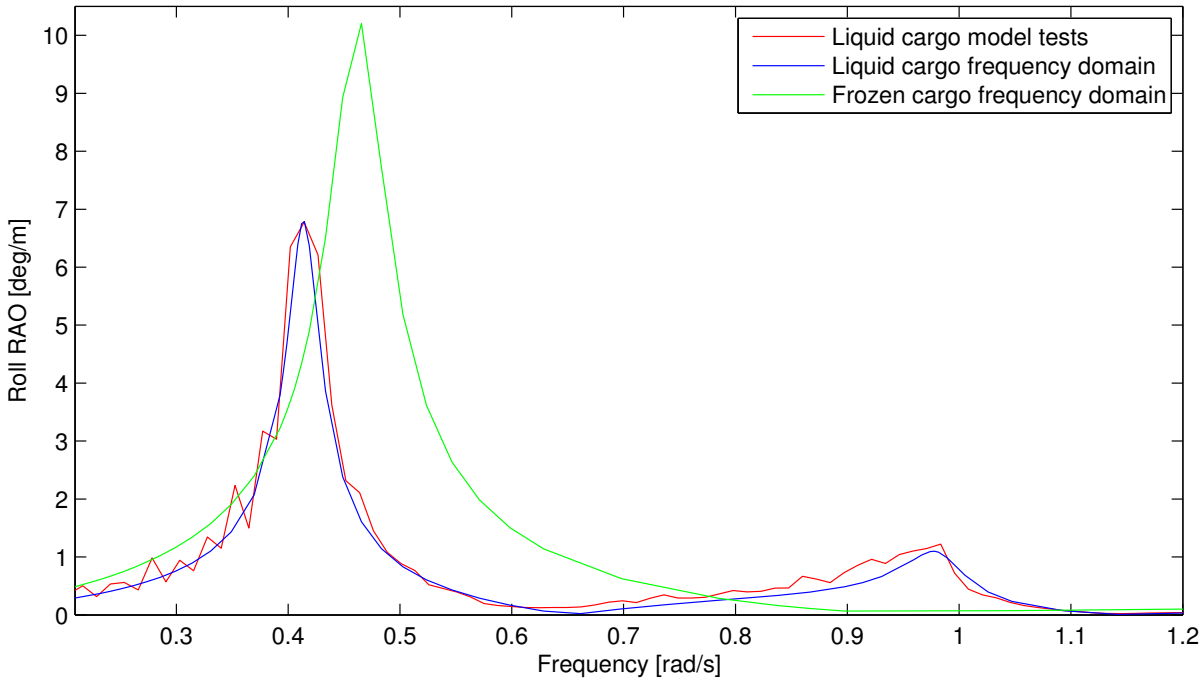

Figure 6.7: Frozen vs liquid cargo for the 50% loaded condition from frequency domain analysis

The results clearly show that frozen cargo results in a higher roll RAO peak around the barge natural frequency, and that this peaks occurs at a higher frequency. The shift in frequency was expected by the literature study performed, and was for example shown by Molin (2008) for membrane type tanks. Now it also shown that this occurs for spherical tanks. This proofs that sloshing of the cargo actually damps the roll motions of the barge around the barge natural frequency, rather than increasing it. The results also shown that sloshing creates a lower natural frequency due to a loss of hydrostatic stability. This is beneficial as it brings the natural frequency further away from commonly experienced sea states. Obviously there is no sloshing induced RAO peak for the frozen cargo, as is the case with liquid cargo.

6.1.4. Influence of wave direction

This section will describe the influence of the wave direction on the main and sloshing induced roll RAO peak. Based on the model tests it is known that the sloshing induced RAO peak almost disappears from beam quartering waves. This has been modelled successfully in the frequency domain as was shown in section 6.1.2. However, more information on the influence of wave direction is not available from the model tests. In this section the influence of wave direction is further investigated for all possible wave directions in intervals of 5 degrees.

In Figure 6.8 two polar plots are given for the 25% loading condition. The left polar plot shows the height of the main roll RAO peak. The right polar plot shows the height of the sloshing induced roll RAO peak.

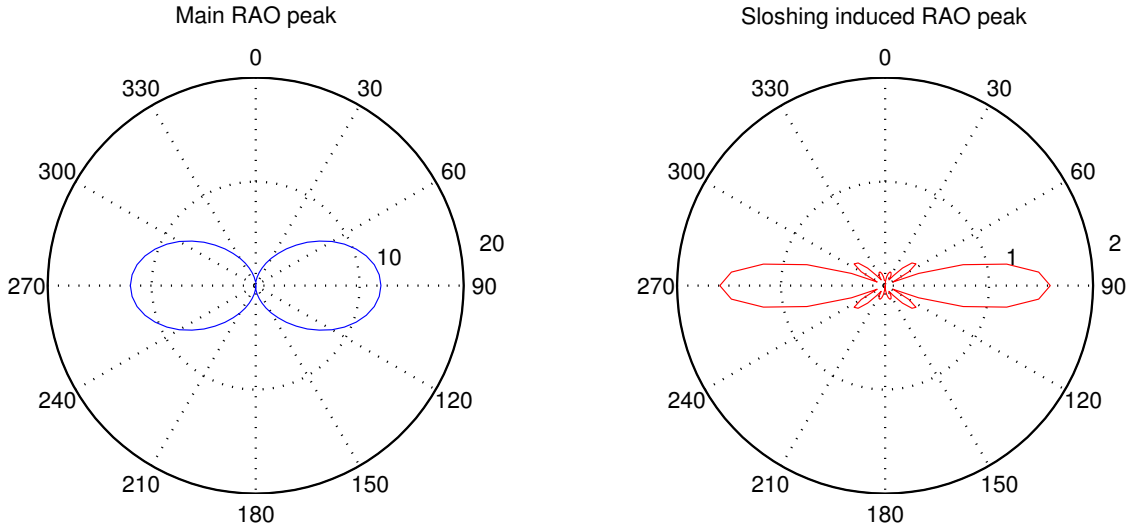

Figure 6.8: Influence of wave direction on the height of the RAO peaks for the 25% filling condition.

Figure 6.8 shows that the height of the main RAO peak is significantly influenced by the wave direction. This was already known from the literature for vessels with no cargo tanks, but is now also shown for partially filled spherical cargo tanks. The influence of wave direction on the height of the sloshing induced RAO peak was not yet known, but is clearly shown in the above results. The height of the sloshing induced roll RAO peak is even more influenced by the wave direction than the height of the main roll RAO peak. The height of the sloshing induced RAO peak has already decreased by 50% for 75 degree incoming waves, compared to 90 degree incoming waves. For 65 degree incoming waves and lower the sloshing induced roll RAO peak has almost completely disappeared.

There are three main explanations for this. The first one is that for for 45 degree waves the barge may start to yaw. Because of yaw the sloshing in the two tanks are getting out of phase with each other, decreasing the sloshing induced roll. The second explanation is that for 45 degree incoming waves the roll and sway of the barge are smaller, and smaller sloshing loads are therefore expected. The third and final explanation is that for 45 degree waves the sloshing does not occur from starboard to port side, but also under an angle creating a smaller moment around the x-axis.

6.1.5. Influence of tank size on roll response

This section will describe the influence of the tank size on the roll response of the barge. This could be of interest as the spherical LNG tanks on board Moss carriers have a different radius than the (full scale) spherical tanks used in the model tests. However, to make a good comparison between different tank sizes a number of properties of the barge and tank must be taken into account:

- The total mass of the system must be preserved to make a good comparison. This means it is not possible to use the same density of the cargo, as this would change the total mass of the system for a different tank size. During the model tests water with a density of 1000 kg/m3 was used as cargo. Therefore LNG, with a density of 435 kg/m3, was used as cargo to investigate the influence of the tank size. Once the density was known the tank radius could be calculated for 3- or 4 spherical tanks on board.
- The centre of mass of the cargo in the tanks must also be preserved. Therefore the locations of the tanks is changed so that for every tank size used the centre of mass is the same. This was done for the vertical, transverse and longitudinal centre of mass.

The results of this analysis are shown for the 50% loading condition in Figure 6.9 below.

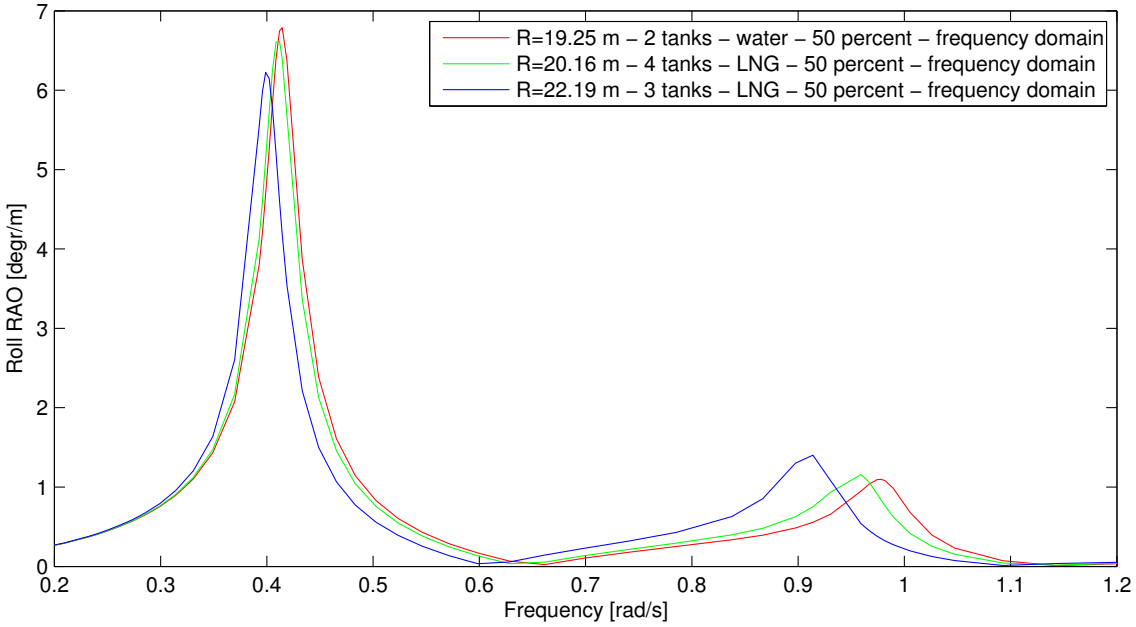

Figure 6.9: Influence of tank size for the 50% filling condition, 90 degree waves.

The results clearly show that for increasing tank size:

- The main response peak decreases in size and moves to a lower frequency
  For an increasing tank radius the moment around the x-axis due to sloshing becomes larger relative to midship, and therefore the influence of sloshing becomes more significant. This supports the hypothesis that sloshing damps the roll motions around the barge natural frequency.
- The sloshing induced roll RAO peak increases in size and moves to a lower frequency
  From McCarty and Stephens (1960) was known that the first mode natural sloshing frequency decreases with increasing tank size. This is also seen in the results presented here. Furthermore, as was explained above; the moments due to sloshing around the x-axis become larger for increasing tank size. The right peak is induced by the sloshing. A larger moment due to sloshing is therefore expected to create a larger roll response.

6.2. Computational Fluid Dynamics

To validate the ComFLOW model only, validation has to be done without taking into account the coupling with aNySIM. This is done in two ways:

1. Comparison between the first two natural sloshing modes and frequencies with sloshing experiments performed by McCarty and Stephens (1960). See section 6.2.1 for more details.
2. Comparison of the videos made during the scale model tests with the ComFLOW output. The motions of the tanks are taken from time traces from the scale model tests. See section 6.2.2.

6.2.1. First two sloshing modes- and frequencies

Validation of the model would ideally be done against model tests during which forces are measured. Currently no solid information about this was identified and therefore an initial validation will be done by considering the natural sloshing frequencies. This is done by reproducing some of the experiments done by McCarty and Stephens (1960).

During one of the experiments performed by McCarty and Stephens (1960) a small spherical tank was excited by a horizontal sinusoidal motion. If the liquid in the tanks is excited at its natural frequency and the external excitation is suddenly removed then the liquid in the tank will move in that specific mode until it is damped out. This only happens when the natural sloshing frequency of a mode is approached very closely, otherwise some other modes will intervene and change the free surface motion. This is difficult with a CFD model, as it takes a while to find the right frequency and run it again. Furthermore, the experiments were done on a small scale and are extrapolated to full scale by simple scaling laws. Therefore a good result would already be if mainly one sloshing mode is observed in the results. From the experiments by McCarty and Stephens (1960) the following dimensionless frequency parameters λ_n and natural sloshing frequency ω_n were obtained:

	λ_n [-]	ω_n [rad/s]
First mode	1.25	0.89
Second mode	2.30	1.65

Table 6.3: Natural sloshing frequencies for R=19.25 meter (McCarty and Stephens, 1960)

The dimensionless frequency parameter λ_n is used to define the relationship between the (approximate) natural sloshing frequency ω_n, the tank radius R and the gravitational acceleration g:

$$\lambda = \omega_n \sqrt{\frac{R}{g}} \tag{6.3}$$

$$\omega_n = \lambda \sqrt{\frac{g}{R}} \tag{6.4}$$

The goal of this part of the validation was to induce the first two free surface modes that were observed during an experiment. The results are shown below in Figure 6.10. From the results follows that the first two sloshing modes were successfully induced during the simulation. This gave a first indication that the CFD model is working correctly.

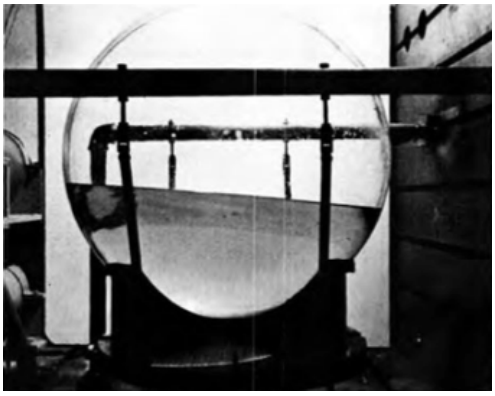

(a) First mode (McCarty and Stephens, 1960)

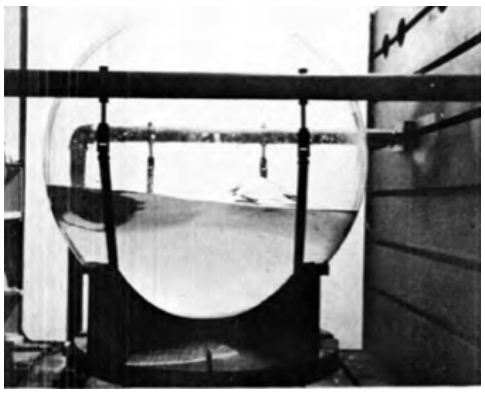

(b) Second mode (McCarty and Stephens, 1960)

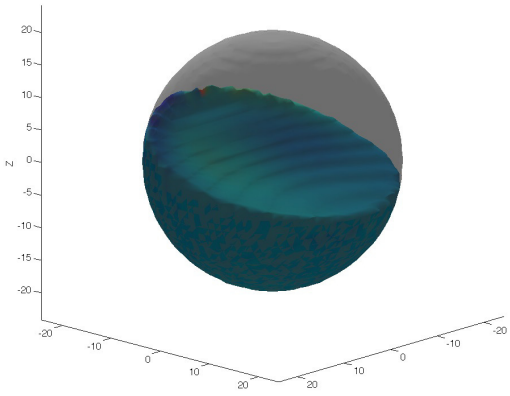

(c) First mode 3D (0.89 rad/s)

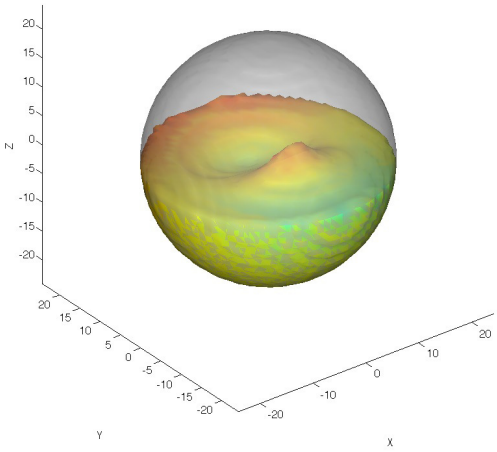

(d) Second mode 3D (1.65 rad/s)

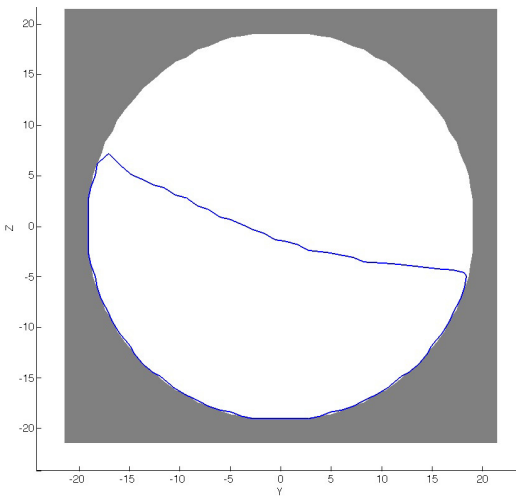

(e) First mode 2D (0.89 rad/s)

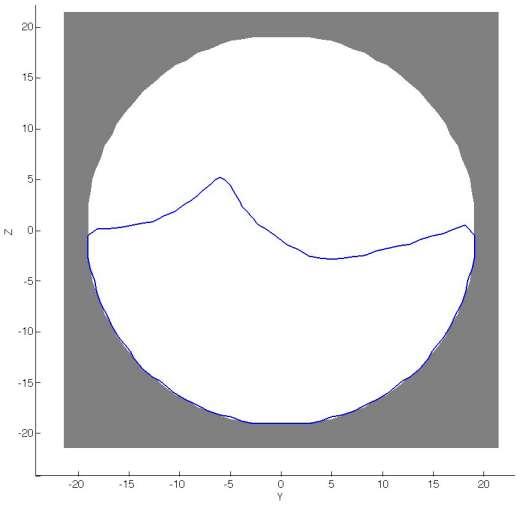

(f) Second mode 2D (1.65 rad/s)

Figure 6.10: First two sloshing modes from experiments and the ComFLOW simulations

6.2.2. Comparing ComFLOW results with scale model test videos

In this section videos recorded during the scale model tests are compared with a visualisation of the results of the ComFLOW simulation. This is done by using the time trace of the barge during the scale model test shown in the videos. This is done for the following (wave) conditions:

Loading cond.	**Direction [deg]**	ω **[rad/s]**	**Amplitude [m]**
25%	90	0.48	3.0
50%	90	0.84	7.0
75%	90	1.01	1.5

Table 6.4: Wave conditions used for comparison of the model test- and comflow videos.

In Figure 6.11 on the next page screenshots are shown taken from the videos of the scale model tests in China and from a visualisation of the ComFLOW results. This is done for the 25, 50, and 75 percent loading conditions. The similarities in bulk movement of the liquid in the tanks for the different filling conditions can be clearly seen.

The 25 percent filling conditions with the considered environmental conditions (Table 6.4) clearly shows a very flat free surface in both the scale model tests and the ComFLOW results. Also the height that the liquid reaches is the same in both videos. In time the shape of the free surface stays roughly the same, but the height peak of the free surface is moving from left to right with a frequency close to that of the waves that are exciting the vessel. This is observed in both the scale model test video as the ComFLOW results.

The 50 percent loading conditions shows a much more chaotic free surface. In this case the peak in the free surface is not moving from port to starboard, but is swirling around the tank with a frequency close to that of the waves. This type of sloshing is found in both the scale model tests and in the visualisation of the ComFLOW results.

The 75 percent filling conditions shows small waves in the tank that are very chaotic. This is observed in both videos. Finally the observations from both videos are quantified by considering their observed sloshing frequencies in Table 6.5 below.

Loading cond.	ω **model tests [rad/s]**	ω **ComFLOW [rad/s]**
25%	0.46	0.48
50%	0.89	0.92
75%	1.01	1.00

Table 6.5: Comparison of observed sloshing periods

In conclusion, both videos show the same bulk moment of the liquid in the tank for all considered filling conditions. Also the observed sloshing frequencies are very close together. Together with the validation in Chapter 6.2.1 this gives a trustful indication that the CFD model is working correctly and that it can be used in the coupling with aNySIM.

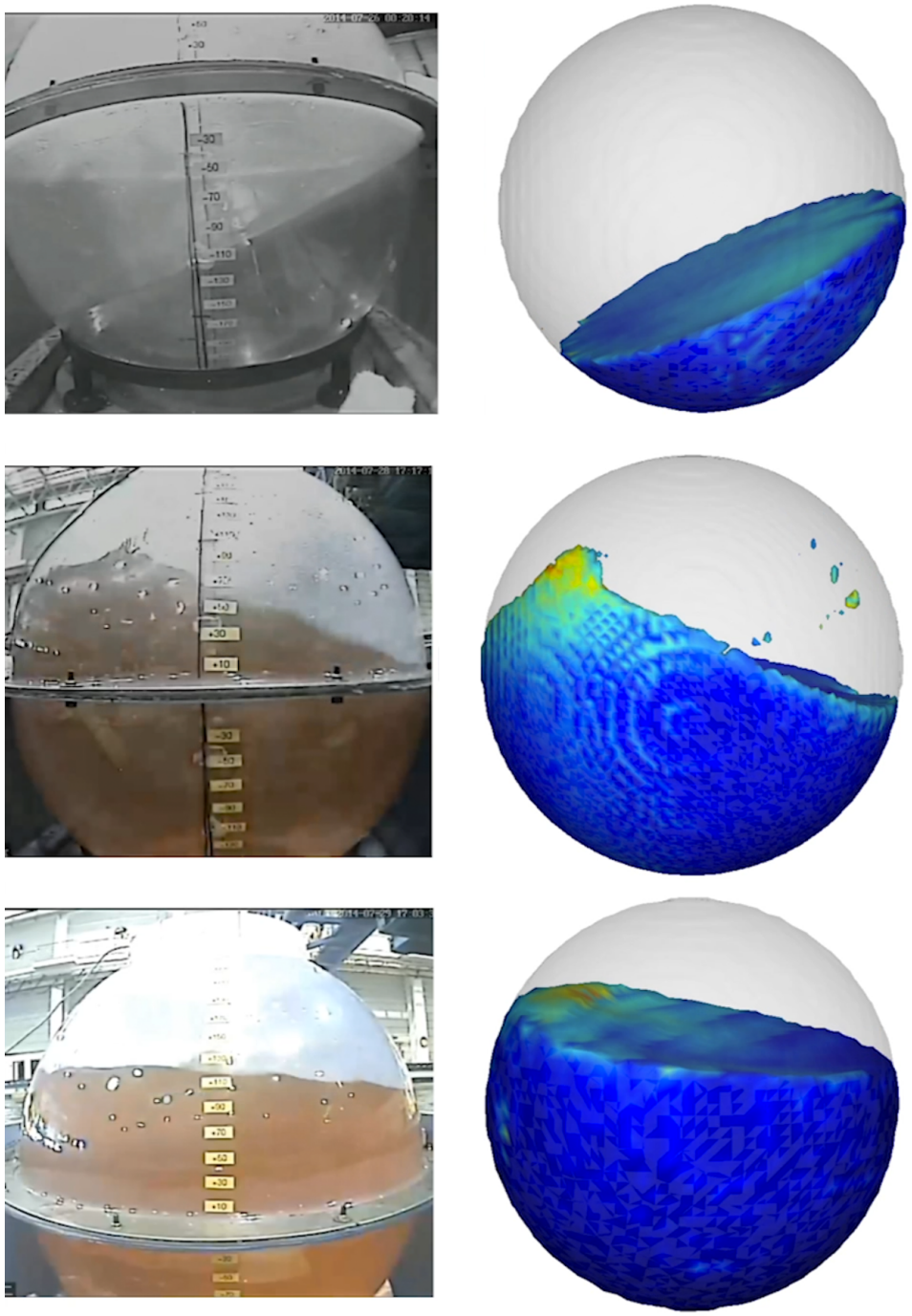

Figure 6.11: Model test (left) and ComFLOW (right) results for the 25, 50 and 75 percent loading condition

6.3. Ship motion model

In this section the ship motions model in aNySIM is validated. This is relevant as it is important to be confident in the ship motions model itself, before it is coupled to aNySIM at a later stage. First the mooring system will be discussed in section 6.3.1 followed by investigating the motions of the barge for the ballasted condition in section 6.3.2.

6.3.1. Mooring system

To investigate if the mooring system is set up correctly (see section 4.7 for details of the mooring system) a sway decay test is performed. From a sway decay test the natural period of the mooring system can be obtained. This test has been done during the scale model tests, and has also been simulated in aNySIM. See Figure 6.12 for the results. The sway period (including mooring system) during the model tests was found to be 163.3 seconds. The sway decay test performed in aNySIM gave a sway period of 163.4 seconds, a difference of only 0.06%. Furthermore, the sway decay test was also used to identify additional sway damping that is not included in the frequency domain input and cannot be determined automatically by aNySIM. The additional sway damping of 240 kN·s/m was identified by matching the amplitudes. Based on the results of the sway decay test the mooring system in aNySIM is successfully validated against the scale model test.

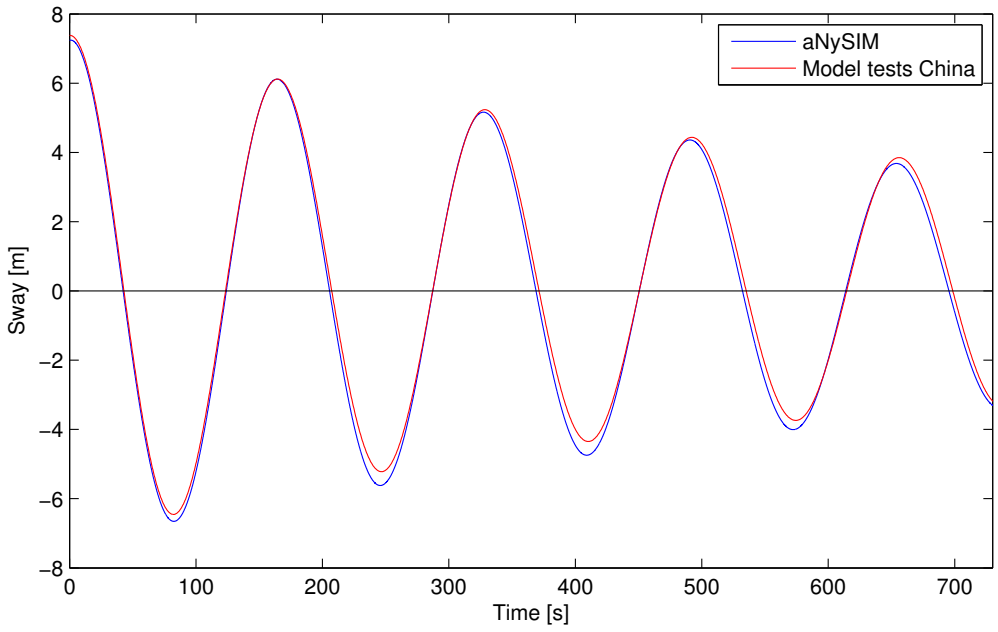

Figure 6.12: Sway decay test to validate the mooring system and sway damping in aNySIM.

6.3.2. Results for the ballasted case

This section will describe a number of tests to check if the aNySIM model is producing realistic results and can be assumed to be working correctly. All tests are done for the barge used in the scale model tests and the ballasted loading condition (no cargo in the tanks) will be considered. The sway decay test was already shown in section 6.3.1 by which the mooring system could be successfully validated. Other tests that will be discussed in this section are the still water test, static heel test and a roll decay test. Regular wave tests are discussed in section 6.3.3.

Still water and heave decay test

In the still water test is mainly checked if the buoyancy and the setup of the hydrostatics is modelled correct. The goal is to have zero heave in the still water test. The goal of the heave decay test is to investigate the natural heave period and to check the restoring force in heave by trying to induce a 1 meter heave by exciting the barge with a vertical force. From the WAMIT analysis the non-dimensional restoring heave coefficient was found to be 0.92. From this the restoring force can be calculated with:

$$\mathrm{C}(3,3) = \overline{\mathrm{C}(3,3)} \cdot \rho \cdot g \cdot \mathrm{ULEN}^2 \tag{6.5}$$

$$= 0.92 \cdot 1000 \cdot 9.81 \cdot 100^2 = 90252 \text{ kN/m} \tag{6.6}$$

Where ULEN is a length scale used in the WAMIT analysis. This means that if we apply 90252 kN we expect a heave of exactly 1 meter. To check this the barge is subjected to a gradually increasing vertical force of 90252 kN, after which the force is suddenly removed and the barge can freely move. The results are shown in Figure 6.13.

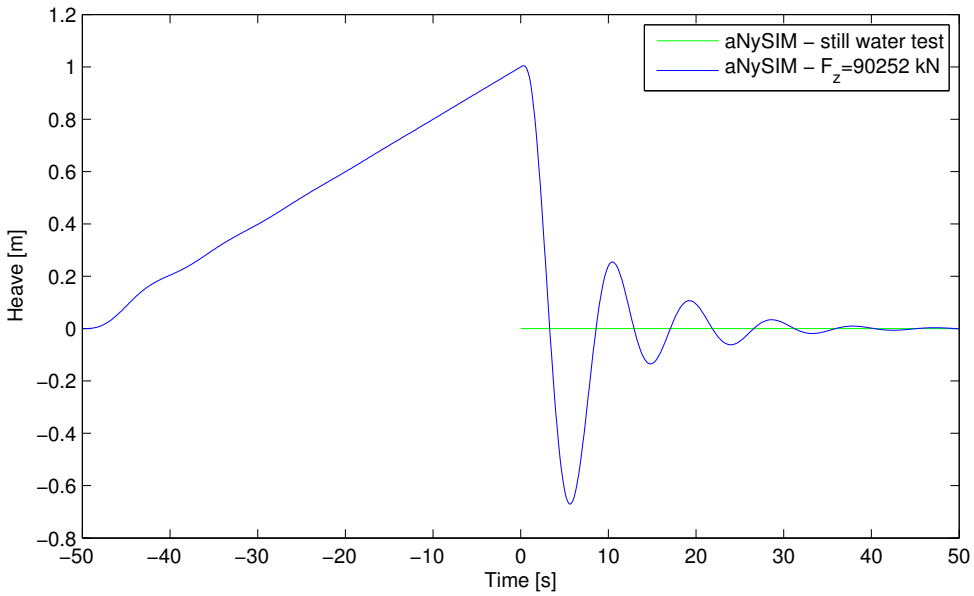

Figure 6.13: Still water, restoring force and heave decay test.

It can be clearly seen that in a still water test a heave of (very close to) 0 meter is found. When a vertical force of 90252 kN is applied a resulting heave of 1.0 meter is obtained. When the barge can freely move after t=0 a heave natural period of 10.1 seconds is found, while in the scale model tests 10.06 was found. A very good result and this test has been completed successfully.

Static heel- and roll decay test

In this test a static roll angle will be reached by exciting the barge with a roll moment around the x-axis, in other words a roll moment. After this the moment will be removed and the vessel can roll freely in its natural frequency. The necessary roll moment can be calculated with the following equations.

$$\mathrm{M_{roll}} = \rho \cdot g \cdot \nabla \cdot \mathrm{GM} \cdot \sin(\phi) \tag{6.7}$$

$$\mathrm{GM} = \mathrm{KB} + \mathrm{BM} - \mathrm{KG} \tag{6.8}$$

$$\mathrm{KM_T} = \mathrm{BM_T} + \mathrm{KB} \tag{6.9}$$

$$\mathrm{BM_T} = \frac{\frac{1}{12} \cdot L \cdot B^3}{\nabla} \tag{6.10}$$

Where ϕ is the required angle and is in this case equal to 8.7°. GM is the distance between the centre of gravity and the metacentric height, K is the keel, B the centre of buoyancy and ∇ is the displaced volume. By considering equations 6.7 to 6.10 $\mathrm{M_{roll}}$ can be calculated:

$$\mathrm{M_{roll}} = 1000 \cdot 9.81 \cdot 8.1475 \cdot 10^5 \cdot 11.91 \cdot \sin(8.7°) = 1.44 \cdot 10^6 \text{ kN/m} \tag{6.11}$$

When this is applied the response in Figure 6.14 is found.

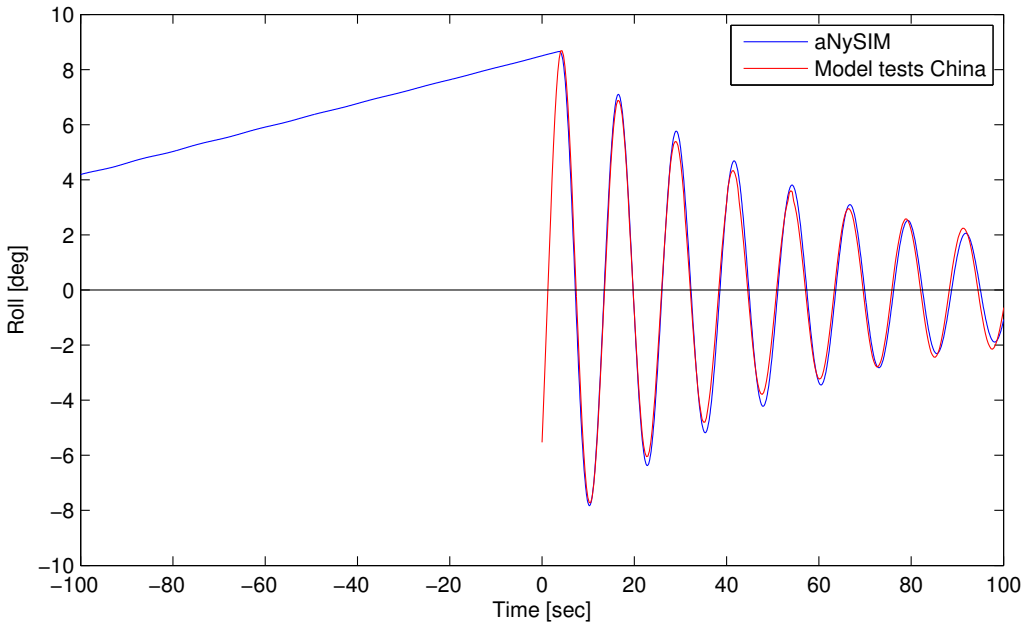

Figure 6.14: Static heel- and roll decay test.

It is clearly visible that the static heel test was completed successfully, a roll angle of 8.7 degrees has been obtained. The natural period found from the roll decay test with aNySIM is 12.55 seconds, while in the model tests this was 12.45 seconds; a very small difference of 0.8%. However, from the white noise wave tests during the scale model campaign a natural frequency of 12.54 seconds was found. This indicates that the type of testing has an influence on the natural frequency or that the uncertainty comes from the spectrum analysis to obtain the RAOs from the white noise tests. However, the difference is small and the aNySIM model is believed to be producing accurate results. The above roll decay test was obtained by considering a linear roll damping ($8.2 \cdot 10^5$ kNms/rad) and quadratic roll damping ($7.5 \cdot 10^5$ kNms^2/rad)

6.3.3. Regular waves

To validate the aNySIM model of the barge in waves, a series of regular wave cases are simulated in aNySIM and the results are compared to the RAOs obtained in the scale model tests. The results are shown below in Figure 6.15. It is immediately visible that the aNySIM results are very similar to the scale model test results. The only difference is that the response around the natural frequency is slightly underestimated, which is caused by the linear and non-linear damping that is not estimated completely correct from the roll decay test (see section 6.3.2) or by an overestimation of the RAOs by the cross-spectrum analysis based on the white noise test performed during the scale model tests. But overall the results show that the barge model in aNySIM is working very well and is hereby validated. The next step is to couple aNySIM to ComFLOW to include the partially filled spherical tanks in the analysis.

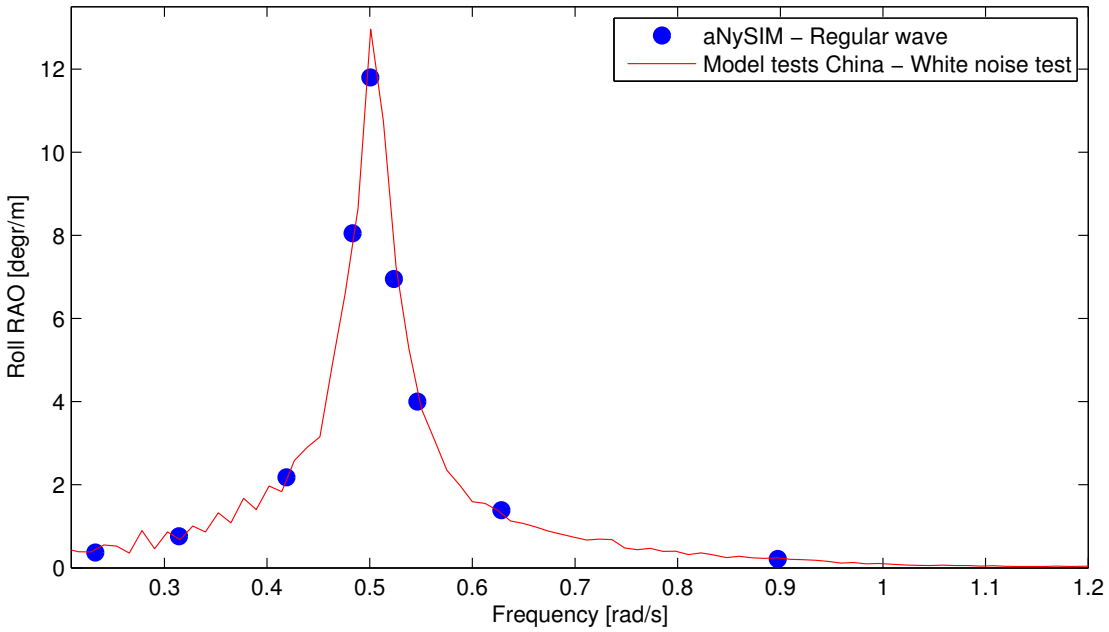

Figure 6.15: Validation of the aNySIM model of the barge in waves.

6.4. Coupled time domain model

In the last two sections the ComFLOW and aNySIM models have been separately discussed and validated. In this section the results obtained from the coupled aNySIM - ComFLOW model are discussed and validated against the scale model tests. The results of the coupled simulation are discussed for the 25, 50 and 75 percent loading condition (same roll radius of gyration is used as in the frequency domain approach). This is done by (1) comparing the roll decay tests and by (2) comparing the obtained RAOs in the coupled model with those found during the scale model tests. Additionally the developed coupled time domain model is used to investigate the frequencies in the coupled response (section 6.4.3), stability of the model (section 6.4.4), the influence of the communication time step between aNySIM and ComFLOW (section 6.4.5), additional interpolation methods that can be used in the coupling (section 6.4.6), non-linearity in the response (section 6.4.7) and the influence of the pump tower on the response of the barge (section 6.4.8).

6.4.1. Roll decay test

After the coupling was finished the first step was to perform a roll decay test. This gave insight in the natural frequency of the coupled systems and the necessary damping. In Figure 6.16 the roll decay test results are shown for the 25% filling conditions, obtained from the scale model tests and the coupled model. Figure 6.17 and 6.18 on the next page show the same for the 50 and 75 percent filling conditions.

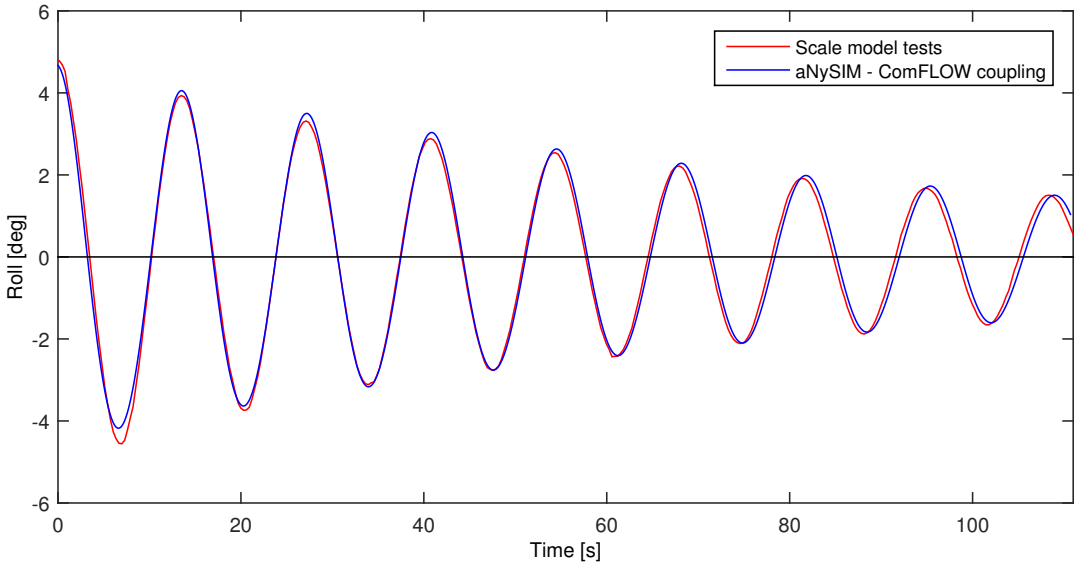

Figure 6.16: Roll decay test for the 25% filling condition.

The natural periods and damping coefficients obtained from the roll decay tests are shown in Table 6.6 below. The damping has been manually added to the external damping matrix of aNySIM to obtain a good agreement of the amplitudes found from the model test- and numerical results.

Filling condition [%]	**Model tests** [s]	**Coupled model** [s]	**Difference** [%]	**Linear damping** [kNms/rad)]	**Non-linear damping** [kNms^2/rad^2)]
25	13.54	13.65	0.76	4.03E5	7.5 E5
50	15.05	14.98	-0.47	3.70E5	7.5 E5
75	16.37	16.37	-0.02	4.15E5	7.5 E5

Table 6.6: Comparison of the natural periods found in the roll decay tests.

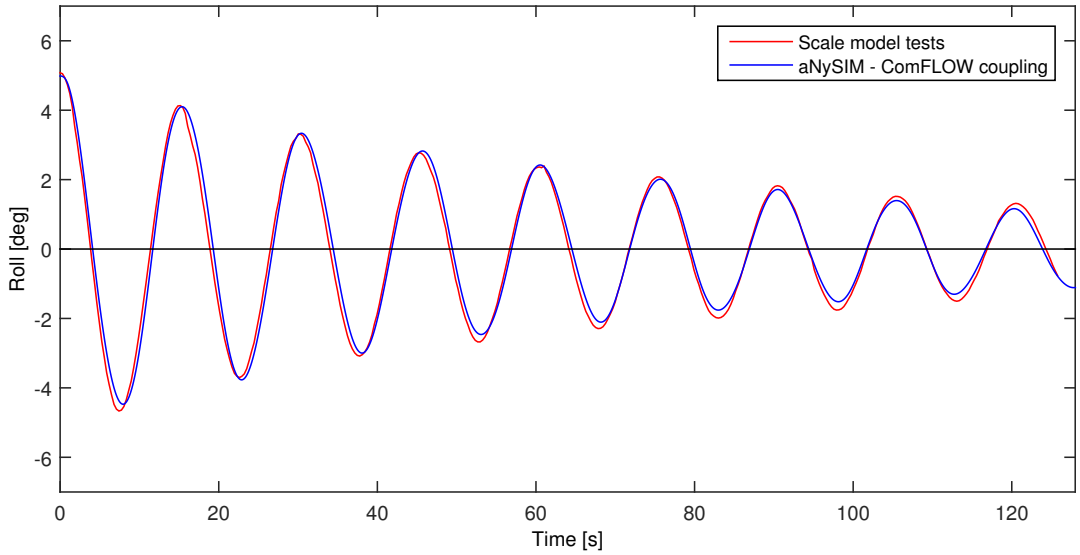

Figure 6.17: Roll decay test for the 50% filling condition.

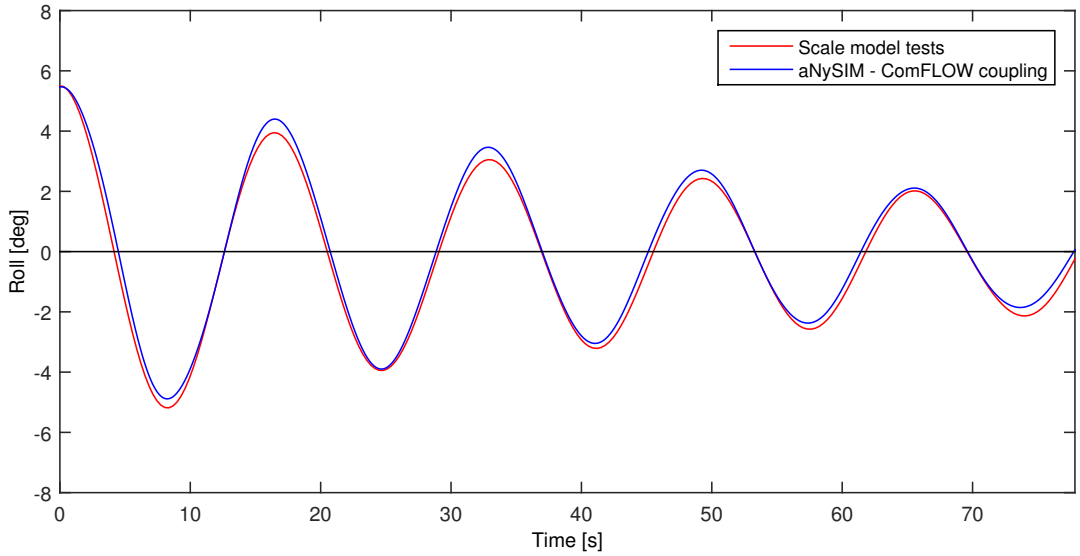

Figure 6.18: Roll decay test for the 75% filling condition.

Figure 6.16 to 6.18 all show the same trend; a great similarity between the aNySIM - ComFLOW coupling and the scale model test results. The natural frequency as well as the amplitude of the response are modelled very accurately. The damping used for this can be seen in Table 6.6. This creates a lot of confidence in the coupled model and the next step is to compare the RAOs obtained from the coupled model with those from the scale model tests.

6.4.2. Response Amplitude Operators

In this section the RAOs that have been determined in the scale model tests will be compared to the RAOs obtained from the coupled model by using regular waves. First the results for a 90 degree wave direction will be discussed, followed by the results for a 45 degree wave direction.

90 degree regular waves

Below in Figure 6.19 the results are compared for the 25% filling condition.

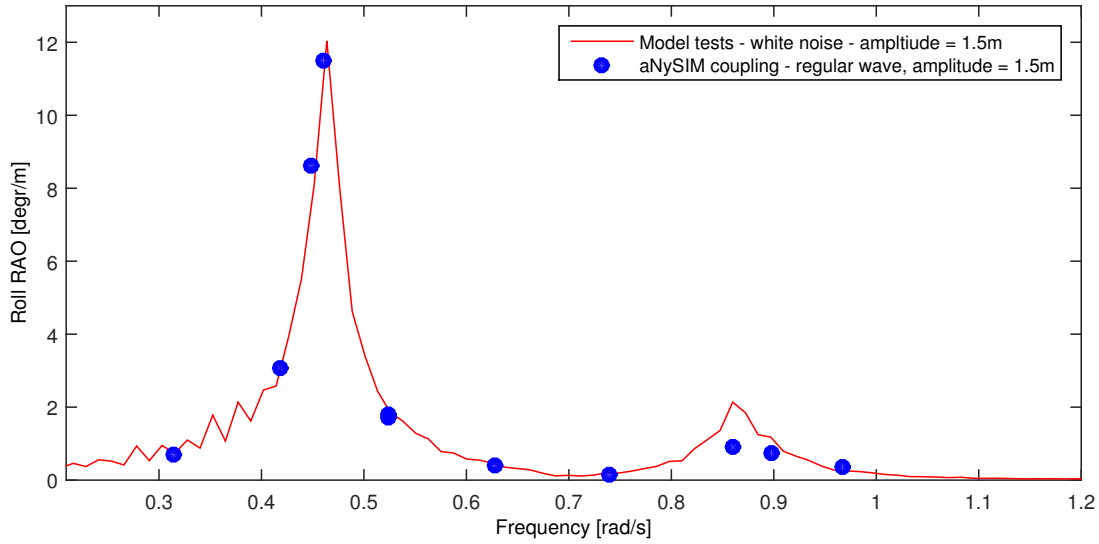

Figure 6.19: RAOs for the 25% filling condition.

It can be clearly seen that in general the results from the coupled aNySIM model match the results from the model tests well. However, natural frequency of the barge is slightly underestimated (by 0.75%), which was known from the roll decay tests and is well within the uncertainties that can be expected in such an analysis. The main peak is also slightly underestimated, which is explained by the amount of damping chosen based on the roll decay tests. Choosing the correct damping is a very sensitive and complex process, and considering the time it takes to do one roll decay tests with the coupled model already a very good damping value is believed to be chosen.

A more significant difference between the coupled model and the scale model tests is found around the sloshing induced roll RAO peak. This peak in the RAOs is underestimated with the coupled aNySIM - ComFLOW model. For this there may be four explanations:

- The main difference is caused by uncertainties in the results obtained from both the scale model tests and coupled time domain simulations. This will be discussed in section 6.5.
- The response of the coupled system (hull + tanks) is different in regular waves than would be expected based on a white noise test. This will be discussed after the results for 45 degree incoming waves.
- There is too much damping created by the coupling between aNySIM and ComFLOW. Especially the communication time step between aNySIM and the type of interpolation of the motions/forces in the coupling may have a significant effect. This is investigated in more detail in section 6.4.5 and 6.4.6.
- There is too much damping in ComFLOW. This has not been investigated in more detail.

For the 50% loading conditions the results are shown in Figure 6.20 below.

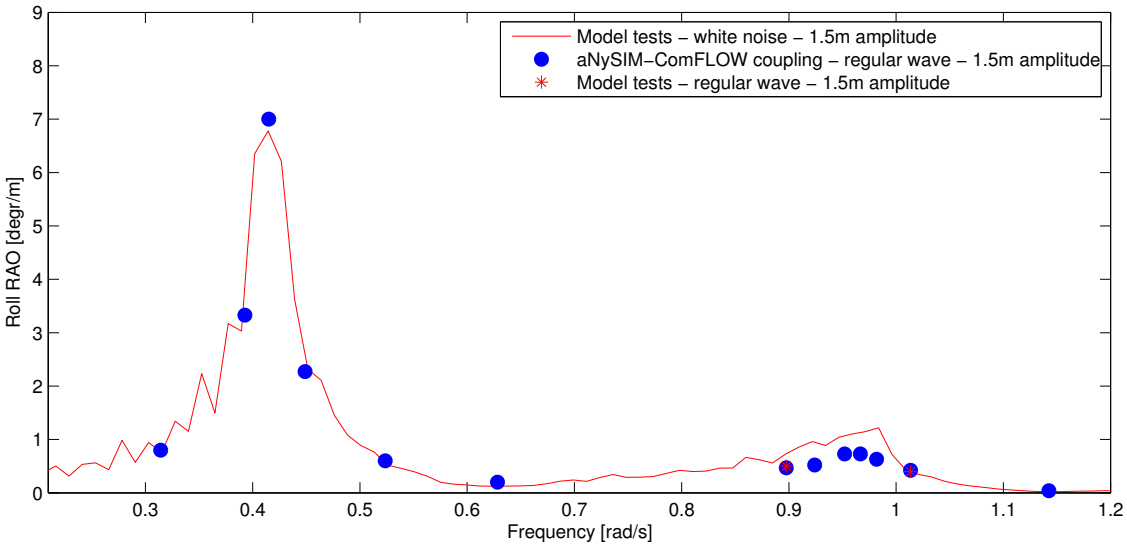

Figure 6.20: RAOs for the 50% filling condition.

It can be clearly seen that the results match well, but the response at the main peak is slightly overestimated in the coupled model, which is contributed to the amount of damping that is chosen based on the roll decay tests. The smaller sloshing induced peak is underestimated just as for the 25% loading condition. However, for comparison two regular wave tests that have been performed during the scale model tests are also included in the results (around 0.9 and 1.03 rad/s). The coupled model matches these results very well, which could indicate that the response of the coupled system is different for regular waves than would be expected based on white noise tests. The results for the 75% loading condition are shown below in Figure 6.21.

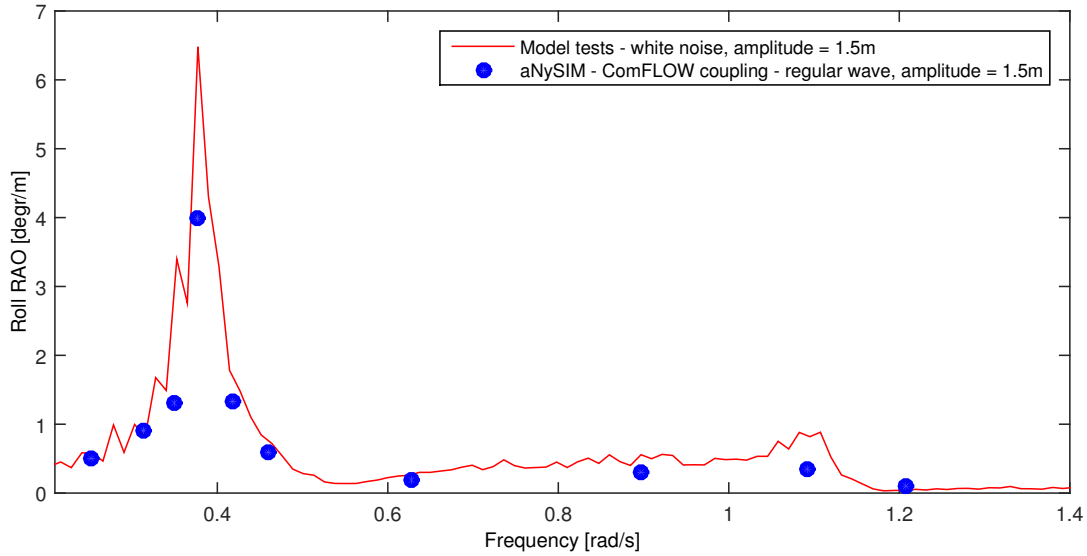

Figure 6.21: RAOs for the 75% filling condition.

The results for the 75% loading condition show that the main peak is underestimated, this may be partly because of the damping chosen. However, it is also expected that there is a lot of uncertainty in the RAOs obtained from the scale model tests. During the white noise tests in the scale model tests a maximum response period of 16.65 seconds was found. However, a roll decay test during the same scale model campaign resulted in a natural period of 16.37 seconds. The roll decay test with the coupled ComFLOW - aNySIM model also indicated a natural period of 16.65 seconds, while the maximum RAO from the coupled model was obtained from a regular wave with a period of 16.37 seconds. Therefore it is expected that the maximum response of the coupled aNySIM- ComFLOW model would also be at 16.37 seconds when regular waves are considered. To be able to give a good explanation of what causes these differences, first the response must be further investigated. For example by starting to consider a regular wave at 16.37 seconds. Due to time limitations this was not possible anymore for this project.

45 degree regular waves

The aNySIM - ComFLOW coupling has also been tested for beam quartering (45 degree) incoming waves. Both the results from the scale model tests for the 45- and 90 degree incoming waves are shown in Figure 6.22. It is clearly visible that for 45 degree waves the main roll RAO peak decreases significantly and that the sloshing induced peak almost disappears completely (see section 58 for an explanation). It was investigated if this could also be simulated by the coupled model, of which the results are included in Figure 6.22 below.

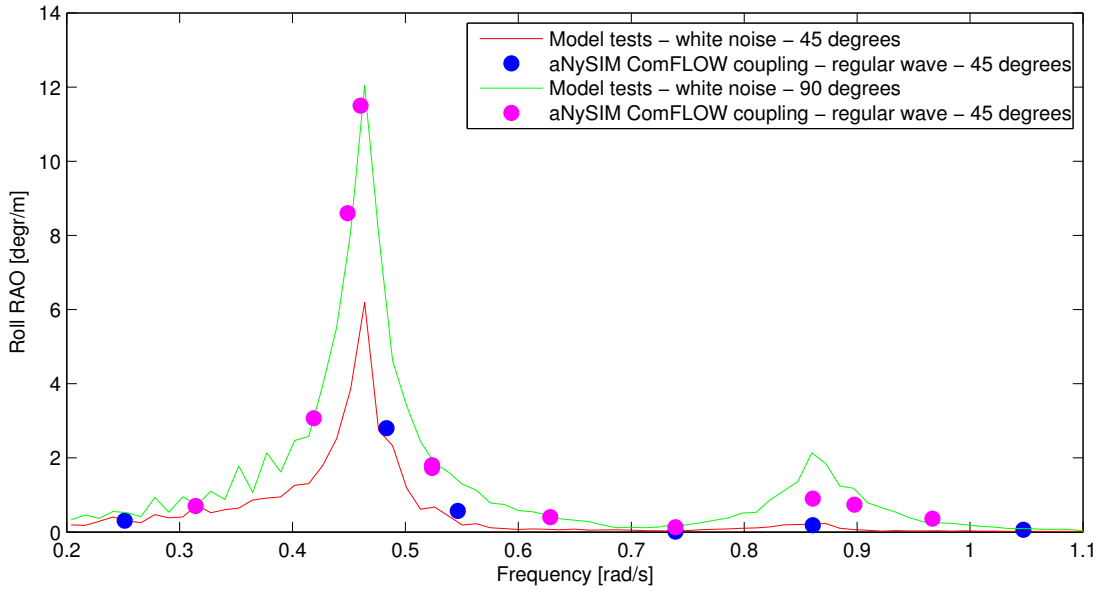

Figure 6.22: 45- and 90 degree incoming waves for 25% filling condition.

The results clearly show that the response is modelled correctly. Not many data point are available, but those that are available show that the sloshing induced roll RAO peak almost completely disappears in the results obtained from the coupled model. This gives a lot of confidence that the above discussed results are not obtained by luck, but that the coupled model consistently gives accurate results for different situations.

JONSWAP and white noise tests

As was discussed in section 6.4.2 the RAOs around the natural sloshing frequency were underestimated when the results from the model tests (white noise) and coupled model (regular waves) were compared. This can be because of uncertainty in the results or because of too much damping in ComFLOW, but can also be caused by the difference in response of the barge (including tanks) to regular- or white noise tests. Performing white noise tests with the coupled model is very time consuming, but may also give more insight in how vessel and tanks are responding to different types of environment. Therefore a white noise tests for one loading condition has been performed with the coupled model. On top of this also a JONSWAP irregular wave test was performed. Both the white noise- and irregular wave test simulated 2 hours of waves. Increasing the length of the test may slightly influence the results. All results are given in Figure 6.23 below.

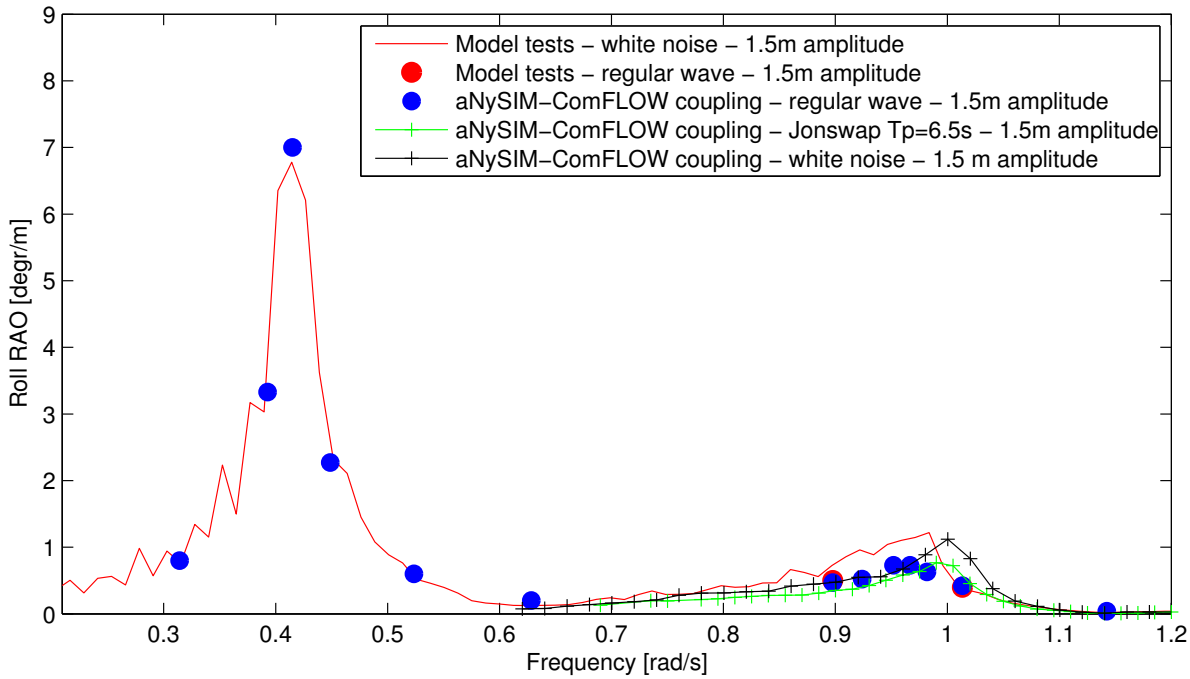

Figure 6.23: Regular, JONSWAP and white noise wave tests for 50% filling condition.

The results from the coupled model clearly show large differences between the different types of tests; regular, white noise and JONSWAP. When this is compared to the RAOs obtained in the model tests with a white noise tests a number of interesting observations can be made:

- RAOs determined from the white noise tests in the coupled model show a similar local maximum around the natural sloshing frequency when compared to the scale model test results. The difference between the frequencies of the local maxima is 1.75%, well within the uncertainty margins of the results.
- The RAOs determined from the regular wave tests are underestimated compared to the white noise test results.
- The RAOs determined from the JONSWAP irregular wave tests with a peak period of 6.5 seconds shows a trend comparable with that of regular wave tests.

Based on the observations it can be concluded that the RAOs found for the barge including partially filled tank are very much dependent on the type of test used, and frequencies in those tests. Two possible explanations are presented for this. The first is the effect of the inertia of the cargo. In case of regular waves the cargo is forced in one frequency (around the natural sloshing frequency) and may develop non-linear over time. This is expected to damp out the motions of the vessel. In case of a white noise test the cargo does not have the time to really respond to the frequencies close to the natural

sloshing frequency and develop non-linear. The second explanation is that during white noise tests not only the barge is exposed to many different wave frequencies with equal energy, but these frequencies are also introduced in the tank. So although the barge may be exposed to a certain wave frequency, that is taken into account in the Fourier transform to obtain the RAOs, there are still different frequencies present in the tank that are also contributing to the RAO but are not directly taken into account in the Fourier transform.

6.4.3. Frequencies in coupled response

When the response to regular waves is simulated with the coupled ComFLOW - aNySIM model it was initially expected that the response would also be regular. However, from analysing the time traces of the roll response it was identified that the roll response of the barge with partially filled tanks to a regular wave is irregular. This was checked by performing a Fast Fourier Transform on the roll response of the vessel in regular waves. This was done for 4 wave frequencies for the 50% filling conditions. These frequencies are:

- Natural sloshing frequency - 0.98 rad/s - 6.4 seconds
- 0.63 rad/s - 10 seconds
- 0.52 rad/s - 12 seconds
- Maximum response frequency (barge natural frequency) - 0.42 rad/s - 15.14 seconds

The results are shown in Figure 6.24 below.

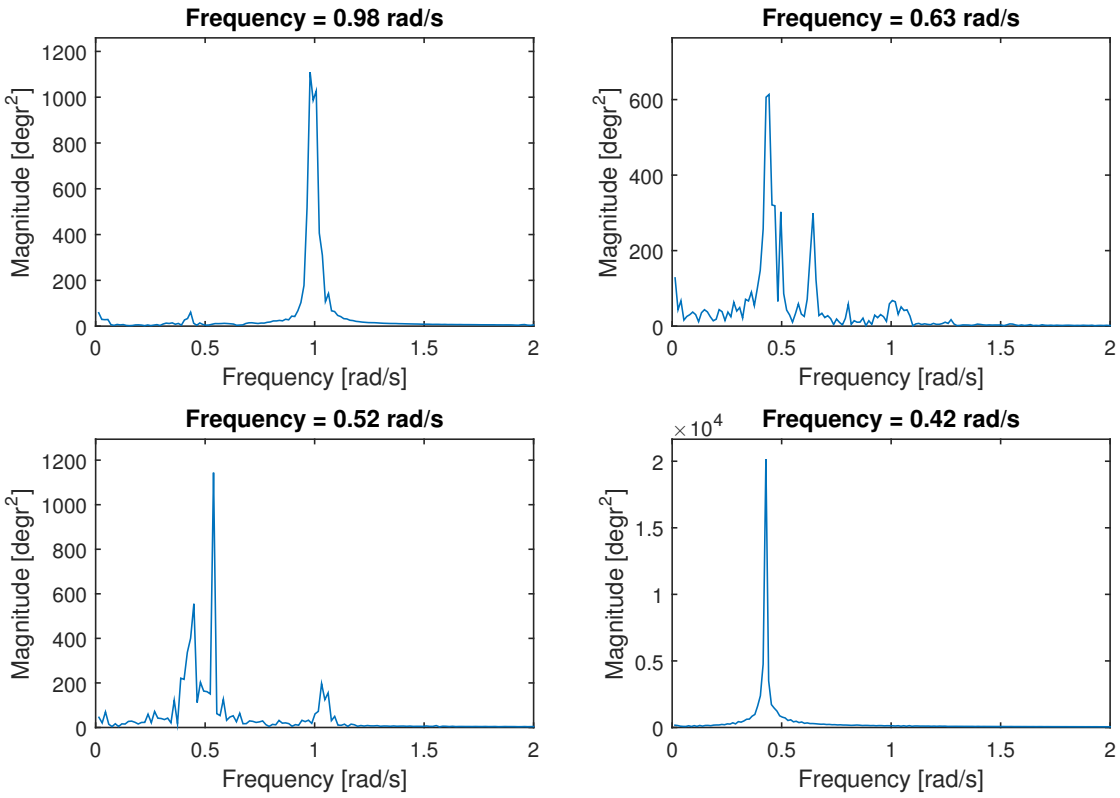

Figure 6.24: Response frequencies for regular waves for the 50% filling condition.

The results indicate that when the wave is close to the natural sloshing frequency or maximum response frequency the response of the vessel is more or less regular at the wave frequency. However, when the

vessel is excited at a frequency in between the natural sloshing- and maximum response frequencies than the response is irregular and several frequencies are present in the roll response. These frequencies are: the wave frequency, the natural sloshing frequency and the maximum response frequency. This is not the case for regular waves, where only the wave frequency is present in the output, regardless of what the wave frequency is.

6.4.4. Stability of the coupled response

The stability of the coupling has initially been tested in a still water test, static heel test, roll decay test and heave decay test. After this regular, white noise and irregular wave tests were performed to obtain the RAOs. A time trace of the vessel motions are shown in Figure 6.25 for a white noise test. This has been done with an aNySIM (and communication) time step of 0.1 seconds.

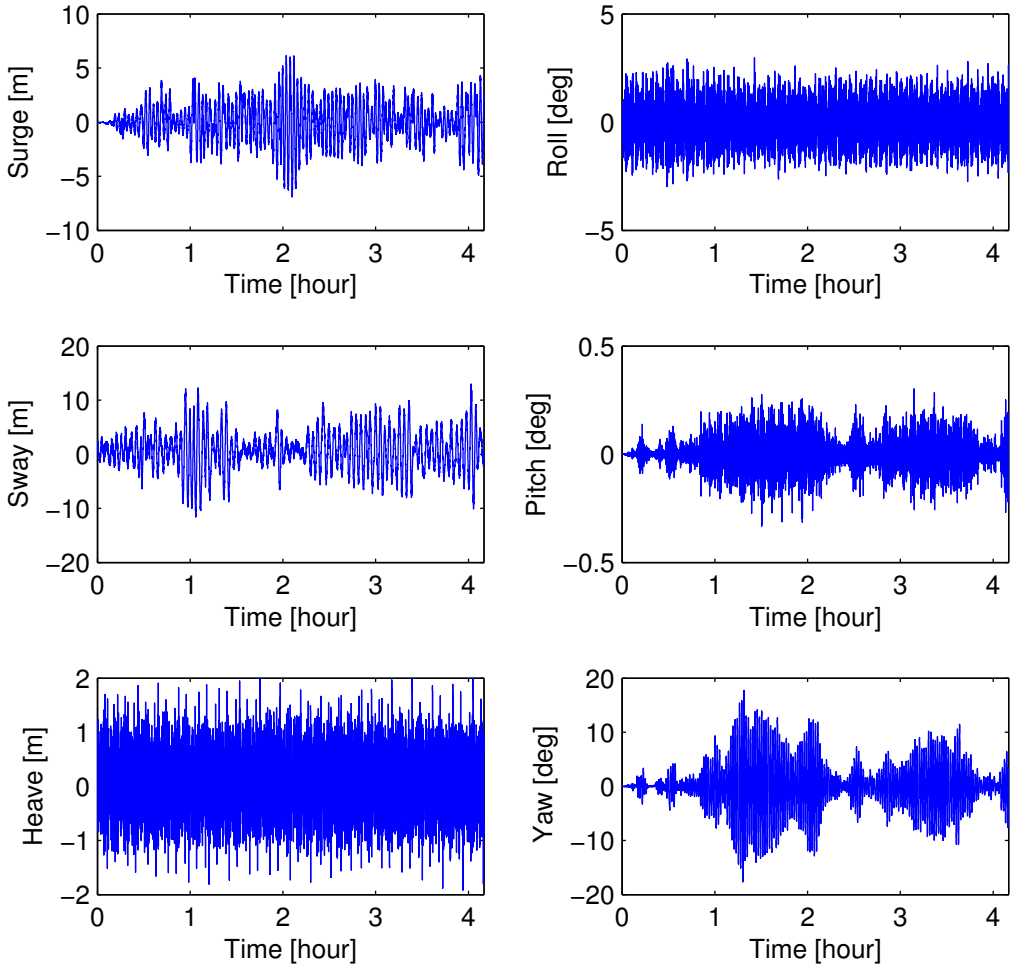

Figure 6.25: White noise wave tests, beam waves and Hs=1.5m for the 50% loading condition.

From Figure 6.25 can be clearly seen that all degrees of freedom seem stable in this simulation. During the test the response of the barge to more than 4 hours of white noise wave tests was simulated. The same stability was observed in other regular, irregular and white noise wave tests. The stability found in the results shown in Figure 6.25, but also in the other tests, creates a lot of confidence that the aNySIM - ComFLOW simulation is stable.

6.4.5. Influence of the communication time step

In the coupled simulation aNySIM and ComFLOW communicate in intervals of the aNySIM time step. This was originally chosen to be 0.1 seconds, which delivered a stable simulation (see section 6.4.4). In this section it is investigated in more detail how the communication time step influences the results. An overview of the results is given in Figure 6.26 for a roll decay test for the 50% loading condition. It is important to consider that the ComFLOW time steps mentioned in the graph are the maximum time step that ComFLOW may use. A roll decay test is chosen for this comparison because from the model tests it is known how the time series will look like and the response is not chaotic as was seen in many regular wave tests with partially filled tanks.

Different aNySIM time steps have been chosen, at which also the communication between ComFLOW and aNySIM takes place. For an aNySIM time steps of 0.035- and 0.05 seconds also the ComFLOW time step is lowered to a maximum of 0.03 seconds. This was done to make sure that the ComFLOW time step stays smaller than the aNySIM time step. For every simulation all other settings and parameters were taken the same. The results are shown below in Figure 6.26.

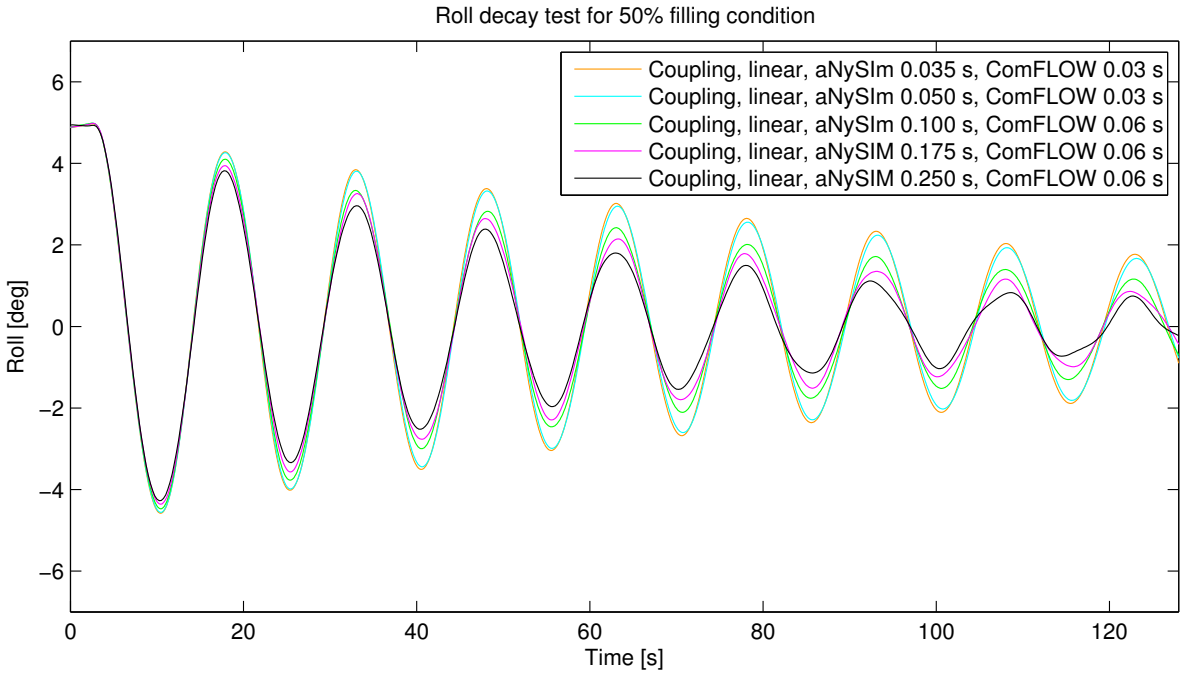

Figure 6.26: Results for different aNySIM time steps and maximum ComFLOW time steps.

The results show that there is a significant difference between the results for the different communication time steps. Besides the fact that a different time step results in a different roll amplitude, the results also show that for a communication time step of 0.25 seconds the results do not show a smooth sine shape. It is expected that the differences are partly caused by the method of interpolation chosen to calculate the motions of the tanks in between aNySIM time steps. When the time step is changed the interval over which interpolation of the motions takes place changes as well. This again influences the accuracy of the coupling method. For example, in case of overestimation of the motions additional energy is introduced in the system. In case of underestimation of the motions energy is taken from the system, introducing additional damping. In all previous results linear interpolation was used (first order accurate) to estimate the motions of the tank. As stability and accuracy of the coupling is a very important part of the project it is investigated how the results will change when third order accurate interpolation for the motions and first order interpolation (currently no interpolation) for the forces is used. Also a coupling is developed for which aNySIM and ComFLOW use exactly the same time step. This is described in more detail in section 6.4.6.

6.4.6. Additional interpolation methods

ComFLOW requires the motions of the tanks at every ComFLOW time step. However, the motions are only known at the aNySIM communication time steps which are larger than the ComFLOW time steps. Therefore interpolation is used to determine the motions of the tank in between the aNySIM time steps. Currently linear interpolation for the motions is used, but in this section the results are investigated when third order interpolation of the motions is used.

Currently there is no interpolation used for the forces that are send to aNySIM. This was done because it was assumed that the ComFLOW time step is much smaller than the aNySIM time step. This would mean that when the forces are sent to aNySIM both ComFLOW and aNySIM are almost at the same time. However, sometimes ComFLOW is using time steps almost as large as aNySIM. Because of this ComFLOW is often significantly further in time than aNySIM, which results in less accurate forces that are sent to aNySIM. Therefore first order interpolation of the forces is also investigated in this section.

Finally it is investigated what the effects are of an equal time step for aNySIM and ComFLOW. In this case no interpolation of the forces or moments is necessary as both aNySIM and ComFLOW exchange information at the same time levels. However, because a fixed time step is used ComFLOW cannot change the time step based on the CFL condition. Because of this the simulation may become unstable or take more time than strictly necessary.

Third order accurate cubic spline interpolation of the motions

Figure 6.27 shows an example of third order vs linear interpolation. With third order cubic spline interpolation a continuous function is found of which the second derivates in the known points are zero. An example is shown in Figure 6.27 below. For this a sine function was used as this greatly represents the ship motions observed in this project.

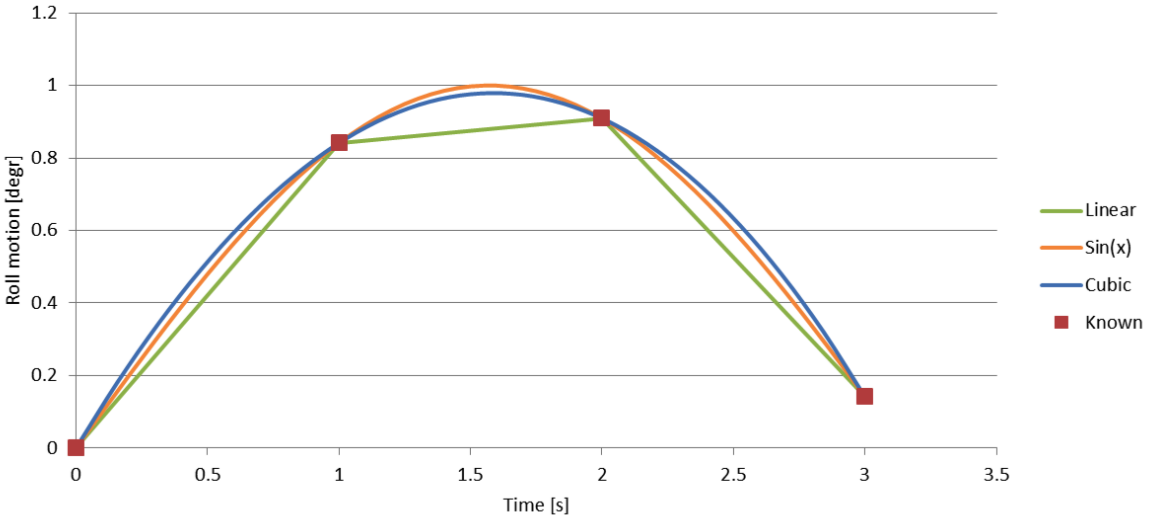

Figure 6.27: Roll decay tests with linear- and cubic splines interpolation for different time steps.

It is assumed that 4 points in time are known, labelled with red squares. When the motions in between those points are interpolated with linear interpolation the solution is often significantly off, and underestimated (and therefore damping the response). With third order interpolation the motions are estimated with a much higher precision. However, in extreme situations third order interpolation could also be less accurate than linear interpolation. But for the motions considered in this project it is expected that cubic spline interpolation is stable and more accurate than first order interpolation.

The cubic spline interpolation used in the coupling is based on the following interpolation method:

$$s(x) = y(i) + b(i) \cdot (x - x(i)) + c(i) \cdot (x - x(i))^2 + d(i) \cdot (x - x(i))^3 \tag{6.12}$$

where $x(i) \leq x \leq x(i+1)$, $s(x)$ is the third order solution, x is the time at which the interpolation is required, $x(i)$ is the time of the known point left of x, $x(i+1)$ is the time of the known point right of x. $y(i)$ is the y-axis value at time $x(i)$. $b(i), c(i)$ and $d(i)$ are the spline coefficients that are calculated for the interval between consecutive known points. The Fortran code for calculating the spline coefficients is obtained from AlexG (2010). This cubic spline method used in this project requires 4 known points. However, at the beginning of the simulation these points are not yet known. Therefore linear interpolation of the motions is used until enough data is available for cubic spline interpolation. The results for the different interpolation strategies are shown at the end of this section in Figure 6.29.

First order interpolation of the forces

In the current coupled simulations ComFLOW progresses in time until it has passed the aNySIM time step. When this is done the latest forces and moments obtained in ComFLOW are sent to aNySIM, without any interpolation. This process is accurate as long as the ComFLOW time step is much smaller than the aNySIM (communication) time step, as in that case ComFLOW will not progress in time much further than the current aNySIM time. However, when the ComFLOW time step is almost as large as the aNySIM time step then ComFLOW can progress significantly past the current aNySIM time. This is visualised in Figure 6.28 below.

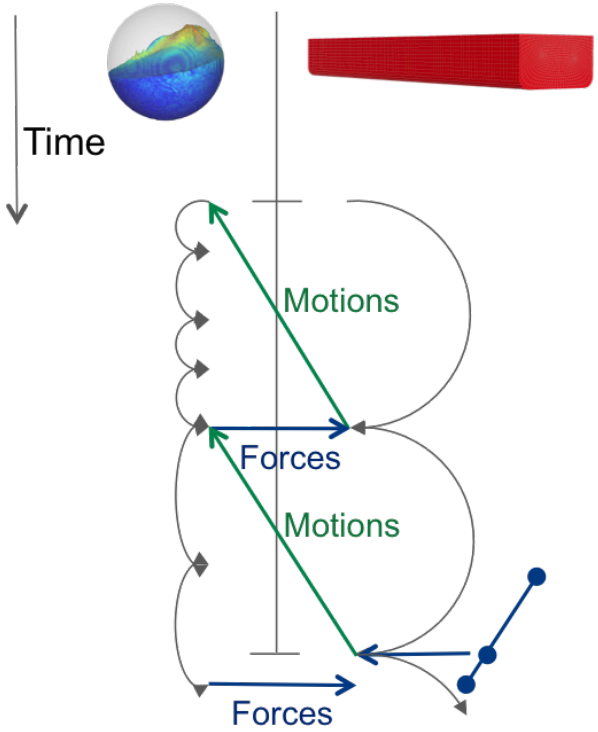

Figure 6.28: Principle of linear interpolation of the forces from ComFLOW to aNySIM.

Figure 6.28 above shows how a relatively large ComFLOW time step could create a situation in which forces are sent to aNySIM based on a time that is relatively far away from the current aNySIM time. In the visualisation can also be seen how the linear interpolation of the forces works. The results of including linear interpolation of the forces is shown in Figure 6.29 at the end of this section.

Synchronised simulation

In the previous sections was described how interpolation can make the simulation more accurate. This section will discuss the approach when no interpolation is used in the coupling. In this case aNySIM and ComFLOW use the same time step, and communicate therefore also at the same times. This means no interpolation of the motions or sloshing loads is necessary. It is however necessary that the time step is fixed in both ComFLOW and aNySIM. This creates some difficulties as both aNySIM and ComFLOW may decrease the time step to make the simulation more stable. Additionally, ComFLOW may increase the time step to decrease the necessary calculation time. It is therefore very important to consider a fixed time step that will results in a stable simulation. For this project time steps have been used that are smaller than the time step that ComFLOW used in the same simulation with a variable time step.

Results

Below in Figure 6.29 the roll decay test results are shown for different interpolation strategies.

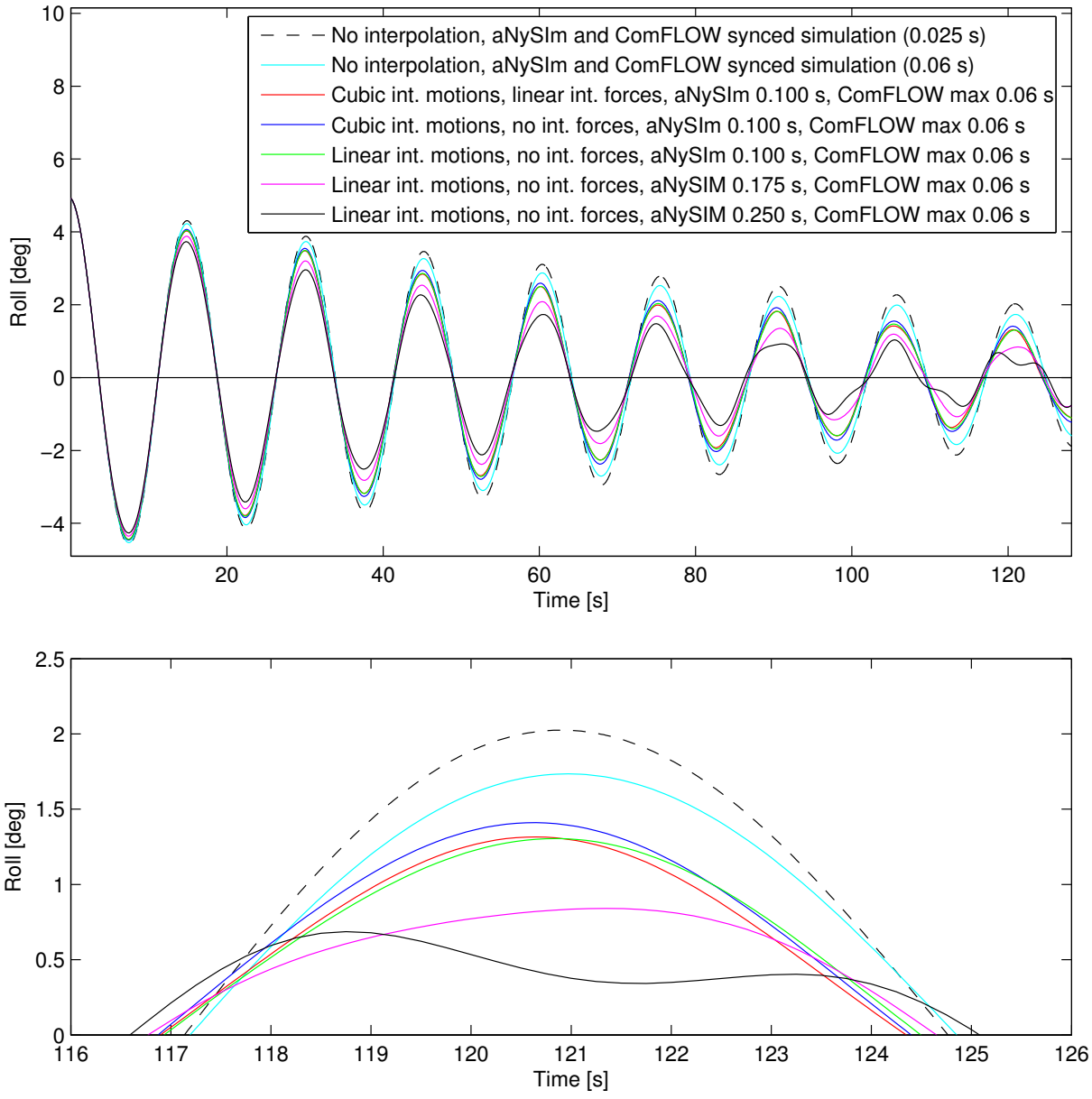

Figure 6.29: Roll decay test when different interpolation strategies are used

The blue curve shows the results when third order cubic spline interpolation of the motions is used. For this case there is no interpolation of the forces, and a communication interval of 0.1 seconds is chosen (just as for the green line). The absolute amplitudes are larger compared to the results obtained with linear interpolation of the motions. This was expected as with linear interpolation the results are underestimated. With third order interpolation the estimated motions are expected to be larger and more accurate for a sine shaped response. When linear interpolation of the forces is also taken into account (red line) the results show a smaller amplitude than without linear interpolation of the forces.

The dotted black- and cyan coloured line represent results obtained with a simulation in which ComFLOW and aNySIM both use the same time step and exchange information at the same time levels. This strategy has been tested for a time step of 0.025 and 0.06 seconds. A time step of 0.06 seconds is often used by ComFLOW. However, depending on the flow velocities ComFLOW normally changes the time step based on the CFL condition. The implications of using a fixed time step is that ComFLOW cannot decrease the time step anymore to create a more stable simulation in case of high fluid velocities or increase the time step to decrease the calculation time. The results obtained with a synchronised simulation show a small phase difference of about 0.33% and a significantly larger absolute amplitudes compared to the results found with a communication interval of 0.1 seconds. The differences between the amplitudes found in the two synchronised simulations is expected to be partly caused by the smaller time step that is also used in ComFLOW. In case of a smaller ComFLOW time step the peaks in the sloshing loads may be better captured and could produce a larger response.

6.4.7. Non-linearity in the response

Besides the irregularity of the response when the barge is excited by regular waves, it is also expected that the response of the coupled system is non-linear, especially when it is excited with waves around the natural sloshing frequency. This is tested by performing regular wave tests, each test with a different wave height while keeping everything else the same. For this a wave period of 6.5 seconds, or wave frequency of 0.96 rad/s is used. From the response the RAO is calculated and the RAOs found for different wave heights are compared. This is shown in Figure 6.30 below.

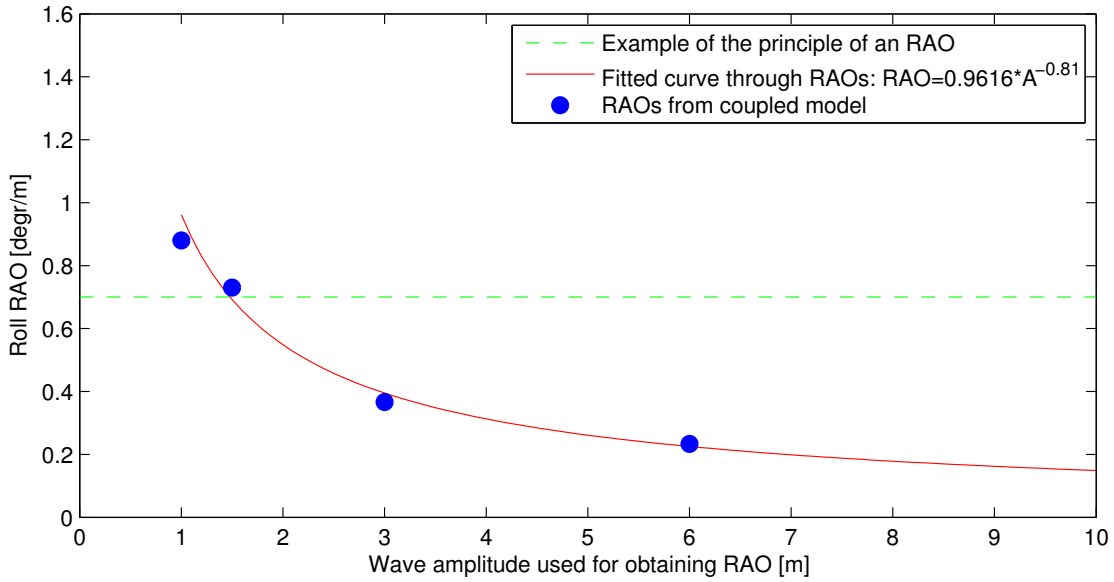

Figure 6.30: Roll RAOs obtained for 50% filling condition from different wave amplitudes.

The principle of an RAO is that whatever wave height you choose, the RAO will stay the same. This is visualised by the straight black dotted line in Figure 6.30 above; the RAO stays the same indepen-

dent of the wave amplitude. However, it can be clearly seen that the obtained results do not match the definition of an RAO. The RAO found in these tests (roll amplitude/wave amplitude) change very much depending on the the wave amplitude that they are based on and decrease with increasing wave amplitude.

However, a very important conclusion from these results is that the motions of a ship with partially filled spherical tanks cannot be considered linear. A fitted curve through the obtained RAOs is also presented which gives an indication of how the results could be extrapolated to other wave amplitudes. However, this type of extrapolation should be used with caution as the RAO for a wave amplitude that approaches zero is not known.

6.4.8. Influence of the pump tower

In reality spherical LNG tanks on board vessels are equipped with a pump tower. This is a cylindrical structure (see cover photo of this report) that contains the pumps and pipes through which the LNG is loaded in- and out of the spherical tanks. The diameter of the pump tower used for this project is 3.0 meter, which is realistic. The influence of the pump tower is first investigated for the RAOs. This is shown in Figure 6.31 below.

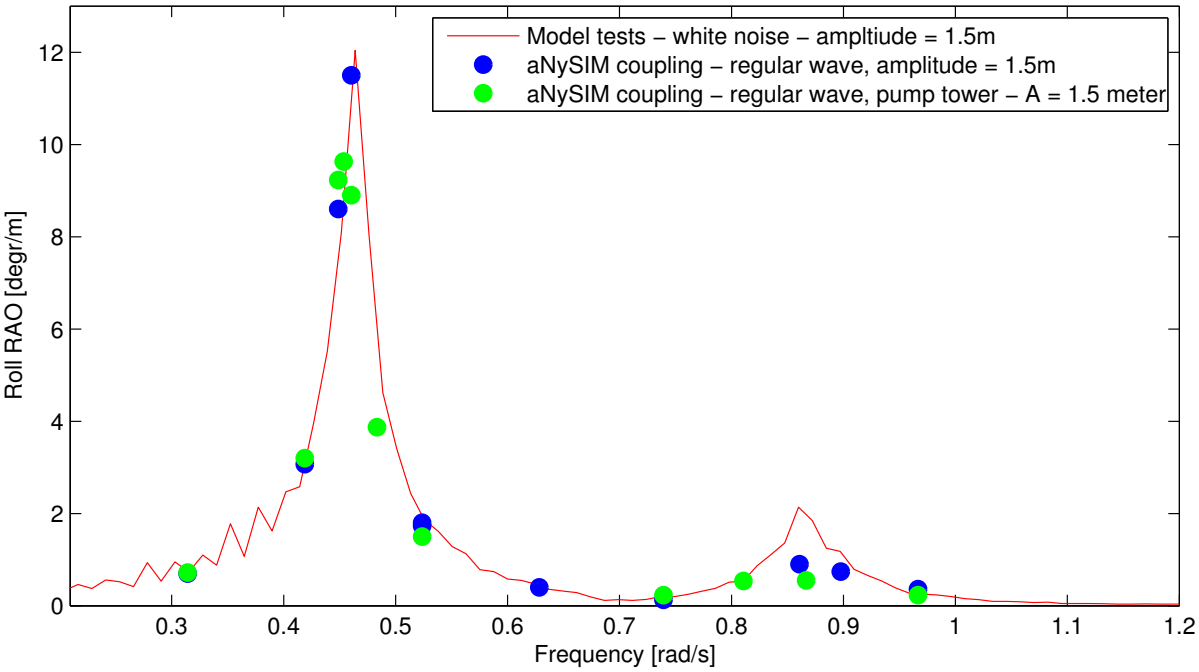

Figure 6.31: Inluence of the pump tower on the roll RAOs for the 25% loading condition

Based on the results a few observations can be made:

- Due to the pump tower the maximum response frequency become smaller
  This observation makes sense, as the pump tower is believed to add damping to the coupled system because waves in the tank are stopped or slowed down by the the pump tower. When additional damping is included in the system the natural frequency becomes smaller.

- The main roll RAO peak became smaller
  This is believed to be caused by the damping that is added to the system because the pump tower is now located inside the tank.

- The sloshing induced roll RAO peak becomes smaller
  This is also believed to be due to the additional damping of the pump tower

All above observations are based on the principle that energy is removed from the system due to the presence of the pump tower. This will be investigated in more detail by looking at screenshots of the flow in the tank with- and without pump tower.

Figure 6.32 shows a visualisation of the sloshing in the spherical tanks with- and without pump tower in the tank.

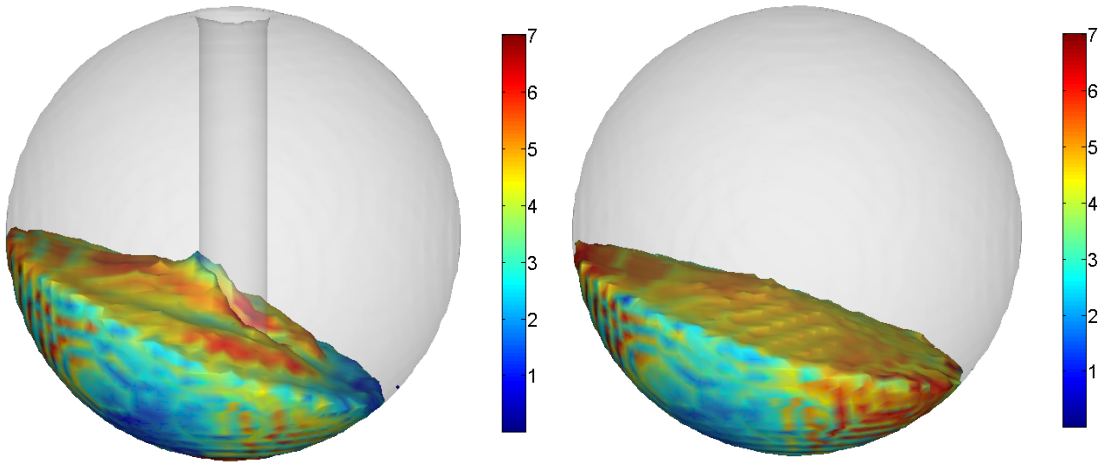

(a) With pump tower (b) Without pump tower

Figure 6.32: Sloshing in the spherical tanks with- and without pump tower for 25% loading condition.

From the visualisations can be seen that the pump tower basically blocks the liquid that is passing through the middle of the tank. By doing this the pump tower removes a lot of energy from the system, but especially from the liquid traveling through the middle of the tank. And exactly this part of the cargo will travel the largest distance in y-direction, to the other end of the tank where the tank is the widest. However, because of the pump tower the liquid traveling through the middle of the tank is slowed down and will not reach the same distance and height in the tank once it reaches the other side. Because of this the sloshing induced moments around midship are believed to be smaller and responsible for creating smaller roll motions of the vessel.

In terms of operability the pump tower has a positive effect on the ship motions. The maximum response frequency moves to a lower frequency (away from commonly experienced sea states) and the overall roll response becomes smaller.

6.5. Uncertainty in the results

Uncertainty in the results for this project are separated in uncertainties in the scale model test results and uncertainties in the numerical results. Uncertainties of measurements during scale model tests or the uncertainty arising from using a CFD model are a study in itself. Therefore the most important uncertainties are described, including their potential effects, but no exact numbers could be given as they are not exactly known.

6.5.1. Uncertainty in the scale model test

According to ITTC (2011) there are two types of uncertainties in scale model test experiments. Type A uncertainties and type B uncertainties. Type A uncertainties are uncertainties related to the repeatability of the experiments. The same results should be obtained when a test is performed multiple times. The repeatability of the tests was investigated during the scale model test, and it was concluded that the repeatability of the tests is good. Therefore no major type A uncertainties are expected.

Type B uncertainties are following from uncertainties in sensors and its calibration, the produced waves, data acquisition system, processing- and analysis of the data. Uncertainties in the sensors is for example relevant for the accelerometers measuring the motions of the barge and the lasers used during the inclination tests. There are strong suspicions that there is a significant uncertainty in the roll radius of gyration measured during the scale model tests. This was originally identified because the numerical results for the ballasted loading condition did not match the scale model test results. An incorrectly measured roll radius of gyration could be an explanation for this. After checking with one of the supervisors of the scale model tests it was acknowledged that it was expected that there was a significant uncertainty in the roll radius of gyration. The effects of this uncertainty on the numerical results are discussed in section 6.5.2.

There is also an uncertainty in the waves that are created. During the scale model tests the wave heights have been achieved with an error of $+/-$ 3.3%, and the wave periods have been been achieved with an error of $+/-$ 0.85%. However, there are also uncertainties in the wave measuring devices.

A data acquisition system was used to acquire the data from the optimal motion system, tension transducers in the mooring system and the wave probes. The uncertainties in this are not known. The last uncertainties that will be discussed for the scale model tests are the uncertainties in the processing- and analysis of the recorded data. A main uncertainty in this is determining the RAOs from the time traces of the white noise tests. The RAOs were delivered to Shell and were produced by the staff of the wave basin in China. The RAOs determined from a cross spectral analysis on time series depend on many variables and the methods used to reduce uncertainty. When it was tried to reproduce the RAOs supplied by the staff of the wave basin differences were found up to 40%. Although it is expected that the software used by the staff of the wave basin is much more sophisticated and accurate than what was used to reproduce the RAOs, there may still be a significant uncertainty.

6.5.2. Uncertainty in the numerical results

Results of the numerical models are subject to uncertainty due to a large variety of sources. For example the accuracy of the barge properties that are used as input for the numerical models, but also the mesh/grid used, the assumptions in the equations that are solved by for example ComFLOW and uncertainty caused by the influence of the time step. The uncertainties that are expected to cause the largest uncertainty will be discussed in this section.

Uncertainties due to assumptions

One of the main assumptions is linearity. This is relevant for the frequency domain approach, but also for modelling the barge in the time domain approach. In this linear approach it is assumed that the

wave steepness and resulting vessel motions and velocities are small. According to Denis (1974) small vessel motions give heave amplitudes smaller than $1/5^{th}$ of the draft, roll amplitudes smaller than 15 degrees and pitch amplitudes smaller than 5 degree. In the frequency approach all these conditions are satisfied for the barge. However, it is expected that this assumption is not valid for the sloshing in the tank during all the different loading conditions. Especially for the 50% loading condition non-linear sloshing was observed during the scale model tests. For the time domain approach this assumption may also not be valid during all conditions. For example, with a wave height of 1.5 meter, sometimes roll motions up to 18 degrees were observed. All frequency domain results and frequency dependent input for the time domain model also assume that the liquid is an ideal fluid (incompressible, free of surface tension, homogeneous) and that the fluid is irrotational. The main implication of this is that additional damping should be added for roll, as viscous effects are not taken into account. The exact value of the additional damping is not explicitly known and is estimated by matching the roll RAO peak in the frequency domain and by using the roll decay tests in the time domain approach. Therefore there is also uncertainty in the amount of linear and non-linear roll damping that is used.

For the CFD model non-linear sloshing motions are taken into account. However, the fluid is assumed to be incompressible, and viscous effects and free surface tension are not taken into account. This is justified by the high Reynolds numbers in both model- and full scale results. Incompressible flow is assumed to be valid for the considered simulations, but should be taken into account when two-phase simulations are performed in the future to account for the pressure in real LNG tanks. There may be many more assumptions made in CFD, but the presented assumptions above are made specifically for this project. It is expected that the more fundamental principles of CFD are taken into account by the developers of ComFLOW.

Uncertainties in the input

The uncertainties in the input are discussed for the barge properties, the panel models, grid and numerical settings.

- Barge properties
  The barge properties are used in both the frequency- and time domain models. Uncertainty in this may come from the measured values during the scale model tests, for example the length or the centre of gravity of the barge. An important uncertainty in the numerical results is caused by the relatively large uncertainty in the roll radius of gyration that is measured during the scale model tests (see section 6.5.1 and Figure 6.33).

  The differences between the corrected and the measured roll radius of gyration are in the range of 1.2 to 5.3 percent. The effects of this on the frequency domain results is shown in Figure 6.33 for the 50% loading condition. The results in Figure 6.33 show that the roll radius of gyration mainly influences the natural frequency of the barge (height of the corresponding peak is matched, as the required damping is uncertain to begin with). The overall shape of the response does not seem significantly influenced by the difference in roll radius of gyration and also the response around the natural sloshing frequency is not significantly influenced. The other barge particulars used in the model are based on the measured values during the scale model tests, rather than the designed values.

- Panel models of barge and tank in the frequency domain
  Panel models are created to model the barge and tank in the frequency domain. Also the barge model in the time domain model is based on the frequency domain results for the barge, for which the same panel model is used. The sensitivity of the results was investigated for different mesh sizes, by which the uncertainty due to the panel models is significantly lowered.

- Grid used for the tank model in ComFLOW
  The number of cells in the grid that is used to model the flow of liquid in the tank in ComFLOW has an effect on the results. Therefore the sensitivity of the results to the number of cells in the grid is investigated and is expected to reduce the uncertaityn due to the choice of grid.

- Numerical settings

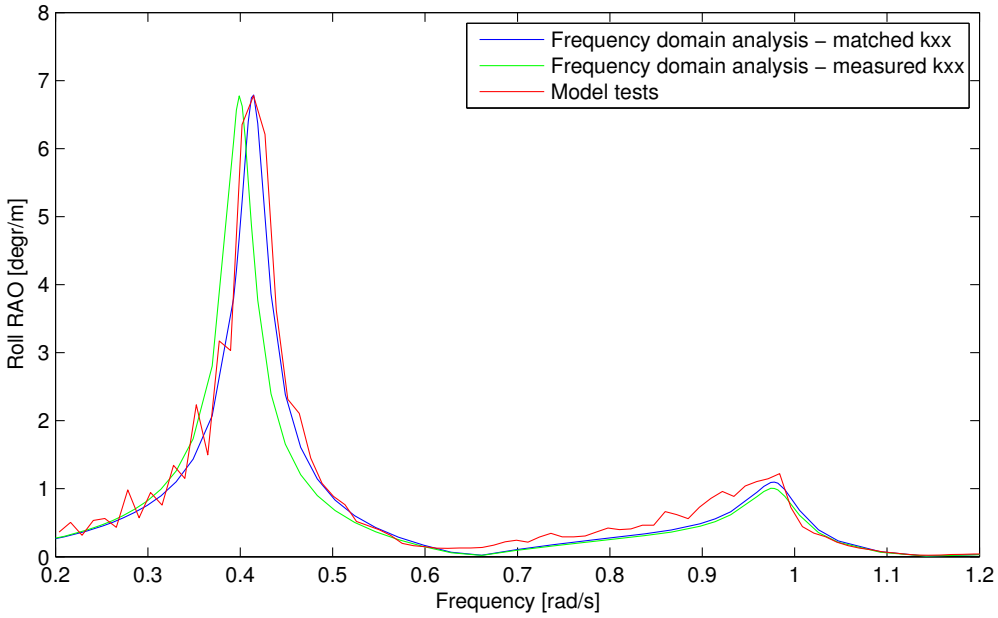

Figure 6.33: Difference in results caused by the roll radius of gyration

The type of numerical schemes and the time step used have an effect on the results. The time step is mainly important for aNySIM, ComFLOW and the coupling. The time step and numerical scheme used in aNySIM has been based on recommendations from MARIN and has shown convergence of the solution. The ComFLOW time step is based on the CFL criteria and is not expected to create significant differences in results as this is a proven method. The influence of the communication time step that is relevant for the coupled model is discussed in section 6.4.5 (but can be significant). The numerical schemes used in ComFLOW are mainly based on recommendations. It was however observed that changing the spatial numerical scheme from second order central difference (used for this project) to first order upwind had a significant influence on the results. Therefore the importance of choosing the most appropriate numerical scheme is recognised.

Uncertainties in processing the output

Another important uncertainty is the roll RAO determined from the coupled aNySIM - ComFLOW model. The uncertainty depends on the type of wave test used:

- Regular waves
  In section 6.4.3 was discussed that the roll response to a regular wave is irregular, which creates uncertainty in the roll RAO. The uncertainty due to an irregular response is the largest in between the two local maxima and is the smallest very close to the two local maxima where the response is (close to) regular.
- White noise- and irregular wave test
  The RAOs that are based on a white noise- or irregular wave test are obtained by cross spectrum analysis. This is mainly relevant for section 6.4.2, but the uncertainty in the cross spectrum analysis is believed to be significant.

6.5.3. Conclusion on uncertainties

In this section many types of uncertainty have been identified that could have an effect on the results. Most of the uncertainties are considered to be of minor or negligible impact. However, the following uncertainties are believed to have a potentially significant impact on the results:

- Uncertainty in the roll radius of gyration
- Uncertainties in the roll RAOs obtained from a (sometimes) irregular response to a regular wave
- Uncertainty in the roll RAOs obtained from a cross spectral analysis for irregular or white noise wave test (for the scale model tests tests as well as for the coupled time domain model).
- Uncertainty created by the coupling between ComFLOW and aNySIM
- Uncertainties due to non-linear effects (especially relevant for the frequency domain approach).

6.6. Chapter summary

In this chapter the main findings of this project have been presented. In section 6.1 first the frequency domain results have been discussed and compared to scale model tests. A good agreement with the scale model tests was found. Additionally the effect of frozen vs liquid cargo, the tank radius and wave direction have been investigated in more detail. The rest of this chapter has been devoted to the time domain coupling between aNySIM and ComFLOW. First in section 6.2 the setup of the computational fluid dynamics model has been discussed. After this the CFD model was validated by inducing the first two free surface modes and by comparing the results to videos of the scale model tests. After this, in section 6.3 the ship motion model in aNySIM has been discussed and successfully validated against the scale model tests for the ballasted condition. In section 6.4 the results of the coupled aNySIM - ComFLOW model have been discussed. The results of the coupled model have been validated against the scale model tests by comparing the roll decay tests and roll RAOs for 45- and 90 degree waves. Also the different frequencies in the response have been investigated, followed by the stability of the model, non-linearity, the influence of the communication time step between aNySIM and ComFLOW and the influence of the pump tower. More complex interpolation methods for the coupled model have also been investigated and compared. Finally in section 6.5 the uncertainty in the results has been investigated.

In Chapter 7 all results discussed in this chapter will be summarised and presented in the form of the conclusions and recommendations of this project.

7

Conclusions and recommendations

At the beginning of this project the following goal was set:

> "To develop a coupled sloshing-ship motion model that is validated with scale model tests, to be used to simulate, and to gain a better understanding of, the effect of sloshing in partially filled spherical tanks on ship motions under operational conditions".

To achieve this goal two separate models were developed; a frequency domain model and a time domain model. In this chapter will be reflected upon the goal set by providing the conclusions (section 7.1) and recommendations (section 7.2).

7.1. Conclusions

The conclusions will be presented separately for the frequency and time domain models. The main difference between the two approaches is the assumption of linearity. Both the frequency- and time domain models are based on linear potential theory for the barge. In the frequency domain the tank is also modelled with linear potential theory, while in the time domain the tank is modeled by using the non-linear Euler equations. The impact of this is discussed in more detail below.

The frequency domain model provides accurate results compared to the scale model tests (45 and 90 degree incoming waves) and is very fast; running the model only takes about one hour and it is relatively easy to set up. However, linearity of the solution is assumed, while it was found that the response (especially around the natural sloshing frequency) is non-linear. This means that the agreement between the roll RAOs obtained from the frequency domain approach and the scale model tests depends on the wave height used during the scale model tests. Also the effect of tank size, wave direction and frozen vs liquid cargo was investigated in the frequency domain. By comparing the roll response of the barge for a 50 percent loaded tank with liquid and frozen cargo it was shown that sloshing creates a lower natural frequency of the barge and also decreases the height of the main response peak. From these findings it could be concluded that sloshing adds damping to the system. By changing the tank size it was shown that for increasing tank size the barge natural frequency moves to a lower frequency and the peak also becomes lower. This was expected because for a larger tank the sloshing moments will increase as the arm between the force location and midship becomes larger. As was known from the comparison between frozen and liquid cargo sloshing actually decreases the natural frequency of the barge and decreases the height of the main peak. Therefore it makes sense that this also occurs for increasing tank size, in which the effect of sloshing becomes larger. It was also shown that for increasing tank size the sloshing induced roll RAO peak becomes larger and moves to a lower frequency. This was expected as this peak is created due to the moments of the sloshing cargo, which becomes larger for increasing tank size. Furthermore, from the literature review it was known that the natural sloshing frequencies moves to a lower frequency for increasing tank size. By investigating the effect of wave direction on the

roll motions of the barge it was shown that both roll RAO peaks are strongly dependent on the wave direction, especially the height of the sloshing induced roll RAO peak. The sloshing induced peak is at its maximum for 90 degree waves, but is already decreased by 50% for 75 degree incoming waves and almost disappears for wave directions smaller than 65 degrees.

The time domain model is based on a coupling between ship motions solver aNySIM and Volume of Fluid solver ComFLOW. In the coupled model the ship motions calculated by aNySIM are based on linear potential theory, but non-linear sloshing motions can be simulated by ComFLOW. Because of this the coupled model can describe non-linear ship motions due to non-linear sloshing in the tank, which is a significant difference compared to the frequency domain approach. The time domain model was validated by comparing the numerically obtained roll decay time traces and the roll RAOs with those obtained during the scale model tests.

The roll decay tests obtained from the time domain model showed a similar response as was found during the scale model tests. Validation of the roll RAOs was done by comparing the results of regular wave tests in the coupled model with the RAOs obtained from a white noise wave test during the scale model tests. The agreement between the results is reasonably good, but showed that the sloshing induced roll RAO peak is underestimated by the coupled time domain model. This is expected to be because the frequencies from the white noise waves are transported into the tank and therefore also influence the response at a later time. The cross spectral analysis, used to obtain the RAO's from the white noise test, only take into account the wave frequencies, and not the frequencies in the tank. Therefore the RAO for a certain wave frequency may also contain influences from other frequencies that are still present in the tank. To gain more insight in this a very time consuming white noise wave test was performed with the coupled model. The resulting RAOs showed a better agreement around the natural sloshing frequency, for the height as well as the frequency of the peak. The regular wave tests also showed that a vessel with partially filled spherical tanks often shows an irregular roll response when exposed regular waves. This was investigated in more detail and it was shown that the wave frequency, natural frequency of the barge and the natural sloshing frequency were all present in the response. The contribution of every frequency to the response largely depends on how close the wave frequency is to the natural sloshing frequency and natural frequency of the barge. Because of the irregularity of the response often no steady state response is found, which creates uncertainty in the RAOs found from regular wave tests, but also shows that the response is non-linear. By investigating the response of the barge to different wave heights it was found that the RAO depends on the wave height used in the test. This is the second indication for a non-linear response of the barge.

The effect of the pump tower, that was previously not taken into account, is also investigated. The results showed that due to the pump tower the two peaks in the roll RAO response decrease and that the natural frequency of the barge has moved to a lower frequency. This makes sense as it is believed that the pump tower adds damping to the system and decreases the moments acting on the barge due to the sloshing. Finally also the effect of the communication time step between ComFLOW and aNySIM was investigated, during which the motions were interpolated linearly in between the communication time steps. This showed that the results were significantly different for different communication time steps. Therefore third order interpolation of the motions and first order interpolation of the forces was included in the coupling. Additionally also a coupling without interpolation was used, during which ComFLOW and aNySIM use exactly the same time step and therefore exchange information at the same times. The use of different interpolation schemes showed different results. Especially the simulation in which aNySIM and ComFLOW use the same step showed a significantly higher roll amplitude.

Both the frequency domain- and time domain approach showed promising results and can both be used to investigate the effect of sloshing on ship motions. However, both approaches have their advantages and disadvantages. The frequency domain approach is very accurate for the sea states considered in the model tests, fast, robust and easy to set up. But due to the linear assumptions the frequency domain approach should be used with caution outside the sea states that it is validated for. The frequency domain approach also cannot model the irregular response of the vessel to regular waves. On the other

hand, the time domain approach is very time consuming and more complex to set up, but also shows good results. More important, the time domain approach can be used to investigate the non-linear response of the vessel in more complex sea states and gives much more insight in what is actually happening.

7.2. Recommendations

At the start of this project very little was known about the effect of sloshing in partially filled spherical tanks on ship motions. Now, at the end of the project and after the scale model tests performed by Shell, the effect of sloshing in spherical tanks on ship motions is much better understood. Furthermore, different approaches that could model the effect of sloshing in spherical tanks on ship motions have been identified and investigated. Many questions have been answered, but new questions also came up. This section will describe the recommendations for future work that could answer those questions and would increase the knowledge on (the modelling of) the effect of sloshing on ship motions.

The main recommendations have been separated into two groups. The first group focuses on increasing the knowledge of the effects of sloshing in spherical tanks on ship motions and the different approaches to model this. The second group is more focused on other areas that the developed coupling could also be used for.

The main recommendations focused on the effects of sloshing on ship motions are discussed per bullet point in the list below:

- *Gain more insight in the influence of wave height and wave type on the coupled motions*
  It was found that the wave height and type of wave spectrum used has a significant impact on the results. By performing additional model tests or simulations more insight could be gained in how the wave height and wave type influence the results. This would not only increase the knowledge on the effects itself, but may also give more insight into what type of environments could, and could not, be modelled under linear assumptions.
- *Investigate the use of baffles, anti roll tanks or compartments*
  The use of baffles, anti roll tanks or compartment may decrease the effects of sloshing on ship motions. This has been extensively investigated for membrane type tanks, but not for spherical tanks. The relevance of this recommendation depends on whether or not sloshing is considered a problem. To determine this the next recommendation is presented.
- *Perform an operability study for a vessel with partially filled spherical tanks*
  This would give a lot of insight in whether or not sloshing in the partially filled spherical tank is a problem or maybe even advantageous. For example, the barge natural roll frequency moved to a lower frequency, further away from often experienced sea states. On the other hand, a second, sloshing induced roll RAO peak is now present in the area of wind waves.
- *Investigate the motions of a more representative LNG carrier with partially filled tanks*
  The model tests performed by Shell and the developed models were all focused on a barge with two spherical tanks. Although this provided a very good understanding of the effects sloshing in spherical tanks has on ship motions, it would also be interesting to investigate the coupled motions for a more representative LNG carrier. This mainly includes a more representative hull shape that contains 4 or 5 spherical LNG tanks.
- *Investigate influence of pressure in the spherical tanks on the results*
  In reality the spherical tanks are pressurised. This has not been included in the model tests or developed numerical models. ComFLOW does offer a two-phase simulation mode in which the pressure could be taken into account. Model tests could also give insight in the effect of pressure on the sloshing.
- *Investigate in more detail the effect of LNG as cargo rather than water*
  In this project mainly water was used as cargo. However, in reality the LNG boiling inside the

tank creates complex free surface interaction with the air around it. This could also be modelled by a two phase ComFLOW simulation for sloshing in spherical tanks.

- *The influence of fenders and mooring lines that connect the LNGC and FLNG*
  In this project the focus was on modelling the motions of the barge that was used in the scale model test. This barge was kept in place with a soft spring mooring system. However, during an offloading situation the LNG carrier is connected to the FLNG by fender and mooring lines. This is not yet taken into account and could give more insight in the motions of a vessel with partially filled spherical tank during an offloading operation.
- *Investigate numerical schemes used in the coupling*
  As was discussed in this report the influence of the communication time step and interpolation schemes on the results was significant. Therefore it is recommended to investigate strategies to improve the quality of the coupling further. Extrapolation of the forces (predictor-corrector method) could be applied to estimate the average forces and moments over an aNySIM time step. It is also recommended to investigate communication between ComFLOW and aNySIM at the aNySIM integration time steps, rather than the overall aNySIM time step. Although MARIN has shared that this is very complicated (both ComFLOW and aNySIM need to use the same integration schemes) and not recommended.
- *Include forward speed of the vessel*
  It may the case that an LNG carrier is sailing with partially filled spherical tanks. In this case the forward speed will influence the sloshing in the tanks. Additionally, the sailing LNG carrier may also experience very rough weather conditions that are not considered during offloading situations.

The next set of recommendations is focused on research outside the scope of sloshing in spherical tanks. For this the focus has been on fields of application that are not directly related to this project, but for which the developed coupling may be of interest:

- *Model the effects of anti roll tanks*
  The modelling of (the effects of) anti roll tanks on ship motions may very well be done with the developed aNySIM - ComFLOW coupling. The principle is the same as with sloshing in the spherical tanks; the motions of the vessel are modelled with aNySIM and the flow of liquid in the anti roll tanks is modelled in ComFLOW.
- *Green water simulations*
  The aNySIM - ComFLOW coupling could also be used for green water simulations. For example the flow of water over a barge during the installation of a jacket.
- *Interaction between flow through risers and ship motions*
  The flow through a riser is depending on the shape of the riser, which is again influenced by the motions of the ship or platform that it is connected to. To investigate the flow through a riser that is connected to a moving platform or ship, the aNySIM - ComFLOW coupling could be very well used. The motions of the ship are modelled in aNySIM and the flow through the riser is modelled in ComFLOW.

Bibliography

AlexG, . Fortran code for cubic spline interpolation, 2010. URL `http://ww2.odu.edu/~agodunov/computing/programs/`.

Andrew, J.S. and Alfred, L.A. Analytical and experimental investigation of forces and frequencies resulting from liquid sloshing in spherical tank. 1962.

Bauer, H.F. Nonlinear mechanical model for the description of propellant sloshing. *AIAA*, J.4(9): 1662–1668, 1966e.

Budiansky, B. Sloshing of liquids in circular canals and spherical tanks. 1958.

Bunnik, T. and Huijsmans, R.H.M. Large scale LNG Sloshing Model Tests. In *International Offshore and Polar Engineering Conference*, 2007.

Bunnik, T. and Veldman, A.E.P. Modelling the effect of sloshing on ship motions. In *OMAE*, 2010.

Claus, F.G.; Testa, D., and Sprenger, F. Coupling effects between tank sloshing and motions of a LNG carrier. In *OMAE*, 2010.

Denis, M. St. Some obser-vations on the techniques for predicting the oscillations of freely-floating hulls in a seaway. *Offshore Technology Conference*, 1974.

Fossen, T.I. *Guidance and Control of Ocean Vehicles*. John Wiley and Sons Ltd, 1994.

Gaillarde, G.; Ledoux, A, and Lynch, M. Coupling between liquefied gas and vessel's motion for partially filled tanks: effects on seakeeping. 2003.

Ibrahim, R.A. *Liquid Sloshing Dynamics*. Cambridge University Press, 2005.

ITTC, . Recommended procedures and guidelines. *26th ITTC International Towing Tank Conference*, 2011.

Journee, J.M. and Massie, W.W. *Offshore Hydromechanics*. Delft University of Technology, 2001.

Lee, S.J. *The effects of LNG sloshing on the global response of LNG-carriers*. PhD thesis, Texas A&M Universit, 2008.

McCarty, and Stephens, . Investigation of the natural frequencies of fluids in spherical and cylindrical tanks. 1960.

Mikishev, G.N. and Dorozhkin, N. Y. An experimental investigation of free oscillations of a liquid in containers (in Russian). *Isv. ALad. Nauk SSSR, OM. Tekh. Nauk, Mekh. i Maahinostr*, pages No. 4, pp. 48–53, July/Aug., 1981.

Miles, J.W. Resonant motion of a spherical pendulum. *Physica*, 11(D):309–323, 1984c.

Molin, B.; Remy, F.; Ledoux, A., and Ruiz, N. Effect of roof impacts on coupling between wave response and sloshing in tanks of LNG-carriers. In *ASME*, 2010.

Rattayya, J. V. Sloshing of liquids in axiasymmetric ellipsoidal tanks. *AIAA Paper No. 65-114*, 1965.

Shell, . FLNG visualisation, 2014. URL `http://d1dep6bscgu00w.cloudfront.net/wp-content/uploads/2012/03/Prelude-FLNG-Project-on-Track-Shell-Says.jpg`.

Sumner, I.E. Experimentally determined pendulum analogy of liquid sloshing in spherical and oblate-spheroidal tanks. 1965.

Wemmenhove, R.; Loots, E.; Luppes, R., and Veldman, A.E.P. Modelling two-phase flow with offshore applications. In *OMAE*, 2005.

Zhao, W.; Yang, J.; Longbin, T., and White, D. Research on the coupling effects between ship motions and sloshing. In *OMAE*, 2014.

A

Fortran code for developed coupling

```
!!=========================================
!!
!!  PURPOSE:   External Fortran DLL to couple ComFLOw and aNySIM
!!
!!  LANGUAGE:  Fortran 90
!!
!!  AUTHOR:    JWikkerink & Emiel van Twillet (student TU Delft - graduate intern Shell)
!!
!!  CREATED:   March 2015
!!
!!  PARAMETER:
!!
!!  GLOBAL:
!!
!!  REFERENCE:
!!
!!
!!  DESCRIPTION OF CHANGE                | DATE     | AUTHOR
!!-------------------------------------------------

!!  1.

    |          |
!!

    |          |
!!===========================
module ExtFortranDLL

implicit none

private

public :: FDLL_init
public :: FDLL_updateState
public :: FDLL_calcForce
public :: FDLL_getForce
public :: FDLL_output
```

```
35 public :: FDLL_close
36
37 ! Start test functionality
38 ! End test functionality
39
40 !-----------------------------------------------
41
42 !#define __EXAMPLE__
43
44 !-----------------------------------------------
45
46 integer                                  ::  fdll_NBody
47 real                                     ::  fdll_time
48 real,   dimension(:,:), allocatable  ::  fdll_sfMotion, fdll_sfVeloc,
      fdll_sfAccel
49 real,   dimension(:,:), allocatable  ::  fdll_efPosition, fdll_lifMot,
      fdll_lifVel
50 real,   dimension(:,:), allocatable  ::  fdll_force
51 integer,    parameter                  ::  DOF = 6
52 integer                                  ::  k
53 real                                     ::  t_nmin1, t_nmin2, dta, t_nmin3
      , error, force_linear(3), moment_linear(3), dforce, dmoment
54 real                                     ::  fdll_pos_n(6), fdll_pos_nmin1
      (6), fdll_pos_nmin2(6), fdll_pos_nmin3(6), pos_linear(6),
      velocity_linear(6), acceleration_linear(6)
55 real*8 pos_min1(6), velocity_min1(6), acceleration_min1(6),
      velocity_cfmin1(6), tc_min1, fdll_lifAcc(6), fdll_lifAcc_check(6),
      pos_min3(6), pos_min2(6),  velocity_n(6), velocity_min2(6),
      velocity_min3(6)
56 real*8 acceleration_n(6), acceleration_min2(6), acceleration_min3(6),
      force_nmin1(3), moment_nmin1(3),  tcom_nmin1
57 real*8 write_force(3),write_moment(3), write_force_linear(3),
      write_moment_linear(3), write_pos_linear(6), write_pos_cubic(6)
58 real*8 pos_check(6), velocity_check(6), acceleration_check(6)
59
60 !
61 ! define parameters for cubic spline
62 !
63 integer, parameter :: n=4      ! base points for interpolation
64 integer, parameter :: nint=7   ! compute interpolation in nint points
65 double precision xmin, xmax     ! given interval of x()
66 double precision, dimension (n) :: xi(n), b(n), c(n), d(n)
67 double precision, dimension (n,6) :: yi
68 double precision x, y, step, ys, errav
69 integer i
70 double precision f, ispline
71 !
72 !
73 !---------------------------------------------------------------------
74
75 CONTAINS
76
77 !---------------------------------------------------------------------
78 !
79 ! FDLL_init is an interface procedure,
80 ! its signature may not be changed.
```

```
81  !
82  !-----------------------------------------------------------------
83
84  subroutine FDLL_init(NBody, error)
85    integer,                intent(in)  :: NBody
86    integer,                intent(out) :: error
87
88    ! Expose subroutine ExtFortranDLL to users of this DLL
89    !
90    !DEC$ ATTRIBUTES DLLEXPORT::FDLL_init
91
92    ! Variables
93
94    ! Body of FDLL_init
95
96  #ifdef __EXAMPLE__
97    write(*,*) 'FDLL_init'
98
99
100 #endif __EXAMPLE__
101   open(unit= 2, file= 'TimeTrace.txt')
102   !open(unit= 3, file= 'ForceMoments.txt')
103   fdll_NBody = NBody
104
105   allocate( fdll_sfMotion(fdll_NBody, DOF) )
106   allocate( fdll_sfVeloc(fdll_NBody, DOF) )
107   allocate( fdll_sfAccel(fdll_NBody, DOF) )
108   allocate( fdll_efPosition(fdll_NBody, DOF) )
109   allocate( fdll_lifMot(fdll_NBody, DOF) )
110   allocate( fdll_lifVel(fdll_NBody, DOF) )
111
112   allocate( fdll_force(fdll_NBody, DOF) )
113
114   error = 0
115
116   ! Initisation phase of ComFLOW
117   ! begin: procedure for GEODEF
118   call initialize(1) !<-- 1=GEODEF
119   call setup !<-- process input files
120   call geoliq !<--
121   call closure !<-- clean up
122   ! Start procedure for ComFLOW
123   call initialize(0) !<-- 0=COMFLOW
124   call setup !<-- process input files
125   ! Finish initisation phase of ComFLOW
126
127 end subroutine FDLL_init
128
129 !-----------------------------------------------------------------------
130 !
131 ! FDLL_updateState is an interface procedure,
132 ! its signature may not be changed.
133 !
134 !-----------------------------------------------------------------------
135
136 subroutine FDLL_updateState(bodyIndex, time, sfMotion, sfVeloc, sfAccel
```

```
    , efPosition, lifMot, lifVel)
  integer,                intent(in)  ::  bodyIndex
  real,                   intent(in)  ::  time
  real,   dimension(6),   intent(in)  ::  sfMotion
  real,   dimension(6),   intent(in)  ::  sfVeloc
  real,   dimension(6),   intent(in)  ::  sfAccel
  real,   dimension(6),   intent(in)  ::  efPosition
  real,   dimension(6),   intent(in)  ::  lifMot
  real,   dimension(6),   intent(in)  ::  lifVel

  ! Expose subroutine FDLL_updateState to users of this DLL
  !
  !DEC$ ATTRIBUTES DLLEXPORT::FDLL_updateState


  ! Body of ExtFortranDLL

  fdll_time                       = time
  fdll_sfMotion(bodyIndex,:)      = sfMotion
  fdll_sfVeloc(bodyIndex,:)       = sfVeloc
  fdll_sfAccel(bodyIndex,:)       = sfAccel
  fdll_efPosition(bodyIndex,:)    = efPosition
  fdll_lifMot(bodyIndex,:)        = lifMot
  fdll_lifVel(bodyIndex,:)        = lifVel

end subroutine FDLL_updateState

!-----------------------------------------------------------------------
!
! FDLL_calcForce is an interface procedure,
! its signature may not be changed.
!
!-----------------------------------------------------------------------

subroutine FDLL_calcForce()

  ! Expose subroutine ExtFortranDLL to users of this DLL
  !
  !DEC$ ATTRIBUTES DLLEXPORT::FDLL_calcForce

  ! Define ComFLOW variables
  integer*4 i,boxnr,tcycle
  real*8 force(3),moment(3),inertia(3)
  real*8 t,tmax,dt,t_next
  real*8 pos(6),velocity(6),acceleration(6)
  real*8 moment_location(3)
  ! End of defining ComFLOW variables

#ifdef __EXAMPLE__
  integer bodyIndex
#endif __EXAMPLE__

  ! Body of FDLL_calcForce
  fdll_force(:,:) = 0
#ifdef __EXAMPLE__

```

```
192   do bodyIndex = 1, fdll_NBody
193     call FDLL_spring( bodyIndex,fdll_force(bodyIndex,:) )
194   end do
195 #endif __EXAMPLE__
196
197   ! Body of FDLL_calcForce
198   fdll_force(:,:) = 0
199  ! fdll_force(1,3) = -2.9312E5 ! Vertical force to compensate for
       liquid in tanks
200  ! if (fdll_time .gt. 2500.0) then
201  !       if (fdll_time .lt. 3000.0) then
202  !           fdll_force(1,1) = 1000.0*(fdll_time-2500.0)/500.0;
203  !       else
204  !           fdll_force(1,1) = 1000.0;
205  !       endif
206  ! endif
207  ! if (fdll_time .lt. 50.0) then
208  !           fdll_force(1,4) = 0.0!8.2127E5/50.0*fdll_time;
209  ! else
210  !           fdll_force(1,4) = 0.0
211  ! endif
212
213  ! Set initial positions, velococities and accelerations going to
       ComFLOW
214   pos = 0.0
215   velocity = 0.0
216   acceleration = 0.0
217  ! Calculate acceleration at timestep of aNySIM
218  if (fdll_time == 0) then
219     fdll_lifAcc=0
220  else
221     fdll_lifAcc(3)=(fdll_lifVel(1,3)-velocity_min1(3))/(fdll_time-
          t_nmin1)
222     fdll_lifAcc_check=(fdll_lifVel(1,:)-velocity_min1)/(fdll_time-
          t_nmin1)
223  endif
224  !
225   boxnr = 1
226   moment_location = 0.0
227   !
228   call get_time(tcycle,t,tmax,dt)
229   ! start time loop
230
231   ! Calculate forces and moments at t=0 to account for gravity of cargo
       .
232   if (t == 0) then
233       print*, 'first comflow time  = ', t
234        call set_moving_frame(t, pos, velocity, acceleration)
235   ! carry out a timestep
236   !
237   call loop
238   call get_time(tcycle,t,tmax,dt)
239   !
240   !
241   ! obtain the forces on the tank
242   call get_force_frcbx(boxnr,force,moment,inertia,moment_location)
```

```
243   fdll_force(1,1)=force(1)/1000
244   fdll_force(1,2)=force(2)/1000
245   fdll_force(1,3)=force(3)/1000
246   fdll_force(1,4)=moment(1)/1000
247   fdll_force(1,5)=moment(2)/1000
248   fdll_force(1,6)=moment(3)/1000
249   !
250   ! if t comflow is unequal to 0, then go through the interpolation
         process.
251   else
252   !
253   !
254   ! start time loop
255   do while (t < fdll_time)
256   !
257   if (fdll_time == 0) then
258       print*, 't_n= ', fdll_time
259       !velocity_cfmin1 = 0
260       !tc_min1 = 0
261       dta=100
262       !print*, 'dt aNySIM     = ', dta
263       t_nmin2=0
264       t_nmin3=0
265   else
266       print*, 't_n-3 aNySIM  = ', t_nmin3
267       print*, 't_n-2 aNySIM  = ', t_nmin2
268       print*, 't_n-1 aNySIM  = ', t_nmin1
269       print*, 't_n aNySIM    = ', fdll_time
270       print*, 't_n comflow   = ', t
271       pos_check(3) = pos_min1(3)+(fdll_lifMot(1,3)-pos_min1(3))/(
             fdll_time-t_nmin1)*(t-t_nmin1)
272       velocity_check(3) = velocity_min1(3)+(fdll_lifVel(1,3)-
             velocity_min1(3))/(fdll_time-t_nmin1)*(t-t_nmin1)
273       acceleration_check(3) = acceleration_min1(3)+(fdll_lifAcc(3)-
             acceleration_min1(3))/(fdll_time-t_nmin1)*(t-t_nmin1)
274       pos_linear=pos_min1+(fdll_lifMot(1,:)-pos_min1)/(fdll_time-
             t_nmin1)*(t-t_nmin1)
275       velocity_linear = velocity_min1+(fdll_lifVel(1,:)-velocity_min1)
             /(fdll_time-t_nmin1)*(t-t_nmin1)
276       acceleration_linear = acceleration_min1+(fdll_lifAcc_check-
             acceleration_min1)/(fdll_time-t_nmin1)*(t-t_nmin1)
277       !print*, 'Print comparison of heave position, velocity and
             acceleration'
278       !print*, '1-by-1 ', pos_check(3), 'matrix' , pos(3)
279       !print*, '1-by-1 ', velocity_check(3), 'matrix' , velocity(3)
280       !print*, '1-by-1 ', acceleration_check(3), 'matrix' ,
             acceleration(3)
281       !acceleration(3) = (velocity(3)-velocity_cfmin1(3))/(t-tc_min1)
282       !acceleration(3) = acceleration_min1(3)+(fdll_sfAccel(1,3)-
             acceleration_min1(3))/(fdll_time-t_nmin1)*(t-t_nmin1)
283       !print*, 'Heave going to ComFLOW: ', pos(3)
284       !velocity_cfmin1(3)=velocity(3)
285       !tc_min1 = t
286       fdll_pos_n=fdll_lifMot(1,:)
287       velocity_n=fdll_lifVel(1,:)
288       acceleration_n=fdll_lifAcc_check
```

```
289         dta=fdll_time-t_nmin1
290         print*, 'dt aNySIM      = ', dta
291         !
292         ! loop for calculating cubic splines
293           if (fdll_time > dta*8) then
294         !
295         ! LOOP FOR DISPLACEMENT
296               do k = 1, 6
297                   xmin=t_nmin3
298                   xmax=t
299                   xi(1)=t_nmin3
300                   xi(2)=t_nmin2
301                   xi(3)=t_nmin1
302                   xi(4)=fdll_time
303                   yi(1,k)=fdll_pos_nmin3(k)
304                   yi(2,k)=fdll_pos_nmin2(k)
305                   yi(3,k)=fdll_pos_nmin1(k)
306                   yi(4,k)=fdll_pos_n(k)
307                   !print*, 'heave_n-3    = ', fdll_pos_nmin3(k)
308                   !print*, 'heave_n-2    = ', fdll_pos_nmin2(k)
309                   !print*, 'heave_n-1    = ', fdll_pos_nmin1(k)
310                   !print*, 'heave_n      = ', fdll_pos_n(k)
311                   ! call spline subroutie
312                   call spline (xi, yi(:,k), b, c, d,n)
313                   ! time at which we want the spline interpolation
314                   x = t
315                   y = pos_linear(k)
316                   !print*, '-----check linear vs spline-------'
317                   !print*, 'roll_linear     = ', y
318                   ys = ispline(x, xi, yi(:,k), b, c, d, n)
319                   !print*, 'roll_cubic      = ', ys
320                   error=abs((ys-y)/y*100)
321                   !print*, 'difference (%)  = ', error
322                   pos(k)=ys
323               enddo
324         !
325         ! LOOP FOR VELOCITY
326               do k = 1, 6
327                   xmin=t_nmin3
328                   xmax=t
329                   xi(1)=t_nmin3
330                   xi(2)=t_nmin2
331                   xi(3)=t_nmin1
332                   xi(4)=fdll_time
333                   yi(1,k)=velocity_min3(k)
334                   yi(2,k)=velocity_min2(k)
335                   yi(3,k)=velocity_min1(k)
336                   yi(4,k)=velocity_n(k)
337                   !print*, 'velocity_n-3    = ', velocity_min3(k)
338                   !print*, 'velocity_n-2    = ', velocity_min2(k)
339                   !print*, 'velocity_n-1    = ', velocity_min1(k)
340                   !print*, 'velocity_n      = ', velocity_n(k)
341                   ! call spline subroutie
342                   call spline (xi, yi(:,k), b, c, d,n)
343                   ! time at which we want the spline interpolation
344                   x = t
```

```
345                 y = velocity_linear(k)
346                 !print*, '-----check linear vs spline-------'
347                 !print*, 'velocity_linear    = ', y
348                 ys = ispline(x, xi, yi(:,k), b, c, d, n)
349                 !print*, 'velocity_cubic     = ', ys
350                 error=abs((ys-y)/y*100)
351                 !print*, 'difference (%)  = ', error
352                 velocity(k)=ys
353             enddo
354       !
355       ! LOOP FOR ACCELERATION
356             do k = 1, 6
357                 xmin=t_nmin3
358                 xmax=t
359                 xi(1)=t_nmin3
360                 xi(2)=t_nmin2
361                 xi(3)=t_nmin1
362                 xi(4)=fdll_time
363                 yi(1,k)=acceleration_min3(k)
364                 yi(2,k)=acceleration_min2(k)
365                 yi(3,k)=acceleration_min1(k)
366                 yi(4,k)=acceleration_n(k)
367                 !print*, 'aceleration_n-3   = ', acceleration_min3(k)
368                 !print*, 'aceleration_n-2   = ', acceleration_min2(k)
369                 !print*, 'aceleration_n-1   = ', acceleration_min1(k)
370                 !print*, 'aceleration_n     = ', acceleration_n(k)
371                 ! call spline subroutie
372                 call spline (xi, yi(:,k), b, c, d,n)
373                 ! time at which we want the spline interpolation
374                 x = t
375                 y = acceleration_linear(k)
376                 !print*, '-----check linear vs cubic-------'
377                 !print*, 'acceleration_linear    = ', y
378                 ys = ispline(x, xi, yi(:,k), b, c, d, n)
379                 !print*, 'acceleration_cubic     = ', ys
380                 error=abs((ys-y)/y*100)
381                 !print*, 'difference (%)  = ', error
382                 acceleration(k)=ys
383             enddo
384       !
385       ! APPLY LINEAR INTERPOLATION BEFORE CUBIC SPLINE IS USED
386         else
387             pos=pos_linear
388             velocity=velocity_linear
389             acceleration=acceleration_linear
390         endif
391       !
392     endif
393     !
394     !print*, 'heave acceleration to comflow    = ', acceleration(3)
395     ! Set moving frame based on current time
396     call set_moving_frame(t, pos, velocity, acceleration)
397     ! carry out a timestep
398     !
399     ! Store forces and moments from previous time step
400     !
```

```
401       if (fdll_time == 0) then
402       tcom_nmin1 = 0.0
403       force_nmin1 = 0.0
404       moment_nmin1 = 0.0
405   else
406       tcom_nmin1 = t
407       force_nmin1 = force
408       moment_nmin1 = moment
409   endif
410   !
411   ! End store forces and moments previous time step
412   !
413   call loop
414   call get_time(tcycle,t,tmax,dt)
415   !
416   !
417   ! obtain the forces on the tank
418   call get_force_frcbx(boxnr,force,moment,inertia,moment_location)
419   !write (3,'(ES14.6, 6ES14.6)') t, force(3)
420   !
421   ! Close loop
422   enddo
423
424     print*, 'Heave force from ComFLOW: ', force(3)
425   write_force=force
426   write_moment=moment
427
428     ! Define time, motions, velocities, accelerations to be used as
          information in next loop for t-1 calculations (extrapolation)
429  !
430   if (fdll_time > dta*6) then
431             t_nmin3 = t_nmin2
432             fdll_pos_nmin3 = fdll_pos_nmin2
433             velocity_min3=velocity_min2
434             acceleration_min3=acceleration_min2
435 else
436 endif
437  !
438   if (fdll_time > dta*5) then
439             t_nmin2 = t_nmin1
440             fdll_pos_nmin2 = fdll_pos_nmin1
441             velocity_min2=velocity_min1
442             acceleration_min2=acceleration_min1
443 else
444 endif
445 !
446     if (fdll_time == 0) then
447       t_nmin1 = 0.0
448       pos_min1 = 0.0
449       velocity_min1 = 0.0
450       acceleration_min1 = 0.0
451   else
452       t_nmin1 = fdll_time
453       pos_min1 = pos
454       velocity_min1 = velocity
455       acceleration_min1 = acceleration
```

```
456         fdll_pos_nmin1=fdll_lifMot(1,:)
457     endif
458
459     !
460     !----- Define forces going from ComFLOW to aNySIM
461     !       tcom_nmin1 = t
462         !force_nmin1 = force
463         !moment_nmin1 = moment
464     !------Apply linear extrapolation to obtain estimate of current
           forces and moments
465     !
466     !       pos_linear=pos_min1+(fdll_lifMot(1,:)-pos_min1)/(fdll_time-
           t_nmin1)*(t-t_nmin1)
467
468     force_linear=force_nmin1+(force-force_nmin1)/(t-tcom_nmin1)*(
           fdll_time-tcom_nmin1)
469     moment_linear= moment_nmin1+(moment-moment_nmin1)/(t-tcom_nmin1)*(
           fdll_time-tcom_nmin1)
470     dforce=(force(2)-force_linear(2))/force_linear(2)*100
471     dmoment=(moment(1)-moment_linear(1))/moment_linear(1)*100
472     !
473     ! Linear interpolated forces and moments
474     fdll_force(1,1)=force(1)/1000
475     fdll_force(1,2)=force(2)/1000
476     fdll_force(1,3)=force(3)/1000
477     fdll_force(1,4)=moment(1)/1000
478     fdll_force(1,5)=moment(2)/1000
479     fdll_force(1,6)=moment(3)/1000
480     write_force_linear=force_linear
481     write_moment_linear=moment_linear
482     !
483     ! End loop that checks if comflow time is zero or not.
484     endif
485     !
486     ! Print force comparison to screen
487       print*, 'Comparison of forces and moments'
488       print*, 'ComFLOW time           = ',t
489       print*, 'aNySIM time            = ',fdll_time
490       !print*, 'Fy_no extr.     = ', force(2)
491       !print*, 'Fy_linear extr. = ', force_linear(2)
492       print*, 'Force difference (%)  = ', dforce
493       ! Print moment comparison to screen
494       !print*, 'Mx_no extr.     = ', moment(1)
495       !print*, 'Mx_linear extr. = ', moment_linear(1)
496       print*, 'Moment Difference (%)  = ', dmoment
497     !
498 contains
499         function ispline(u, x, y, b, c, d, n)
500 !======================================================================
501 ! function ispline evaluates the cubic spline interpolation at point z
502 ! ispline = y(i)+b(i)*(u-x(i))+c(i)*(u-x(i))**2+d(i)*(u-x(i))**3
503 ! where  x(i) <= u <= x(i+1)
504 !----------------------------------------------------------------------
505 ! input..
506 ! u       = the abscissa at which the spline is to be evaluated
507 ! x, y    = the arrays of given data points
```

```
508 ! b, c, d = arrays of spline coefficients computed by spline
509 ! n       = the number of data points
510 ! output:
511 ! ispline = interpolated value at point u
512 !
    ===========================================================================
513 implicit none
514 double precision ispline
515 integer n
516 double precision  u, x(n), y(n), b(n), c(n), d(n)
517 integer i, j, k
518 double precision dx
519
520 ! if u is ouside the x() interval take a boundary value (left or right)
521 if(u <= x(1)) then
522   ispline = y(1)
523   return
524 end if
525 if(u >= x(n)) then
526   ispline = y(n)
527   return
528 end if
529
530 !*
531 !  binary search for for i, such that x(i) <= u <= x(i+1)
532 !*
533 i = 1
534 j = n+1
535 do while (j > i+1)
536   k = (i+j)/2
537   if(u < x(k)) then
538     j=k
539     else
540     i=k
541    end if
542 end do
543 !*
544 !  evaluate spline interpolation
545 !*
546 dx = u - x(i)
547 ispline = y(i) + dx*(b(i) + dx*(c(i) + dx*d(i)))
548       end function ispline
549
550 end subroutine FDLL_calcForce
551
552 !---------------------------------------------------------------------
553 !
554 ! FDLL_getForce is an interface procedure,
555 ! its signature may not be changed.
556 !
557 !---------------------------------------------------------------------
558
559 subroutine FDLL_getForce(bodyIndex, force)
560   integer,                intent(in)  ::  bodyIndex
561   real,   dimension(6),   intent(out) ::  force
```

```
562
563   ! Expose subroutine ExtFortranDLL to users of this DLL
564   !
565   !DEC$ ATTRIBUTES DLLEXPORT::FDLL_getForce
566
567   ! Variables
568
569   ! Body of FDLL_getForce
570   !
571
572   if (fdll_time == 0) then
573         force(:) = fdll_force(bodyIndex,:)
574   else
575         force(1:3)= force_linear(:)/1000
576         force(4:6)= moment_linear(:)/1000
577   endif
578
579   !force(1:3)= force_linear(:)
580   !force(4:6)= moment_linear(:)
581   print*, 'Fz to aNySIM = ', force(3)
582
583
584
585
586 end subroutine FDLL_getForce
587
588 !-----------------------------------------------------------------------
589 !
590 ! FDLL_output is an interface procedure,
591 ! its signature may not be changed.
592 !
593 !-----------------------------------------------------------------------
594
595 subroutine FDLL_output()
596   ! Expose subroutine ExtFortranDLL to users of this DLL
597   !
598   !DEC$ ATTRIBUTES DLLEXPORT::FDLL_output
599
600   ! Variables
601
602   ! Body of FDLL_output
603
604 #ifdef __EXAMPLE__
605    integer  :: columnCount
606    write (2,'(ES14.6, 6ES14.6)') fdll_time, (fdll_force(1 ,columnCount)
          ,columnCount=1,6)
607 #endif __EXAMPLE__
608    integer  :: columnCount
609    write (2,'(ES14.6, 6ES14.6, 6ES14.6, 6ES14.6, 6ES14.6, 6ES14.6, 6
          ES14.6, 6ES14.6, 6ES14.6, 6ES14.6)') fdll_time, (fdll_efPosition
          (1 ,columnCount),columnCount=1,6), (fdll_lifMot(1 ,columnCount),
          columnCount=1,6), (fdll_lifVel(1 ,columnCount),columnCount=1,6),
           (fdll_sfMotion(1 ,columnCount),columnCount=1,6), (fdll_sfVeloc
          (1 ,columnCount),columnCount=1,6), (write_force(columnCount),
          columnCount=1,3), (write_moment(columnCount),columnCount=1,3), (
          write_force_linear(columnCount),columnCount=1,3), (
```

```
      write_moment_linear(columnCount),columnCount=1,3)
end subroutine FDLL_output

!---------------------------------------------------------------------
!
! FDLL_close is an interface procedure,
! its signature may not be changed.
!
!---------------------------------------------------------------------

subroutine FDLL_close

  ! Expose subroutine ExtFortranDLL to users of this DLL
  !
  !DEC$ ATTRIBUTES DLLEXPORT::FDLL_close

  ! Variables

  ! Body of FDLL_close

#ifdef __EXAMPLE__
  write(*,*) 'FDLL_close'
  ! Close TimeTrace.txt:

#endif __EXAMPLE__
  close(2)
  !close(3)
  if (allocated( fdll_sfMotion) )    deallocate( fdll_sfMotion )
  if (allocated( fdll_sfVeloc ) )    deallocate( fdll_sfVeloc )
  if (allocated( fdll_sfAccel ) )    deallocate( fdll_sfAccel )
  if (allocated( fdll_efPosition ) ) deallocate( fdll_efPosition )
  if (allocated( fdll_lifMot ) )     deallocate( fdll_lifMot )
  if (allocated( fdll_lifVel ) )     deallocate( fdll_lifVel )

  if (allocated( fdll_force ) )      deallocate( fdll_force )

  call closure !<-- clean up again and close ComFLOW

end subroutine FDLL_close

!---------------------------------------------------------------------

#ifdef __EXAMPLE__
subroutine FDLL_spring(bodyIndex, force)
    integer,                intent(in)  :: bodyIndex
    real,   dimension(6),   intent(out) :: force

    force(1) = 0
    force(2) = 0
    force(6) = 0

end subroutine FDLL_spring
#endif __EXAMPLE__

!
!
```

```
!
! include function
!
!

!
!
    end module ExtFortranDLL

       subroutine spline (x, y, b, c, d, n)
!======================================================================
!  Calculate the coefficients b(i), c(i), and d(i), i=1,2,...,n
!  for cubic spline interpolation
!  s(x) = y(i) + b(i)*(x-x(i)) + c(i)*(x-x(i))**2 + d(i)*(x-x(i))**3
!  for  x(i) <= x <= x(i+1)
!  Alex G: January 2010
!----------------------------------------------------------------------
!  input..
!  x = the arrays of data abscissas (in strictly increasing order)
!  y = the arrays of data ordinates
!  n = size of the arrays xi() and yi() (n>=2)
!  output..
!  b, c, d  = arrays of spline coefficients
!  comments ...
!  spline.f90 program is based on fortran version of program spline.f
!  the accompanying function fspline can be used for interpolation
!======================================================================
implicit none
integer n
double precision x(n), y(n), b(n), c(n), d(n)
integer i, j, gap
double precision h

gap = n-1
! check input
if ( n < 2 ) return
if ( n < 3 ) then
  b(1) = (y(2)-y(1))/(x(2)-x(1))   ! linear interpolation
  c(1) = 0.
  d(1) = 0.
  b(2) = b(1)
  c(2) = 0.
  d(2) = 0.
  return
end if
!
! step 1: preparation
!
d(1) = x(2) - x(1)
c(2) = (y(2) - y(1))/d(1)
do i = 2, gap
  d(i) = x(i+1) - x(i)
  b(i) = 2.0*(d(i-1) + d(i))
  c(i+1) = (y(i+1) - y(i))/d(i)
  c(i) = c(i+1) - c(i)
end do
```

```
721 !
722 ! step 2: end conditions
723 !
724 b(1) = -d(1)
725 b(n) = -d(n-1)
726 c(1) = 0.0
727 c(n) = 0.0
728 if(n /= 3) then
729   c(1) = c(3)/(x(4)-x(2)) - c(2)/(x(3)-x(1))
730   c(n) = c(n-1)/(x(n)-x(n-2)) - c(n-2)/(x(n-1)-x(n-3))
731   c(1) = c(1)*d(1)**2/(x(4)-x(1))
732   c(n) = -c(n)*d(n-1)**2/(x(n)-x(n-3))
733 end if
734 !
735 ! step 3: forward elimination
736 !
737 do i = 2, n
738   h = d(i-1)/b(i-1)
739   b(i) = b(i) - h*d(i-1)
740   c(i) = c(i) - h*c(i-1)
741 end do
742 !
743 ! step 4: back substitution
744 !
745 c(n) = c(n)/b(n)
746 do j = 1, gap
747   i = n-j
748   c(i) = (c(i) - d(i)*c(i+1))/b(i)
749 end do
750 !
751 ! step 5: compute spline coefficients
752 !
753 b(n) = (y(n) - y(gap))/d(gap) + d(gap)*(c(gap) + 2.0*c(n))
754 do i = 1, gap
755   b(i) = (y(i+1) - y(i))/d(i) - d(i)*(c(i+1) + 2.0*c(i))
756   d(i) = (c(i+1) - c(i))/d(i)
757   c(i) = 3.*c(i)
758 end do
759 c(n) = 3.0*c(n)
760 d(n) = d(n-1)
761     end subroutine spline
```

B

Theory

This chapter will provide some background information on the equations that are used by WAMIT and ComFLOW. Reference and a thank you is made to Journee and Massie (2001) for providing an excellent overview of the equations for potential flow. The derivation of the Navier Stokes equations has been created by considering a large range of sources, among others the ComFLOW manual.

B.1. Navier-Stokes equations

The Navier-Stokes equations will be derived by considering the continuity equation (Section B.1.1) and the momentum equations (Section B.1.2)

B.1.1. Continuity equation

An important constraint for fluid motions is mass conservation, expressed by the continuity equation. For the derivation a fluid element is considered that is small enough so that the flow through the faces can be expressed by the first two terms of the Taylor expansion. The considered fluid element has dimensions dx, dy and dz .

Figure B.1 below shows the inflow- and outflow of mass through the sides of the element. For example, for the flow in the x-direction the total mass going into the element is $[\rho u]dydz$, while the mass going out is equal to $[\rho u + \frac{\partial(\rho u)}{\partial x}dx]dydz$ (higher order terms have been neglected). The same can be done for all other direction.

The increase of mass in the element can be expressed by considering:

1. The rate of increase of mass inside the element:

$$\frac{\partial}{\partial t}(\rho dxdydz) = \frac{\partial \rho}{\partial t}(dxdydz) \tag{B.1}$$

2. The flux of mass going out of the element

$$\begin{aligned}\left[\rho u + \frac{\partial(\rho u)}{\partial x}dx\right]\ dydz - [\rho u]\ dydz + \left[\rho v + \frac{\partial(\rho v)}{\partial y}dx\right]\ dxdz - [\rho v]\ dxdz \\ + \left[\rho w + \frac{\partial(\rho w)}{\partial z}dz\right]\ dxdy - [\rho w]\ dxdy\end{aligned} \tag{B.2}$$

which is equal to:

$$\frac{\partial(\rho u)}{\partial x}\ dxdydz + \frac{\partial(\rho v)}{\partial y}\ dxdydz + \frac{\partial(\rho w)}{\partial z}\ dxdydz \tag{B.3}$$

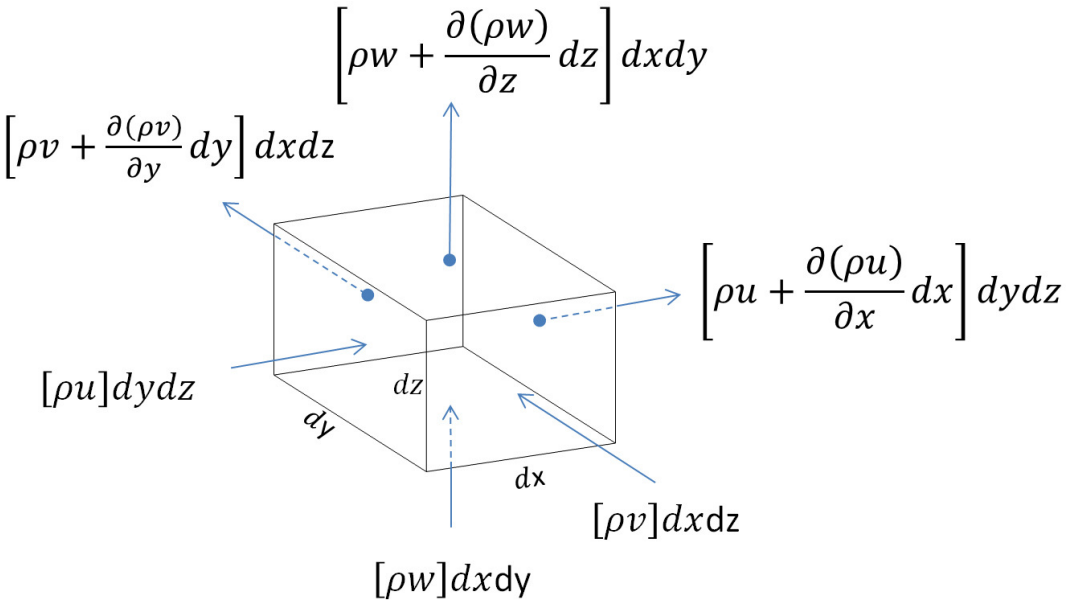

Figure B.1: Flow through an element with volume $dx\ dy\ dz$.

As the rate of change of the mass inside the element decreases when the mass going out of the element increases, the total increase of mass inside the element is given by:

$$\frac{\partial \rho}{\partial t}(dxdydz) = -\frac{\partial(\rho u)}{\partial x}\, dxdydz - \frac{\partial(\rho v)}{\partial y}\, dxdydz - \frac{\partial(\rho w)}{\partial z}\, dxdydz \tag{B.4}$$

$$\tag{B.5}$$

After reordering Equation B.4 and dividing by $dxdydz$ the three-dimensional mass conversation or continuity equation for compressible flow is obtained:

$$\frac{\partial \rho}{\partial t} + \frac{\partial(\rho u)}{\partial x} + \frac{\partial(\rho v)}{\partial y} + \frac{\partial(\rho w)}{\partial z} = 0 \tag{B.6}$$

Which can also be written as:

$$\frac{\partial \rho}{\partial t} + \nabla \cdot (\rho \boldsymbol{u}) = 0 \tag{B.7}$$

Where $\boldsymbol{u} = \boldsymbol{i}u + \boldsymbol{j}v + \boldsymbol{k}w$ ($\boldsymbol{i}, \boldsymbol{j}$ and $\boldsymbol{k}$ are the unit vectors for an x,y,z reference frame) and ∇ is the divergence.

However, if incompressible flow (μ is constant) is assumed than the continuity equations simplifies to:

$$\frac{\partial u}{\partial x} + \frac{\partial v}{\partial y} + \frac{\partial w}{\partial z} = 0 \tag{B.8}$$

$$\nabla \cdot \boldsymbol{u} = 0 \tag{B.9}$$

B.1.2. Momentum equations

The momentum equations are very important in the derivation for obtaining the Navier-Stokes equations. Newton's Second Law states that the rate of change of momentum of a fluid particle is equal to the forces on this fluid particle:

$$\boldsymbol{F} = m\boldsymbol{a} \tag{B.10}$$

$$\boldsymbol{F} = \rho dxdydz \frac{D\boldsymbol{u}}{Dt} \tag{B.11}$$

Where the acceleration of a fluid particle is given by the Lagrangian $\frac{D}{Dt}$ of the fluid velocity:

$$\frac{D\boldsymbol{u}}{Dt} = \frac{\partial \boldsymbol{u}}{\partial t} + \frac{\partial u}{\partial x}u + \frac{\partial v}{\partial y}v + \frac{\partial w}{\partial z}w = \frac{\partial \boldsymbol{u}}{\partial t} + (\boldsymbol{u}\cdot\nabla)\boldsymbol{u} \tag{B.12}$$

The next step is to obtain the rate of increase of the momentum in the fluid element. This is done in the same way as for obtaining the continuity equation in Section B.1.1. However, instead of considering a mass flux of $[\rho\boldsymbol{u}]dxdydz$ now a momentum flux is considered. This results in the momentum equations:

$$\rho dxdydz\frac{Du}{Dt} = \left(\frac{\partial \rho u}{\partial t} + \frac{\partial(\rho uu)}{\partial x} + \frac{\partial(\rho uv)}{\partial y} + \frac{\partial(\rho uw)}{\partial z}\right)dxdydz \tag{B.13}$$

$$\rho dxdydz\frac{Dv}{Dt} = \left(\frac{\partial \rho v}{\partial t} + \frac{\partial(\rho uv)}{\partial x} + \frac{\partial(\rho vv)}{\partial y} + \frac{\partial(\rho vw)}{\partial z}\right)dxdydz \tag{B.14}$$

$$\rho dxdydz\frac{Dw}{Dt} = \left(\frac{\partial \rho w}{\partial t} + \frac{\partial(\rho uw)}{\partial x} + \frac{\partial(\rho vw)}{\partial y} + \frac{\partial(\rho ww)}{\partial z}\right)dxdydz \tag{B.15}$$

The final step is to consider the forces that are acting on the fluid element.

1. Pressure forces
   If the element in Figure B.1 is considered, than the net pressure forces in the x, y and z-direction are:

$$F_{px} = [p]dydz - \left[p + \frac{\partial p}{\partial x}dx\right]dydz = -\frac{\partial p}{\partial x}dxdydz \tag{B.16}$$

$$F_{py} = [p]dxdz - \left[p + \frac{\partial p}{\partial y}dy\right]dxdz = -\frac{\partial p}{\partial x}dxdydz \tag{B.17}$$

$$F_{pz} = [p]dxdy - \left[p + \frac{\partial p}{\partial w}dz\right]dxdy = -\frac{\partial p}{\partial x}dxdydz \tag{B.18}$$

   Or in vector notation:

$$\boldsymbol{F} = [\nabla p]dxdydz \tag{B.19}$$

2. Viscous forces
   The viscous forces are obtained by considering the Cauchy stress tensor $\boldsymbol{\sigma}$:

$$\sigma_{ij} = \begin{bmatrix}\sigma_{xx} & \tau_{xy} & \tau_{xz}\\ \tau_{yx} & \sigma_{yy} & \tau_{yz}\\ \tau_{zx} & \tau_{zy} & \sigma_{zz}\end{bmatrix} = -\begin{bmatrix}\pi & 0 & 0\\ 0 & \pi & 0\\ 0 & 0 & \pi\end{bmatrix} + \begin{bmatrix}\sigma_{xx}+\pi & \tau_{xy} & \tau_{xz}\\ \tau_{yx} & \sigma_{yy}+\pi & \tau_{yz}\\ \tau_{zx} & \tau_{zy} & \sigma_{zz}+\pi\end{bmatrix} = -\pi\cdot I + T \tag{B.20}$$

   where τ- and σ are the shear- and normal stresses, T is the deviator stress tensor, and π is the mean normal stress, which equal to the mechanical pressure:

$$\pi = -\frac{1}{3}\left(\sigma_{xx} + \sigma_{yy} + \sigma_{xx}\right) \tag{B.21}$$

   And the viscous force is given by:

$$\boldsymbol{F_v} = [\nabla\boldsymbol{\sigma}]dxdydz \tag{B.22}$$

   In order to include viscous forces in the Navier-Stokes equations, Stokes made the following assumptions:

   (a) The stress tensor is linear depending on the strain rates (μ is not constant)

   (b) The fluid is isotropic

   (c) When the fluid is at rest, only the hydrostatic pressure results, so $\boldsymbol{T} = 0$.

Applying the above assumptions to the stress tensor gives:

$$T_{ij} = \mu \left(\frac{\partial V_i}{\partial X_j} + \frac{\partial V_j}{\partial X_i} - \frac{2}{3}\delta_{ij}\frac{\partial V_k}{\partial X_k} \right) + \delta_{ij}\lambda \frac{\partial V_k}{\partial X_j} \tag{B.23}$$

Where μ is the dynamic viscosity, λ is the second coefficient of viscosity, and δ_{ij} is the Kronecker delta. Substituting Equation B.23 in the momentum equations (B.13 to B.15) will result in Navier-Stokes equations for compressible flow, which will not be discussed here as incompressible flow is assumed for this project. To obtain the solution for incompressible flow the following assumptions are made:

(a) The viscosity μ is constant

(b) The second viscosity effect $\lambda = 0$

(c) The simplified (incompressible) continuity equation $\boldsymbol{\nabla} \cdot \boldsymbol{u} = 0$ can be used to simplify the Navier-Stokes equations

Applying these assumptions to the solution for compressible flow gives:

$$F_{vx} = \nabla \cdot \boldsymbol{\sigma} = \nabla \cdot \mu \nabla u = \mu \nabla^2 u \tag{B.24}$$

$$F_{vy} = \mu \nabla^2 v \tag{B.25}$$

$$F_{vz} = \mu \nabla^2 w \tag{B.26}$$

Which can also be written in vector form:

$$\boldsymbol{F}_v = \mu \nabla^2 \boldsymbol{u} \tag{B.27}$$

Substitution of the pressure- and viscous forces in the momentum equations (equations B.13 to B.15) give a commonly used expression of the Navier-Stokes equations:

$$\rho dxdydz \frac{Du}{Dt} = \left(-\frac{\partial p}{\partial x} + \mu \nabla^2 u \right) dxdydz + F_{ext,x} \tag{B.28}$$

$$\rho dxdydz \frac{Dv}{Dt} = \left(-\frac{\partial p}{\partial y} + \mu \nabla^2 v \right) dxdydz + F_{ext,y} \tag{B.29}$$

$$\rho dxdydz \frac{Dw}{Dt} = \left(-\frac{\partial p}{\partial z} + \mu \nabla^2 w \right) dxdydz + F_{ext,z} \tag{B.30}$$

Where $\boldsymbol{F}_{ext}$ is the vector with external forces acting on the fluid. Dividing by $\rho \cdot dxdydz$ and writing the above equation in vector notation gives:

$$\frac{Du}{Dt} = -\frac{1}{\rho}\nabla p + \frac{\mu}{\rho}\nabla^2 \boldsymbol{u} + F_{ext} \tag{B.31}$$

Or by expanding the Lagrangian:

$$\frac{\partial \boldsymbol{u}}{\partial t} + \boldsymbol{u} \cdot \nabla \boldsymbol{u} = -\frac{1}{\rho}\nabla p + \frac{\mu}{\rho}\nabla \cdot \nabla \boldsymbol{u} + \boldsymbol{F}_{ext} \tag{B.32}$$

Which gives the expression of the Navier-Stokes equation used in the ComFLOW manual. External forces acting on the fluid element are for example the gravity force, which is given by:

$$F_{g,x} = 0 \tag{B.33}$$

$$F_{g,y} = 0 \tag{B.34}$$

$$F_{g,z} = -[\rho g] dxdydz \tag{B.35}$$

B.2. Diffraction code

B.2.1. Principles of linear potential theory

In this section the basic principles of linear potential theory will be described. First the assumptions and boundary conditions will be elaborated on, followed by a discussion on the effects of the linear approach on ship motions.

Assumptions

Potential flow theory is based on the following assumptions:

- The fluid is an ideal fluid
  For an ideal fluid it is assumed that the viscosity $\mu = 0$. As a result, for example, the normal σ- and shear τ stresses in the momentum equation take the following form:

$$\sigma_{xx} = -p + 2\mu\frac{\partial u}{\partial x} = -p \tag{B.36}$$

$$\tau_{xy} = \mu\left(\frac{\partial v}{\partial x} + \frac{\partial u}{\partial y}\right) = 0 \tag{B.37}$$

  Because an ideal fluid is considered the following assumptions are implicitly made:

  - The fluid is frictionless
  - The fluid is homogeneous
    All fluid considered has uniform properties
  - The fluid is free of surface tension
  - The fluid is incompressible
    The density of the fluid ρ is constant, so that:

$$\frac{D\rho}{Dt} = \frac{\partial \rho}{\partial t} + \rho\nabla \cdot \boldsymbol{u} = 0 \tag{B.38}$$

- The fluid is irrotational
  $\boldsymbol{\nabla} \cdot \boldsymbol{u} = 0$, meaning that the divergence of $\boldsymbol{u}$ is equal to zero, where $\boldsymbol{u} = \boldsymbol{u}(\boldsymbol{X}, t)$ is the velocity of an element of fluid at a position $\boldsymbol{X}$ and time t.
- The wave steepness (ζ/λ), and resulting vessel motions and velocities are small.
  According to Denis (1974) small vessel motions give heave amplitudes smaller than $1/5^{th}$ of the draft, roll amplitudes smaller than 15 degrees and pitch amplitudes smaller than 5 degrees.

  When the wave steepness, vessel motions and vessel velocities are small the higher order terms in the free surface boundary condition, kinematic boundary condition and in the Bernoulli equation can be neglected. This assumptions makes the linear approach valid in which total potential can be decomposed into a number of separate potentials.

Decomposing the total potential

As small motion amplitudes are assumed, the total potential $\Phi(x, y, z, t)$ can be decomposed in three components:

1. The undisturbed incident wave potential $\Phi_w(x, y, z, t)$
2. The wave diffraction potential $\Phi_d(x, y, z, t)$
3. The wave radiation potential $\Phi_r(x, y, z, t)$

So that:

$$\Phi(x, y, z, t) = \Phi_w(x, y, z, t) + \Phi_d(x, y, z, t) + \Phi_r(x, y, z, t) \tag{B.39}$$

or simply: $\Phi = \Phi_w + \Phi_d + \Phi_r$. Next to the fact that the total potential can be decomposed, also the vessel motions can be decomposed in six degrees of freedom. If it is also assumed that the waves and motions are sinusoidal and that the potential can be separated in a time- and place dependent part

the potentials. Finally, the radiation potential is normalised by using the oscillation velocity v_j. This yields:

$$\Phi_w(x,y,z,t) = \phi_w(x,y,z)e^{-i\omega t} \tag{B.40}$$

$$\Phi_d(x,y,z,t) = \phi_d(x,y,z)e^{-i\omega t} \tag{B.41}$$

$$\Phi_r(x,y,z,t) = \sum_{j=1}^{6} \phi_j(x,y,z)e^{-i\omega t} = \sum_{j=1}^{6} v_j\phi_j(x,y,z)e^{-i\omega t} \tag{B.42}$$

Boundary conditions

The potentials can be solved by applying the following boundary conditions:

1. Laplace equation for homogeneous and incompressible fluid
   By substituting the water particle velocities in the three translational directions (that following from the definition of the velocity potential)

   $$u = \frac{\partial \Phi}{\partial x} \qquad v = \frac{\partial \Phi}{\partial y} \qquad w = \frac{\partial \Phi}{\partial z} \tag{B.43}$$

   in the Continuity Condition:

   $$\frac{\partial u}{\partial x} + \frac{\partial v}{\partial y} + \frac{\partial w}{\partial z} = 0 \tag{B.44}$$

   the Laplace Equation for homogeneous and incompressible flow is found:

   $$\nabla^2\Phi = \frac{\partial^2 \Phi}{\partial x^2} + \frac{\partial^2 \Phi}{\partial y^2} + \frac{\partial^2 \Phi}{\partial z^2} \tag{B.45}$$

2. Sea bed boundary condition
   The vertical water particle velocity at the sea bed is zero so that no water can leak through the sea floor:

   $$\frac{\partial \Phi}{\partial z} = 0 \qquad \text{for: } z = -h \tag{B.46}$$

3. Free surface dynamic boundary condition
   At the free surface ($z = \zeta$) the pressure p is equal to the atmospheric pressure. Using the Bernoulli equation an expression for the free surface pressure can be given in terms of the potential Φ:

   $$\frac{\partial \Phi}{\partial t} + \frac{1}{2}\left(u^2 + v^2 + w^2\right) + \frac{p}{\rho} + gz = C^* \tag{B.47}$$

   Assuming two dimensions ($y = 0$) and small wave steepness (u and v are small) gives the linearised Bernoulli equation:

   $$\frac{\partial \Phi}{\partial t} + \frac{p}{\rho} + gz = C^* \tag{B.48}$$

   Or with $z = \zeta$:

   $$\frac{\partial \Phi}{\partial t} + \frac{p_0}{\rho} + g\zeta = C^* \tag{B.49}$$

   The next step is to include $\frac{p_0}{\rho} - C^*$ into $\frac{\partial \Phi}{\partial t}$ as this will not influence the velocities from the potential Φ:

   $$\frac{\partial \Phi}{\partial t} + g\zeta = 0 \tag{B.50}$$

To find the derivative of Φ Taylor expansion is used at the potential at the free surface:

$$\{\Phi(x,z,t)\}_{z=\zeta} = \{\Phi(x,z,t)\}_{z=0} + \zeta \cdot \left\{\frac{\partial\Phi(x,z,t)}{\partial z}\right\}_{z=0} + \zeta^2 \cdot \left\{\frac{\partial\Phi^2(x,z,t)}{\partial z^2}\right\}_{z=0} + ... \quad \text{(B.51)}$$

Assuming a small wave steepness and small resulting vessel motions the derivative of the potential can be written as:

$$\left\{\frac{\partial\Phi(x,z,t)}{\partial t}\right\}_{z=\zeta} = \left\{\frac{\partial\Phi(x,z,t)}{\partial t}\right\}_{z=0} + \mathcal{O}(\epsilon^2) \quad \text{(B.52)}$$

In which linearisation of the boundary condition is used, yielding the free surface dynamic boundary condition (for $z = 0$):

$$\frac{\partial\Phi}{\partial t} + g\zeta = 0 \quad \text{(B.53)}$$

So that the wave profile can be written as:

$$\zeta = -\frac{1}{g}\frac{\partial\Phi}{\partial t} \quad \text{(B.54)}$$

However, the goal is to obtain the free surface kinematic boundary condition, which includes the relationship between T and λ. This is achieved by assuming that the vertical velocity of a water particle at the free surface is the same as the vertical velocity of the free surface itself. For the wave surface this gives:

$$\frac{\partial z}{\partial t} = \frac{\partial\zeta}{\partial x} \cdot \frac{\partial x}{\partial t} \qquad \text{for } z = \zeta \quad \text{(B.55)}$$

However, the second term is a product of two small values (because of the assumed wave steepness). By multiplying those two small values a very small (second order) relation is found that can be ignored. This linearisation gives:

$$\frac{\partial z}{\partial t} = \frac{\partial\zeta}{\partial t} \quad \text{(B.56)}$$

$$\frac{\partial\Phi}{\partial z} = \frac{\partial\zeta}{\partial t} \quad \text{(B.57)}$$

Just as for Equation B.53 these conditions are also valid for $z = 0$ (by Taylor expansion). By taking the derivative of Equation B.53 with respect to t gives:

$$\frac{\partial^2\Phi}{\partial t^2} + g\frac{\partial\zeta}{\partial t} = 0 \qquad \text{for } z = 0 \quad \text{(B.58)}$$

Substitution of Equation B.57 in B.58 gives:

$$\frac{\partial^2\Phi}{\partial t^2} + g\frac{\partial\Phi}{\partial z} = 0 \quad \text{(B.59)}$$

$$\text{(B.60)}$$

Or after rearranging the terms:

$$\frac{\partial\Phi}{\partial z} + \frac{1}{g}\frac{\partial^2\Phi}{\partial t^2} = 0 \quad \text{(B.61)}$$

Or alternatively, in the form of the Cauchy Poission Condition by substituting Equation B.57 and B.56 in Equation B.61:

$$\frac{\partial z}{\partial t} + \frac{1}{g} \cdot \frac{\partial^2\Phi}{\partial t^2} = 0 \qquad \text{for } z = 0 \quad \text{(B.62)}$$

4. Kinematic Boundary Condition on the oscillating body surface
   The water particle velocity at a point at the surface of the body is equal to the velocity of this point itself. Therefore, the outward normal (n) velocity v_n at a point $P(x, y, z)$ which is at the outside of the body is given by:

$$\frac{\partial \Phi}{\partial n} = v_n(x, y, z; t) \tag{B.63}$$

   And because the solutions for the potentials will be linearised this can be written as:

$$\frac{\partial \Phi}{\partial n} = v_n(x, y, z; t) = \sum_{j=1}^{6} v_j \cdot f_j(x, y, z) \tag{B.64}$$

   where v_j and f_j are the oscillatory velocities and generalised direction cosines on the vessel respectively. f_j is given by:

$$f_1 = \cos(n, x) \tag{B.65}$$
$$f_2 = \cos(n, y) \tag{B.66}$$
$$f_3 = \cos(n, z) \tag{B.67}$$
$$f_4 = y \cdot \cos(n, z) - z \cdot \cos(n, y) = y \cdot f_3 - z \cdot f_2 \tag{B.68}$$
$$f_5 = y \cdot \cos(n, x) - z \cdot \cos(n, z) = y \cdot f_1 - z \cdot f_3 \tag{B.69}$$
$$f_6 = y \cdot \cos(n, y) - z \cdot \cos(n, x) = y \cdot f_2 - z \cdot f_1 \tag{B.70}$$

   Which are normalised as $\sqrt{f_1 + f_2 + f_3} = 1$.

5. Radiation condition
   As the distance from the body R increases the radiation potential approaches zero:

$$\lim_{R \to \infty} \Phi = 0 \tag{B.71}$$

6. Symmetric or Anti-symmetric Condition
   In some situation, where the vessel is symmetric with respect to its middle line plane, the potential equations can be simplified with:

$$\Phi_2(-x, y) = -\Phi_2(x, y) \tag{B.72}$$
$$\Phi_3(-x, y) = +\Phi_3(x, y) \tag{B.73}$$
$$\Phi_4(-x, y) = -\Phi_4(x, y) \tag{B.74}$$

   Which are also used in the WAMIT analysis described in this report.

Applying the boundary conditions (1-5) to the radiation potential $\Phi_r(x, y, z, t) = \sum_{j=1}^{6} v_j \phi_j(x, y, z) e^{-i\omega t}$ (Equation B.42) and by considering deep water ($k = \omega^2/g$) gives:

$$\nabla^2 \phi_j = \frac{\partial^2 \phi_j}{\partial x^2} + \frac{\partial^2 \phi_j}{\partial y^2} + \frac{\partial^2 \phi_j}{\partial z^2} \qquad \text{For complete fluid region} \tag{B.75}$$
$$\frac{\partial \phi_j}{\partial z} = 0 \qquad \text{for: } z = -h \tag{B.76}$$
$$\frac{\partial \phi_j}{\partial z} - k\phi_j = 0 \qquad \text{for } z = 0 \tag{B.77}$$
$$\frac{\partial \phi_j}{\partial n} \cdot e^{-i\omega t} = f_j \cdot v_j \qquad \text{On the body surface} \tag{B.78}$$
$$\lim_{R \to \infty} \left[\frac{\partial \phi_j}{\partial R} + ik\phi_j \right] = 0 \qquad \text{(Sommerfield) Radiation Condition} \tag{B.79}$$

Doing the same for the undisturbed wave potential $\Phi_w(x,y,z,t) = \phi_w(x,y,z)e^{-i\omega t}$ and diffracted wave potential $\Phi_d(x,y,z,t) = \phi_d(x,y,z)e^{-i\omega t}$ gives:

$$\nabla^2\phi_w = \nabla^2\phi_d = 0 \qquad \text{For complete fluid region} \tag{B.80}$$

$$\frac{\partial\phi_w}{\partial z} = \frac{\partial\phi_d}{\partial z} = 0 \qquad \text{for: } z = -h \tag{B.81}$$

$$\frac{\partial\phi_w}{\partial z} - k\phi_w = \frac{\partial\phi_d}{\partial z} - k\phi_d = 0 \qquad \text{for } z = 0 \tag{B.82}$$

$$\frac{\partial}{\partial n}(\phi_w + \phi_d) \qquad \text{On the body surface} \tag{B.83}$$

$$\lim_{R\to\infty}\left[\frac{\partial\phi_d}{\partial R} + ik\phi_d\right] = 0 \qquad \text{(Sommerfield) Radiation Condition} \tag{B.84}$$

B.2.2. Solution strategies for linear potential flow

Solving the potentials is generally done in two ways:

- Two dimensional strip theory
  In 2D strip theory the forces and moments on the 3D body are approximated by considering 2D strips over the submerged length of the body. Because of this interaction between the strips is neglected.
- Three dimensional Boundary Element Method (diffraction code)
  With BEM the submerged surface of the vessel is divided into panels over which the potentials are solved by using a source distribution. WAMIT, the software package used for solving potential flow theory in this project, is an example of a 3D Boundary Element Method.

B.2.3. Solving the potentials with WAMIT

Below a very brief overview will be given on how WAMIT solves the velocity potentials, taken from the WAMIT manual. Green's theorem is used to obtain integral equations for the velocity potentials on the body boundary. For the radiation potential this integral equation takes the form:

$$2\pi\phi_j(\boldsymbol{x}) + \iint_S \phi_j(\boldsymbol{\zeta})\frac{\partial G(\boldsymbol{\zeta};\boldsymbol{x})}{\partial n_\zeta}\,d\zeta = \iint_S n_j G(\boldsymbol{\zeta};\boldsymbol{x})\,d\zeta \tag{B.85}$$

and for the diffraction and incident wave velocity potential this is:

$$2\pi\phi_d(\boldsymbol{x}) + \iint_S \phi_d(\boldsymbol{\zeta})\frac{\partial G(\boldsymbol{\zeta};\boldsymbol{x})}{\partial n_\zeta}\,d\zeta = 4\pi\phi_w(\boldsymbol{x}) \tag{B.86}$$

Where $(n_1,n_2,n_3) = \boldsymbol{n}$, $(n_3,n_4,n_5) = \boldsymbol{x}\cdot\boldsymbol{n}$, $\boldsymbol{x} = (x,y,z)$ and the undisturbed wave velocity potential ϕ_w is:

$$\phi_w = \frac{igA}{\omega}\frac{\cosh\left[\nu(z+H)\right]}{\cosh\left[\nu H\right]}e^{-i\nu x\cos\beta - i\nu y\sin\beta} \tag{B.87}$$

where β is the angle between the direction of propegation of the undisturbed incident wave and the positive x-axis and ν is the wavenumber given by the real root of the dispersion relation:

$$\frac{\omega^2}{g} = \nu\tanh(\nu H) \tag{B.88}$$

Furthermore, the Green's function $G(\boldsymbol{\zeta};\boldsymbol{x})$ is the wave source potential and is defined as the velocity potential at point $\boldsymbol{x}$ due to a point source of strength -4π located at point ζ, and satisfies the free surface and radiation conditions. Equation B.85 and B.86 are solved by discretisation. This can be done with the high order method (B-spline approach) or low order (a collection of quadrilaterals is used to approximate the wetted surface of the body). In this report the low order method is used which will

be shortly elaborated upon below. When the mesh size is small enough the quadrilaterals will approach a plane surface. Now, for each plane the velocity potential can be solved by considering the linear systems that follows from discretisation of equations B.85 and B.86. For the radiation potential this is:

$$2\pi\phi(\boldsymbol{x_i}) + \sum_{k=1}^{N} D_{ik}\phi_k = \sum_{k=1}^{N} S_{ik}\left(\frac{\partial\phi}{\partial n}\right)_k \tag{B.89}$$

with $i = 1, ..., N$ where N is the number of panels. For the diffraction potential is used:

$$2\pi\phi(\boldsymbol{x_i}) + \sum_{k=1}^{N} D_{ik}\phi_k = 4\pi\phi_w(\boldsymbol{x_i}) \tag{B.90}$$

In which the following matrixes are used:

$$D_{ik} = \iint_{S_k} \frac{\partial G(\boldsymbol{\zeta}; \boldsymbol{x_i})}{\partial n_\zeta}\, d\boldsymbol{\zeta} \tag{B.91}$$

$$S_{ik} = \iint_{S_k} G(\boldsymbol{\zeta}; \boldsymbol{x_i})\, d\boldsymbol{\zeta} \tag{B.92}$$

where s_k is the surface of the k-th panel and the points $\boldsymbol{x_i}$ are the points for which the velocity potentials are calculated which are located at the panel centroids.

B.2.4. Determine pressures and forces

The first order pressures on the body can be obtained by linearising the the Bernoulli equation:

$$\frac{\partial\Phi}{\partial t} + \frac{1}{2}\left(u^2 + v^2 + w^2\right) + \frac{p}{\rho} + gz = 0 \tag{B.93}$$

Yielding:

$$\frac{\partial\Phi}{\partial t} + \frac{p}{\rho} + gz = 0 \tag{B.94}$$

$$p^1 = -\rho gz - \rho\frac{\partial\Phi}{\partial t} \tag{B.95}$$

Substitution of Equation B.40 to B.42 in Equation B.95 gives:

$$p = -\rho gz - \rho\left(\frac{\partial\Phi_w}{\partial t} + \frac{\partial\Phi_d}{\partial t} + \frac{\partial\Phi_r}{\partial t}\right) \tag{B.96}$$

$$= -\rho gz + i\rho\omega e^{-i\omega t}\left(\phi_w + \phi_d + \sum_{j=1}^{6}\phi_j\right) \tag{B.97}$$

The forces $\boldsymbol{F}$ and moments $\boldsymbol{M}$ on the body surface S can now be obtained by:

$$\boldsymbol{F} = -\iint_S (p\cdot\boldsymbol{n})\cdot dS \tag{B.98}$$

$$\boldsymbol{M} = -\iint_S p\,(\boldsymbol{r}\cdot\boldsymbol{n})\cdot dS \tag{B.99}$$

With $\boldsymbol{n}$ the outward normal vector of the surface dS and $\boldsymbol{r}$ the position vector of the surface dS in the body fixed axis system.

B.2.5. Restoring coefficients

The restoring coefficients in $\boldsymbol{C}_b$ are given by:

$$C(3,3) = \rho g \iint_S n_3 \, dS \tag{B.100}$$

$$C(3,4) = \rho g \iint_S y n_3 \, dS \tag{B.101}$$

$$C(3,5) = -\rho g \iint_S x n_3 \, dS \tag{B.102}$$

$$C(4,4) = \rho g \iint_S y^2 n_3 \, dS + \rho g \nabla z_b - m g z_g \tag{B.103}$$

$$C(4,5) = -\rho g \iint_S x y n_3 \, dS \tag{B.104}$$

$$C(4,6) = -\rho g \nabla x_b \tag{B.105}$$

$$C(5,5) = \rho g \iint_S x^2 n_3 \, dS + \rho g \nabla z_b - m g z_g \tag{B.106}$$

$$C(5,6) = -\rho g \nabla y_b + m g y_g \tag{B.107}$$

In addition, $C_{ij} = C_{ji}$ except for C_{46} and C_{56}. Also, $C_{ij} = 0$ for all other restoring coefficients that are not given above.

B.3. Scaling laws

For scaling from full size (subscript s) to model scale (subscript m) Froude scaling (Section B.3.1 is used for the model scale experiments. Robert Edmund Froude, son of William Froude, used that inertia and pressure forces are almost universally important. Furthermore, he stated that it is therefore appropriate to keep the ratio of inertia or pressure forces divided by the gravity forces constant. Taking the square root of this ratio gives the Froude number on which Froude scaling is based upon.

Froude scaling does not ensure that the viscous forces are correctly scaled, for this Reynolds scaling (Section B.3.2) is necessary. However, Froude- and Reynods scaling cannot be applied simultaneously without changing the viscosity of the fluid. This does not matter for as long as in both the full size- and scaled model the same Reynold regime is observed.

Other scaling laws that can be applied, and that are not discussed in this report are based on the Weber (inertia/surface tension)-, Mach (inertia/elasticity)-, Strouhal- and Keulegan-Carpenter (drag/inertia) number.

B.3.1. Froude scaling

The Froude number is, as explained above in Section B.3, based on:

$$F_n = \frac{\text{inertia or pressure forces}}{\text{gravity forces}} \tag{B.108}$$

If we now assume a scaling factor for density α_ρ, α_V for volume, α_L for length and α_g for gravity we

can write Equation B.108 as follows:

$$F_n = \frac{\alpha_\rho \cdot \alpha_V^2 \cdot \alpha_L^2}{\alpha_\rho \cdot \alpha_L^3 \cdot \alpha_g} \tag{B.109}$$

$$= \frac{\alpha_v}{\sqrt{\alpha_g \cdot \alpha_L}} \tag{B.110}$$

$$= \frac{V}{\sqrt{gL}} \tag{B.111}$$

If it is now assumed that the Froude number has to be constant for the full size (subscript s) and model scale (subscript m), and that the gravitational acceleration is constant in scaling then the following applies:

$$F_n = \frac{V_m}{\sqrt{g \cdot L_m}} = \frac{V_s}{\sqrt{g \cdot L_s}} \tag{B.112}$$

$$= \frac{V_m}{V_s} = \frac{\sqrt{g \cdot L_m}}{\sqrt{g \cdot L_s}} \tag{B.113}$$

$$= \frac{V_m}{V_s} = \frac{\sqrt{L_m}}{\sqrt{L_s}} = \sqrt{\frac{L_m}{L_s}} \tag{B.114}$$

$$= \alpha_V = \sqrt{\alpha_L} \tag{B.115}$$

From Equation B.115 is found that when the model is built with a scaling factor for length

$$\alpha_L = \frac{\sqrt{L_s}}{\sqrt{L_m}} = \frac{L_s}{L_m} \rightarrow L_m = \frac{L_s}{\alpha_L} \tag{B.116}$$

the relation between the scaling factor for velocity and length is given by $\alpha_V = \sqrt{\alpha_L}$ and that the scaled model velocity is:

$$V_m = \frac{V_s}{\alpha_V} \tag{B.117}$$

$$= \frac{V_s}{\sqrt{\alpha_L}} \tag{B.118}$$

Other scaling factors can be derived accordingly. For example the scaling factor for time can be derived for considered the relation $x = V \cdot t$. This gives:

$$\alpha_L = \alpha_V \cdot \alpha_t \tag{B.119}$$

$$\alpha_t = \frac{\alpha_L}{\alpha_V} = \frac{\alpha_L}{\sqrt{\alpha_L}} = \sqrt{\alpha_L} \tag{B.120}$$

For acceleration the following relation can be used:

$$V = \ddot{V} \cdot t \tag{B.121}$$

$$\alpha_V = \alpha_{\ddot{V}} \cdot \alpha_t \tag{B.122}$$

$$\alpha_{\ddot{V}} = \frac{\alpha_V}{\alpha_t} = \frac{\sqrt{\alpha_L}}{\sqrt{\alpha_L}} = 1 \tag{B.123}$$

Which is a logical result, as also the gravitational acceleration g is kept constant for scaling between full- and model scale. The scaling factor for displacement can now also be easily calculated as displacement has the unit of length to the power of three, so:

$$\alpha_V = \alpha_L^3 \tag{B.124}$$

Another important scaling factor is force, which can be found by:

$$F = m \cdot \ddot{V} \propto \rho \cdot \nabla \cdot \ddot{V} \tag{B.125}$$

$$\alpha_F = \alpha_\rho \cdot \alpha_\nabla \cdot \alpha_{\ddot{V}} \tag{B.126}$$

$$= \alpha_\rho \cdot \alpha_L^3 \cdot 1 = \alpha_\rho \cdot \alpha_L^3 = \alpha_L^3 \tag{B.127}$$

Finally, the last scaling parameter derived here is the wave frequency ω. As angles are identical for full size and model scale, the following is found:

$$\alpha_\omega = \frac{1}{\alpha_t} = \frac{1}{\sqrt{\alpha_L}} \tag{B.128}$$

A number of other scaling factors are given below. Any scaling factors not mentioned here, but used during the project, will be elaborated upon in the relevant chapter.

$$\alpha_M = \alpha_L^4 \tag{B.129}$$

$$\alpha_m = \alpha_L^3 \tag{B.130}$$

$$\alpha_{\ddot{\omega}} = \alpha_L^{-1} \tag{B.131}$$

$$\alpha_T = \sqrt{\alpha_L} \tag{B.132}$$

$$\alpha_{S(\omega)} = \alpha_L^{2.5} \tag{B.133}$$

Froude scaling works very well when in both the full- as model scale situation the flow is turbulent, where viscous forces do not dominate. This is the case for the situations considered in this project and therefore Froude scaling is believed to be the best method of scaling in this project.

B.3.2. Reynolds scaling

In Reynolds scaling the ratio between the inertia and viscous forces stay the same, so that the viscous forces are correctly scaled:

$$\frac{\text{Inertia forces}}{\text{Viscous forces}} = \frac{F_i}{F_v} \propto \frac{\rho V^2 L^2}{\mu V L} = \frac{UL}{\nu} = Re \tag{B.134}$$

Where ν is the kinematic viscosity m/ρ. With Reynolds scaling the Reynolds number has to be the same for the scaled and full size model:

$$Re = \frac{\rho V_m D_m}{\mu_m} = \frac{\rho V_s D_s}{\mu_s} \tag{B.135}$$

Of course the density of the fluid is the same at model scale as at full size scale, so Equation B.135 can be written in the form:

$$\frac{V_m D_m}{\nu_m} = \frac{V_s D_s}{\nu_s} \tag{B.136}$$

Or in terms of scaling factor α:

$$\frac{\alpha_V \cdot \alpha_L}{\alpha_\mu} = 1 \tag{B.137}$$

With $\alpha_V = \alpha_L / \alpha_T$ this becomes:

$$\alpha_T = \frac{\alpha_L^2}{\alpha_\nu} \tag{B.138}$$

When the same fluids are used at full- and model scale, or are almost the same as in case of for example simulating sea water in a tank, α_ν and α_ρ can be assumed to be almost equal to 1.0, resulting in:

$$\alpha_T \approx \alpha_L^2 \tag{B.139}$$

This would mean that time would go very quickly at model scale. Furthermore, if substitutions are made to derive the scale factor for force, it would be derived that α_F is equal to 1.0, meaning that forces would be as big for the scaled model as for the full size model. Both these findings are of course very impractical.

It is also possible to relate the presence of viscous forces to the Navier Stokes equation. With $Re = \frac{\rho V D}{\mu}$ it can be seen that for increasing tank size and increasing velocities in the tank the Reynolds number will be larger. This is important as for small Reynolds numbers viscous forces are dominant and become less important for larger Reynolds numbers. This is shown by rewriting the dimensionless Navier-Stokes equation:

$$\frac{Dv}{Dt} = -\nabla p + \frac{\mu}{\rho V D}\nabla^2 V + f \tag{B.140}$$

If we now assume that

$$\frac{\mu}{\rho V D} = \frac{1}{Re} \tag{B.141}$$

it can be seen in Equation B.142 that the viscous term in the Navier-Stokes equations disappears as $Re \to \infty$

$$\frac{Dv}{Dt} = -\nabla p + \frac{1}{Re}\nabla^2 V + f \tag{B.142}$$

B.4. Derivation of the moment of inertia of a hemisphere

This section will describe the procedure to obtain the moment of inertia of a partially filled spherical tank. This is used to simulate the frozen cargo condition, see Section 2.5.

B.4.1. Calculate volume- and free surface of the partially filled tanks

For the analysis it is necessary to know the volume, but also the height of the free surface level of the partially filled tanks and the corresponding horizontal location of the tank wall at the free surface level. These are necessary for creating the panel model, which should be created up to the free surface level, and not higher.

B.4.2. Derivation for the completely filled tank

In this section the moment of inertia of the completely filled spherical tanks only is considered. First the derivation in cartesian coordinates is given, which can also be applied to partial filled spherical tanks. The basis of the analysis is that a sphere can be divided in infinite small thin (horizontal) disks with radius y. Considering the moment of inertia of a solid cylinder as $I = \frac{1}{2}mR^2$, resulting in the moment of inertia for the thin disks:

$$dI = \frac{1}{2}y^2 dm \tag{B.143}$$

Substituting $dm = \rho\, dV$ and $dV = \pi y^2 dz$ gives:

$$dI = \frac{1}{2}y^2 \rho\, dV = \frac{1}{2}y^2 \rho \pi y^2\, dz = \frac{1}{2}\rho\pi y^4\, dz \tag{B.144}$$

The moment of inertia for the completely filled sphere can now be obtained by:

$$I = \frac{1}{2}\rho\pi \int_{-R}^{R} y^4\, dz \tag{B.145}$$

The radius y of this thin horizontal disk at any location in the sphere can be expressed in the radius R and vertical location z of the disks in the sphere by using Pythagoras' theorem:

$$y^2 = R^2 - z^2 \tag{B.146}$$

Substitution of this in Equation B.145 gives:

$$I = \frac{1}{2}\rho\pi \int_{-R}^{R} (R^2 - z^2)^2\, dz = \frac{8}{15}\pi R^5 \tag{B.147}$$

By considering the mass of a completely filled tank the density ρ can be expressed as:

$$\rho = \frac{m}{V} = \frac{m}{\frac{4}{3}\pi R^3} \tag{B.148}$$

Substitution of the density of the cargo in Equation B.147 gives the moment of inertia for a completely filled spherical tank around the centre of gravity of the tank in all three directions:

$$I_{xx} = I_{yy} = I_{zz} = \frac{8}{15}\left(\frac{m}{\frac{4}{3}\pi R^3}\right)\pi R^5 = \frac{2}{5}mR^2 \tag{B.149}$$

Next to the moment of inertia itself, it is also relevant to know the centre of mass of the spherical tank as this is relevant for determining the moment of inertia of the spherical tanks around the global axis system of the barge. Obviously for a completely filled spherical tank z_{cm} is located in the centre of the

sphere. However, for a partially filled spherical tank the vertical location of the centre of gravity will change and can be determined with:

$$\bar{x} = \frac{\int x\, dm}{\int dm} \tag{B.150}$$

By substituting $dm = \rho\pi \left(\sqrt{R^2 - x^2}\right)^2$ Equation B.150 becomes for a completely filled sphere:

$$z_{cm,100\%filled} = \frac{\int_{-R}^{R} x \cdot \pi\rho \left(\sqrt{R^2 - x^2}\right)^2 dx}{\int_{-R}^{R} \pi\rho \left(\sqrt{R^2 - x^2}\right)^2 dx} = \frac{1}{2}R \tag{B.151}$$

B.4.3. Derivation for the partially filled spherical tank

The equations used for calculation the moment of inertia- and centre of mass for the completely filled tank can also be used for the partially filled tanks. However, now the centre of mass in the z-direction is not in the centre of the sphere anymore. To obtain the moment of inertia around its center of mass the parallel axes theorem can be used:

$$I_{xx} = \bar{I}_{xx} - m(\delta y^2 + \delta z^2) = \bar{I}_{xx_{tank}} - m z_{cm}^2 \tag{B.152}$$
$$I_{yy} = \bar{I}_{yy} - m(\delta x^2 + \delta z^2) = \bar{I}_{yy_{tank}} - m z_{cm}^2 \tag{B.153}$$
$$I_{zz} = \bar{I}_{zz} - m(\delta x^2 + \delta y^2) = \bar{I}_{zz_{tank}} \tag{B.154}$$
$$I_{yz} = \bar{I}_{yz} - m\delta y \delta z = 0 \tag{B.155}$$
$$I_{xz} = \bar{I}_{xz} - m\delta x \delta z \tag{B.156}$$
$$I_{xy} = \bar{I}_{xy} - m\delta x \delta y = 0 \tag{B.157}$$

Where I_{xx}, I_{yy}, I_{zz}, I_{yz}, I_{xz} and I_{xy} are the (cross) moments of inertia around the relevant axis going through the centre of the liquids mass in the (partially filled) tank, $\bar{I}_{i,j}$ are the (cross) moments of inertia around the axis going through the undisturbed free surface of the liquid in the tank, $\delta x = \delta y = 0$ as the centre of gravity is horizontally still in the middle of the tank, and $\delta z = z_{cm}$.

The complete process of finding the moment of inertia for the partially filled tank around the mass centre will be given below for the 50% filling condition. If Equation B.147 and B.148 are used for the the half-full tank the following is obtained:

$$\bar{I}_{50} = \frac{1}{2}\rho\pi \int_{-R}^{0} (R^2 - z^2)^2\, dz = \frac{4}{15}\pi R^5 \tag{B.158}$$
$$\rho_{50} = \frac{m}{V} = \frac{m}{\frac{8}{3}\pi R^3} \tag{B.159}$$
$$\bar{I}_{xx_{tank}} = \bar{I}_{yy} = \bar{I}_{zz} = \frac{4}{15}\left(\frac{m}{\frac{8}{3}\pi R^3}\right)\pi R^5 = \frac{2}{5}mR^2 \tag{B.160}$$

Equation B.160 gives the moments of inertia around the axis going through the center of the free surface of the liquid in the half full tank. This is the same result as found for the completely filled tank, with the exception that now the mass of the half full tank is used. Which is logical as a sphere can be seen as two hemispheres on top of each other. The next step is to obtain the moment of inertia around the axis going through the center of the liquid that is in the tank. For this we are interested in the vertical location of the mass centre:

$$z_{cm_{50}} = \frac{\int_{0}^{R} x \cdot \pi\rho \left(\sqrt{R^2 - x^2}\right)^2 dx}{\int_{0}^{R} \pi\rho \left(\sqrt{R^2 - x^2}\right)^2 dx} = \frac{3}{8}R \tag{B.161}$$
$$= \frac{3}{8} \cdot 19.25 = 7.22\ m \tag{B.162}$$

The final step is to calculate the moment of inertia around the centre of mass of the liquid in the tank. This is done by substitution of Equation B.160 and B.162 in Equation B.153 to B.155:

$$I_{xx_{tank}} = \bar{I}_{xx_{tank}} - m(\delta y^2 + \delta z^2) \tag{B.163}$$

$$= \bar{I}_{xx_{tank}} - m\delta z^2 = \frac{2}{5}mR^2 - m\left(\frac{3}{8}R\right)^2 = \frac{83}{320}mR^2 \tag{B.164}$$

$$I_{yy_{tank}} = \bar{I}_{yy_{tank}} - m(\delta x^2 + \delta z^2) \tag{B.165}$$

$$= \bar{I}_{yy_{tank}} - m\delta z^2 = \frac{2}{5}mR^2 - m\left(\frac{3}{8}R\right)^2 = \frac{83}{320}mR^2 \tag{B.166}$$

$$I_{zz_{tank}} = \bar{I}_{zz_{tank}} - m(\delta x^2 + \delta y^2) \tag{B.167}$$

$$= \bar{I}_{zz_{tank}} = \frac{2}{5}mR^2 \tag{B.168}$$

B.4.4. Inertia around the centre of gravity of barge including tanks

Now that the moments of inertia of the liquid in the tank around its own centre of gravity are known, the moments of inertia around the centre of gravity of the barge without cargo tanks can be calculated. This is done by using the parallel axes theorem (see Equation B.153 to B.157). The barge is equipped with two tanks which have to be taken into account separately. For both tanks δy is equal to zero as both tanks have their centre of gravity at $y = 0$. $\delta_{x_1} = 50m \wedge \delta_{x_2} = -50m$ as one of the tanks is placed 50 meter aft of midship while the other tanks is placed 50 meter fore of midship. δz changes depending on the filling condition and also has to be taken into account for both tanks separately. Summing the moments of inertia of the barge and the tanks, and applying the parallel axes theorem gives:

$$I_{xx} = I_{xx_{barge}} + 2 \cdot \left[I_{xx_{tank}} + m_{tank} \cdot \delta z^2\right] \tag{B.169}$$

$$= I_{xx_{barge}} + 2 \cdot \left[I_{xx_{tank}} + m_{tank} \cdot 0.67^2_{cm}\right] \tag{B.170}$$

$$I_{yy} = I_{yy_{barge}} + 2 \cdot \left[\bar{I}_{yy_{tank}} + m_{tank} \cdot (\delta x^2 + \delta z^2)\right] \tag{B.171}$$

$$= I_{yy_{barge}} + 2 \cdot \left[\bar{I}_{yy_{tank}} + m_{tank} \cdot (50^2 + 0.67^2_{cm})\right] \tag{B.172}$$

$$I_{zz} = I_{zz_{barge}} + 2 \cdot \left[\bar{I}_{zz_{tank}} + m_{tank} \cdot \delta x^2\right] \tag{B.173}$$

$$= I_{zz_{barge}} + 2 \cdot \left[\bar{I}_{zz_{tank}} + m_{tank} \cdot 50^2\right] \tag{B.174}$$

Which summarise the moments of inertia around the x-, y-, and z-axis going through the centre of gravity of the barge including the two spherical cargo tanks. The value of δz is found by:

$$\delta z = 2.5 + R - z_{cm} - z_{CoGbarge} \tag{B.175}$$

$$= 2.5 + 19.25 - 7.22 - 13.86 = 0.67 \tag{B.176}$$

Where 2.5 is the distance between the keel and bottom of the tank and z_{cm} is the distance between centre of gravity of the tank and the free surface in the tank, see Equation B.162.